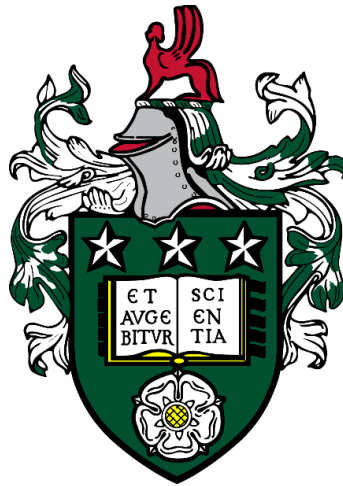# Auto-ignition and heat release of alternative engine fuels.

Inna Gorbatenko

Submitted in accordance with the requirements for the degree of
Doctor of Philosophy

The University of Leeds

The Centre for Doctoral Training in Fluid Dynamics

September, 2019

The candidate confirms that the work submitted is his/her own, except where work which has formed part of jointly-authored publications has been included. The contribution of the candidate and the other authors to this work has been explicitly indicated below. The candidate confirms that appropriate credit has been given within the thesis where reference has been made to the work of others.

Chapter 4 represents work from a published manuscript:

Bates, L., Bradley, D., Gorbatenko, I. and Tomlin, A.S. Computation of methane/air ignition delay and excitation times, using comprehensive and reduced chemical mechanisms and their relevance in engine autoignition. *Combustion and Flame.* 2017, **185**, pp.105-116.

For the above, the author of the present thesis has carried out all the detailed chemical kinetic modelling, related numerical simulations, evaluations and data analysis of the results presented in the above manuscript under the guidance of the Prof. D. Bradley and Prof. A. S. Tomlin. All the figures were entirely or partly based on the information and the results of the study performed by the current candidate, who is accounted for the production of most of them. Dr. L. Bates is fully responsible for the reduced global scheme numerical work. All authors are jointly responsible for writing, revising, editing and technical discussion of the manuscript.

Part of work presented in Chapter 5 appeared in the following manuscript:

Gorbatenko, I., Tomlin, A.S., Lawes, M. and Cracknell, R.F. Experimental and Modelling Study of the Impacts of n-Butanol Blending on the Auto-Ignition Behaviour of Gasoline and its Surrogate at Low Temperatures. *Proceedings of the Combustion Institute.* 2019, **37**(1), pp.501-509.

For the above, the candidate was the first author and the lead investigator. The present author was responsible for the experimental acquisition of the data, numerical analyses and detailed chemical kinetic modelling work. The supervisory team Prof. A. S. Tomlin, Dr. M. Lawes and Prof. R. F. Cracknell provided invaluable insights on the topic, guidance and technical discussion of the work. The candidate wrote the first draft paper. Prof. A. S. Tomlin proof read the draft, re-worded and wrote part of the discussion. All authors contributed to the revision and edition of the manuscript.

This copy has been supplied on the understanding that it is copyright material and that no quotation from the thesis may be published without proper acknowledgement.

The right of Inna Gorbatenko to be identified as Author of this work has been asserted by her in accordance with the Copyright, Designs and Patents Act 1988.

This thesis is dedicated to

My wonderful parents, who have raised me to be the person I am today,

My amazing sister, who has always been there for me.

"Success isn't a result of spontaneous combustion. You must set yourself on fire." –
Arnold H. Glasow

Acknowledgements

Abstract

Diversification of energy sources and transport decarbonisation are growing concerns of modern societies. Alternative fuels play an important role in addressing these challenges. For the spark ignition (SI) engine, the propensity of the fuel and fuel blends to auto-ignite is a critical characteristic that limits engine efficiency, which can be assessed by the ignition delays (τ_i). Severity of knock is also dependent upon the duration of heat release rate - the excitation time (τ_e).

In this thesis, detailed evaluations of τ_i and τ_e are employed to study the tendency of methane to detonate in comparison with other fuels, employing the detonation peninsula on the ξ/ε diagram. The ξ parameter is the ratio of acoustic to auto-ignitive velocity, whereas ε is the ratio of the acoustic wave resistance time in a hot spot to the τ_e. It is shown that stoichiometric methane/air exhibits very good anti-knock properties in comparison with other fuels under turbocharged engine running conditions.

The changes in the auto-ignition behaviour caused by the progressive addition of n-butanol (at 10%, 20%, 40% and 85% vol n-butanol) to gasoline (RON 95, MON 86.6) and its toluene reference fuel (TRF) are studied computationally and experimentally in a rapid compression machine (RCM) under stoichiometric condition at 2 MPa and at 678-916 K. At low temperatures, n-butanol acts as an octane enhancer, reducing low temperature heat release and increasing ignition delays, with marginal additional effects for blends above 40%. This is supported by the results from ξ/ε diagram, where higher n-butanol blends lie further away from the developing detonation region.

A brute-force sensitivity analysis of the surrogate model suggests that the main reaction inhibiting ignition at low temperatures is H abstraction from the α-site of n-butanol, even for the 10% blend. At higher temperatures, the behaviour reverses as the chain branching routes from H abstraction by OH from the γ-site of n-butanol and from the α-site by HO_2 become more dominant, promoting ignition. For the lower blends, the largest discrepancies between simulations and experiments are found in the negative temperature coefficient (NTC) region, where a larger number of reactions contribute to the uncertainty in predicting τ_i. For the higher blends, the largest discrepancies occur at low temperatures, indicating that uncertainties within the low temperature n-butanol chemistry need to be resolved. Regarding τ_e, the addition of n-butanol to the TRF blends has a negligible effect. Furthermore, τ_e, is not influenced by NTC chemistry.

Table of Contents

List of Figures

List of Tables

Nomenclature

A	Pre-exponential factor	-
a	Acoustic speed	m/s
c_p	Specific heat capacity at constant pressure	J/kg/ K
c_v	Specific heat capacity at constant volume	J/kg/ K
E	Activation energy	J/mol
$\bar{E}$	Detonation stability dimensionless group, $(\bar{E}=(\tau_i/\tau_e)(E/RT)\ )$	-
H	Standard enthalpy	J/mol
k	Rate constant	-
k_f	Rate constant (forward reaction)	-
k_r	Rate constant (reversed reaction)	-
K_{eq}	Equilibrium rate constant	-
M	Molecular weight	kg/mol
m	Mass	kg
m_0	Initial mass of the fuel	kg
N	Total number of species	-
n	Polytropic coefficient, $(PV^n = const)$	-
P	Pressure	Pa
P_c	Pressure at the end of compression	Pa
P_i	Initial pressure	Pa
$\dot{Q}_{chem}$	Rate of heat released	J/s
R	Ideal gas constant	J/mol/ K
r_0	Hot spot radius	m
$\bar{r}$	Normalised hot spot radius $(\bar{r} = r/r_0)$	-
S_i	Sensitivity coefficient of reaction i	-
$S^{\ominus}$	Standard entropy	J/mol/ K
T	Temperature	K
t	Time	s
T_c	Temperature at the end of compression	K
T_i	Initial temperature	K
U	Specific internal energy	J/kg
u_a	Auto-ignition velocity	m/s

V	Volume	m^3
v	Stoichiometric coefficient	-
W_{piston}	Rate of work done by the piston	J/s
w	Molar rate of production	-
Y	Mass fraction	-

Greek Symbols

γ	Ratio of specific heats	-
ε	Residence time of pressure wave in hot spot normalised by excitation time ($\varepsilon = r_0 / a\tau_e$)	-
ξ	Acoustic speed normalised by auto-ignition velocity ($\xi = a/u_a$)	-
ξ_l,	Lower limits	-
ξ_u	Upper limits	-
π	Knock intensity parameter	-
τ_e	Excitation times	s
τ_i	Ignition delay time	s
τ_1	First-stage ignition delay time	s
τ_2	Second-stage ignition delay time	s
φ	Equivalence ratio	

Subscripts and Superscripts

AI	Instance of auto-ignition
cyl	Cylinder
in	Flow into the system
max_exp	Maximum experimental
max_isoc	Maximum isochoric
nr	Non-reactive case
out	Flow out of the system
$\ominus$	Standard

Acronyms

aHR	Accumulated Heat Release
BDC	Bottom Dead Centre
BMF	Burned Mass Fraction.
BTU	British Thermal Unit
CI	Compression Ignition
CFD	Computational Fluid Dynamic
CFR	Cooperative Fuel Research
CNG	Compressed Natural Gas
CPU	Central Processing Unit
CR	Compression Ratio
DI	Direct Injection
EGR	Exhaust Gas Recirculation
FACE	Fuels for Advanced Combustion Engines
GCI	Gasoline Compression Ignition
GDP	Gross Domestic Product
GHG	Greenhouse Gas
HCCI	Homogeneous Charge Compression Ignition
HRA	Heat Release Analysis
HRR	Heat Release Rate
HTHR	High Temperature Heat Release
ICE	Internal Combustion Engine
ITHR	Intermediate Heat Release Rate
KAUST	King Abdullah University of Science and Technology
LDV	Light Duty Vehicle
LHV	Lower Heating Value
LLNL	Lawrence Livermore National Laboratory
LNG	Liquefied Natural Gas
LTC	Low Temperature Combustion
LTHR	Low Temperature Heat Release
Mb/d	Million barrels per day
MBDOE	Million Barrels Oil Equivalent per Day
MON	Motor Octane Number
Mt	Million tonnes

NASA	National Aeronautics and Space Administration
NDC	Nationally Determined Contribution
NTC	Negative Temperature Coefficient
ON	Octane Number
ODE	Ordinary Differential Equations
OI	Octane Index
PCCI	Premixed Charge Compression Ignition
PRF	Primary Reference Fuel
POLIMI	Politecnico di Milano
RCCI	Reactivity Controlled Compression Ignition
RCM	Rapid Compression Machine
RED	Renewable Energy Directive
RON	Research Octane Number
S	Octane Sensitivity
SI	Spark Ignition
TDC	Top Dead Centre
VHRR	Volumetric Heat Release Rate

1. Introduction to the topic and scope of the research study

1.1 Outline of the problem and rational

Energy is fundamental for modern life and affects the economy, security, sustainability and environmental goals. By 2040, the global population is projected to reach 9.2 billion people [1]. At the same time the global Gross Domestic Product (GDP) is likely to almost double, with the continuing trends towards increased urbanisation and significant expansion in the middle class [1-3]. Largely, the growth in energy demand comes from developing countries such as China and India, which are predicted to substantially increase their transportation needs [1-3]. In 2017, over 70% of global energy demand growth was met by oil, natural gas and coal, with the fossil fuels accounting for 81% of total energy demand [3]. Therefore, our society is still heavily reliant on the finite resources of fossil fuels. Despite the finite reserves, the world is quite far from exhausting the fossil fuel reserve. There are approximately 13-15 trillion barrels of oil, 50 quadrillion cubic feet of natural gas, and 14 trillion tons of coal in the world [4]. However, only a small part of these resources are of viable recovery and utilisation. Most of them are located in the unreliable and variable markets of often politically unstable regions. At the present day, effective exploitation capacity is close to being entirely utilised. Therefore, the economical reserves will not be able to accommodate the world's growing demand for refined products and can only be fulfilled with additional capacity [5].

In 2018, the global primary energy consumption grew by 2.9% - the fastest growth since 2010, as shown in Figure 1.1 (a) [6]. This growth took place despite a backdrop of moderate GDP growth and increasing energy prices [6]. The transport sector accounts for around 20% of the world's energy use [3, 7, 8]. Oil remains the world's dominant fuel with an approximate consumption of 4.66 billion tonnes and a growth rate of 1.5% or 1.4 million barrels per day (Mb/d) [6]. It constitutes approximately one third of all energy consumed [6]. Moreover, according to BP Global [2, 6] and ExxonMobil [1], oil is expected to continue to dominate the world's energy mix, reaching up to 105 Mb/d by 2040. This growing demand is primarily driven by commercial transportation (including aviation and shipping), and the chemical industry [1-3, 9-11]. Although, the introduction of strict policies and regulations of emissions, driven by environmental concerns, or a technological breakthrough in the energy sector, may lead to a different outcome. The

global energy mix by sector in 2017 is presented in Figure 1.1 (b), along with projections for 2025 and 2040.

Figure 1.1: a) Global energy consumption growth. Adopted from [6]. b) Global energy consumption by sector in quadrillion British thermal units (BTUs). Adapted from [12].

Historically, liquefied hydrocarbons have become the energy source of choice. In 2017, conventional crude and condensate accounted for around two thirds of the liquid supply [12]. This is due to their high energy density, low cost, ease of handling, reliability and highly integrated infrastructure for their production, transport, storage and distribution. At present, around 95% of the transport energy is supplied by liquid fuels [7, 8, 13]. These fuels are derived by refining petroleum, which is overwhelmingly oil dependent and accounts for around 60% of global oil demand [7, 8, 13]. Light duty vehicles (LDVs), predominantly passenger cars, account for more than 70% of all transport modes and around 44% of the global transport energy demand [3, 7, 8, 13]. These are typically (about 80%) powered by spark ignition (SI) engines running on gasoline with the immense global demand of more than 4.85 billion litres a day [7, 8]. Figure 1.2 (a) illustrates the LDV demand by fuel type. According to ExxonMobil projections [11], the LDV demand for internal combustion engine (ICE) fuels is going to culminate before 2025 and then reduce to levels of the 2010 by 2040. The former is attributed to an increase in personal vehicle ownership, whereas the latter is driven by electrification and higher efficiency gains in engine technologies [11]. In Europe, diesel engines have a higher proportion of the market with a global daily demand of 4.83 billion litres [7, 8]. The road and marine commercial sectors are overshadowed by diesel engines [14]. Due to their affordable price, durability, high reliability and fast refuelling, conventional ICE are predicted to continue

to play a leading role in the global fleet in the future, as demonstrated in Figure 1.2 [11]. The ICE technology is particularly important for air travel, trucking and shipping [9, 11]. Figure 1.2 (b) demonstrates the commercial transportation demand by sector and fuel.
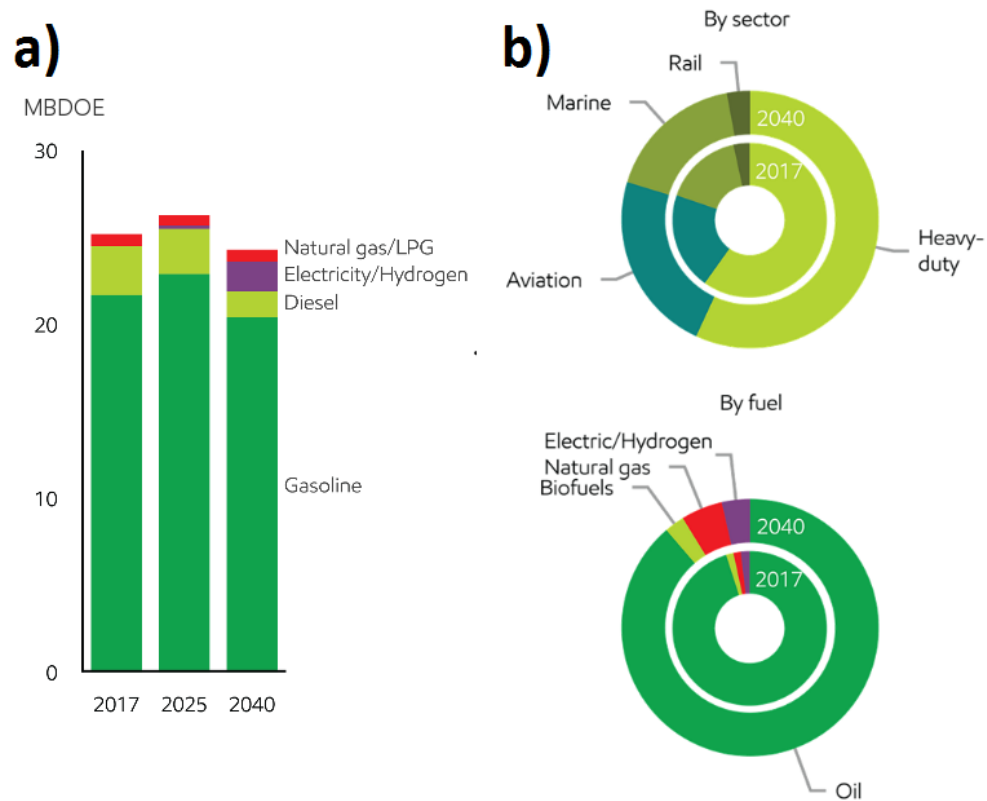
Figure 1.2: a) Light duty demand by fuel in million oil equivalent barrels per day (MBDOE) b) Commercial transportation demand by sector and fuel [11].

A steady growth in energy consumption, as well as its overwhelming dependence on fossil fuels and ICE technology, makes the transportation sector a critical driver of future world anthropogenic emissions. On-road and non-road ICE combined emissions account for approximately 41% of anthropogenic nitrogen oxides emissions [15]. The global greenhouse gas (GHG) emissions rose by a shocking 91% between 1970 and 2012 [16]. An approximate 55% increase in carbon emissions has occurred in the last 25 years [2]. While most sectors were able to decrease their GHG emissions, emissions from transportation increased by almost 21% between 1990 to 2010 [15]. Advances in engine technologies and emission control systems, as well as fuel quality, have helped to stall the growth in emissions of pollutants closely related to the combustion processes. These include nitrogen oxides (NO_x), carbon monoxide (CO), carbon dioxide (CO_2), hydrocarbons (HC), particulate matter (PM) and sulphur dioxide (SO_2) [15]. However, the transport sector is still confronted with problems of decarbonisation and reduction of emissions, particularly in developing countries.

Emissions from the transport sector have detrimental environmental effects. They impact the atmospheric chemistry, result in smog formation and acid rain, and drive global average surface temperature increases and climate change. Nowadays, extreme and unpredicted weather patterns, including hurricanes, flooding and tropical cyclones, occur more frequently. Global warming causes the reduction of the sea ice in both the Arctic and Antarctic, the melting of land ice and increases in ocean heat content [4, 5, 17-20]. This subsequently increases the sea level and results in the flooding and erosion of coastal areas [4, 5, 17]. Currently, sea level is rising at a rate of ~3.2 mm per year, as a result of land ice loss, the melting of ice sheets in Greenland and Antarctica, and thermal expansion due to the storage of heat in the oceans [19, 20]. Between 1980 and 2011 floods impacted the lives of more than 5.5 million people and caused direct economic losses of more than €90 billion [17]. It is very probable that adverse and extreme weather patterns, heat waves and heavy precipitations will become even more frequent in future. Moreover, an increase in air pollution from transport directly affects the air quality in urban areas and public health. Worldwide, ambient air pollution contributed to 7.6% of all deaths in 2016 [21]. It claims approximately 4.2 million lives every year [21]. The influence of urban air pollution on public health is only beginning to be understood. This is associated with an increased risk of respiratory and cardio-metabolic diseases, reduction of quality of life, and premature deaths in the most vulnerable populations [4, 5].

Environmental concerns have led to the introduction of strict counter measures and regulations of emissions, which have been often influenced by the fundamental and applied research of combustion processes. The recent Paris Agreement [22] on climate change has clearly demonstrated the governments' intentions to reduce GHG emissions with the ambition to develop an agreement of nationally determined contributions (NDCs) [1]. The Paris Agreement requires each country to prepare, outline, communicate and maintain NDCs that it aims to achieve [23]. This subsequently would provide policies that could change the energy consumption and supply, encourage new technology or discourage the use of an existing technology [1].

Since 2009, EU legislation sets mandatory CO_2 emission reduction targets for new vehicles in order to cut down its GHG emissions. A binding target of 130 grams of CO_2 per kilometre (g CO_2/km) was implemented for the EU fleet-wide average emission of new vehicles since 2015 [24]. From 2021, this will be decreased to 95 g CO_2/km [24]. As part of the EU's 2030 climate and energy framework and contribution to the Paris Agreement, a binding target has been set to reduce emissions in the EU by at least 40%

below 1990 levels by 2030 [24]. Another target is related to the energy efficiency throughout the full energy chain. This is a headline target of at least 32.5% improvement in energy efficiency by 2030 [24]. To promote energy from renewable sources and to help the EU to meet its emission reduction commitments under the Paris Agreement, the EU has established the renewable energy directive (RED). The EU RED (2009/28/EC) has set mandatory national targets for gross final consumption and for the share of energy from renewable sources in transport. It sets a binding target of 20% gross energy consumption from renewable sources by 2020 [24]. To achieve this, each EU member state is required to have at least 10% of their transport fuels from renewable sources by 2020 [24]. In 2018, 9.5% of the primary energy consumption in the EU was attained by renewable energy, which continues to grow considerably more rapidly than any other form of energy [6]. In 2015, the increased deployment of renewables resulted in a €16 billion saving in fossil fuel imports and the reduction of GHG emissions by the equivalent of Italy's total emissions [25]. However, the transport sector contributed to only 6% of renewable energy in 2015. Hence, some EU members must maximise their efforts to attain the 10% binding target for transport by 2020 [25].

In December 2018, a new RED (2018/2001/EU), known as RED II, entered into force [24, 26]. The RED II sets a binding renewable energy target for the EU of at least 32% of final energy consumption by 2030, with a minimum of 14% of the energy consumed in road and rail transport as renewable energy [24, 26]. The RED II details sustainability and GHG emission minimum requirements that biofuels used in transport must comply with in order to be counted towards the transport target of 14%. Within the 14% transport target, there is a specific target for advanced biofuels. These biofuels must contribute at a minimum 0.2% of transport energy in 2022, 1% in 2025 and 3.5% by 2030 [24, 26]. Hence, biofuels that are economically and environmentally sustainable play an important role in the future transport. They are seen as immediate (but short-term) solutions to the decarbonisation of the transport sector. EU countries have to increase their biofuel usage in transport in order to maximise their ability to reach these targets. For example, blending biofuels with fossil fuels at higher concentrations can offer a route to increase the biofuel use in transport.

1.2 Motivation of the research

CO_2 is the principal greenhouse gas, attributing to 64% of anthropogenic global warming and 81% of total UK GHG emissions [24, 27]. In 2018, the UK saw some declines in

GHG and CO_2 emissions, primarily due to a change in the fuel mix for electricity generation [6, 27]. There has been a lower usage of coal and a higher deployment of the renewables [6, 27]. Figure 1.3 shows the latest estimates of CO_2 and GHG emissions in the UK between 1990 and 2018. GHG emissions are reported in CO_2 equivalent units. In the UK, between 2017 and 2018, the total GHG emissions have declined by 2.5% or 11.7 million tonnes (Mt), whereas CO_2 emissions have decreased by 2.4% or 9.1 Mt [27]. The highest share of 33% CO_2 emissions, at 121.4 Mt, was related to the transport sector in 2018 [27]. The majority of these emissions are attributed to road transport [27]. Since 1990, the total CO_2 emissions have decreased by 39% in the UK [27]. Nonetheless, CO_2 emissions from the transport sector have declined by less than 3.2% in the same amount of time [27]. Sadly, in 2018, total global carbon emissions increased by 2.0%, the fastest growth in the last 7 years [6]. Meanwhile, there was a 44% decline in GHG emissions in the UK between 1990 and 2018 [27]. This is less than half of the UK's 2050 commitment to decrease its emissions by a minimum of 100% from the levels of 1990 [28].

2018 UK greenhouse gas emissions are provisionally estimated to be lower than in 2017
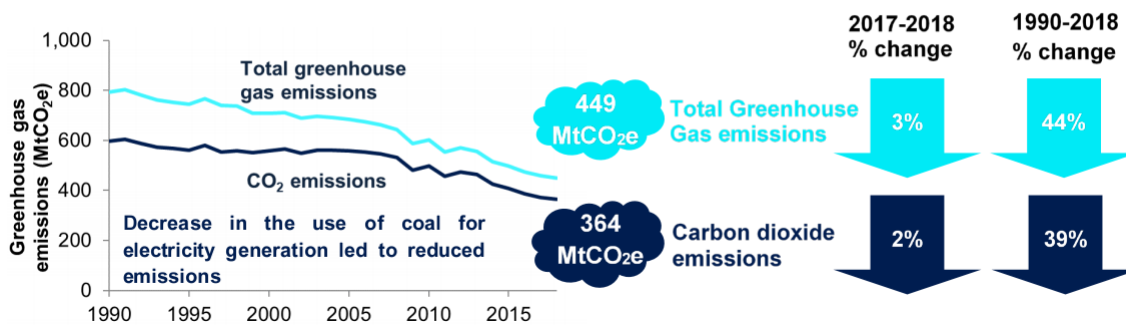
Figure 1.3: The provisional figures of GHG emissions and CO_2 emissions based on UK energy statistics between 1990 and 2018 [27].

This highlights that the current efforts to combat the GHG emissions are far from sufficient. The world requires practical and robust solutions to meet the needs of societies and governments, and to reinforce the response to the threat of climate change. Further research and development into innovative methods can improve their efficiencies and reduce emissions associated with the combustion processes of existing energy conversion devices in compliance with regulations. This can facilitate the development of low or zero-emission energy sources, which can provide energy security without environmental consequences. There are two potential areas of research that focus on both advances in combustion technology and alternative sources of energy.

Alternative fuels can be renewable and used either on their own or blended with the conventional petroleum-based fuels. They aim to reduce the dependency on the traditional fossil fuels in order to ensure the energy security and diversity. These fuels include both gaseous and liquid fuels such as synthetic fuels, hydrogen, natural gas and biofuels (e.g. bio-methanol, bio-ethanol and bio-butanol) among many others. Alternative fuels have the potential to provide carbon neutral or even carbon negative cycles. In addition, they seek to offer scalable demand and similar energy densities, as well as physical and chemical properties to fossil fuel. Subsequently, this will enable their direct use within the existing infrastructures. For example, the development of a hydrogen infrastructure is a main constraint of the rapid expansion of the hydrogen fuel cell vehicles. It is estimated to be in the range of several hundreds of billion dollars over several decades ($0.1-1.0 trillion for pipelines and $0.2 - 0.7 trillion for refuelling stations) to transport, store and deliver hydrogen to the end user [29].

At present, alternative fuels account for around 5% of total transport energy demand [8] and their share is expected to continue to increase [1, 2, 30]. They often have a chemical composition and structure that is considerably distinctive to the conventional fossil fuels, as well as different levels of unsaturation, oxygenation and substitution. Renewable energy can fuel transport demand directly with biofuels - substituting gasoline or diesel in ICE, or indirectly through the electrification of transport modes [13]. Biofuels are liquid or gaseous fuels derived from biomass [5, 31]. The EU renewable energy policy has been a driving force in increased deployment of biofuels, and their blending with conventional fossil fuels. They are believed to be one of the most promising and strategically important fuel sources in short-term solutions to increase the renewable energy usage, and to reduce carbon impact of the transport sector (when produced sustainably). The chemical compositions of biofuels usually differ from that of conventional fossil fuels. This, subsequently, may lead to substantially different combustion behaviours of these biofuels compared to that of fossil fuels. With the diverse choice of biofuels available, a profound understanding of the fundamental combustion processes and characteristics under various operating conditions is required. This can facilitate the optimisation of these combustion strategies and the implementation of advanced technologies. This in turn can help to meet the efficiency and emissions targets, as well as facilitate their commercialisation.

Advanced combustion technologies seek to improve or achieve a similar efficiency to existing technologies, while reducing the harmful emissions. There are increasing

industry trends towards downsized, boosted direct injection engines. These engines improve combustion efficiency by operating at a higher brake mean effective pressure, while reducing pumping, friction and heat losses. This is commonly achieved through intake air charging strategies (super- and turbo-charging), cam phasing devices, plasma assisted devices and cooled external exhaust gas recirculation (EGR) [32]. Proposed advanced technologies include homogeneous charge compression ignition (HCCI), reactivity controlled compression ignition (RCCI), gasoline compression ignition (GCI), premixed charge compression ignition (PCCI) and their variants. These technologies usually tend to operate at fuel lean equivalence ratios (with premixed reactants) and at high pressures and low temperatures. This can impact multiple fundamental parameters and impose stability, safety and control problems [33]. These issues arise partly due to uncertainties in low temperature chemistry. Moreover, there is an increased likelihood and effect of abnormal combustion phenomena such as knock or misfiring in ICE, or flashback and early ignition events in these engines [34]. Hence, it is of paramount importance to gain understanding of these factors and the effects of their interaction.

1.3 Focus of the research

This research seeks to understand the role and the effects of some of the key fundamental combustion properties (in particular ignition delay time, excitation time and heat release), and their interaction in combustion and ignition processes. It also seeks to understand the chemistry that drives these processes for different fuels at conditions relevant to advanced combustion strategies. It is of particular interest to see how alcohol fuel with Arrhenius-type behaviour will impact the ignition delay time (total, first- and second- stage), heat release profile and excitation time of the blend, under various blending ratios with fuels that exhibit NTC behaviour (e.g. gasoline).

Auto-ignition is one of the principal fundamental combustion characteristics that influences the performance of practical combustion devices. Auto-ignition can be defined as the spontaneous exothermic heat release from the oxidation of the fuel - the onset of self-sustained combustion of the mixture - in the absence of an external source of ignition, such as a spark or flame. In practice, the fuel/air mixture is non-uniformly dispersed and auto-ignition first appears at apparent "*hot spots*" after a characteristic ignition delay time, τ_i. Ignition by hot spot consists of three almost subsequent phases - induction, excitation and propagation. The induction phase is primarily controlled by chemical kinetics, diffusion and heat conduction when ignition delays are sufficiently long. During this

phase the elevated temperature in the hot spot generates a radical pool that leads to ignition. It is followed by the excitation phase, or *excitation time*, τ_e, during which the hot spot ignites. This is governed by chemical kinetics and gas dynamic processes. During this time the exothermic chemical reactions accelerate, and rapidly deposit thermal energy in the centre. The exothermic power, or rate of chemical energy release, evolves until the reactants are depleted, then declines as the remaining chemical energy is dissipated. The excitation time can be defined by the growth of the power pulse, which is measured from the beginning of the heat release to the point of the maximum power. Lastly, the flame front propagation proceeds, which is mostly controlled by chemical kinetics and transport processes [35, 36].

Knock is an abnormal and stochastic combustion phenomenon which limits the performance of spark ignition (SI) engines. In SI engines, fuel and air are pre-mixed and compressed, and a chemical energy release occurs in the form of a growing turbulent flame which is introduced by an electrical spark. The temperature and pressure in the unburned mixture ahead of the propagating flame front (the end gas) rise as combustion proceeds. Even in the case of premixed fuel and air, the mixture is never truly completely homogeneous. This is mainly due to the turbulent premixing of hot gases in the combustion chamber with the fresh air, which causes hot spots to prevail. Changes in the thermodynamic conditions of pressure and temperature history, together with the anti-knock quality of the fuel, promote auto-ignition - accumulated around one or numerous hot spots. A significant proportion of the chemical energy embodied in the end gas may be rapidly released by auto-ignition. This causes a sharp pressure rise and standing pressure waves inside the cylinder. The term knock refers to the arising sound caused by the vibration of the engine. High intensity knock can have a detrimental impact on the engine and cause severe damages, as demonstrated in Figure 1.4. Therefore, a key operating principle in SI engines is to avoid knock [37, 38].

SI engine design has progressively advanced towards turbocharging and downsizing concepts, with increased compression ratio, in pursuit of enhanced efficiency and lower pollutant emissions. The increase in compression ratio leads to larger pressure and temperature in the end gas. Hence, there is a stronger possibility of engine knock. Indeed, one of the key challenges in combustion is the trade-off between fuel efficiency and knock mitigation. Despite the selection of engine operating conditions to expressly avoid knock in existing technologies, super-knock events are sometimes observed. Super-knock is an extremely high intensity knock which is a manifestation of a developing detonation. Here

the pressure wave generated by the auto-ignition is reinforced by the reaction front. It limits the scope for turbocharging and therefore downsizing [37, 38].
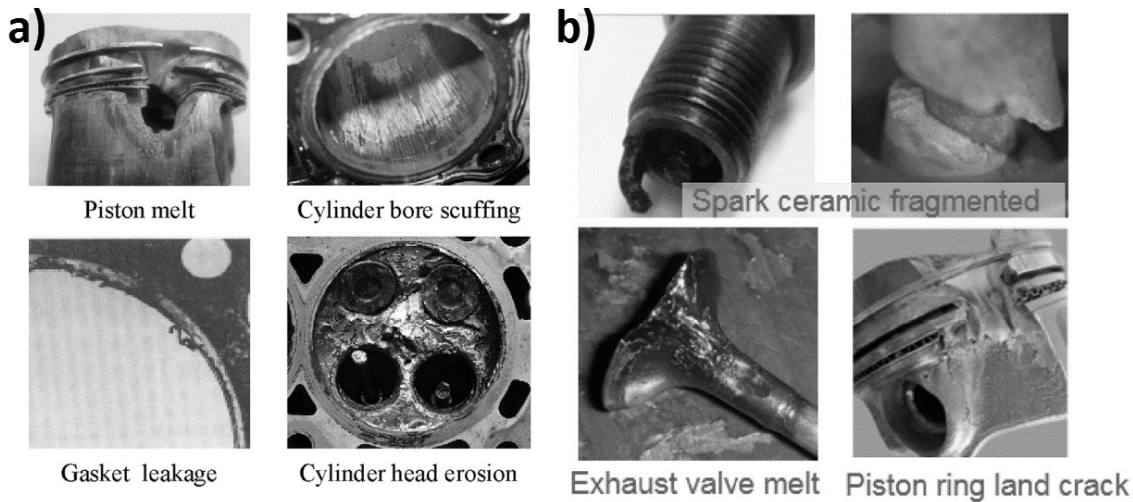
Figure 1.4: Typical damage caused by a) conventional engine knock and b) super-knock [39].

Characterisation of auto-ignition phenomena is vital for the assessment and potential prediction of the transition from harmless auto-ignition to undesirable knocking combustion. It is a prerequisite in the implementation and development of SI technologies. Under controlled conditions, auto-ignition can be helpful, dispensing with spark ignition. This is due to the fact that it offers additional energy for the power stroke of the compression ignition (CI) engine cycle. Moreover, the auto-ignition event itself necessitates detailed research. Engine knock is a result of an auto-ignition in the end gas, but not each auto-ignition event causes engine knock. Also, the auto-ignition phenomena can present a severe hazard. It was considered as a possible cause of the tragedy on the Piper Alpha oil platform in 1988. Owing to their combustible characteristics, there is a serious risk associated with storing large quantities of fuel at high temperature with exposure to the oxidising atmosphere. Clearly, the study of auto-ignition is essential for the prevention and mitigation of auto-ignition in fuel storage facilities, chemical plants, refineries and transport.

With practical engine systems, there are two typical categories of hydrocarbon fuels based on their ignition characteristics. In the first category are those that exhibit Arrhenius-type behaviour, where τ_i decreases exponentially with an increase in temperature. These types of fuels, such as aromatics and alcohols, portray a single-stage auto-ignition behaviour. In the second category are those that do not exhibit Arrhenius-type behaviour and display

two-stage auto-ignition, such as *n*-paraffins, *iso*-paraffins and *cyclo*-paraffins. A two-stage auto-ignition usually occurs at low temperature conditions below 850 K. The negative temperature coefficient (NTC) region of total ignition delay time stretches over this low temperature region. The NTC is the region where τ_i does not decrease exponentially, and can even increase in magnitude with an increase in the temperature. There have been few studies that looked at blends of these two fuel types (such as [40-43]) to explore the influence of blending an Arrhenius-type fuel with a fuel that has an NTC. However, this research is important due to the need to blend increased amounts of biofuels (e.g. alcohols) with traditional gasoline (which exhibits NTC behaviour). Hence, this motivates the research carried out in this thesis.

The two-stage auto-ignition of paraffinic fuels is primarily controlled and affected by the heat release from the first-stage auto-ignition, and intermediate species created. After a first-stage ignition, a low-temperature heat release (LTHR) stage in a "*cool flame*" is followed by the main heat release - a high temperature heat release (HTHR) stage. The LTHR is an essential parameter that affects auto-ignition delay time, while the HTHR is a critical parameter in determining the excitation time. Consequently, the HTHR is an important parameter in the uncontrolled auto-ignition during the active ignition process, e.g. knock, pre-ignition, detonation and super-knock. In advanced technologies, where engine processes are controlled by the kinetics of the fuel (such as in HCCI), combustion is most likely occur in two stages. A better understanding of these combustion phenomenon and their interaction is fundamental in the control of combustion phasing and the extension of the HCCI operating range, as well as the development towards optimal fuel economy and lower emissions [44].

1.4   Aims and objectives

Various auto-ignition behaviours are apparent at conditions that are relevant to practical combustion systems. These are strongly dependent on the unburned thermodynamic state and fuel composition. A detailed understanding of the ignition behaviour of hydrocarbon fuels, as well as the effects of the addition of an oxygenated constituent on key fundamental parameters (i.e. ignition delay time, heat release and excitation time) is crucial to the advancement of combustion technologies. In these technologies, inhomogeneous behaviours and instances of abnormal combustion behaviour are prevalent. The present study concentrates on the properties of methane, *n*-butanol, toluene

reference fuel (TRF) and *n*-butanol/TRF blends using experiments in a rapid compression machine (RCM) and numerical modelling.

This work aims to investigate the ignition behaviour of fuels relative to their constituents. Also, the role of the addition of an oxygenated compound within non-Arrhenius type fuels is studied in terms of key fundamental properties of the combustion processes. The predictive accuracy of well-developed chemical kinetic mechanisms in modelling auto-ignition delay time is also scrutinised.

Therefore, the objectives of this research are:

1. To provide novel data on the excitation times of methane, *n*-butanol, TRF and *n*-butanol/TRF blends.

2. To present experimental measurements of ignition delay times of *n*-butanol/TRF and *n*-butanol/gasoline mixtures at various blending ratios which could aid the development of chemical kinetic mechanisms.

3. To assess the ability of proposed surrogate fuel in representing the auto-ignition response of real gasoline fuels at various blending ratios.

4. To assess accuracy and reliability of the experimental measurements in an RCM.

5. To evaluate the performance of chemical kinetic mechanisms in the modelling of ignition delay times at various blending ratios.

6. To conduct a heat release rate analysis of the collected experimental data to derive the chemical exothermicity for a range of fuels.

7. To assess the predictive capability of the chemical kinetic mechanism in modelling heat release data.

8. To investigate the role and impacts of the heat release rate in the cool flame and main heat release stages, in terms of the ignition behaviour of fuels and the conditions that could lead to abnormal combustion processes.

9. To assess the chemistry controlling auto-ignition behaviour. To determine the main reactions which influence ignition delay times, excitation time and heat release rates at low-temperature conditions for different fuels particularly with respect to the blending ratios of an oxygenated additive.

10. To gain a deeper understanding of the factors that drive abnormal ignition events, such as knock, super-knock, deflagration and developing detonation.

1.5   Thesis structure

Chapter 2 provides a literature review and a crucial content of the research. It presents the background knowledge of the combustion processes, abnormal combustion behaviour, knocking combustion, alternative fuels, combustion chemistry, numerical modelling, and key experimental approaches to study auto-ignition.

Chapter 3 details the experimental facility, equipment and operating procedures used to collect the experimental ignition delays reported in this work, as well as sources of uncertainties and errors. The approach used to model the ignition delay times, excitation times and to assess the controlling chemistry is presented here. Details on the detonation theory are provided in this Chapter. Also, the heat release analysis is detailed here.

Chapter 4 presents results of a computational investigation into the auto-ignition behaviour of a methane - a relatively simple fuel which is known to have good anti-knock qualities. Ignition delay times and excitation times for stoichiometric methane/air mixtures are modelled using a comprehensive chemical kinetic scheme within a pressure range of 0.1 and 10 MPa, and a temperature range of 700 and 1670 K. To determine the main reactions that effect ignition delays and excitation times, brute-force local sensitivity analyses are performed at the four temperatures and the two pressures of 0.1 MPa and 10 MPa.

Chapter 5 investigates the impacts of the addition of n-butanol to conventional gasoline and its TRF surrogate fuel at different blending ratios (10%, 20%, 40% and 85% vol n-butanol). In particular, the study investigates the ignition delay times in a Rapid Compression Machine (RCM), through experimental measurements and numerical modelling for the low temperature region 678-916 K at a pressure of 2 MPa under stoichiometric conditions. The performance of a detailed chemical kinetic scheme in representing the auto-ignition behaviour of studied blends is assessed. Through the use of a brute-force sensitivity analysis, the chemistry controlling the auto-ignition of the n-butanol/TRF blends is investigated to determine the main reactions which influence τ_i at selected conditions and blending ratios.

Chapter 6 further analyses the acquired experimental data by assessing the preliminary exothermicity of n-butanol/TRF blends studied in Chapter 5. It investigates the effects of

n-butanol addition on the low temperature heat release (LTHR), accumulated heat release (aHR), intermediate heat release (ITHR) and high temperature heat release (HTHR) of the blends through brute-force sensitivity analyses. The excitation times of *n*-butanol, toluene reference fuel (TRF) and *n*-butanol/TRF blends are reported here. The effects of *n*-butanol addition to TRF on excitation times are assessed. Also, this study further investigates the conditions that lead to knock, super-knock and different auto-ignition modes.

Chapter 7 concludes the key research findings and contributions of this research, and giving suggestions for future research.

2. Background and literature review

This chapter provides background information and reviews existing knowledge governing auto-ignition phenomena and associated processes. It describes the processes occurring during knocking combustion, and introduces theory of hot spot auto-ignition and developing detonation. An overview of experimental techniques available to study auto-ignition phenomena is presented. The chemistry governing auto-ignition phenomena at different temperatures for alkanes and alcohols is also discussed, along with the modelling approaches and methods for the kinetic model assessment. Finally, a brief discussion of alternative fuels and the recent progress in ignition studies of butanol is given in this chapter.

2.1 Auto-ignition and knocking combustion

A detailed understanding of the auto-ignition in the end gas is a prerequisite in controlling, reducing, and eliminating the engine knock and its associated limitations on advancement of practical combustion technologies. Hence, one of the core aims of this research is to gain an improved understanding of auto-ignition phenomena and associated processes. The auto-ignition phenomenon is a spontaneous self-ignition of a fuel-air mixture due to increases in local pressures and temperatures through compression in engines, or through compression in a shock wave created ahead of a propagating flame at high flame speeds [45]. It is a physico-chemical phenomenon, as a result of thermal feedback and chemical chain branching, rendering an auto-acceleration of the overall reaction rate, amplified by the exothermicity of the reaction, which is apparent at both low and high temperatures. First slow thermal reactions with a substantial chain-branching constituent enhance oxidation, subsequently leading to an increase in radical concentrations and increasing reaction rates that ultimately manifest in a rapid explosive surge in oxidation rate and temperature – hence ignition. Having strong dependence on temperature and pressure, these reactions transform the chemical energy into heat and a relatively small proportion of light energy. The heat released consequently raises the temperature of the overall system resulting in a complex interaction between positive and negative loops that define the time of ignition event, the ignition delay time [46]. The tendency of a fuel air mixture to auto-ignite is generally assessed by this property and it is commonly used as a proxy for the knocking potential of a fuel, which can significantly impact the combustion cycle of reciprocating engines. A pictured example of homogeneous auto-ignition of *iso*-octane

and associated pressure time-history for the definition of ignition delay time is provided in Figure 2.1.
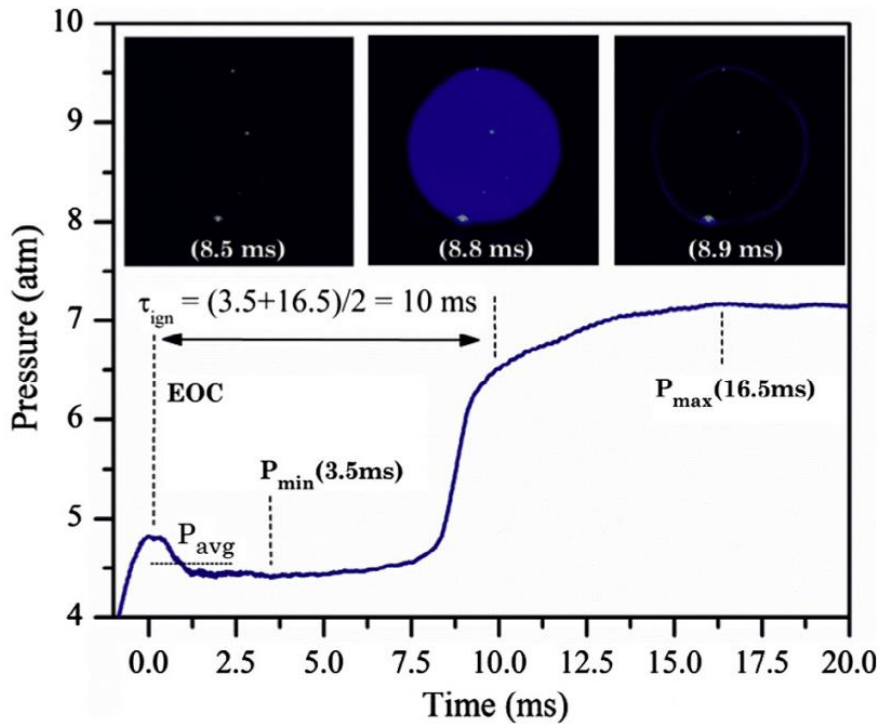
Figure 2.1: A typical experimental pressure time history during homogeneous ignition, for *iso*-octane at P=0.46 MPa, T=1035 K, φ=0.25; where τ_{ign} is the ignition delay time. Three frames illustrate uniform chemiluminescence during auto-ignition [33].

2.1.1 Spark ignition engine operation

The four stroke Otto cycle of an SI engine includes an induction, compression, power and exhaust stroke, with each stroke consisting of 180° of crank angle. Figure 2.2 illustrates the steps of the basic four stroke cycle. During the induction stroke (Figure 2.2 (a)), the fuel-air mixture is drawn into the cylinder as the piston travels from top dead centre (TDC) to bottom dead centre (BDC). The compression stroke (Figure 2.2 (b)) compresses the fuel-air mixture to high temperatures and pressures, as the piston travels back to TDC. Near the end of this stroke, before the piston reaches the TDC the spark plug ignites the mixture and initiates the combustion within the chamber (Figure 2.2 (c)). The spark ignited flame expands and propagates through the volume of the combustion chamber in a controlled fashion, significantly increasing temperature and consequently peak pressure, which provides the force required to drive the piston down during the power stroke (Figure 2.2 (d)). This is the stroke which causes the piston to drive the engine. At the end of power stroke, the exhaust valve is opened and exhaust blowdown takes place (Figure 2.2 (e)). During the exhaust stroke (Figure 2.2 (f)) the piston travels from BDC

16

to TDC, forcing the remaining burned or partially oxidised gases out of the chamber. The exhaust valve closes as the piston reaches TDC and the intake valve starts to open so that next cycle advances [47].
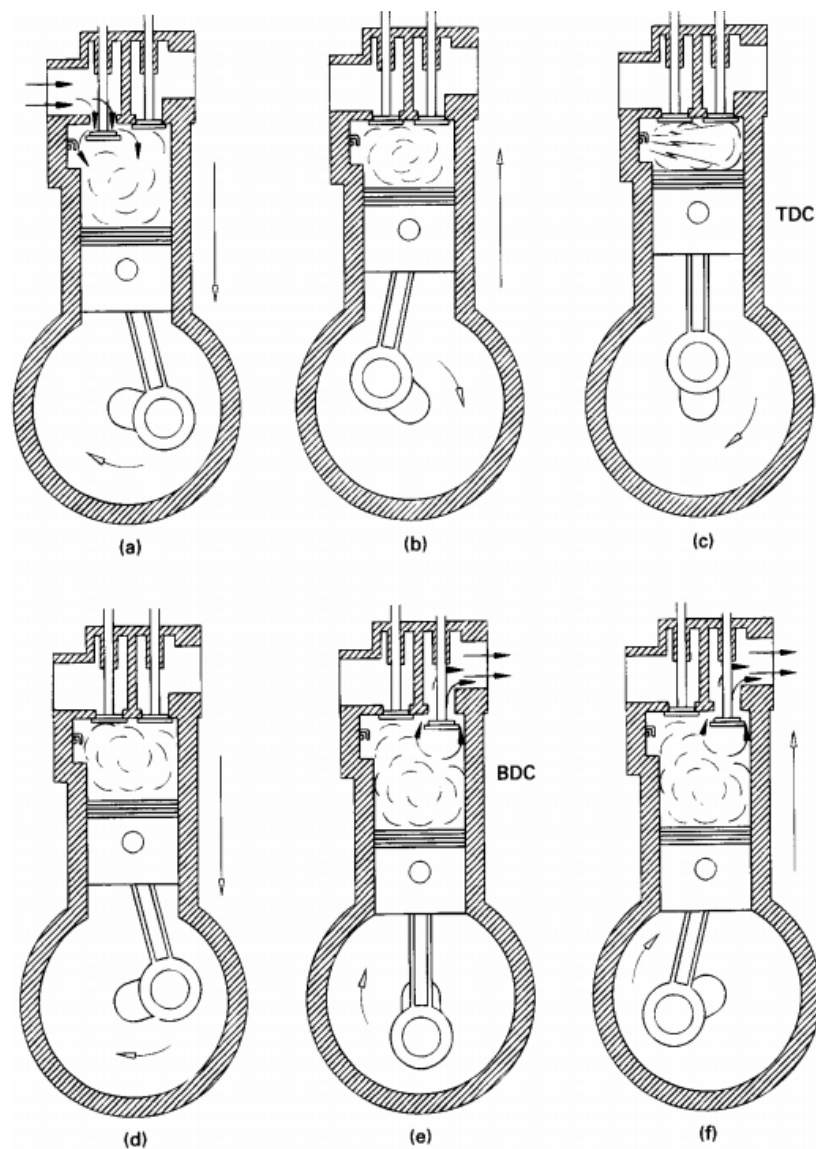
Figure 2.2: Four stroke SI engine operating cycle. (a) Induction stroke, (b) compression stroke, (c) combustion at almost constant volume near TDC, (d) power stroke, (e) exhaust blowdown when exhaust valve opens towards the end of power stroke, (f) exhaust stroke [47].

Under normal, non-knocking operation, the end gas is consumed in a controlled fashion by the flame front before auto-ignition can take place, with the combustion processes mainly governed by the chemical kinetics of the oxidation. Nevertheless, the propagating turbulent flame originated by the spark plug imparts further compression and heating on the end gas, which can potentially cause auto-ignition of the mixture and ignition prior to

17

the arrival of the flame front, leading to a rapid increase of the in-cylinder pressure and extremely localised temperatures [48]. The fuel-air mixture combusts rapidly releasing energy (between 5 to 25 times faster than during normal combustion), causing large and high amplitude pressure waves [49]. These pressure waves cause high frequency oscillations of the in-cylinder pressure, subsequently creating a sharp sound, like metallic ringing – knock [48]. Figure 2.3 illustrates high-speed images and representative in-cylinde pressure traces comparing normal and knocking cycles.
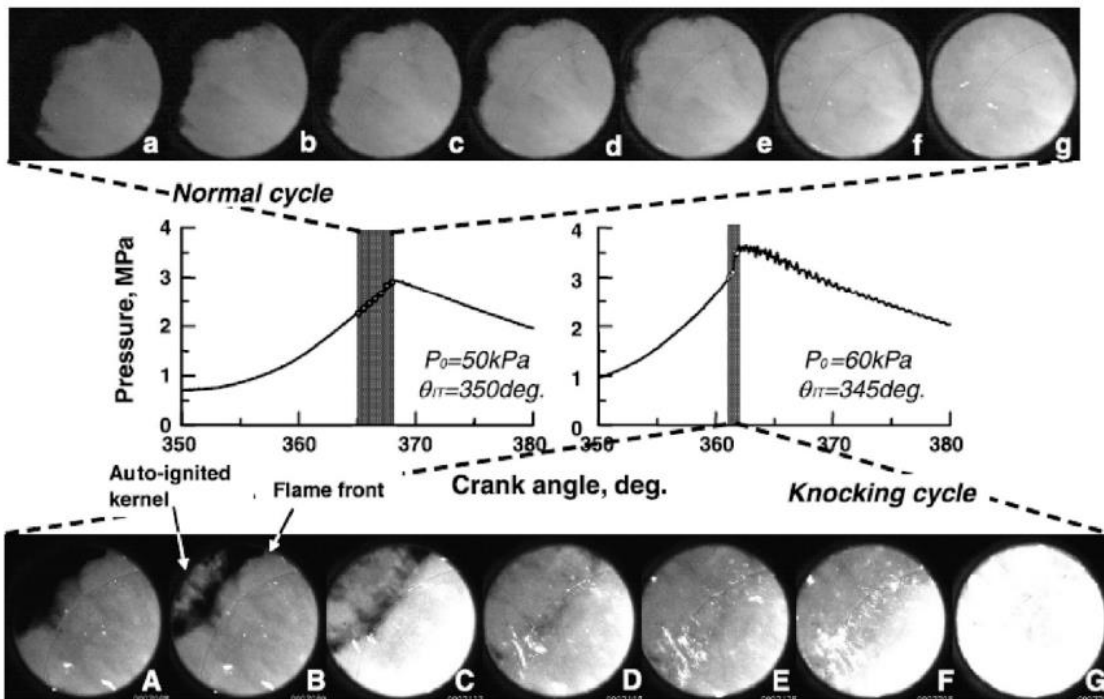
Figure 2.3: Series of high-speed direct images and representative in-cylinde pressure traces for normal and knocking cycles [39].

The events of knocking combustion reflect the competition between the time for the complete consumption of the reactants by the propagating flame, and the time of pre-combustion reactions of the end gas auto-ignition to occur, i.e. the ignition delay time. Knocking, therefore, would not take place if the flame front uses up the entire mixture before the pre-combustion reactions attain the end gas auto-ignition. Fuels with longer ignition delay times can withstand auto-ignition and survive the additional compression and heating by the propagating spark ignited flame. Auto-ignition may occur within the end gas in the cylinder, leading to the substantial increase in the chamber pressure, which

18

subsequently excites an acoustic resonance between the gas in the cylinder and the engine block [48]. This causes enormous exothermic oxidation with temperature jumps of more than 1000 K [48]. The combination of high temperatures and pressures degrades the material, and thus engine knock can lead to piston crown melting, piston ring sticking, cylinder bore scuffing, piston ring-land cracking, cylinder head gasket leakage and cylinder erosion [39]. Knocking incidence depends on many factors including the design of combustion chamber, the equivalence ratio, the fuel chemical composition, the intake pressure and the intake temperature [50].

2.1.2   Fuel rating

Fuels in SI engines are therefore designed to resist auto-ignition under engine operating conditions until the spark. The current standard for fuel quality testing in SI engine is to measure the octane rating using a Cooperative Fuel Research (CFR) engine [51]. Octane numbers (ON) are used to describe the fuel knock propensity. This rating system has been adopted for gasoline fuels since the 1920s [45]. The higher the ON, the longer the ignition delay time, and the higher the fuel resistance to auto-ignition (see Figure 2.4). The ON is defined as the percentage by volume of *iso*-octane blended with *n*-heptane in the Primary Reference Fuel (PRF), that gives rise to engine knock in the research method or motor method with CFR engines under the same conditions as the actual fuel [52]. During the measurements various blends of PRF are tested until the knock behaviour of the test fuel is replicated. The Research Octane Number (RON) tests fuel performance under low severity engine operation at an engine speed of 600 rpm and a temperature of 325 K, while Motor Octane Number (MON) replicates engine operation conditions of 900 rpm and 422 K [53]. RON is generally higher than MON for most non-PRF fuels. To quantify these differences between RON and MON, the fuel sensitivity (*S*) is commonly used, which is related to how the chemical reactivity of the fuel changes with temperature and pressure. Larger *S* values indicate that the fuel has auto-ignition characteristics that are more sensitive to operating conditions [54] and is defined as :

$$S = RON - MON \qquad\qquad (2.1)$$
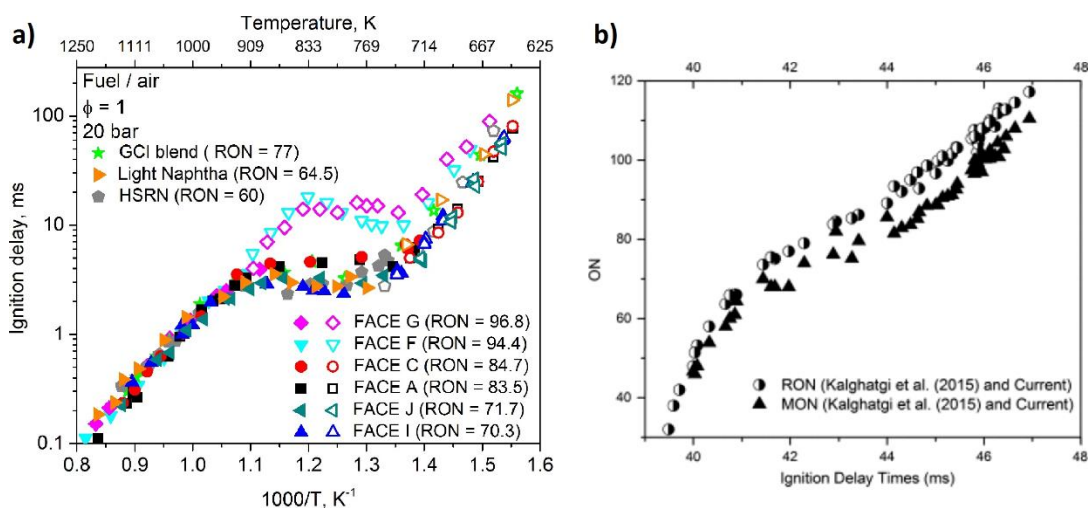
Figure 2.4: Dependence of ignition delay times on octane numbers. a) Experimental data for various fuels from shock tubes, RCMs and CFR engines. Figure adopted from [55]. b) Calculated ignition delay times taken from [53]. Fuels with higher octane numbers tend to exhibit longer ignition delay times.

Iso-octane (RON 100) and *n*-heptane (RON 0) have been selected as reference fuels for the octane rating scale because of their distinctly different reactivity during oxidation and their similar physical properties (such as vapour pressure and viscosity). In real life, gasoline is made up of only approximately 5% *iso*-octane and 0.3% *n*-heptane. Therefore, using these fuels to characterise gasoline may not be representative, in particular when an increasing use of alternative fuels substantially alters the fuel chemical composition for SI engines compared to that when octane rating was developed [52, 56]. The octane rating of conventional gasoline can be enhanced by blending it with oxygenated fuels (e.g. ethanol or butanol), which have higher anti-knock properties [57]. However, the effects of these oxygenated compounds on the auto-ignition behaviour is not fully understood. Hence, the effects the addition of *n*-butanol to gasoline and its representative surrogate mixture on auto-ignition behaviour of the mixture are studied in Chapter 5. Meanwhile, in-cylinder conditions under which knock takes place, such as engine temperatures, pressures, and mixture strengths can considerably differ from those in the CFR tests with the adoption of modern engine technologies, and hence RON and MON values are an insufficient guide to the practical performance of engines and description of anti-knock qualities of the fuels [52]. In order to cover the whole operating range, the octane index (OI) was developed that provides the rating of the PRF that only causes knocking under the same conditions as the tested fuel [52] and is defined as:

$$OI = K * MON + (1 - K) * RON \qquad\qquad (2.2)$$

where K is an empirical constant, which depends only on the pressure and temperature history of the unburned mixture in the chamber and is supposed to be independent of fuel properties and show the relevance of RON and MON tests. For RON tests, the K index is 0 and K is 1 in the MON test. When K=0.5 for the fuel, the average of the RON and the MON value, is a good indicator of anti-knocking qualities of the fuel [58]. The development of engine designs (such as those using advanced cooling systems, boost systems, and injection systems) have led to decreases in K values [58]. K is often found to be negative in turbocharged direct injection SI engines and varies substantially with operating conditions [56]. There is a good correlation for K with unburned gas temperature. Figure 2.5 illustrates data on K against T_{comp15} (unburned gas temperature at a compression pressure of 15 bar) from various studies (adopted from [39]). It shows that at 15 bar, values for K decreased from 6 at 1000 K to 0 at 700-800 K, down to -2.5 at 500 K.
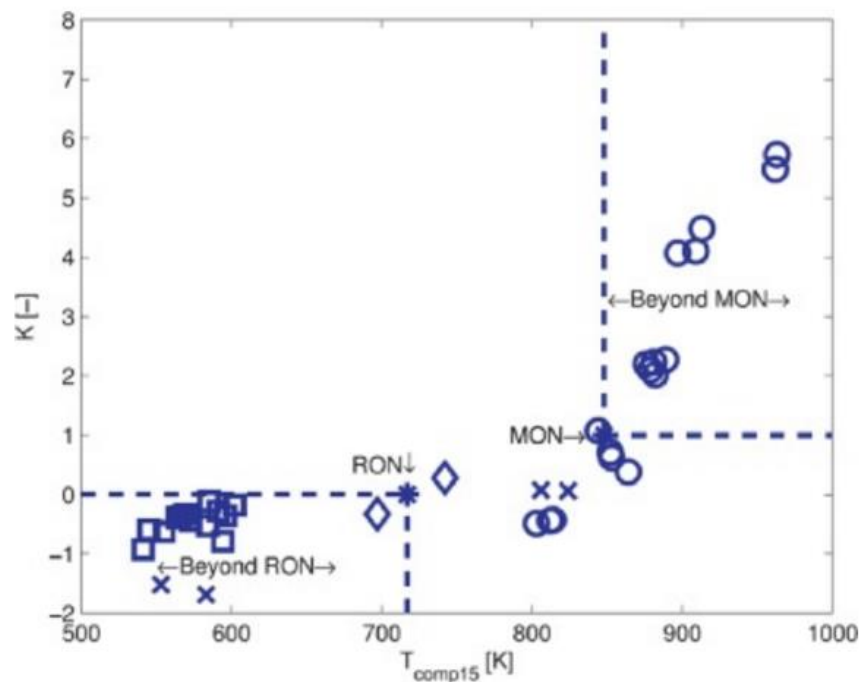
Figure 2.5: K against T_{comp15} (unburned gas temperature at a compression pressure of 15 bar). Symbols illustrate different studies. Adopted from [39].

Applying ON to modern SI technologies requires therefore extrapolation of the conventional ON to predict the fuel's anti-knock quality. The relevance of such extrapolation is debatable. For example, for negative K values at a given RON, fuels with

21

greater S have better anti-knock properties. Thus an increase in RON or MON values does not ultimately manifest in improved knock resistance, and operating conditions for modern engines tend to exceed the boundary defined by the operating conditions of CFR tests [38, 58]. The OI, in attempting to characterise the knocking propensity, is in fact just an indicator of the auto-ignition potential [57]. This is inversely proportional to the ignition delay time of the fuel, the principle combustion characteristic, which would provide a more accurate description of auto-ignition phenomenon and can be measured directly as a function of the pressure and temperature profiles over time [52]. Therefore, it is important to obtain ignition delay times measurements for various fuel mixtures over a wide range of conditions. This motivates the research carried out in Chapter 5. In spite of all these deficiencies, automotive and oil industries continue to use RON and MON as primary parameters in describing auto-ignition.

2.1.3   Compression ignition engine operation

CI engines on the other hand depend on auto-ignition to combust the fuel. Diesel engines compress air to elevated pressures and temperatures, and then inject vaporised fuel into combustion chamber at the end of the compression stroke to initiate the combustion processes via auto-ignition. The auto-ignition tendency of a CI fuel is defined in terms of the ignition delay time which depicts cetane number. The cetane number is obtained in a Waukesha CFR engine with a pre-combustion chamber and adjustable compression ratio (CR), as the relationship between the ignition delay time and ratio of cetane and alpha-methylnaphthalene. Higher cetane numbers imply shorter ignition delay times and stronger auto-ignition tendencies, thus better CI performance because shorter ignition delay times provide more time for combustion within a cycle [59]. Since only air is compressed rather than an air-fuel mixture, diesel engines are not affected by pre-ignition problems associated with high compression SI engines, thus enabling higher attainable CR. Higher CRs are desirable because the effective thermal efficiency of the engines increases with CR. CRs are, on the other hand, restrained by their upper limit due to knocking combustion, since at high CR the attainable pressures and temperatures are higher at the end of the compression stroke. This subsequently promotes the likelihood of auto-ignition in the end gas. The higher values CR of CI engines necessitate stronger and heavier engine components and slower engine speeds, consequently increasing maintenance requirements and costs. Diesel CI engines have higher thermodynamic cycle efficiency compared to SI engines, because they operate on lean mixtures, lack the

throttling of the intake charge and have higher compression ratios (CI CR: 16-18; versus SI CR 9-11).

CI engines are a popular choice in heavy duty vehicles and other commercial applications due to their high efficiency and durability. These engines are larger and heavier compared to those used in passenger vehicles, hence they have to operate at lower speeds, where knock is more prevalent due to the longer time available for auto-ignition. Auto-ignition at low engine speeds takes place earlier because of the availability of sufficient time for chemical reactions to occur at low temperatures and because of the presence of substantial amounts of unburned amount of mixture in the zone of the end gas, which promotes strong knock. An increase in the engine speed causes higher turbulence intensities of the mixture within the chamber, thereby raising the propagation speed of the flame front, decreasing the duration of combustion and decreasing likelihood of knocking [48]. Also, the efficiency of SI engines at low loads is especially low due to increased pumping losses since they operate at fixed air-to-fuel ratio and use throttle to decrease the amount of intake air. Throttling increases the pumping work under low loads and therefore decreases the efficiency. Pumping losses are also greater in SI engines compared to CI engines since they compress the fuel-air mixture rather than only air before heat release [14]. This makes SI engine technology less attractive for heavy duty vehicle applications compared to CI engines. Nonetheless, the major disadvantage of diesel engines is their emission of air pollutants, specifically particulate matter (PM) and nitrogen oxides (NOx), whereas SI engines are able to control tailpipe emissions effectively through three-way catalysts [14]. In diesel engine soot is found in the fuel rich zones and NOx in the hot stoichiometric zones, which makes it challenging to cut down both PM and NOx emissions at the same time through combustion improvement technologies. To control PM and NOx emissions, modern diesel engines use high pressure fuel injection and complex after-treatment systems that consequently make these technologies substantially more expensive compared to SI engines. Moreover, in theory, when comparing ideal cycle efficiencies, the Otto cycle has always higher efficiency and higher work area compared to the diesel cycle at the same CRs, since in the diesel cycle the isentropic compression ratio is greater than the isentropic expansion ratio, while in the Otto cycle they are equal. CI engines only become more attractive than petrol engines because of throttling losses and the knock limitations on CR. Hence, knocking combustion in SI is a major limitation of implementation and development of these technologies.

2.1.4 Advanced engine technologies

While there are various strategies and concepts present for engine advancement to attain better efficiencies, engine downsizing coupled with high boosted direct injection technologies is a mainstream industry trend. It provides enhanced power density (increased power ratio per unit space) and reduced fuel consumption by operating at a higher specific output for the same torque at a given engine speed, and reduced pumping and frictional losses [32]. Engine downsizing uses smaller engines in the car that give the power of larger engines through the implementation of advanced technologies. This concept is associated with number of benefits such as 1) reduction in CO_2 and NOx emissions due to the reduced fuel consumption through the optimisation of the intake and exhaust valve timing at low engine speeds with scavenging that subsequently leads to reduced residual gas content within the cylinder; 2) decrease in the engine weight and thus the load on the engine; 3) the smaller swept volume by the piston results in decrease in friction between the piston and the engine bore, thus reduced frictional losses [60].

The performance of downsized engines is maintained by injecting more air into the combustion chamber to combust additional fuel through supercharging, where an air-charging device is driven mechanically, or by turbocharging technologies (where the device is driven by the exhaust gases). The higher the air pressure or charge density, the greater the amount of air and oxygen that can be supplied to the combustion chamber, and hence the greater the amount of fuel that is burned. Turbocharging or supercharging achieves lower NOx emissions because these devices decrease the total amount of fuel in fuel-air mixture, burning leaner mixtures at lower flame temperatures at the expense of decreased power output [61]. This can be compensated by increased air charge density [61]. In boosted direct injection (DI) systems, a fuel injector diffuses atomised fuel directly into the combustion chamber of each cylinder, rather than the pre-combustion chamber of traditional gasoline engines. Coupled with computer management systems, DI enables more precise control over the amount of fuel injected and its timing over the engine map for any given flywheel torque, so that the throttle is wider open, thus resulting in reduced pumping losses [60].

According to Alriksson and Denbratt [62] research, to escape high NO emissions at low equivalence ratios, the combustion should take place at temperatures below approximately 2200 K. At high equivalence ratios, the temperature is required to decrease even further to avert extremely heavy soot formation. Both high soot and NO emissions are prevented if the temperature is kept below approximately 1650 K, regardless of the

equivalence ratio value. This concept is known as low temperature combustion (LTC) [63]. Moreover, it was also suggested that CO to CO_2 oxidation becomes low below 1400 K [63]. According to the LTC concept, the most of the energy released while avoiding excessively high soot, NO_x, and CO/UHC formation zones is indicated by the yellow cloud in the φ-T map in Figure 2.6
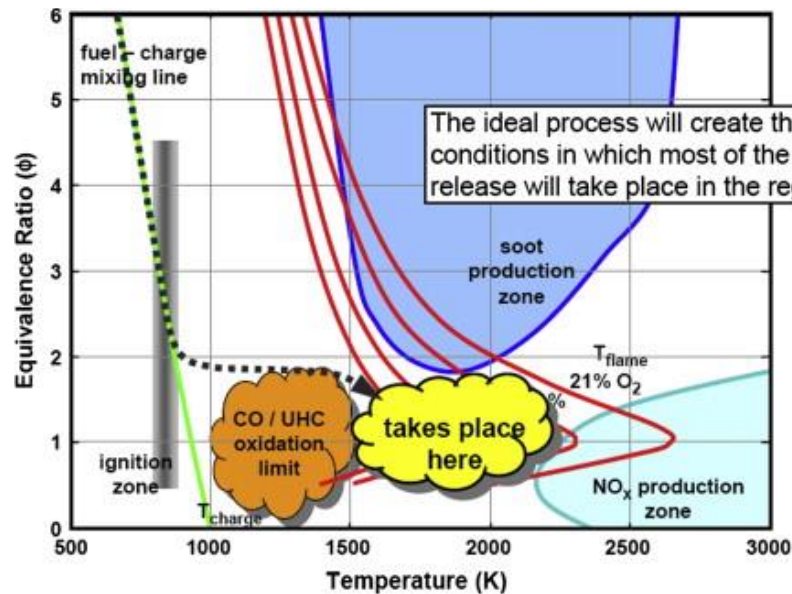
Figure 2.6: Regions of high soot, NO_x and CO/UHC production zones. Optimum conditions for lower emissions according to the low temperature combustion concept are indicated by the yellow cloud. Replicated from [63].

The knocking in these new technologies is an obstacle for engine designers, which prevents engines from attaining optimised combustion phasing and higher CRs, in particular in low speed, high-load operating regimes. A new form of abnormal combustion, which is commonly apparent at low engine speeds, called super-knock, has become a challenge in these technologies [39]. Such a phenomena differs from conventional knock, in which the end gas auto-ignites ahead of the spark-ignited propagating flame front, because the pressure and temperature of the unburned mixture are tremendously amplified by the compression effect due to thermal expansion of the burned zone (that potentially can overlap the moving piston) [64]. Rapid compression machine (RCM) experiments [33, 44, 65] have shown that the super-knock mechanism can be expressed by hot spot induced deflagration to detonation transition, succeeded by high pressure oscillation. Figure 2.7 illustrates the comparisons of typical pressure traces and heat release rates of a normal combustion, a conventional knock cycle and a super-knock cycle. The major discrepency between super-knock and conventional knock is an

amplitude of the maximum pressure rise at knock onset. For super-knock, an amplitude of the maximum pressure rise (Δp) is more than an order of magnitude higher compared to that of conventional knock [39]. Super-knock events appear sporadically and show little direct relationship to engine control parameters, and hence the common knock mitigation methods, such as retarding spark timing, enriching mixture, cooling intake charge, and enhancing heat transfer would be deficient in suppressing super-knock [65]. Hence, super-knock is the serious barrier for further advancing the boost level of turbocharged SI engines.

a) Three typical combustion pressures traces   b) continuous engine cycles with random super-knock
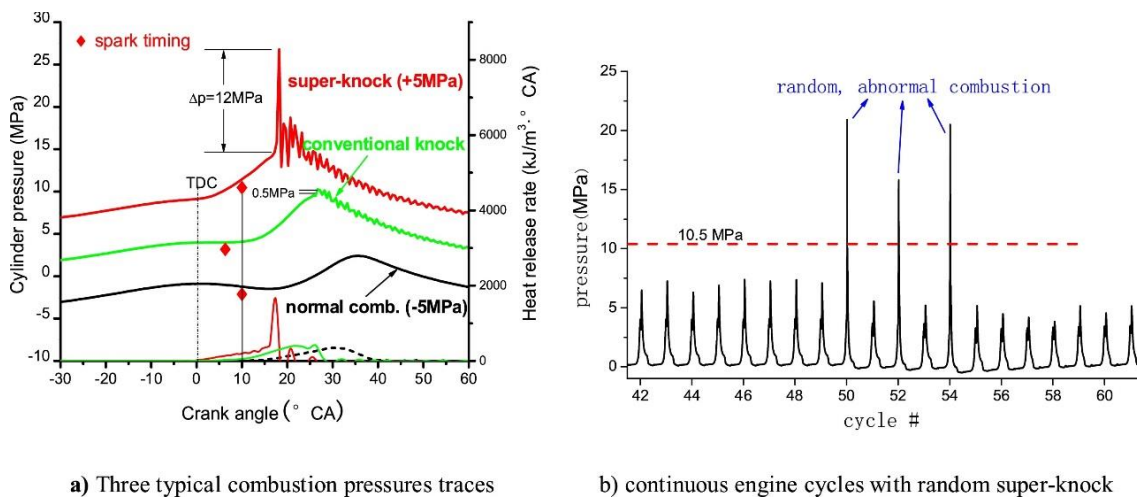
Figure 2.7: a) Comparisons of typical pressure traces and heat release rates of a normal combustion, a conventional knock cycle and a super-knock cycle. b) Continuous engine cycles illustrating super-knock. Adopted from [39].

2.1.5 HCCI engines

Another combustion concept, Homogeneous Charge Compression Ignition (HCCI) has recently drawn attention due to its high thermal efficiency, and potentially low NOx and PM emissions. HCCI operates by merging both SI and CI combustion principles in a manner that the air-fuel mixture is premixed in the intake manifold, or in the cylinder with DI, before the combustion, in order to create a homogeneous charge. It is then auto-ignited to initiate combustion within the compression stroke similar to the conventional CI engine operation [63]. Comparisons of SI, CI and HCCI engines are provided in Figure 2.8 and Table 2.1.
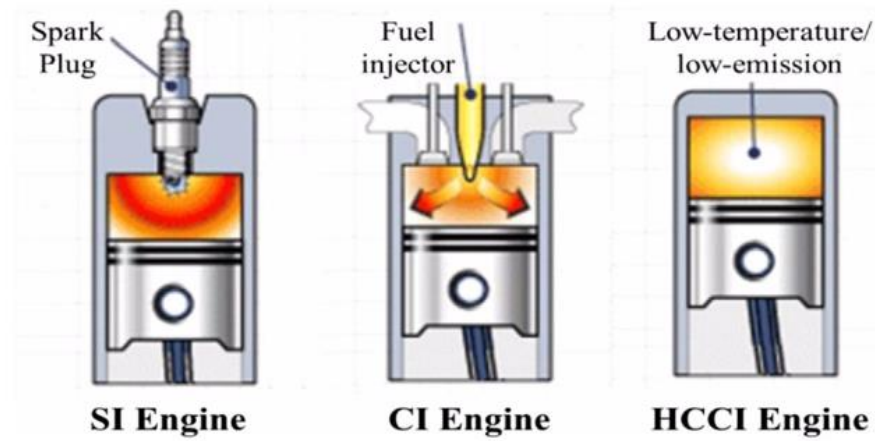
Figure 2.8: Schematic diagram of HCCI operation [66].

Table 2.1: Comparisons of SI, CI and HCCI combustion engines [66, 67].

Engine Type	SI	CI	HCCI
Ignition method	Spark ignition	Auto-ignition	Auto-ignition
Charge	Premixed homogeneous mixture before ignition	In-cylinder homogeneous	Premixed homogeneous charge
Ignition point	Single	Multiple flame propagation	At multiple without a discernible flame propagation
Throttle loss	Yes	No	No
Compression ratio	Low	High	High
Combustion flame	Flame propagation	Diffusive flame	Multi-point auto-ignition
Fuel economy	Good	Better	Best
Max. efficiency	30%	40%	>40%
Major emissions	HC and CO	NO_x and PM	HC and CO
Injection type	Port injection	Direct injection	Both port and direct injection
Equivalence ratio	~1	Lean or too rich	Lean mixture

The charge is heated through heating the intake air or by storing some of hot combustion products in the combustion chamber at the beginning of the compression stroke to attain auto-ignition conditions at the end of the compression stroke. This raises the gas temperature throughout the compression process, which accelerates the chemical reactions that subsequently result in combustion. Despite the fact that the start of the main

27

heat release is generally apparent at temperatures of 1050-1100 K for gasoline, or less than 800 K for diesel, most of the hydrocarbons in gasoline and diesel release low temperature heat, accounting for up to 10% of the total energy released. The amount of low temperature heat release required for auto-ignition, as well as the heat release rate from the HCCI combustion, depends on both the unique chemical kinetics of the fuel, and the thermal conditions used. HCCI has no flame propagation, instead the fuel-air mixture combusts almost homogeneously, and almost instantaneously throughout the chamber, causing a high rapid rate of heat release. To avoid runaway heat release rates, and to limit combustion rates, HCCI operates on lean or/and diluted fuel air mixtures with burned gasses. This is achieved through the use of excess air, exhaust gas recycling or water injection [68, 69]. However, using highly diluted mixtures substantially decreases the achievable engine load, so that the power density of the engine drops. This situation can be improved through supercharging [70].

The coupling of a diluted premixed fuel and air mixture with numerous, almost simultaneous, auto-ignition points throughout the cylinder removes the high combustion temperature regions and limits soot particles. This therefore results in extremely low NOx and PM emissions. Figure 2.9 demonstrates the zones of NOx, soot, CO and UHC emission in φ-T map, along with the representative operating ranges of conventional diesel combustion (CDC) and different modes of LTC, thus optimal combustion temperatures and equivalence ratios for attaining emission reductions can be detected. The adoption of lean or more often diluted air-fuel mixtures with recycled burned gases enables the unthrottled use of an HCCI gasoline engine, thus resulting in better engine efficiency and improved fuel consumption compared to SI engines. Therefore, the HCCI strategy concurrently decreases both NOx and PM emissions from a CI engine and offers a potential to decrease fuel consumption and NOx emissions of an SI engine to meet current and future emission legislation without costly, sophisticated and often ineffective exhaust gas after-treatment systems. Nonetheless, this combustion strategy has shown different problems to overcome before implementing these technologies at the commercial scale. These include difficulty in controlling the combustion phasing, a restrained operating range, large hydrocarbon emissions, high levels of noise, cold start problems, challenges in homogeneous mixture preparation [63, 69].
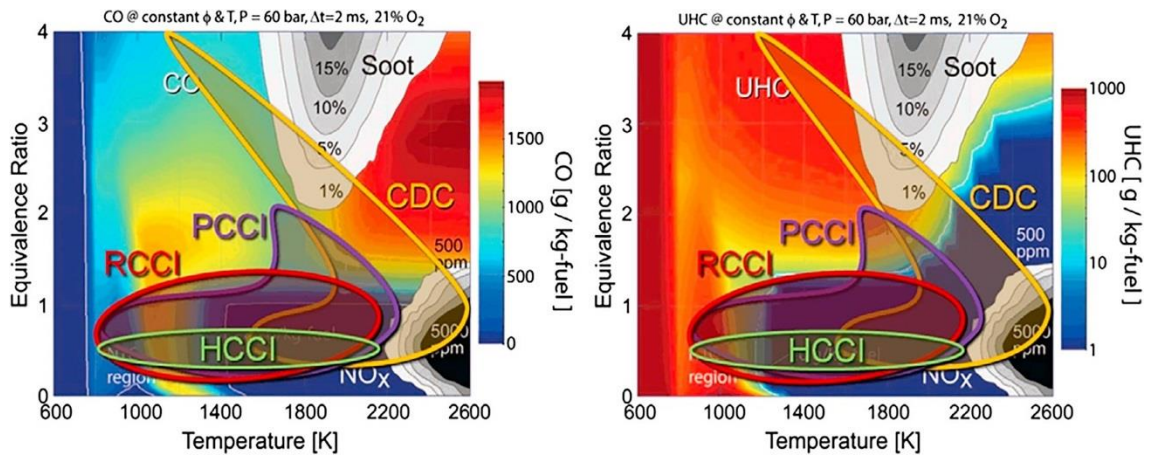
Figure 2.9: Countour plots of emissions portraying the operating zones of LTC modes, namely reactivity controlled compression ignition (RCCI), premixed charge compression ignition (PCCI) and homogeneous charge compression ignition (HCCI), compared to the conventional diesel combustion (CDC) mode. Replicated from [67].

The maximum load is limited by a very high pressure rise rate that accompanies auto-ignition events within this new combustion mode, which subsequently results in extremely noisy operation and unacceptable mechanical strains on an HCCI engine. There is no direct control of the onset of combustion, since there is no ignition event (such as a spark in SI engine or an injection in conventional CI engine), and it solely depends on instantaneous auto-ignition. The ignition timing can be only controlled indirectly, and requires the detailed understanding of the auto-ignition properties for the potential fuels to ensure that the fuel-air mixture auto-ignites under the desired compression conditions within HCCI [68, 71]. Hence, this research aims to improve understanding of the auto-ignition behaviour of fuel mixtures with respect to its constituents over a wide range of operating conditions, relevant to LTC strategies. This is achieved through experimental measurements of ignition delay times in a fundamental device (an RCM), accompanied by detailed chemical kinetic modelling investigations and theoretical analyses. Chemistry that governs important combustion characteristics and influences auto-ignition behaviour of fuels is also investigated.

HCCI combustion of diesel-like fuels shows a distinct two-stage heat release. The first-stage heat release is related to low temperature kinetic reactions. Low temperature kinetics is accountable for engine knock in SI engines and could be related to ONs. Smaller values of ON correspond to more apparent low temperature heat release energy. For gasoline like fuels with high ONs, the low temperature heat release from the first-stage ignition is lower compared to fuels similar to diesel at the identical conditions [63].

29

Therefore, this research also seeks to improve understanding of links between the low temperature kinetics and auto-ignition processes. The oxygenated compounds, such as *n*-butanol, generally have similar or higher octane rating compared to conventional hydrocarbon fuels. Blending these oxygenated fuels with hydrocarbons can result in higher anti-knock properties of the blend. However, their effects on the auto-ignition response are not fully understood. Also, their role in low temperature kinetics necessitates an improved understanding. Hence, the effects of addition of *n*-butanol to hydrocarbon mixture on auto-ignition behaviour and associated low temperature heat release are investigated in Chapter 6.

2.1.6 The chemistry of auto-ignition

To understand engine knock and the auto-ignition phenomenon, it is paramount to understand the kinetics and main reactions influencing ignition delay times, and hence the fundamental chemistry of hydrocarbon oxidation. The oxidation of hydrocarbons and related compounds is an intricate process with series of thousands of distinct elementary reactions. It comprises many intermediate compounds, which, in theory, result in the final products of combustion, CO_2 and H_2O. The process of oxidation evolves through a radical chain mechanism. A chain reaction mechanism generally entails four steps: initiation, propagation, branching and termination. An essential phenomenon of this mechanism is chain branching which depicts the process of self-acceleration, amplified by the exothermicity of reaction, which occurs at both low and high temperatures [72]. A static combustion system can potentially be described to entail two regions: a low temperature region with slow reactions, and high temperature region with explosive reactions [73]. The shift in temperature causes the rate of chain branching reactions to alter. These chain branching reactions are primarily components that control the chemistry of auto-ignition and decide how the oxidation proceeds.

Chain initiation

The chain reaction mechanism initiates when energy input into the compressed fuel-air mixture from the compression stroke of engine attains the minimum activation energies of the endothermic initiation reactions between fuel molecules (RH) and either molecular oxygen or radical species. Activation energy can be defined as the minimum energy required to be added to a chemical system in order to initiate a chemical reaction [74]. The most common chain carriers of the radical chain mechanism are radical species O, H,

OH, CH_3, and HO_2, which are capable of reacting via the same reactions in the combustion chemical systems raising the intricacy of combustion kinetics [74].

During the initiation step, the initial decomposition of the reactants takes place, during which atoms or radicals are formed by either dissociation of the relatively stable fuel molecule (reaction (2.3)), e.g. $C_6C_5CH_3{\rightarrow}C_6H_5CH_2+H$, or by reaction between fuel and oxygen (reaction (2.4)), e. g. $C_3H_6+O_2{\rightarrow}C_3H_5+HO_2$ [75, 76]. Since unimolecular dissociation necessitates the same or larger activation energies compared to the bond dissociation of the fuel molecule, these dissociation reaction are generally relatively slow, and decomposition of RH is apparent generally at high temperatures [75].

$$RH \rightarrow R \bullet + H \qquad\qquad (2.3)$$

$$RH + O_2 \rightarrow R \bullet + HO_2 \bullet \qquad\qquad (2.4)$$

Propagation

Fuel radicals generated during the initiation step further react in exothermic propagation and branching reactions. During the propagation step, the reactive intermediate species react with stable species to produce only one radical for each one consumed, e.g. $C_2H_6+OH{\rightarrow}C_2H_5+H_2O$.

Branching

In the branching step reaction of one reactive species with a stable species form two or more radicals for each one consumed, each of which can then propagate another reaction chain, thus boosting the amount of radicals exponentially, e.g. $O+H_2O{\rightarrow}HO+HO$, $CH_4 + O {\rightarrow}CH_3+OH$.

Termination

Besides the chain propagation and branching, the fuel radicals may also undergo a chain termination route, which stops the chain with no further radicals generated. It removes active species from the system, as radicals combine and produce stable species. For example, chain termination reaction is reducing stable radicals in $C_2H_5+C_2H_5{\rightarrow}C_4H_{10}$. These reactions are generally not temperature sensitive.

31

The overall oxidation rate relies on the elementary steps which change the number of the radicals. An explosion can result at the point where branching reactions overwhelm the termination reactions when originally slow, low and intermediate temperature reactions create a sufficiently extensive radical pool to sustain and accelerate oxidation. Initiation reactions are paramount but have only a linear effect on the number of radicals. On the contrary, branching and termination reactions have a significantly greater influence on the number of radicals. The exponential increase in radical build up due to excess of branching over termination is accountable for the auto-ignition. The low temperature kinetics primarily controls the ignition delay times and dictates whether the auto-ignition takes place or not. Combustion stops either when all of RH are consumed or when there is not sufficient energy present to promote further combustion reactions [74, 76].

2.1.7 The chemistry of low and intermediate temperature hydrocarbon oxidation

The low and intermediate temperature regions (500-1000 K) typically involve ignition and start of combustion before the temperature in combustion chamber attains or exceeds 1000 K, owing to the compression event and the exothermic reactions. This is important in understanding auto-ignition phenomenon and engine knock. The majority of alkanes follow a similar mechanism of oxidation in the low to intermediate temperature region, as outlined in Figure 2.10. A comprehensive detailed low temperature oxidation (500-750 K) scheme has been presented by Battin-Leclerc et al. [77], with only a brief description being given here. Except at very high temperatures (above 1200 K), the common radical chain mechanism of hydrocarbons begins with the initiation step, $RH+O_2$ or $RH+OH$, which removes a hydrogen atom (H-abstraction) from the alkane producing an alkyl radical (R•). Under low temperature conditions (below 700 K) the H-abstraction is mainly undertaken by OH, because it can produce water with abstracted hydrogen radical in the exothermic reaction. The OH radical is generally less particular of the H atom position in H-abstraction, compared to other radical species [72, 74].
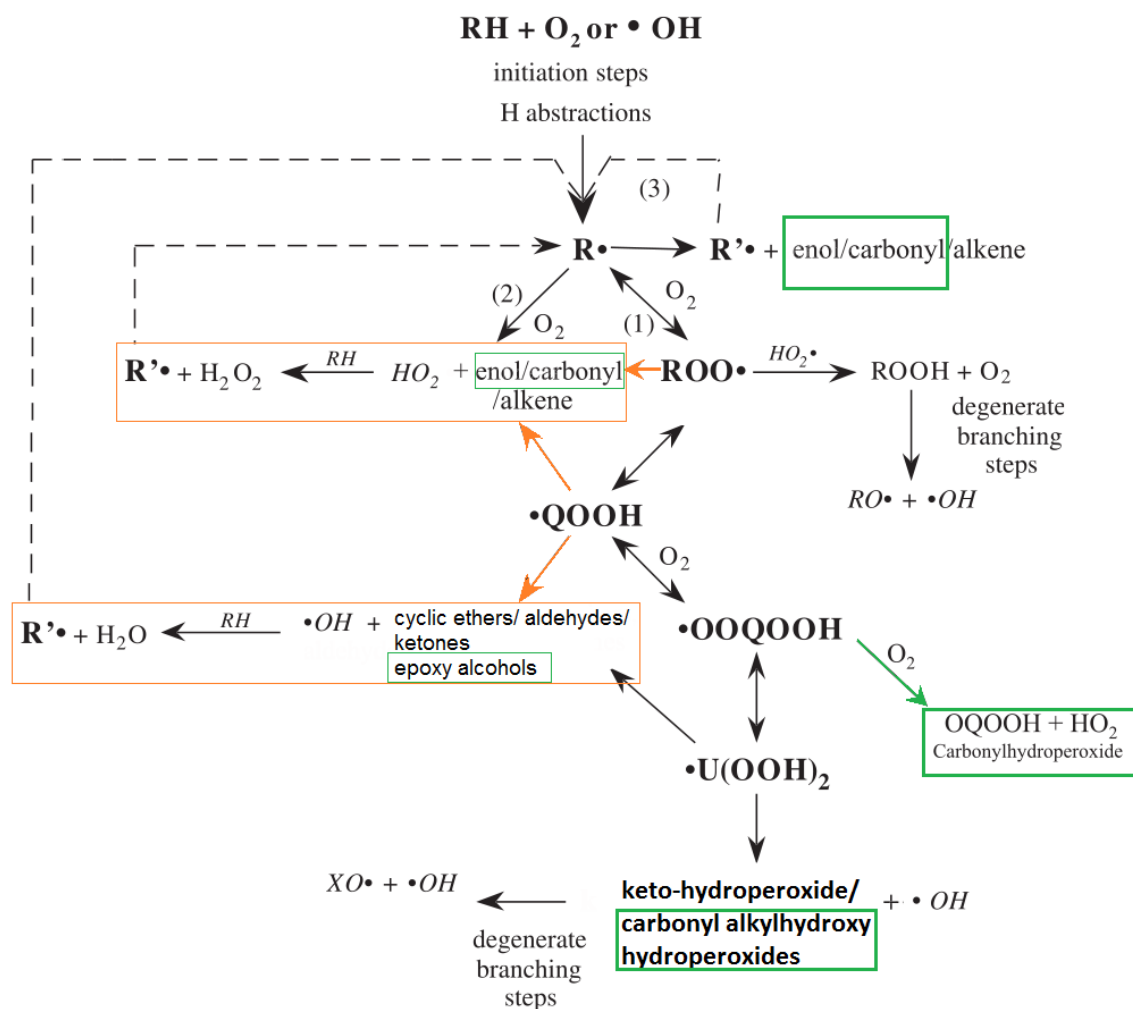
Figure 2.10: A simplified scheme for the primary mechanism of hydrocarbon oxidation at low temperatures. The orange colour highlights the pathways that are responsible for the NTC behaviour. The green colour indicates the pathways and species that are distinctive of the alcohol oxidation. Adapted from [57].

The rate of H-abstraction by the OH radical changes depending on the type of C-H bond being broken in the parent alkane. H-abstraction appears from the weakest C-H bond of the fuel molecule. For alkanes, tertiary C-H bonds are more easily broken, followed by secondary C-H bonds, and then the strongest C-H bonds on a primary carbon atom. The longer carbon chains of alkanes generally indicate faster ignition. However, for sufficiently large carbon chains this effect on the ignition delay is smaller. H-abstraction of tertiary branched carbon atoms is easier compared to secondary straight chain alkanes. However, branching increases the number of primary C-H bonds. It is believed that ignition delays increase with the increased level of branching. Therefore, rate constants of this type of reaction for the branched molecules, such as *iso*-octane, are lower compared with those of straight ones, such as *n*-heptane. Moreover, the strength of the

bond is also affected by the type of bonds and the type of the atoms bonded. For example, in the case of alcohols, the higher electronegativity of the oxygen atom compared to that of carbon hydrogen atoms makes H-abstraction from the alpha carbon position faster than from the secondary position of an alkane. At the same time, H-abstraction from the beta and gamma site is harder and slower than from primary carbon atom of an alkane. H-abstraction from delta site is somewhat equivalent to that of primary carbon atom of an alkane. Therefore, different behaviours emerge from different isomeric structures of the fuel molecule and the overall H-abstraction is generally more difficult for alcohols compared to alkanes [74].

After H-abstraction, molecular oxygen then reacts with the alkyl radical through reaction (2.5) (reaction (1) in Figure 2.10) to create an alkylperoxy radical (ROO) or reaction (2.6) (reaction (2) in Figure 2.10). The competition between these two propagating reactions is responsible primarily for the transition between low and intermediate temperature combustion. At low temperatures, the alkylperoxy radical is the primary product, since the forward reaction has a negligible barrier to the reaction (2.5). This is due to the free radical site and the unpaired electrons on the oxygen. Hence, their association is favoured and slow degenerate branching occurs. As the temperature increases, the higher activation energy dissociation of the alkylperoxy radical becomes favoured so that reactions of R radicals rather than alkylperoxy radicals influence the oxidation. This can subsequently lead to the formation of hydroperoxy HO_2 and a conjugate alkene (reaction (2.6)). In this intermediate temperature region the predominant propagating free radical is HO_2 which tends to abstract a further H-atom to form hydrogen peroxide, H_2O_2. However, at low temperatures, HO_2 is thermodynamically stable and unreactive and slows or effectively terminates the reaction chain [72, 74].

$$R \bullet + O_2 \leftrightarrow ROO \bullet \qquad (2.5)$$

$$R \bullet + O_2 \rightarrow alkene + HO_2 \bullet \qquad (2.6)$$

The alkylperoxy radical produced in reaction (2.5) can undergo intramolecular hydrogen migration through a five- to eight-membered transition state ring via isomerisation forming another carbon centred alkylhydroperoxide radical ($\bullet$QOOH) (reaction (2.7)). This type of reaction goes through a cyclic transition, whose activation energies for isomerisation consist of both the activation energy for H-abstraction and the strain energy

of a cyclic transition state. This reaction generally dictates the overall chain branching sequence and hence influences the formation rate of the radical pool: the higher tendency of a fuel molecule to isomerise leads to faster production of radicals and earlier ignition. Isomerisation takes place through a transition state ring formation, where rings of five or six carbons are preferred due to their small strain energies [74, 78, 79]. Hence, a faster isomerisation is apparent for longer carbon chains (above five or six) compared to shorter fuel molecule chains, and this can potentially increase the likelihood of knock [79]. Then, an unstable alkylhydroperoxide radical may decompose to cyclic ethers or produce oxygenated products such as aldehydes, or ketones and a highly reactive hydroxyl radical, which may further propagate the chain [74, 78].

$$ROO \bullet \leftrightarrow \bullet QOOH \qquad (2.7)$$
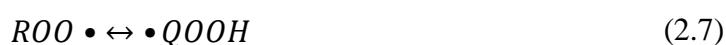
The oxidation 2-methylpentane is a good illustration of the importance of molecular structure in determining a mechanism. Its reaction mechanism is illustrated in Figure 2.11. The C-C bonds in hydrocarbons are approximately 108 degrees. From Figure 2.11, the structure of the 90 degrees (COO) bonding defines the intermediate ketone, aldehyde, and hydroxyl radicals that form. Here, the isomerisation step (indicated by (3.63) in Figure 2.11) determines the overall rate of formation of alkylperoxy radical and subsequent chain branching [79].

The unpaired electron of the carbon atom of alkylhydroperoxide radical ($\bullet$QOOH) is vulnerable to the attack from the second oxygen molecule (reaction (2.8)) to form an unstable intermediate peroxy alkylhydroperoxide ($\bullet$OOQOOH). A peroxy alkylhydroperoxide reacts further by a second internal isomerisation to form alkyl perhydroperoxide radical ($\bullet$U(OOH)$_2$), and then decomposes to form keto-hydroperoxides and release OH. This reaction is a main chain branching reaction promoting low temperature oxidation, because it releases OH radicals and keto-hydroperoxides, which can further decompose and form more OH radicals. These degenerate branching steps involve a multiplication of the number of radicals, which in a chain mechanism increases an exponential acceleration of reaction rates potentially causing spontaneous auto-ignition [77].

$$\bullet QOOH + O_2 \leftrightarrow \bullet OOQOOH \qquad (2.8)$$
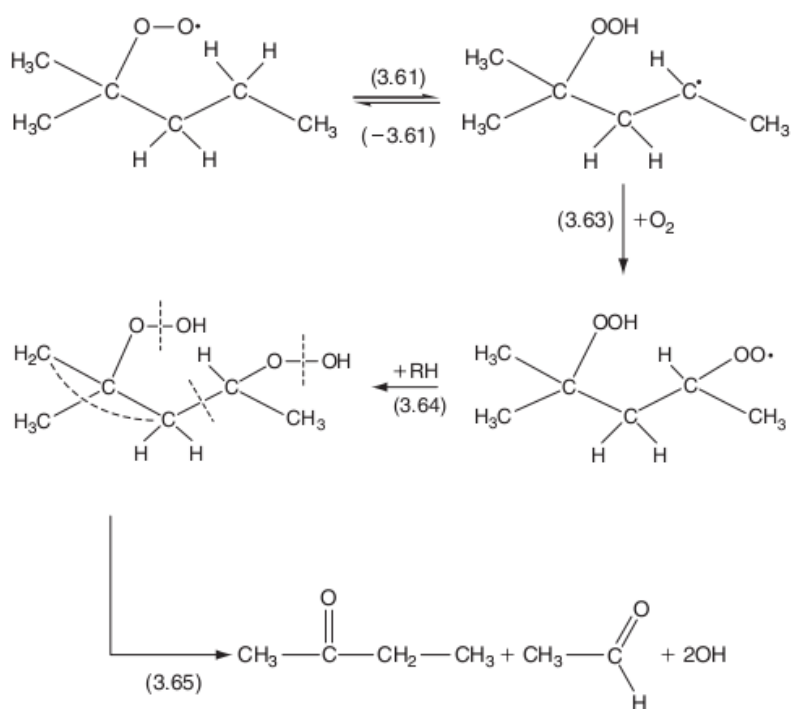
Figure 2.11: The reaction scheme for 2-methylpentane oxidation. Adopted from [79].

2.1.8 The chemistry of high temperature hydrocarbon oxidation

The instability of fuel radicals at high temperature conditions 1000-3000 K and the vast range of intermediate species produced from thermal decomposition (reaction (2.3)), makes the chemical kinetics of combustion complex in this temperature region. The thermal decomposition of RH (reaction (2.3)) appears to become important and to compete with the reaction (2.4) when the cylinder temperature attains 850 K. Above this temperature reaction (2.3) is the prevailing initiation reaction, where either C-C bonds or C-H bonds can be broken [74].

Above 900-1000 K, alkyl radicals (R•) produced in reaction further decay to give a smaller alkyl radicals and a 1-alkene molecule according to reaction (2.10) (reaction (3) in Figure 2.10). This is the predominant mechanism of most alkyl radicals consisting of more than three carbon atoms. Reaction (2.10) adopts the β-scission rule, which says that the bond to be broken is one position away from the radical site [74, 77]. H-abstractions are succeeded by isomerisation and successive decomposition of alkyl radicals until the quite well-recognised chemistry of C_1-C_2 species [80] is attained. This comprises the high temperature mechanism as first described by Westbrook and Dryer [81], that eventually produces CO, part of which oxidises further to CO_2 as part of complete combustion process.

36

$$RH + X \bullet \rightarrow \bullet R + XH \tag{2.9}$$

$$R \bullet \rightarrow \bullet R' + alkene \tag{2.10}$$
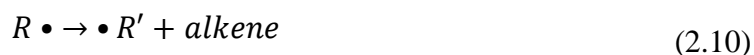
2.1.9   Negative temperature coefficient region

A specific characteristic of hydrocarbon oxidation is a zone of temperature in which the global rate of reaction decreases with temperature, the so called negative temperature coefficient (NTC) region. This behaviour is opposite to the Arrhenius temperature dependence of the reaction rate constant where a monotonic increase in the global reaction rate is observed with an increase in temperature. In RCM studies, the logarithm of the ignition delay time is plotted against inverse temperature, indicating that ignition delay time has a similar dependence on temperature as the reaction rate constant. Therefore, the NTC region can be easily detected by decreasing portion of the curve (Figure 2.12).
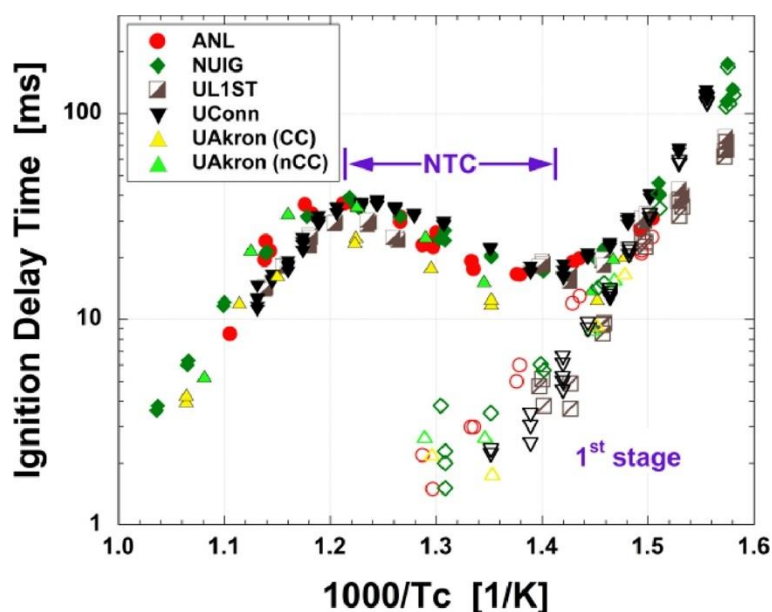
Figure 2.12: Arrhenius plot of *iso*-octane ignition delay time at *P*=2 MPa from different RCMs. The NTC region is clearly highlighted. The variability of the data is high in this region. Adopted from [82].

The presence of the NTC region is related to another peculiarity of the oxidation of alkanes — the potential development of cool flame phenomenon at temperatures several hundred degrees below the minimum auto-ignition temperature. During a cool flame, or multiple cool flames, there is a substantial raise in the temperature and the pressure over a specific temperature region (commonly up to 500 K), however the reaction ceases before the complete combustion is reached owing to the decline in reactivity of the system

37

in the NTC region. A common temperature rise related to cool flame propagation is in the range of 50-200 K, hence a term "*cool flame*". Cool flames are paramount in the spontaneous ignition phenomena since they are related to the first stage of two-stage ignition [77].

The chemical kinetic foundation of NTC can be explained by the displacement in the R•/ROO• equilibrium at the ceiling temperature and the attributed conversion from low temperature degenerate branching to non-branching oxidation modes. The temperature at which ROO•/R• ratio is equal to unity, the ceiling temperature, indicates the limits of the temperature ranges where either the forward or backward reaction is favoured [83]. This is dependent on the structure of the alkyl radicals and on the partial pressure of O_2. The reversibility of the addition of alkyl radicals to oxygen molecules (reaction (2.5)), when temperature raises to facilitate the formation of the HO_2 and the conjugate alkenes reaction (2.6) is favoured, and causes the reduction in the overall reaction rate [77]. Here, the large oxygenated radical intermediates (alkylperoxy radicals and alkylhydroperoxide radicals) can overcome energy barriers for dissociation, molecular elimination reactions producing alkenes and HO_2 radicals, and cyclisation reactions producing cyclic ethers and OH radicals, and propagation reactions leading to formation of β-scission products. These pathways form less reactive products compared to the aforesaid chain branching and lead to the formation of highly reactive peroxide species. Hence, in this intermediate temperature region the accumulation of critical radicals (i.e. OH) is lowered and the overall rate of fuel consumption is decreased [77, 84]. The main propagating radical is then HO_2. Important pathways responsible for the NTC behaviour are highlighted in orange in Figure 2.10.

In addition, the unimolecular decomposition of alkylhydroxide radical starts to compete with the molecular oxygen addition to alkylhydroxide radical (reaction (2.8)), forming peroxy alkylhydroperoxide radical (•OOQOOH), which can undergo internal H-atom isomerisation producing alkyl perhydroperoxide radicals (•U(OOH)$_2$) and which subsequently can decompose generating a carbonyl-peroxide species and a hydroxyl radical. The cleavage of the O-O bond in this peroxide yields a carbonyl-alkoxy radical and another OH radical. This chain branching process results in the generation of three (a carbonyl-alkoxy and 2 OH) radicals. Nonetheless, as temperature increases above approximately 700 K the activation energy barriers for the propagation reactions from alkylhydroperoxide radicals resulting in the formation of cyclic ethers and other β-scission products, along with the concerted elimination of an alkene and hydroperoxyl

radicals from alkylperoxy radical, can be overcome. This leads to the decrease in reactivity of the system and NTC behaviour, since only one radical species is produced rather than three radicals through the chain branching process [85].

Griffiths [86] reported that multiplication of reaction chains is curtailed by displacement from branching to non-branching reaction modes. The author showed that the OH radical is considerably more reactive than the HO_2 radical. Griffiths [86] also stated that considerable exothermicity is associated with OH radical propagation, while HO_2 propagation leading to H_2O_2 formation is virtually thermoneautral. Hence, the overall heat release rate is reduced. H_2O_2 is produced through the reactions (2.11) and (2.12) which at higher temperatures dissociates to form reactive OH radicals. Moreover, below approximately 850 K, the rate of H_2O_2 decomposition to OH radicals is rather low and thus does not advance autocatalysis rapidly enough. This leads to the increased concentration of H_2O_2 in the system, which with the further rise of temperature (above 900 K) will decompose at a growing rate [72]. The reactivity of the system is enhanced here through a new branching step (reaction (2.13)), which increases the radical build up leading to the ignition.

$$HO_2 + H \rightarrow H_2O_2 \tag{2.11}$$

$$HO_2 + HO_2 \rightarrow H_2O_2 + O_2 \tag{2.12}$$

$$H_2O_2(+M) \rightarrow 2OH \bullet (+M) \tag{2.13}$$

Therefore, the fuel oxidation route and chain branching processes are controlled by two different mechanisms in these two distinct temperature regimes, which subsequently are determined by the type of intermediate species produced in the combustion process that can either accelerate or retard reactions. This influences the overall auto-ignition characteristics of a fuel at various temperatures and can manifest as a two-stage ignition (see Figure 2.13). An early, weak ignition or cool flame, where the OH/ROO radical process prevails, is succeeded by a subsequent relatively more powerful second ignition, induced by H_2O_2 decomposition and then chain branching involving H and O [72].
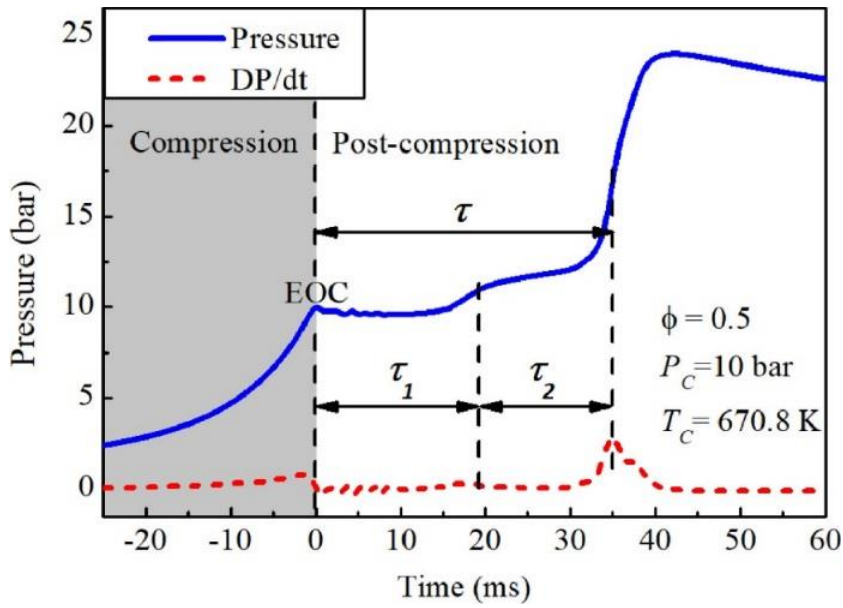
Figure 2.13: A typical RCM pressure trace for the auto-ignition illustrating two-stage ignition behaviour of the diesel surrogate fuel. P=1 MPa, T=671 K and φ=0.5. Adopted from [87].

The fuel concentration also plays an important role in determining the overall rate of the combustion and the ignition delay. For alkanes, at low and intermediate temperatures, an increase in fuel concentration increases the overall rate of the combustion, while at high temperatures this behaviour is opposite. At low temperatures, reaction (2.14) dominates over reaction (2.15), forming hydrogen peroxide, which subsequently leads to chain branching through reaction (2.13) and hence fuel rich mixtures are the fastest to ignite.

At the intermediate temperatures, the reactions of RH with HO_2 radicals and the molecular elimination reactions of alkylperoxy radicals forming an alkene and HO_2 all depend on fuel concentration, with the faster rate of oxidation for the higher fuel concentration mixtures. On the other hand, at high temperature, RH competes with reaction (2.15) for H radicals, which becomes faster than reaction (2.15) at this conditions, and thus an increase in fuel concentration can reduce the rate of the combustion [74, 85].

$$H \bullet + O_2 \rightarrow HO_2 (+M) \tag{2.14}$$

$$H + O_2 (+M) \rightarrow O \bullet + OH \bullet \tag{2.15}$$

2.1.10 The oxidation of methane

Methane displays a peculiar oxidation behaviour that differs from those of alkanes, detailed in earlier sections. Methane has a higher resistance to auto-ignition compared to that of other hydrocarbons. This can be related to its stronger C-H bond in the fuel molecule compared to other hydrocarbons [79]. At low temperatures, even O_2 attack is very slow [79]. Methane auto-ignition behaviour is investigated in Chapter 4 in this work, hence it is important to gain an overview of its oxidation processes and governing reactions. The following sections briefly describe the oxidation of methane.

2.1.10.1 Low temperature methane mechanism

A simplified scheme detailing the low temperature methane oxidation is illustrated in Figure 2.14. It can be seen that there is no H_2O_2 dissociation reaction to OH radical. Glassman [79] reported that this reaction becomes active at the temperatures above approximately 900 K. As highlighted in earlier section, the chain initiation reaction of oxygen addition to parent fuel molecule (reaction (3.71) in Figure 2.14) is slow. The chain propagating reactions (reactions (3.72), (3.73), (3.76) and (3.77) in Figure 2.14) and the chain branching reactions (reaction (3.75) in Figure 2.14) are faster, since they contain a radical and one initial reactant. The chain propagating reaction (reaction (3.76) in Figure 2.14) produces the CO, whereas water is produced in the chain branching reaction [79].

41

$$CH_4 + O_2 \rightarrow \dot{C}H_3 + H\dot{O}_2 \left.\right\} \qquad \text{(chain initiating)} \qquad (3.71)$$

$$\left. \begin{aligned} \dot{C}H_3 + O_2 &\rightarrow CH_2O + \dot{O}H \\[4pt] \dot{O}H + CH_4 &\rightarrow H_2O + \dot{C}H_3 \\[4pt] \dot{O}H + CH_2O &\rightarrow H_2O + H\dot{C}O \end{aligned} \right\} \qquad \text{(chain propagating)} \qquad \begin{aligned} &(3.72) \\[6pt] &(3.73) \\[6pt] &(3.74) \end{aligned}$$

$$CH_2O + O_2 \rightarrow H\dot{O}_2 + H\dot{C}O \left.\right\} \quad \text{(chain branching)} \qquad (3.75)$$

$$\left. \begin{aligned} H\dot{C}O + O_2 &\rightarrow CO + H\dot{O}_2 \\[4pt] H\dot{O}_2 + CH_4 &\rightarrow H_2O_2 + \dot{C}H_3 \\[4pt] H\dot{O}_2 + CH_2O &\rightarrow H_2O_2 + H\dot{C}O \end{aligned} \right\} \qquad \text{(chain propagating)} \qquad \begin{aligned} &(3.76) \\[6pt] &(3.77) \\[6pt] &(3.78) \end{aligned}$$

$$\left. \begin{aligned} \dot{O}H &\rightarrow \text{wall} \\[4pt] CH_2O &\rightarrow \text{wall} \\[4pt] H\dot{O}_2 &\rightarrow \text{wall} \end{aligned} \right\} \qquad \text{(chain terminating)} \qquad \begin{aligned} &(3.79) \\[6pt] &(3.80) \\[6pt] &(3.81) \end{aligned}$$

Figure 2.14: A simplified scheme for the low temperature methane oxidation. Adopted from [79].

The reaction (3.72) in Figure 2.14 proceeds through a metastable intermediate complex - the methyl peroxy radical (see Figure 2.15). At the lower temperatures, the formaldehyde and OH is formed due to the shift in the equilibrium state towards intermediate. At the higher temperatures (above 1000 K) this equilibrium is shifted toward the reactants. This therefore restrains the speed of methane oxidation at these temperatures [79].

$$(3.82)$$
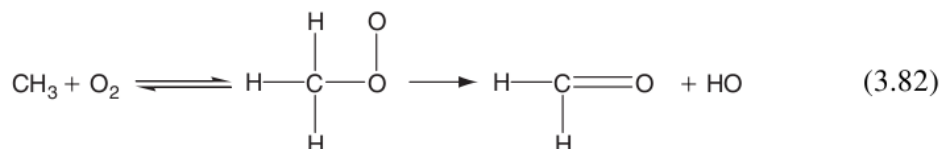
Figure 2.15: A simplified scheme for the low temperature methane oxidation. Adopted from [79].

2.1.10.2 High temperature methane mechanism

Figure 2.16 presents a simplified scheme of the methane oxidation at high temperatures. The chain branching process in the methane oxidation is initiated by reaction (3.83) in Figure 2.16. This triggers the H_2-O_2 chain branching processes and creates pool of OH, O, and H radicals. These radicals can then progress according to equation (2.9) (reaction (3.83) in Figure 2.16). Rate constants of these abstraction reactions are relatively fast [79].

$$CH_4 + M \rightarrow CH_3 + H + M \qquad (3.83)$$

$$CH_4 + X \rightarrow CH_3 + XH \qquad (3.84)$$

$$CH_3 + O_2 \rightarrow CH_3O + O \qquad (3.85)$$

$$CH_3 + O_2 \rightarrow H_2CO + OH \qquad (3.86)$$

$$CH_3O + M \rightarrow H_2CO + H + M \qquad (3.87)$$

$$H_2CO + X \rightarrow HCO + XH \qquad (3.88)$$

$$HCO + M \rightarrow H + CO + M \qquad (3.89)$$

$$CH_3 + CH_3 \rightarrow C_2H_6 \qquad (3.90)$$

$$CO + OH \rightarrow CO_2 + H \qquad (3.91)$$
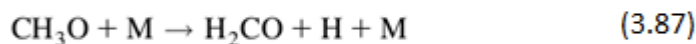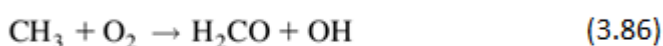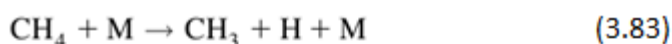
Figure 2.16: A simplified scheme for the high temperature methane oxidation. Here, M denotes the third body species and X represents any radical. Adapted from [79].

The slow oxidation of methane compred to other alkanes can be related to the fact that reaction (3.82) may not undergo the reaction path illustrated in Figure 2.15. The consumption of CH_3 radicals is slow. This leads to the accumulation of CH_3 and the formation of C_2H_6 through a chain termination reaction (3.90) in Figure 2.16. The oxidation of C_2H_6 are considerably different. In some systems the two parallel oxidation pathways in methane system can coexist: one via the CH_3 oxidation and the other via C_2H_6 oxidation. A destruction of CH_3 radicals occurs through reaction (3.85) in Figure 2.16. This is highly endothermic reaction, hence it is responsible for relatively slow chain branching processes in methane oxidation. Formed CH_3O radicals decompose fast and mainly through the reaction (3.87) in Figure 2.16 [79].

2.1.11 The oxidation of alcohols

From earlier discussions, an addition of alcohol fuel to conventional fossil fuels can alter their combustion behaviour and result in higher anti-knock properties of the blend. Therefore, it is important to understand chemical kinetics governing auto-ignition processes of alcohols. The study presented in Chapter 5 investigates the effects of *n*-butanol addition at different blending ratios to a conventional gasoline and its representative surrogate mixture on the auto-ignition response of the blend. The following sections briefly outline the alcohol oxidation.

Alcohols contain a hydroxyl group that makes their combustion kinetics a fascinating deviation of the alkane oxidation [57, 79, 88]. These effects entail pre-reaction system when reacting with OH that lead to the NTC behaviour at low temperatures [88]. Also, in alcohols, the α C-H bond (where the carbon alpha is bound to the hydroxyl moiety) is weaker than all other bonds [57]. Hence, abstraction from 1-hydroxy (i.e., *α*-hydroxy) radical is faster compared to others when reacting with OH and HO_2 radicals [57]. Consideration of the alcohol fuel oxidation mechanism is based almost directely on [57, 88, 89].

2.1.11.1 High temperature alcohol mechanism

Similarly to alkane chemistry, at high temperatures (above 1500 K) and under fuel rich conditions, the unimolecular alcohol decomposition prevails. These are simple C-C and C-H bond scission reactions in alcohols. Dehydration reactions are also important in the alcohol kinetics [57]. Fuel is consumed primarily through H-atom abstraction to form fuel radicals [89]. In butanol, hydrogen atom can be described as hydroxyl, *α, β, γ*, and *δ,* as well as primary, secondary, or tertiary [88]. Figure 2.17 illustrates these characteristic H atom positions and C-H bond dissociation energies for four butanol isomers. Rate constants for these reactions are dependandant on the radical species and the type of hydrogen atom being abstracted [57]. For *n*-butanol, hydrogend bond in the OH moiety is the strongest and the most difficult to abstract [89]. Tertiary bonds are the weakest and are the most easily abstracted [57]. Similarly, the vicinity of OH group makes *α* C-H bond strengths weaker, while *β* C-H bonds are somewhat stronger compared to similar bonds in alkanes [57].
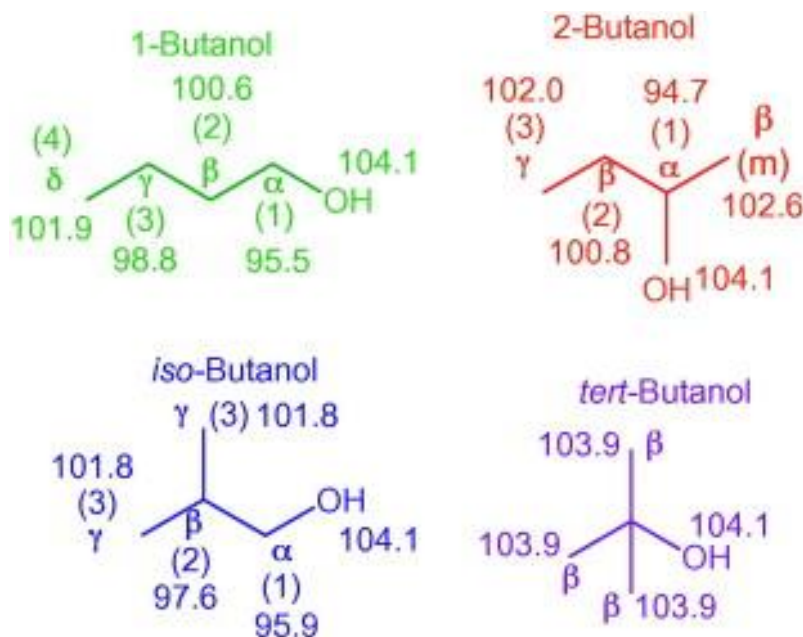
Figure 2.17: C-H bond energies for butanol isomers in kcal/mol calculated at the CBS-QB3 level of theory at 298.15 K. Adopted from [88].

H-abstraction and β-scission of parent alcohol can lead to the formation of aldehydes/ketones at high temperatures. At lower temperatures carbonyls, such as formaldehyde, acetone, butanol etc., can form from α-hydroxyalkyl radical reaction with oxygen [57]. Enols can be produced via dehydration reactions. In gas-phase kinetics their isomerisation to aldehydes or ketones is slow. On the other hand, enol+HO_2 forming aldehyde and HO_2 are faster [57]. The reaction pathway which contains O_2 addition to 1-hydroxylbutyl radicals to produce aldehyde/ketone and HO_2 is rapid at atmospheric conditions [57]. This reaction essentially inhibits low temperature ignition of alcohols and becomes important in oxyden-rich systems, where it starts competing with β-scission reactions [57].

2.1.11.2 Low temperature alcohol mechanism

At low temperatures, alkyl radicals react with O_2 forming alkylperoxy radicals, and thus initiate the chain branching process. Similarly to alkanes, the rate constant of these reactions depends on whether the radical carbon is a primary, secondary or tertiary site [57]. A scheme of the low temperature oxidation mechanism of alcohols is also portrayed in Figure 2.10. The green colour in Figure 2.10 shows the pathways and species that are different with respect to alkane oxidation mechanism. A characteristic of alcohol oxidation at low temperatures is that α-hydroxyalkylradical interacts with oxygen to rapidly form HO_2 and the parent aldehyde or ketone [89]. This distinctive alcohol

45

pathway is in a strong competition with the alkane analogous low temperature branching channel. This can explain the relatively high octane numbers of alcohols [89].

The second step in the low temperature chain branching is ROO•↔•QOOH. The crucial isomerisations consist of five-, six-, and seven-member transition state rings. Reaction rate constants for these reactions depend on the characteristic C-H bond and on the ring strain energy barrier [57]. In the n-butanol system, the β-alkylperoxy radical udergo a six-member ring isomerisation to abstract hydrogen from the OH moiety. This leads to formation of propanal, formaldehyde and OH. Also this results in an inhibition of the low temperature reactivity, since these reactions are chain propagating and compete directly with chain branching pathways [88].

The ROO↔QOOH pathway competes with ROO↔enol+HO_2 pathway. Hence, this pathway competes with chain branching pathway and reduces the overall reactivity of the system [57]. It is also a dominant producer of enols and HO_2 at low and intermediate temperatures. The cyclisation of an alkylhydroperoxide radical to form an epoxy alcohol is comparable to a cyclic ether in alkane oxidation pathway. This pathway competes with the crucial third step in the low temperature oxidation chain branching pathway •QOOH+O_2↔•OOQOOH [57]. The carbon radical (α, primary, secondary, or tertiary) site determines the rate of this reaction [57].

The forth step in the low temperature chain branching process is an isomerisation of peroxy alkylhydroperoxide radical and the formation of a carbonyl alkylhydroxy hydroperoxide species (analogous to carbonyl alkyl hydroperoxide in alkane oxidation, i.e. keto-hydroperoxide) [57]. The final step in the low temperature chain branching is the decomposition of carbonyl alkylhydroxy hydroperoxides to form an OH radical, a smaller oxygenated radical, and a stable oxygenate (such as aldehyde or ketone) [57].

2.1.12 Hot spot auto-ignition

As discussed in earlier sections, engine knock is associated with auto-ignition in the end gas. Auto-ignitions may arise randomly in space and time during an engine cycle. They appear in exothermic centres, called "*hot spots*", and can result in different auto-ignition modes. These, in turn, are associated with auto-ignition processes related to conventional knock and super-knock. An improved understanding of mechanisms leading to different auto-ignition modes can help characterisation of engine auto-ignition over a wide range of conditions, ranging from benign auto-ignition, through mild knock to super-knock. It

can also help to identify conditions that lead to violent or low engine knock. Therefore, the research on hot spots ignition is important to combustion processes and this thesis.

The hot spots, or exothermic centres formed in the end gas are caused by the inhomogeneities in temperature and/or in charge and are capable of igniting the combustible mixture [35]. They can appear close to the boundary layer of cylinder walls or through charge stratification, for example, as a consequence of imperfect hot gas and burned products mixing, heat transfer from hot surfaces or turbulence [90]. Since the *ignition delay*, τ_i, is predominantly temperature sensitive, the hot spot ignites earlier than its slightly cooler surrounding gas, known as the auto-ignition phenomenon [35, 36, 91]. The auto-ignition can take place as a result of elevated temperatures as small as 1 K or active species concentrations. This subsequently leads to space and time dependant processes governed by the superposition of chemistry, gas-dynamics and transport [35, 36, 91]. Hot spot ignition has two functions: it initiates a significant temperature jump across the boundary, and it forces the compression wave to propagate outwards into the surrounding mixture at the local sound speed. The transfer of energy by the compression wave is the critical dynamic effect of the hot spot on the bulk mixture and auto-ignition [36].

Zeldovich et al. [92] demonstrated that gradients of reactivity can generate propagating auto-ignitive reaction fronts at hot spots and subsequently can result in different auto-ignition modes. These include (i) an almost spontaneous *thermal explosion*, (ii) a *supersonic auto-ignitive deflagration*, (iii) a coalescence of pressure and reaction front in a *developing detonation*, (iv) a *subsonic auto-ignitive deflagration*, or (v) a *conventional flame* propagating by molecular and conductive processes.

The combustion corresponding to the deflagration mode is apparent in most engineering applications, where the molecular transport of heat and mass drive the processes following weak ignition. It portrays the subsonic mode of combustion and the chemical reactions take place at constant pressure since compressible effects are negligible in the burnt and unburnt mixtures due to low initial velocities of these flames [93]. On the other hand, the detonative mode of combustion is differentiated by supersonic front propagation velocities of the order of a couple of thousand meters per second.

At one extreme, if the temperature gradient reaches a critical value for a specific mixture and condition, the front of the pressure wave triggered by the rate of change of heat release rate at a hot spot can couple with the auto-ignition front. The auto-ignition front is the

reactive front that propagates into the unburned medium at approximately the sound speed, a. Both fronts jointly reinforce to generate a destructive pressure spike traversing at accelerated velocities in a developing detonation wave if a mixture is sufficiently reactive with sufficient chemical energy feeding into the pressure wave [90, 91]. To trigger a detonation, the heat released by auto-ignition must be discharged sufficiently rapidly into the pressure wave as it propagates through the hot spot. The example of developing detonation from hot spots is demonstrated in Schlieren images in Figure 2.18. The period of heat release is measured by the excitation time, τ_e [36, 94]. The heat release rate is the rate at which thermal energy is released or absorbed by combustion due to a change in energy between products and reactants in reactions. If chemical bonds are formed the energy is released and if the chemical bonds are broken, the energy is absorbed in the form of heat, light, or both according to Conservation of Energy Law, which states that the total energy of system must remain the same.
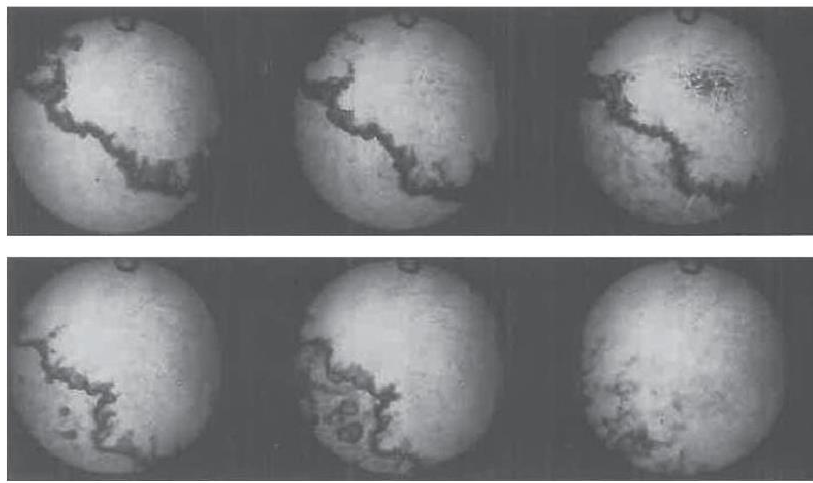
Figure 2.18: Turbulent flame and hot spot auto-ignition in engine. Time increases from left to right and top to bottom [95].

If a mixture is insufficiently auto-ignitive, large scale temperature gradients can subsequently lead to the subsonic auto-ignitive deflagration or more conventional flame driven just by molecular transport and chemical reactions. On the other hand, very small gradients can potentially cause supersonic deflagration in the absence of reaction front and pressure wave fronts coupling or a thermal explosion when gradient is approaching zero [91]. In the event of coupling, the developing detonation that comprises the supersonic combustion with extreme pressure peaks of relatively short existence, may vary in intensity ranging from benign auto-ignition or knock with sufficiently large temperature gradients, to severe knock or super-knock with sufficiently small temperature

gradients. Severe engine knock is associated with the intense heat release rate during the excitation time short enough for it to feed sufficient energy into, and strengthen the pressure wave. Therefore, both ignition delay time and excitation time are important factors controlling potential knock in engines. This requires sufficiently small values of ignition delays and reactivity gradient to generate an auto-ignitive propagating velocity that is greater than the deflagrative velocity and approaches the acoustic velocity [90]. Figure 2.19 illustrates cylinder pressure traces for end gas detonation (super-knock), end gas deflagration (super-knock, heavy knock, and slight knock) and normal flame propagation (non-knock).
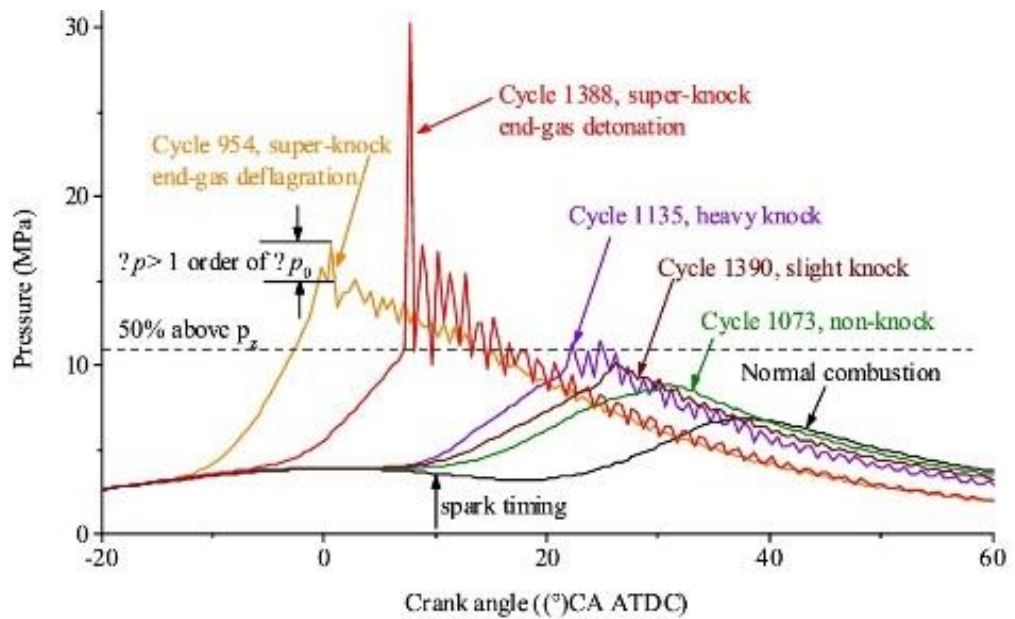
Figure 2.19: Cylinder pressure traces of different engine cycles [39]

2.1.13 Detonation theory

The following section describes a theoretical approach used to characterise the auto-ignition behaviour of studied fuels. This theoretical approach enables the determination of the auto-ignition mode according to the characteristics of a single hot spot and the surrounding mixture. This presents a fundamental methodology for assessing the anti-knock properties of fuels, which was applied in studies described in Chapters 4 and 6.

A spatial distribution of auto-ignition delay time, τ_i, must hold if the original temperature dispersions of temperature or active radicals are inhomogeneous. Subsequently, localised ignitions occur at different points in time and locations. In this way, the reaction develops faster at a hot spot, with the temperature gradients creating an auto-ignition wave that propagates from a hot spot in one dimension and τ_i enlarges with the distance normal to

the gradient from the hot spot, r. The auto-ignition front transverse at a velocity relative to the unburned mixture, u_a, which is inversely proportional to the gradient of the auto-ignition delay time [45, 91, 96] is given by:

$$u_a = \left(\frac{\delta \tau_i}{\delta r}\right)^{-1}$$ (2.16)

An Arrhenius-type equation of the form suggested in Equation (2.17) can be used to express the auto-ignition delay time at a given pressure:

$$\tau_i = A e^{\left(\frac{E}{RT}\right)}$$ (2.17)

Growth of the reacted mixture imposes a further gas velocity to produce a corresponding flame front speed compared to static coordinates. On the assumption that the composition is homogenous and the heterogeneity is caused completely by the temperature gradients $(\delta T/\delta r)$ [45, 91, 96], then:

$$u_a = \left(\frac{\delta T}{\delta r}\right)^{-1} \left(\frac{\delta \tau_i}{\delta T}\right)^{-1}$$ (2.18)

The gradient of ignition delay with temperature from Equation (2.17) can be given by:

$$\frac{\delta \tau_i}{\delta T} = -\tau_i \left(\frac{E}{RT^2}\right)$$ (2.19)

where E is the activation energy, R the ideal gas constant, and their ratio is the localised activation temperature.

So that from Equation (2.19):

$$u_a = \left(\frac{\delta r}{\delta T}\right) \left(\frac{\tau_i E}{RT^2}\right)^{-1}$$ (2.20)

Zeldovich et al. [92] have demonstrated that if the temperature gradient is of a critical value $(\delta T/\delta r)_c$, such that the auto-ignition front would propagate into the unburned mixture at approximately the same magnitude as an acoustic speed, a, the front of the pressure wave set off by the rate of the heat release can combine and grow, with the mutual reinforcement of both fronts, to a developing detonation. The critical condition for such a chemical resonance between the chemical and acoustic waves where the two velocities must be the same, $u_a = a$, can be expressed as [96]:

$$\left(\frac{\delta T}{\delta r}\right)_c = \frac{1}{a\left(\frac{\delta \tau_i}{\delta T}\right)} \tag{2.21}$$

The resonance parameter describing the incidence of a coupling mechanism can be indicated in terms of non-dimensional parameter ξ, the ratio of the local speed of sound to the reaction velocity:

$$\xi = \frac{a}{u_a} = a\left(\frac{\delta T}{\delta r}\right)\left(\frac{\delta \tau_i}{\delta T}\right) = -\tau_i\left(\frac{E}{RT^2}\right)\left(\frac{\delta T}{\delta r}\right)a \tag{2.22}$$

If $\xi \geq 1$, then the speed of sound is significantly larger compared to the reaction velocity and no coupling takes place. Here, the pressure pulse moves ahead of auto-ignitive deflagration and the subsonic auto-ignition regime is entered with no harmful damage to the engine. These modes of auto-ignition are forced by τ_i, rather than by molecular transport processes, as in the more conventional flame [37, 91].

Thermal explosion takes place when $\xi = 0$, which could be characterised in instances where the reaction velocity is significantly higher than the speed of sound and the reaction wave is running ahead of the acoustic wave. Here, all fresh gasses outstanding in the combustion chamber auto-ignite simultaneously owing to a minor temperature gradient. This auto-ignition mode is analogous to the one detected in HCCI engines.

The auto-ignition reaction front and the pressure wave are fully coupled and the chemical resonance takes place when $\xi = 1$, provided that sufficient energy is fed into the wave to create a high pressure ratio of a detonation front. Nevertheless, there is insufficient room for this condition of detonation to be fully achieved in the enclosed space of SI engine and therefore we can only contemplate the developing detonation [37].

The original value of ξ at the hot spot on its own is an incomplete guide of the subsequent mode of auto-ignition. Heat conduction, species diffusion and chemical reaction alter the temperature gradient. This holds especially in cases for larger ignition delay times with the conditions for chemical resonance remaining unmet and local values of ξ are everywhere less than unity. In contrast, for more reactive mixtures and smaller values of τ_i, ξ could locally reach the value of unity and subsequently develop a detonation wave [91].

To trigger the detonation, the chemical energy release rate by auto-ignition must be transferred sufficiently fast into the developing acoustic front as it propagates through the

hot spot at transit time. The duration of the heat release rate can be expressed as the excitation time, τ_e, which is in the order of microseconds. At a hot spot, an approximate quantification of this is the number of excitation times that can be enclosed within an acoustic time defined as the dimensionless hot spot radius divided by sound speed, r_0/a, creating a 'reactivity parameter', ε, as proposed by Bradley and co-workers [91, 96]. Therefore, ε is a measure of the hot spot reactivity and indicates the resistance time of the developing acoustic wave in the hot spot, given by:

$$\varepsilon = \frac{r_0}{a\tau_e} \tag{2.23}$$

The higher the value of ε, the greater the reinforcement of the potentially damaging acoustic wave and therefore the larger the extent of the regime over which the detonation can potentially take place.

Bradley et al. [91] plotted ξ against ε as is illustrated in Figure 2.20 for $0.5\,H_2 - 0.5\,CO$ fuel mixed with air at various equivalence ratios. It defines a detonation peninsula, within which localised detonation can establish from a hot spot and which is bounded by upper and lower limits for the development of detonation, ξ_u and ξ_l, based on the original values of ε and the regimes for the five auto-ignition modes. Therefore, detonation can form within the bounds of the peninsula, but not outside the boundaries. The developing detonations are enclosed to the lower values of ξ, approaching unity, within the narrow toe of the peninsula [91].

Figure 2.20 shows that with greater values of ε, and hence low τ_e and high r_0, the detonation can propagate outside the hot spot and hence there is greater scope of a developing detonation regime. Supersonic deflagration occurs at values of ξ above zero but lower than ξ_l, indicated by letter P in Figure 2.20. Conditional to the distance, the reaction wave front transverses before the lapse of the ignition delay time, which can include a thermal explosion mode. At values of ξ below ξ_l, thermal explosions are more rapid with less intense pressure fronts and smaller temperature gradients. Above ξ_u regime B is apparent in Figure 2.20 where subsonic deflagration takes place. The conventional laminar flame can potentially occur at relatively high values of ξ. The propagation of the reaction front after hot spot auto-ignition evolves into progressively more deflagrative as ξ increases. As equivalence ratio (fuel/air), ϕ, decreases, τ_e increases, ε decreases, the detonation regime narrows and vice versa. This indicates that at high ε values more of the chemical energy can be transferred into and strengthen the acoustic front, and hence the

detonation can commence over a full range of ξ values. The lower values of ξ_u and the narrowing of the toe in the region of the small values of ε appear due to the deficiency of the chemical energy transfer into the developing acoustic front [91, 94]. Therefore, it is important to study these parameters for different fuels to assess their anti-knock properties over a wide range of conditions. Accurate evaluations of ignition delay times and excitation times facilitate the assessment of the tendency of different fuels and their blends to detonate by employing the detonation peninsula on the ξ/ε diagram. These analyses were carried out for methane/air, toluene reference fuel (TRF) surrogate mixture, n-butanol and n-butanol/TRF blends. These studies are detailed in Chapter 4 and 6.
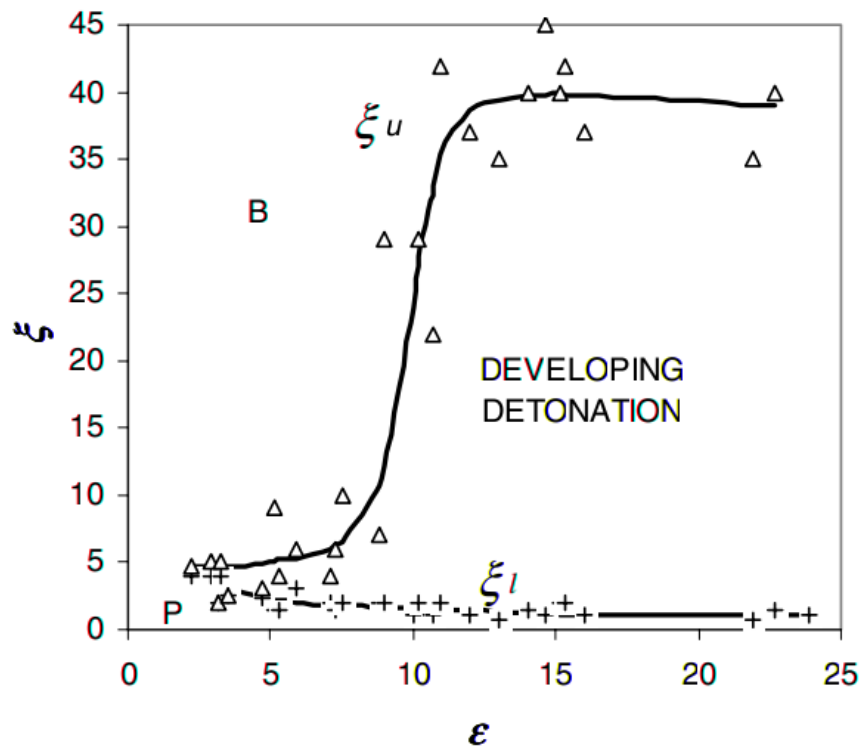
Figure 2.20: Developing detonation peninsula in terms of resonance parameter, ξ, and reactivity parameter, ε, for a H_2-CO/air mixture. Supersonic and subsonic deflagration appears in regions P and B respectively. Δ symbols show the data points which indicate the upper limit of detonation, ξ_u, and $+$ symbols demonstrate data points which reveal the lower limit of detonation, ξ_l [91].

The structure of the developed detonation, a one-dimensional planar detonation, is originally unstable with regard to the propagating waves, but it can be stabilised when it interacts with a leading shock wave. At ξ values close to unity, and smaller values of E/RT, the detonation wave front is apparently flat and stable with relatively weak propagating waves and an associated cellular pattern. If these smaller values of E/RT are

merged with negligible τ_i/τ_e values, the reaction front is spatially relatively uniform, with separate power pulses coupling in time and strengthening the overall stability and strongly coupling with the shock wave. On the other hand, the instabilities could arise due to the sensitivity of τ_i to temperature, with an increase in *E/RT* values or due to an increase in the τ_i/τ_e ratio where the apparent non-uniformity of the power pulse and the spiky heat release leads to the instabilities. Therefore, the coherence and stability of a detonation can be increased by lower values of both terms E/RT and τ_i/τ_e, and their product giving an approximate estimation of stability [45, 90]:

$$\bar{E} = \frac{\tau_i}{\tau_e}\frac{E}{RT} \tag{2.24}$$

Smaller values of $\bar{E}$ describe more stable detonations, while larger values unstable detonations with irregular cellular structures. This could be expressed in terms of non-dimensional parameters ξ and ε through the driving hot spot dimensionless temperature gradient, $lnT/\delta\bar{r}$, where their product ($\xi\varepsilon$) indicates the stability of the detonation and could be implemented in the ξ/ε diagram [90]:

$$\xi\varepsilon = -\bar{E}\left(\frac{\delta lnT}{\delta\bar{r}}\right) \tag{2.25}$$

where $\bar{r} = r/r_0$, r the radius of hot spot within the hot spot of initial radius r_0.

This term can be approximated by $\ln(T/T_0)$ [90], with T_0 the peak temperature at the centre of the hot spot.

Figure 2.21 illustrates the ξ/ε diagram for hot spot auto-ignition with the detonation peninsula confined by ξ_u and ξ_l. It is showing important auto-ignition regimes, namely developing detonation, thermal explosion, subsonic auto-ignition and deflagration. Also dashed curves of two $\bar{E}(\delta lnT/\delta\bar{r})$ parameters, from Equation (2.25), are illustrated. These parameters are representative of the intensity of ignition. The stability of detonation amplifies when $\bar{E}$ value becomes small, whereas small temperature gradients increase probability of detonation and super-knock occurrence.
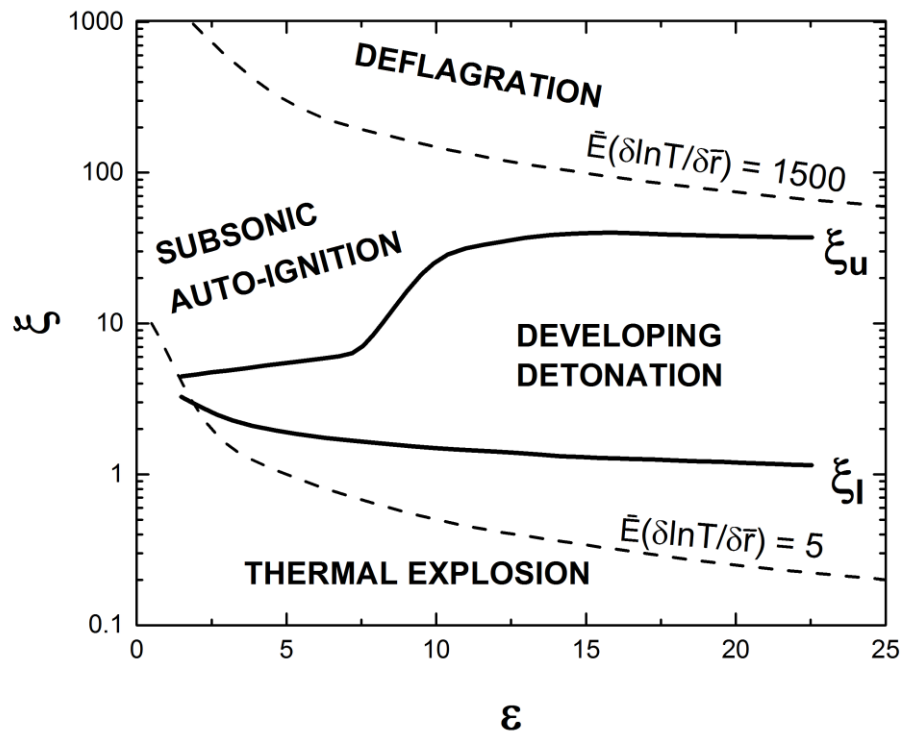
Figure 2.21: *The ξ/ε diagram* for hot spot auto-ignition with addition of curves of constant values of the $\bar{E}(\delta lnT/\delta\bar{r})$ parameters, showing the detonation peninsula and other regimes.

These methodologies undeniably provide invaluable insights, as well as a quantitative criteria on abnormal combustion behaviour, which was applied to study auto-ignition phenomena in this work. They enabled characterisation and assessment of anti-knock properties of various fuels over a wide range of conditions, relevant to advanced engine technologies. Previously, Bradley and Kalghatgi [97] demonstrated by theoretical analyses on ignition delay gradient, that severe knock is induced in the NTC regime. Therefore, these analyses were complemented by further research on the potential effects of low temperature chemistry on various combustion modes, as detailed in Chapter 6. Low temperature chemistry is known to fundamentally affect auto-ignition kinetics and amplify non-monotonicity in combustion systems. The effects of the oxygenated fuel, *n*-butanol, on low temperature kinetics and associated auto-ignition were investigated to improve a current understanding of the processes governing auto-ignition phenomena.

2.1.14 Low and high temperature heat release

Leppard [98] was among the first to demonstrate two-stage ignition kinetic behaviour for alkane fuels. Here, low temperature heat release (LTHR) is preceded by a NTC region and then the apparent high temperature heat release (HTHR) event. HTHR is representative of high temperature combustion where the major heat release takes place.

The transition between LTHR and HTHR can be characterised by the intermediate temperature heat release (ITHR) regime, which often is more difficult to identify. ITHR entails a more gradual pressure increase that can be attributed to coupled self-heating without a sharp inflection point preceding the main ignition [99, 100]. From Figure 2.22, it can be seen that the rate of heat release (ROHR) is an intricate function of multi-stage kinetic behaviour of the fuel air mixture with apparent LTHR, ITHR and HTHR.
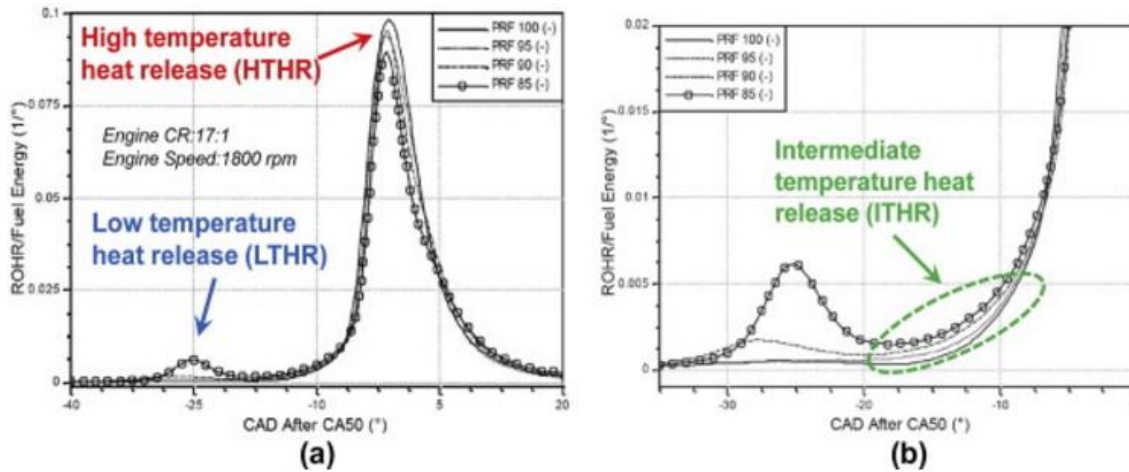
Figure 2.22: Rate of heat release (ROHR) plotted against crank-angle degree (CAD) for different primary reference fuel (PRF), which are scaled by total energy input. a) Illustrated LTHR and HTHR. b) Zoomed LTHR behaviour with different ITHR profiles as a function of PRF. HCCI combustion for a 1.9L Volkswagen turbocharged direct injection engine operation at a compression ratio of 17:1, intake pressure, 1.4 bar, 1800 rpm, φ=0.4 and 50% heat release (CA50). Adopted from [99].

Recently, Westbrook et al. [101] have elucidated further the chemical origins of multi-stage ignition processes and demonstrated that molecular-specific effects on local electron destabilisation is probably the main mechanism for LTHR reaction pathways in alkanes. Alcohol fuels such as *n*-butanol do not exhibit this peculiar behaviour. As discussed in earlier sections, oxidation pathways of alcohols differ from that of alkanes. It is possible to decrease the overall LTHR magnitude of the mixture by blending alkanes with other high ON fuels, such as alcohols. Figure 2.23 illustrates heat release profiles for ethanol/*n*-heptane and *n*-butanol/*n*-heptane blends, where an increase in alcohol concentration within the fuel blend results in decreased LTHR magnitude and delayed ignition. Hence, an addition of the alcohols to alkanes can result in retarded ignition timing, longer ignition delay times and better anti-knock properties of the mixture. The effects of addition alcohol fuel fraction to other fuels have been studied by Saisirirat et al. [102]. The authors found that ethanol and *n*-butanol addition to diesel delayed the HTHR

and the auto-ignition event. This can be related to LTHR, where a decrease in LTHR magnitude has been observed, as well as a reduction in activated intermediate species after LTHR. Also, Saisirirat et al. [103] showed that the rate of production of OH is smaller for alcohol/n-heptane blends compared to a pure n-heptane fuel.
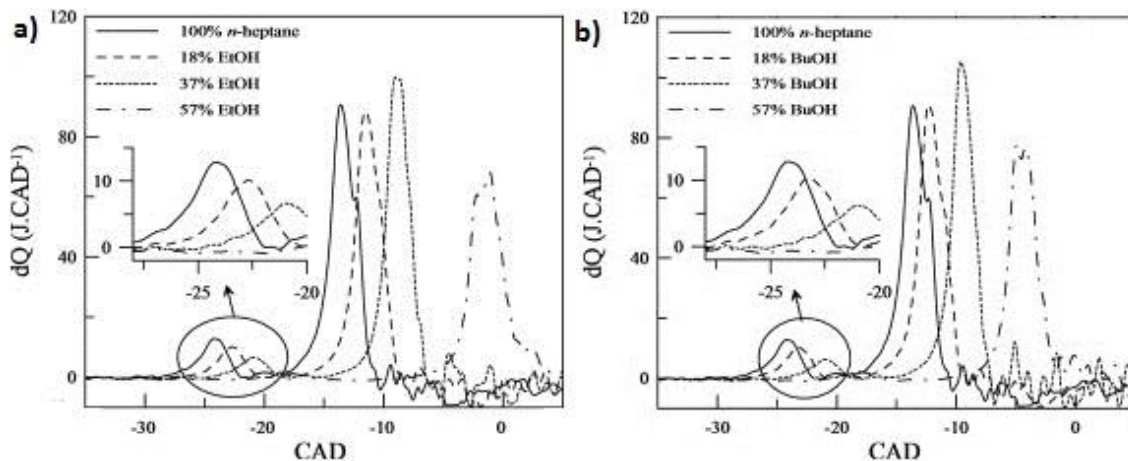
Figure 2.23: Heat release evolution for a) ethanol/n-heptane blends b) n-butanol/n-heptane blends. Heat release rates deduced from the pressure history of HCCI engine experiments and plotted against crank-angle degree (CAD) for 18%, 37% and 57% volume of alcohol in n-heptane. (φ=0.3, T_{inlet}=353 K, 1500 rpm) [103].

The fundamental studies in shock tubes and RCMs have contributed to improved understanding of the fuel kinetic processes of LTHR, but heat release analysis generally is more the focus in HCCI combustion studies where LTHR as well as the NTC is known to have a significant impact on auto-ignition behaviour of the fuel [104]. LTHR usually emits heat during the compression stroke, raising charge temperature prior to TDC and hence advancing ignition [105-107]. Moreover, LTHR kinetics influence ITHR activity that generates a radical pool that is capable of both facilitating ITHR and advance HTHR that can contribute to advancing crank angle location for HTHR. Fuels exhibiting two-stage ignition have been found to offer benefits in controlling combustion phasing and extending the HCCI operating range [108, 109], hence fuel design and blending can offer a route to control the kinetics. This is one of the primary drivers for this research. Despite the fact that LTHR and ITHR in HCCI combustion can improve certain aspects, such as combustion stability and intake temperature, it might also increase the likelihood of knocking and degrade the efficiency of engine [100]. Therefore, a thorough investigation in LTHR and ITHR is required to understand the interplay between LTHR, ITHR and HTHR and to understand chemical effects of range of fuel blends that lead to abnormal combustion.

57

The development of advanced low temperature engine technologies coupled with a current trend of intake boost and engine downsizing, which generally shifts the NTC region to the high temperature regime, reinforces the importance of low temperature combustion behaviour and associated two-stage ignition for conventional gasoline [110]. Heat release analysis can help quantify the trends of preliminary exothermicity of various fuels to facilitate improved understanding of abnormal combustion phenomenon. It can also offer extra targets for the evaluation and validation of chemical kinetic models. Therefore, the study on effects of *n*-butanol addition to TRF on fuel preliminary exothermicity and associated auto-ignition behaviour was undertaken, as detailed in Chapter 6. In this study, investigations of the role of LTHR and ITHR on auto-ignition and abnormal combustion phenomena, especially in the NTC region, has been conducted. Also the main reactions governing these processes were studied.

2.1.15 Experimental studies of auto-ignition

Characterisation of fuels continues to be a crucial prerequisite in the development and implementation of future advanced engine technologies. Fuel combustion in ICEs is a complicated process potentially involving fuel injection, spray, vaporisation, fuel-air mixing, heat and mass transfer, ignition, and combustion. Designed engine experiments can be performed to study the fuel behaviour to assess its knocking potential at specific, usually quite limited, operating conditions that often fail to capture the entire operating scope of practical systems. Observed trends change depending on physical and chemical properties of fuels [7]. Also wide-ranging engine tests carry high costs and cannot be used directly to develop and validate detailed chemical kinetics used in improving understanding of the auto-ignition behaviour of various fuels.

On the other hand, fundamental combustion tests performed in well-constructed chemical reactors and/or canonical flames present valuable data related to detailed chemical oxidation mechanisms, the relative reactivity of different fuels and the effect of the external control parameters on the reactivity of the system. All this information can be used either in the direct assessment of the combustion characteristics of the system or to develop and validate chemical kinetic models. These in turn can be used to aid understanding of trends and comparisons among various fuels, in order to predict their behaviours over a wide range of engine operating conditions facilitating investigations of the main factors controlling knock. Also such fundamental experiments provide a

valuable tool to decouple the physical and chemical aspects of fuel behaviour and aid improved understanding of the effects of molecular fuel structure on fuel auto-ignition. Ignition delay time is a global indicator of fuel oxidation behaviour and is often used as a proxy for assessing knocking potential, and hence the ability to accurately model delay times for a range of fuels under different T, P conditions is important. Ignition delay time is greatly affected by the fundamental elementary reactions and offers an important target for kinetic model development and validation.

Scientists have developed and employed numerous fundamental tests in an attempt to improve knowledge of combustion chemistry over the years. If the focus is primarily on fuel chemistry, the fundamental experiments are designed in the way that the chemical kinetic processes define the fuel oxidation assuming idealised flow fields, while physical/mixing processes have insignificant effects. Typical operational boundaries of the most common experimental devices facilitating the study of auto-ignition behaviour of various fuels are illustrated in Figure 2.24, and comprise motored engines, flow/jet stirred reactors, shock tubes and rapid compression machines (RCMs). In the present research, the attention is directed to this later experimental apparatus (detailed description presented in Chapter 3) which perhaps shows the most potential in enhancing understanding of auto-ignition chemistry of fuel–air mixtures relevant to low temperature advanced technologies. The main characteristics of all these experimental facilities are briefly summarised below and for detailed comparisons and descriptions the reader is referred elsewhere [77, 82, 111-113]. Each experimental device provides information on specific aspects of the chemical kinetic behaviour of the fuel, and each has its own advantages and its own limitations. Hence, data collected from these experimental apparatuses must be handled with care when developing chemical kinetic models and using this information for understanding fuel chemistry [7].
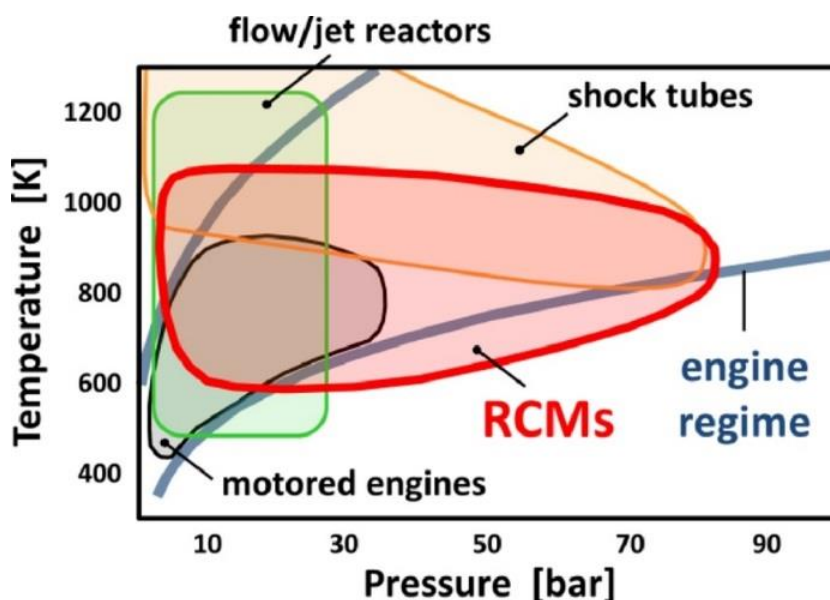
Figure 2.24: Typical operating boundaries of the most common experimental facilities enabling study combustion and auto-ignition characteristics of the fuels [82].

Motored engines [111] are typically single cylinder continuously reciprocating CFR engines driven by an electrical motor, without direct fuel injection or spark, which can exhibit repeated compression events for the fuel. Despite the lack of the additional compression of the flame or consumption by it, the charge does experience compression and heating, which may result in auto-ignition. Although, the combustion processes in this experimental apparatus more accurately replicate the typical operation of a real engine, the flow inside the cylinder is turbulent which results in disruption of temperature and velocity, affecting reaction rates, and leading to variation in each single stroke. This makes it difficult to interpret ignition delay times from motored engines in order to accurately determine the effects of chemical kinetics. One advantage of motored engines is that species evolution can be inferred from timed sampling events at consequent crank angle positions, or by exhaust gas analysis [82].

Flow reactors or *jet-stirred reactors* [77, 112] try to divide the concurrence of mixing and reaction by presenting very efficient mixing conditions throughout the system in a way that renders fluctuations of temperature and species concentration through the volume of the jet-stirred reactor or across the radial dimension of plug flow reactor insignificant. The difficulty in these reactor operations is to maintain a high and homogeneous temperature and high pressure conditions at which reaction timescales and mixing timescales become very similar. The advantage of these experimental facilities is their ability to vary composition, temperature and pressure individually, as well as providing direct measurements of the concentrations of intermediate species and products

60

of fuel oxidation. The measurement of ignition delay times in flow reactors is defined as a time difference between the point at which fuel and oxidiser are sufficiently mixed and the point at which auto-ignition takes place, identified by light emission or a pressure spike. The primary limitation of flow reactor systems is their operating range of up to 1000 K and low pressures of approximately 0.1-3.0 MPa depicting limited ignition delay data, based on the location downstream of the jet. Jet-stirred reactors are able to operate only at very dilute conditions, e.g., less than 1% O_2, to ensure temperature homogeneity [82].

Shock tubes [113] are used for measurements of ignition delay times at high temperature and pressure conditions. A plane shock wave is generated in the long closed tube by the sudden bursting of a diaphragm (e.g. aluminium or copper foil) separating the drive gas at high pressure, from the test gas at low pressure, which subsequently enables propagation of high pressure gas into the low pressure reactive mixture. Conservation of mass, momentum and energy relations, coupled with the equation of state of the test gas and the measured speed of the shock wave, facilitate the calculation of the step change in temperature and pressure of the moving test gas behind the wave. Upon reflection of this incident shock wave from the tube end wall of the driven section, the test gas is further compressed and heated to its initial pre-reaction temperature and pressure while it propagates back across the driven section, and is efficiently stagnated. Owing to the virtually one-dimensionality of the shock tube flow and essentially planar structure of the shock wave, measurements of the incident shock speed can be accurately determined. The combination of efficient step change in shock conditions and the effective stagnation of the test mixture, enables effective modelling of the environment behind the reflected shock wave as a zero-dimensional homogeneous reactor [82, 113] .

A particular strength of shock tube studies remains high temperature dilute conditions with ignition delay times of less than typically 5 ms [82]. Over this period shock tubes exhibit the best performance with the pressure behind the reflected shock waves remaining almost constant avoiding complex flow conditions. At low temperature conditions and in the NTC region, ignition delay times may be relatively longer, and the resistance time of shock tubes is insufficient for the temperature of the test mixture to achieve equilibrium [7]. Measurements of ignition delay time values in shock tubes are thus limited by the time between the point at which the incident shock wave compresses the mixture to the required pressure and temperature within the driven section, and the time for the reflective shock wave to travel back. Thus, the reactivity of the system might

be too slow compared to the time during which shock tubes are capable of maintaining constant conditions, and the gradual increase in pressure behind the reflected shock waves become significant. In the recent past however, longer driver sections and driver gas tailoring have been shown to increase the distance between the shock wave and the driving gas contact surface facilitating, much longer achievable test times, although this necessitates considerable effort and experimentation [7, 113].

Rapid Compression Machines (RCMs) [82], are piston-cylinder devices rapidly compressing a fuel-air mixture to pre-set temperatures and pressures to trigger combustion, thus emulating the compression stroke of a combustion engine. They provide an experimental facility with well-controlled conditions for studying the auto-ignition properties of various fuels and are commonly used to measure longer ignition delay times which are not attainable by shock tubes. Physical sampling is therefore possible and the ignition delay time is attained through the acquisition of pressure traces within the chamber. Generally, RCMs are capable of investigating combustion regimes characterised by low to intermediate temperatures (600-1200 K), and moderate to high pressures (0.5-8 MPa) [82]. Therefore, they play a critical role in improving understanding of auto-ignition behaviour of various fuels for low temperature and NTC behaviour, commonly apparent in modern engines. The changes among various fuels are magnified in the NTC and low temperature regions, and experimental observations are more likely to exhibit stronger sensitivity to coupled physico-chemical processes within this regime. Hence it is essential to characterise the fuel reactivity at low temperatures and within the NTC to accurately describe the LTHR and ITHR, which are critical in the design of modern low temperature combustion technologies [7, 82].

In theory, the ideal RCM apparatus should compress a homogenous fuel air mixture instantaneously, adiabatically and without triggering any reactions, to a homogeneous pressure and temperature, with a systematic auto-ignition appearing in a thermal explosion thereafter [114]. However, in practice, the compression is sufficiently rapid but not spontaneous, and could potentially entail some chemical pre-reactions during the pressure and temperature rise of compression. With slow compression, very reactive fuels in particular, with relatively short ignition delay times may undergo quite significant extents of reactions during the compression phase [114]. Also, some heat is lost to the surrounding environment after compression, the piston rebound is quite probable, and auto-ignition does not entail a fully homogeneous nature [114]. This makes comparisons of experimental ignition delay measurements between different RCMs quite challenging.

Differences in measurements between different sets of results can appear due to variation of their designs and therefore flow dynamics, the use of different buffer gasses which have different thermodynamic properties attributing potentially to different chemical kinetic consequences, differences in compression ratios which affect the rate of heat transfer etc. [7]. Therefore, valid comparisons can only be made with addition of numerical modelling techniques that attribute the heat losses of specific apparatuses. A great deal of historical and recent effort has been devoted to tackle problems associated with RCMs, such as heat transfer induced boundary layer growth, as well as others. A more detailed description of the RCM used in this work, its limitations, operating principles and procedures are presented in Chapter 3.

2.2 Chemical Kinetic Modelling

In the recent years, chemical kinetic modelling has become an imperative technique in the analysis of combustion devices and prediction of fuel behaviours. It is a powerful tool in obtaining quantitative knowledge into kinetic interactions at the elementary reaction level governing the global processes. Availability of the elementary kinetic data, improved methods for reaction rate estimation, progress in efficient 'stiff equation' solution methods, and advancements in computational technologies have all facilitated the application and use of detailed chemical kinetic modelling. Nowadays, chemical kinetic models are commonly used in the analysis of many practical combustion systems, assessment of the influences of kinetic factors on safety of fuel storage and transportation, as well as prediction of combustion behaviours and processes in advanced engine technologies. A thoroughly validated kinetic model is capable of providing accurate simulation of engine experiments and chemical systems, especially under the conditions that may not be accessible otherwise [81, 115].

Chemical kinetics is the branch of physical chemistry that studies the chemical transformation as a process that takes place in time according to a defined mechanism with the predictabilities relevant to this process [116]. It is a science that is concerned with the understanding, measurement and interpretation of the rates of chemical reactions. In contrast to chemical thermodynamics, which only study the initial states of the reactants and the final state of the system when equilibrium is reached, chemical kinetics predicts the speed of the reaction and the effect of reaction conditions. Moreover, it also attempts to understand how exactly the transformation of reactants into products occurs, the reaction mechanism. Chemical kinetics help to determine from which elementary

steps the reaction mechanism consists, what intermediate species are produced in it, via what pathways the reaction takes place, what factors lead to the chemical composition of the products. Therefore, the subject of the chemical kinetics is the detailed study of the chemical reaction. This entails consistency of its development in time, the dependence on the conditions, the mechanism, a relationship between the kinetic characteristics with the structure of reactants, energy of the process, and physics of particle activation [78, 116].

In the past, chemical kinetics related to combustion processes generally targeted the research of chemical systems at the conditions of explosive reaction. Recently, however, the rates and mechanisms of steady (non-explosive) chemical reactions have attracted a lot of attention driven by the development of low temperature technologies as well as higher environmental requirements, since complex pollutants are generally produced in the zones of steady low-temperature reactions during and after combustion [79]. The rate of each individual chemical reaction can potentially influence many processes in an ICE such as heat release, flame stabilisation, soot and pollutant formation, cool flame characteristics, ignition behaviours and auto-ignition modes [78].

2.2.1 Rates of reactions

Chemical processes are governed by a number of reversible (or irreversible) reactions that consist of N chemical species. All chemical reactions occur at a specific rate and are defined by the conditions of the system, such as concentrations of the reactants, pressure, temperature, radiation effects, the presence of catalyst or inhibitors. The reaction rate is a rate at which the substances involved in chemical reaction are transformed into products. For the elementary, one step reaction, the law of mass action states that the rate at which reactants are consumed is proportional to the product of the concentration of each reactant raised to a power equal to the corresponding stoichiometric coefficient and can be represented by the equation:

$$\sum_{i=1}^{N} v_i' A_i \leftrightarrow \sum_{i=1}^{N} v_i'' A_i \qquad (2.26)$$

where v_i' is the stoichiometric coefficient of the reactant i, v_i'' is the stoichiometric coefficient of the product with respect to species i, A_i is an arbitrary specification of all chemical species, and N is the total number of species [79].

Therefore, for any reaction the rate law represents the time dependence of the chemical reaction and is basically the equation that defines the speed of the reaction and its

relationship to the concentration of the chemical species involved. The rate law for reaction (2.26) can be expressed as:

$$\frac{dc_i}{dt} = v_i k_f \prod_{i=1}^{N} c_i^{n_{i,1}}$$

(2.27)

where $v_i = v_i'' - v_i'$ since v_i'' moles of c_i are produced for every v_i' moles of c_i consumed, c_i is the concentration of species i, k_f is the proportionality constant called the specific reaction rate coefficient, the operator $\prod$ means that the product of all terms behind it should be calculated and $n_{i,1}$ is the reaction order with the respect to species i [79].

In theory, all thermal elementary reactions are reversible, implying that the products may react with each other to reform the reactants [117]. The rate law for the reversed form of reaction (2.26) can be written as:

$$\frac{dc_i}{dt} = -v_i k_r \prod_{i=1}^{N} c_i^{n_{i,2}}$$

(2.28)

where, $n_{i,2}$ is the reaction order of the i-th product species. The equilibrium can be attained when the forward and backward reactions have the same microscopic rate and no net reaction is apparent on a macroscopic level. Hence, the equilibrium constant expressed in molar concentrations, K_{eq} can be expressed as [78]:

$$K_{eq} = \frac{k_f}{k_r} = \prod_{i=1}^{N} c_i^{v_i}$$

(2.29)

For an ideal gas, K_{eq} can be calculated from the thermodynamic properties of the species through [117]:

$$K_{eq} = \frac{k_f}{k_r} = \left(\frac{p^{\ominus}}{RT}\right)^{\sum_{i=1}^{N} v_i} exp\left[\frac{\Delta_r S^{\ominus}}{R} - \frac{\Delta_r H^{\ominus}}{RT}\right]$$

(2.30)

where $p^{\ominus}$ is standard pressure, $\Delta_r S^{\ominus}$ and $\Delta_r H^{\ominus}$ are the standard molar reaction entropy and entropy changes, respectively, calculated from the respective standard molar entropies and enthalpies of the species involved in the reaction, R is the universal gas constant.

$$\Delta_r S^{\ominus} = \sum_{i=1}^{N} v_i S_i^{\ominus}$$

(2.31)

$$\Delta_r H^\ominus = \sum_{i=1}^{N} v_i H_i^\ominus \tag{2.32}$$

These standard molar entropies and enthalpies of the species are commonly determined from the thermodynamic properties, in turn obtained from 14 fitted polynomial coefficients called NASA (National Aeronautics and Space Administration) polynomials for each species. The NASA polynomials are the polynomials fitted to tables of thermodynamic or thermochemical properties of a distinct species applying the least square method, which are successively determined based on experimental data, complemented by theoretical calculations such as electronic structure calculations and bond additivity rules. Seven polynomials are used for the low temperature range generally between 300 K and 1000 K and seven for the high temperature range typically between 1000 K and 5000 K. Then these NASA polynomials can be used to calculate different properties at any given temperature (T), such as standard molar heat capacity ($C_p^\ominus$), enthalpy ($H^\ominus$) and entropy ($S^\ominus$) according to following equations:

$$\frac{C_p^\ominus}{R} = a_1 + a_2 T + a_3 T^2 + a_4 T^3 + a_5 T^4 \tag{2.33}$$

$$\frac{H^\ominus}{RT} = a_1 + \frac{a_2}{2} T + \frac{a_3}{3} T^2 + \frac{a_4}{4} T^3 + \frac{a_5}{5} T^4 + \frac{a_6}{T} \tag{2.34}$$

$$\frac{S^\ominus}{R} = a_1 ln\{T\} + a_2 T + \frac{a_3}{2} T^2 + \frac{a_4}{3} T^3 + \frac{a_5}{4} T^4 + a_7 \tag{2.35}$$

where a_n parameters are NASA polynomial coefficients [78, 117].

2.2.2 Arrhenius law

Despite the relationship between the chemical reaction rate and the concentration of the reactants in the law of mass action, the rate constant is independent of concentration but dependent on the conditions, primarily, temperature. This is due to a stable structure of each atom, which necessitates weakening of certain bonds and subsequently requires energy consumption. This energy, the activation energy, is needed for the chemical conversion of the reactants which breaks the reactants chemical bonds. The fraction of collisions of reactants, whose energy is greater than certain amount, *E*, would react and is equal to *exp(-E/RT)* according to Boltzmann's law [116]. Therefore, the rate constants' dependence on the temperature can be expressed in the form of an Arrhenius equation:

$$k = A exp\left(-\frac{E}{RT}\right) \qquad (2.36)$$

where A is the pre-exponential factor or A-factor, which is a constant specific to each reaction that depends on the chance the particle will collide in the correct orientation accounting for the steric factor and the terms in the collision frequency other than the concentrations, E is activation energy, R is the gas constant and T is the temperature, while E/R is called activation temperature. If equation (2.36) can describe the temperature dependence of the rate constant showing an increase of rate constant with the temperature that permits straight line correlation of data on $ln(k)$ versus $1/T$ (Arrhenius plot) then it is said that the data is following Arrhenius kinetics. The slope of this line is $(-E/R)$ and the intercept is $ln(A)$. Low activation energy processes commonly take place faster compared to high activation energy processes at low temperatures and are much less temperature sensitive, while at high temperatures, this behaviour could be opposite due to their temperature sensitivity [79, 117].

In high temperature gas phase kinetic systems found in combustion, 'non-Arrhenius' behaviour of rate constants is typically standard rather than an irregularity, especially for processes that have a small energy barrier [79, 117]. Therefore, for these cases the temperature dependence of the rate constant can be described by the modified Arrhenius equation where the A-factor is not a constant but rather a function accounting for the temperature variation of rate data:

$$k = A T^n exp\left(-\frac{E}{RT}\right) \qquad (2.37)$$

where the power n of T accounts for all the pre-exponential temperature dependent terms. If n is known, E can be calculated from the slope of the plot of $ln(k/T^n)$ against $1/T$ [117]. Typically, the values of n are only relevant over a specific temperature range, and they may be calculated by the techniques of thermochemical kinetics [79].

2.2.3 Pressure dependence of reaction rates

Almost all reactions are initiated by bimolecular collisions, but some particular bimolecular reactions may display first-order kinetics. A popular combustion example is the decay of hydrocarbon radical to an olefin and an H atom (e. g. $C_2H_5 \rightarrow C_2H_4 + H$). The order of such reaction, and hence the form of the applicable rate constant expression may vary with the pressure. Also, the rate constants of thermal decomposition or isomerisation reactions of some small organic species have been shown to be pressure dependent at a

certain temperature [79, 117]. These are unimolecular reactions, since only one species goes through chemical transformation. In the simplest case the pressure dependence can be interpreted using the Lindemann model [118], which gives a simplified representation of the physical processes involved in these reactions. According to this model, unimolecular decomposition is only possible, if the energy in the molecule is high enough to break the bond. Hence, before the decomposition reaction, the energy is increased by collision of the molecule with other molecules M (third body) for the excitation of the molecular vibrations [119]. This third body can be a molecule of bath gas or any other species of the reaction system. These collisions produce excited reactant species which have a broad range of rovibrational energies, that can travel up and down the energy ladder, hence the rate constant is defined by the energy of the excited reactant [117]. The excited species may decompose into products or it can deactivate by another collision before it decomposes. If A is the reactant molecule and M is a non-reacting collision partner, the Lindemann approach can be presented as follows:

$$A + M \overset{k_f}{\to} A^* + M \ (activation)$$ (2.38)

$$A^* + M \overset{k_b}{\to} A + M \ (deactivation)$$ (2.39)

$$A^* \overset{k_p}{\to} P(roducts) \ (unimolecular \ reaction)$$ (2.40)

The rate of decay of species A is given by

$$\frac{d[A]}{dt} = -k_f[A][M] + k_b[A^*][M]$$ (2.41)

Due to the activation and deactivation of the species A^*, its concentration is relatively small, so that it can be assumed that the concentration of A^* is in steady state and does not change with time (quasi-steady state approximation) [119]. Hence, the rate of change of the activated species A^* is given by:

$$\frac{d[A^*]}{dt} = k_f[A][M] - k_b[A^*][M] - k_p[A^*] \cong 0$$ (2.42)

Hence, the concentration of the activated species A^* and the formation of the product P are [119]:

$$[A^*] = \frac{k_f[A][M]}{k_b[M] + k_p} \tag{2.43}$$

$$\frac{d[P]}{dt} = \frac{k_f k_p[A][M]}{k_b[M] + k_p} \tag{2.44)}$$

Due to the size, complexity and a possible presence of the energy exchange, the efficiency of a collision partner (third body) can be different. Generally, the collision efficiency is not important, however for some reactions particular species can have a significant impact [79].

At high pressures, the collision partner M has a large concentration, $M \rightarrow \infty$. When the rate of collisional deactivation is significantly higher compared to the unimolecular decomposition, $k_b[A^*][M] \gg k_p[A^*]$ or $k_b[M] \gg k_p$, the decomposition process becomes first order:

$$\frac{d[P]}{dt} = \frac{k_f k_p}{k_b}[A] = k_\infty[A] \tag{2.45}$$

where k_∞ is a high pressure rate constant. Here the reaction rate does not depend on the concentration of the collision partners, since at high pressures the probability of the collision is high and frequent, so that the decomposition of the activated molecule A^* is rate limiting instead of the activation [119]. Therefore, at the high pressure limit, the rate constant does not depend on the pressure and is constant for a given temperature.

At low pressures, the concentration of the collision partner M is very small. When the rate of collisional deactivation is much smaller compared to the rate of reaction, $k_b[M] \ll k_p$, then:

$$\frac{d[P]}{dt} = k_f[A][M] = k_0[A][M] \tag{2.46}$$

where k_0 is a low pressure rate constant. The process is second order. The reaction rate is proportional to the concentration of species A and collision partner M, because the activation is slow (rate limiting) at low pressures. Hence, above the low pressure limit, the rate constant of the unimolecular reaction is proportional to pressure [78, 119].

The Lindemann model [118] shows that the reaction orders of non-elementary reactions depend on the concentration and conditions chosen. However, this does not cover the mechanisms of the energy processes. More precise results for the pressure dependence of unimolecular reactions can be deducted from the *theory of unimolecular reactions* (see

[120-122]). This theory is capable of taking into the account a vast number of activated species with different levels of activation and presenting fall-off curves which illustrate the pressure dependence of k for different temperatures, where $d[P]/dt=k[A]$. A typical fall-off curve is presented in Figure 2.25 (a). For $p \rightarrow \infty$, $k=k_f k_p/(k_b[M]+k_p)$, tends to the limit, k_∞, and the rate constant becomes independent of the pressure, while for $p \rightarrow 0$ k is proportional to $[M]=p/RT$, yielding a linear dependence. In a similar way, k will decrease with temperature if the effective activation energy of k_∞ is small. Figure 2.25 (b) illustrates the resulting temperature dependence of rate constants, if the fall-off curves are combined with k_∞ [119].
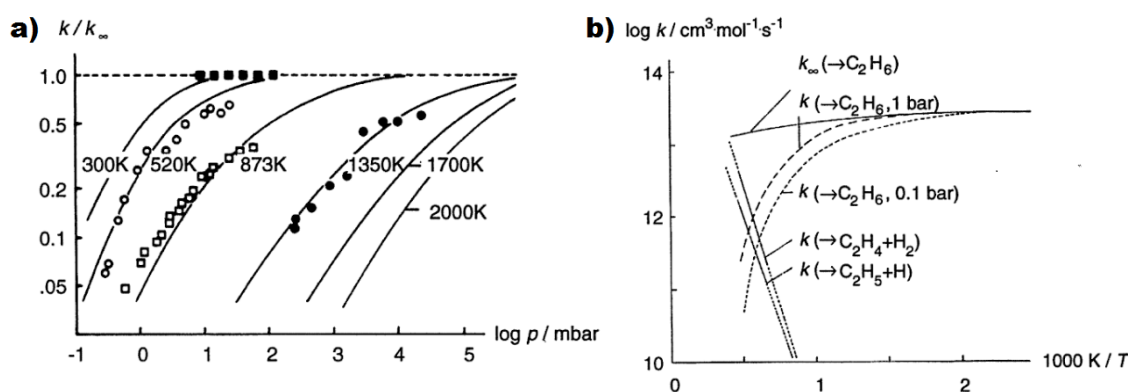
Figure 2.25: Example of fall-off curves for the unimolecular reaction $C_2H_6 \rightarrow CH_3 + CH_3$ (a) and temperature dependence resulting (b) [119].

The deviation from the Lindemann model can be described by the application of the pressure and temperature dependent broadening factor F for each reaction considered [117]. A popular representation of the broadening factor is the TROE formulation [123]:

$$logF = logF_{cent} \left[1 + \left[\frac{logP_r + c}{n - d(logP_r + c)} \right]^2 \right]^{-1} \qquad (2.47)$$

where $c=-0.4-0.67logF_{cent}$, $n=-0.75-1.271logF_{cent}$, $d=0.14$, P_r is reduced pressure given by:

$$P_r = \frac{k_0[M]}{k_\infty} \qquad (2.48)$$

and

$$F_{cent} = (1-\alpha)exp\left(-\frac{T}{T^{***}}\right) + \alpha exp\left(-\frac{T}{T^*}\right) + exp\left(-\frac{T^{**}}{T}\right) \qquad (2.49)$$

70

so that four additional parameters, α, T^{***}, T^{*}, and T^{**}, have to be defined to represent the fall-off curves with TROE parameterisation. The two first terms are important in atmospheric conditions, but the last term becomes important only at high temperatures [117].

Many fall-off reaction cannot be fitted using a single Arrhenius function, hence another formulation known as PLOG was introduced. This is a generalised polynomial fit of the temperature-dependent and pressure-dependent polynomials [85, 124]. Rate constants are calculated over a range of pressures $(P=P_1, P_2,.., P_N)$ as:

$$k_u(T,P_i) = \sum_{j=1}^{M} A_{ij} T^{nij} \exp\left(-\frac{E_0^{ij}}{RT}\right), \ i = 1, \dots, N, M \geq 1 \qquad (2.50)$$

where N is the user defined number of pressures included in PLOG parameterisation and M is the number of duplicate pressures. The rate constant at a given pressure is the summation of the internally duplicate reactions. An extrapolation is bounded by the two pressure limits, P_1 and P_N. This equation is only applicable for a single pressure P_i in the PLOG statement. To calculate $k_u(T,P)$ for any other pressure, $logk_u$ is interpolated as a linear function of $logP$ [85]. If P is between P_i and P_{i+1} for any temperature, a rate constant can be deduced using the following expression [85]:

$$logk_u(T,P_i) = logk_{u,i} + (logP - logP_i) * \frac{logk_{u,i+1} - k_{u,i}}{logP_{i+1} - logP_i} \qquad (2.51)$$

The PLOG formalism shows more accurate performances compared to TROE formalism, when the composition of the gas is kept constant [85]. On the other hand, if the average third body collision efficiency of the mixture substantially alters, then the PLOG calculated rate coefficient can vary [85]. Also, a particular attention should be given to the method the falloff data for a single third body collision efficiency is converted to the third body collision efficiency for a mixture.

2.2.4 Numerical modelling

Numerical modelling of chemically reacting flow problems can be achieved by solving equations for conservation of mass, momentum, energy and the concentration of every chemical species along with equations of state and thermodynamic relationships. Chemical kinetics couples chemical species with the energy equation via the enthalpy of reaction. Combustion problems where the spatial transport influence can be ignored, such as plug flow reactors can be characterised by the conservation equations expressed via

the kinetic system of coupled *ordinary differential equations* (ODEs) for the species concentrations and energy (temperature) with time as the independent variable. On the other hand, when the transport properties are important (e.g. laminar flames), the conservation equations are coupled partial differential equations with characteristic time and space derivatives [81].

Accuracy of the prediction of the time-dependent behaviour of a chemical system is affected by the performance of the chemical kinetic mechanism and the level of its chemical detail, which for hydrocarbon combustion could be in the range of hundreds of chemical species and thousands of elementary reactions. As the chemical processes grow in complexity, the requirements for simulations and analysis of rather extensive systems of chemical species and reaction mechanisms also increase, while the computational cost of modelling such processes strongly depends on the details of the chemical kinetic mechanism. In adiabatic systems or in systems with a defined heat loss rate, where the transport term is neglected, the number of equations in the kinetic systems of ODE is equal to number of chemical species N in the reaction mechanisms plus the energy (or temperature) equation, yielding $(N+1)$ equations. Both the computer memory and the CPU time required increase approximately as $(N+1)^2$. In case of the presence of transport properties this has to be solved for each spatial zone, additionally to conservation of mass and each momentum equation, with as many as 30-40 spatial zones required for each dimension for a simple problem, so that two dimensional problems can contain 1000 zones, whereas 30000 zones can be observed for three dimensional problems. As detail and complexity of the problem grows, the required number of spatial zones rises rapidly. Moreover, these equations have to be solved at each time step and, since these equations are coupled, they have to be solved simultaneously to determine the state of the system. Hence, the computational load increases enormously and the implementation of fully detailed chemical kinetic mechanisms into three-dimensional computational fluid dynamic (CFD) simulations is extremely computationally expensive [81, 117]. While more expensive computational techniques increase the accuracy in the prediction of heat release rates and peak pressures, single-zone simulations are favoured for studying trends and relative fuel properties. Often a trade-off has to be made between the intricacies of fluid dynamics and the level of detail in chemical kinetic mechanism depending on the objective of the study. Single-zone simulations, that assume spatial homogeneity and no multi-dimensional fluid transport, are computationally efficient and reliable for simulating ignition delay times in fundamental devices, such as an RCM [125]. The

following sections provide a brief description of the governing equations required for numerical modelling of zero-dimensional (single-zone) homogeneous reactors, which was employed in detailed chemical kinetic modelling investigations in this thesis.

2.2.5 Conservation of mass

The model of the thermodynamic system of an RCM reactor is a closed system, thus there is no mass flowing in and out of the system. Therefore, the total mass of the mixture is constant:

$$m = \sum_{j=1}^{K} m_j, \quad and \quad \frac{dm}{dt} = 0 \qquad (2.52)$$

where m is the mass of the reactor content, t is time, m_j is the mass of the jth species and K is the total number of species in the mixture [126].

2.2.6 Conservation of species

The chemical reactions are the source term in the energy equation, where the temperature changes based on the energy being converted from one state to another due to reactions. Therefore, the source term of the species conservation equation details the formation or consumption of species j in chemical reactions [126]. The rate at which specie j is produced in a homogeneous phase reactions and closed system of an RCM reactor is:

$$\dot{m}_{j,gen} = V\dot{w}_j M_j \qquad (2.53)$$

where M_j is the molecular weight of each species, w_j is the molar rate of production of each species by gas-phase chemical reaction per unit volume, and V is the volume of the reactor, which may vary in time.

If the surface reactions are not considered, the rate of change in the mass of each species is given by:

$$\frac{d(mY_j)}{dt} = v\dot{w}_j M_j \qquad (2.54)$$

where Y_j is the mass fraction of each species, $v = V/m$ is the specific volume, M_j is the molecular weight of each species and w_j is the molar rate of production of each species by gas-phase chemical reaction per unit volume.

2.2.7 Conservation of energy

Thermal energy is conserved in the chemical reacting flow systems, and the energy equation is used as the basis for such reactors. The equation derived from the first law of thermodynamics for a pure substance in an adiabatic, closed system is:

$$\frac{dU}{dt} + P\frac{dV}{dt} = 0 \tag{2.55}$$

where U is the specific internal energy, P is the reactor pressure and V is instantaneous reactor volume. The law of conservation of energy for the ideal gasses in the reaction chamber is:

$$c_v \frac{dT}{dt} = -P\frac{dv}{dt} - \sum_j u_j \frac{dY_j}{dt} \tag{2.56}$$

where c_v is the specific heat at constant volume of the mixture, v is the specific volume, u_j and Y_j are the specific internal energy and mass fraction of the species j, and t is time[127].

2.2.8 Solving the governing equations

Finding a numerical solution require solving the system of differential equations describing mass, energy and species concentration that calculate the chemical kinetic and thermodynamic properties in each differential element as time proceeds. This enables simulation of reactions that result in heat release and the ignition characteristics of the fuel-air mixtures, such as ignition delay times. The integration of these equations is performed in time steps through the implementation of the integration control. This is required to maintain the convergence of the solution ensuring that the species, temperature and pressure do not change significantly in any one time step providing the accuracy of the overall calculation [85]. These predictions then can be compared to or validated against experimental data from one or more well-characterised combustion apparatuses, in this work from RCM experiments. There are different software packages available that are used in simulating chemical reacting flow systems such as Reaction Design's CHEMKIN suite and Chemkin-Pro[128], OPENSMOKE [129], CANTERA [126], LOGESoft [130], FlameMaster [131], DETCHEM [132]and Workbench [133] etc. This study models the chemical reaction flow systems using CANTERA and CHEMKIN software packages.

2.2.9 CANTERA

The Cantera software was originally written and developed by Prof. Goodwin, D. G. of California Institute of Technology with significant contributions from Moffat, H. at Sandia National Laboratories and several [134]. The Cantera C++ library for chemical kinetics, thermodynamics and transport processes is an open source and object-oriented software that integrates with Python, MATLAB, C++ and Fortran. Cantera is able to read and interpret a range of reaction mechanism formats and thermodynamic data formats, such as those used by Chemkin and NASA, and set up a framework for modelling combustion using detailed chemical kinetic mechanism [134]. It has capabilities to perform stiff chemical kinetic integration and work in conjunction with built-in reactor functions. The rate of reaction steps can vary and may spread over many (10-25) orders of magnitude. Such differential equations are known as stiff ODEs. The numerical solution of stiff systems of ODEs can impose severe step-size limitations on the numerical method [117].

In Cantera, extensive thermodynamic data is stored in the Solution classes. For this work, the Solution classes required two independent properties, namely temperature and pressure, plus composition to set the state. The thermodynamic data for each species is read from a file in the CTI format. To model homogeneous reacting systems, such as RCMs, the two objects namely Reservoir for air, and IdealGasReactor for fuel mixture were used. The state of the Reservoir is fixed, whereas for the IdealGasReactor it is not fixed [127]. Cantera presents more user controllability, and is an appealing tool for scientists interested in creating model specific to their research question. It enables full control and versatility in terms of both the simulations and the results. This was found especially beneficial in conducting a brute-force sensitivity analysis in this work.

2.2.10 CHEMKIN

Chemkin is a Fortran-based software tool that was designed at Sandia National Laboratories to provide general capabilities to represent multicomponent thermodynamics, transport and reacting chemistry in chemically reaction flow simulations to model Continuous Stirred Reactor (CSTR) reactions and premixed flames as well as carry out sensitivity analysis [134]. Chemkin is a popular choice for chemical reacting flow problems due to its built-in models for such. Chemkin-Pro combines the leading functionality and most recent numerical algorithms and methods to deliver accurate and fast results, which enable the solver to perform complex simulations 100 times faster than previous versions of Chemkin and competing codes. Among others, it

incorporates a Reaction Path Analyser useful in investigations of reaction paths and Reactor Networks, which enables simulation of complex chemical reactors, such as RCMs [128].

2.2.11 Zero dimensional model

Zero dimensional (0-D) models function on basis of the first law of thermodynamics and mass balance by using the mass and energy conservation equations, along with the gas state equation, which are solved in their differential form, so that the parameters of the gas within the reactor, such as pressure, temperature and gas composition can be simulated. The mixture is considered to be perfectly mixed with a spatially uniform temperature and chemical composition so that the entire reactor is assumed to be a single homogeneous zone. Therefore, there is no spatial gradient throughout the combustion chamber and spatial variation of thermodynamic (pressure, temperature, composition, etc.) and transport (viscosity, thermal conductivity, diffusion coefficients) properties are assumed to be negligible, which eliminates the need to spatially define the temperature. However, in real chemical reacting systems the temperature flow field is rarely homogeneous with the presence of a boundary layer and non-uniform heat release, especially during the two-stage ignition phenomenon. In the RCM, the core temperature region deviates from the temperature that would be calculated based on an isentropic compression due to heat loss and radical pool effects. Several empirical heat release models with time as the only independent variable try to replicate the heat losses, considering a constant volume after the end of the compression. Although the implementation of these heat loss models in the zero-dimensional approach attempts to capture these multi-dimensional effects, they tend to overestimate the overall heat release rate, because they underestimate heat losses. Alternatively, the adiabatic core assumption to an effective volume, $V_{eff}(t)$, which is the volume that is obtained from the non-reactive experimental pressure considering an isentropic compression. More details on this are provided in Chapter 3. Finally, in the zero-dimensional model, the conservation of momentum is not considered and all chemical species are considered to behave as an ideal gas [78, 135, 136].

2.2.12 Chemical kinetic mechanism

Models based on detailed chemical kinetic mechanisms are capable of replicating hydrocarbon oxidation process, which can be attributed to their core methodology in describing at the molecular level the chemical transformations of reactants to intermediate and product species, as well as thermal energy, taking place during the reactions [77, 80].

A chemical kinetic mechanism consists of the comprehensive record of species with their thermodynamic parameters and elementary reactions, which are the stoichiometric equations of the reaction step corresponding to real molecular changes, and their associated rate constants and third body collision efficiencies. In addition, numerical problems encompassing diffusion involve the values of all transport parameters [85, 117]. This molecular method has two consequences. First of all, it facilitates the systematic and hierarchical development of kinetic mechanisms by sequentially implementing similar reaction classes and gathering well-recognised general reaction schemes to the primary oxidation reactions of the fuel molecule and its derived species [137]. However, there are some dissimilarities in reaction classes between different research groups as comprehensively detailed in the Battin-Leclerc literature review [77] of the combustion of alkanes. Secondly, fuels involving heavy molecules, generally above 6 carbon atoms, contain complex mechanisms. This subsequently results in two approaches used in developing these chemical reaction mechanisms based on whether they are computer aided or not [137]. Schemes produced without computer assistance, are generally created iteratively by modules, starting with smaller esters and advancing to larger ones. These includes some of mechanisms from Lawrence Livermore National Laboratory (LLNL). On the contrary, computer-aided schemes do not capture the earlier sub-mechanisms and are generally smaller, owing to tailoring of mechanisms to the problem. Therefore, for example, EXGAS software may only initiate the major classes of reactions for the specific temperature range [137].

The process for developing and validating chemical kinetic models has been formerly outlined by Frenklach et al. [138] and summarised by Simmie [80]. Generally, these models are validated by modelling a broad range of experimental targets at various temperature and pressure regimes, such as ignition delay times, flame speeds and species concentration data in flow and jet-stirred reactors, shock tubes and RCMs as described earlier in Section 2.1.15. Details of experimental physical environments and measurements including any uncertainty bounds, as well as potential standardisation of experimental results and physical conditions to enable comparisons between the results of different scientific groups/experimental facilities, are required to facilitate the development and validation of chemical kinetic mechanisms. The comprehensiveness and detail of a chemical kinetic mechanism can be defined by its competence in performing well in describing combustion phenomenon broadly. Indeed, as it has been demonstrated in Sections 2.1.7 and 2.1.8, there are quite substantial differences in the reaction

mechanisms driving chemistry at low temperatures compared to that of the high temperatures, which can lead to different chemical consequences. A comprehensive chemical reaction mechanism should be able to model a fuel's oxidation covering an extensive range of physical conditions including mixture compositions, temperatures and pressures. The scope, performance and predictive capability of a chemical kinetic mechanism depends on whether or not all of the required reaction pathways and relevant product channels are incorporated within the mechanism and whether the values/accuracy of the rate constants, thermochemical and transport data are appropriate [85].

2.2.13 Surrogate mixtures

The chemical kinetic processes that result in fuel oxidation and the potential auto-ignition phenomenon may entail thousands of elementary reactions with different reaction rates. The size of the chemical kinetic mechanism is usually governed by the magnitude and the complexity of the parent fuel molecule [78]. It is well recognised that the number of reactions and species involved in a chemical mechanism grows almost exponentially with carbon number [139]. Figure 2.26 shows that the size of the mechanism increases almost exponentially as a function of the number of heavy (non-hydrogen) atoms in the reactant molecule(s). On the other hand, there is a linear correlation between the number of the reactions and the number of species in the mechanism [140]. Typically, it is desired that the reaction mechanism details the chemistry as accurately as required for the understanding of particular phenomenon of interest. However, it is generally required to enhance the prediction of the process performances. Due to these immense reaction system networks, especially for complex fuels such as petroleum refined products, and the limitations in computer hardware and software, it becomes extremely difficult to handle these huge chemical reaction mechanisms during simulations [139].
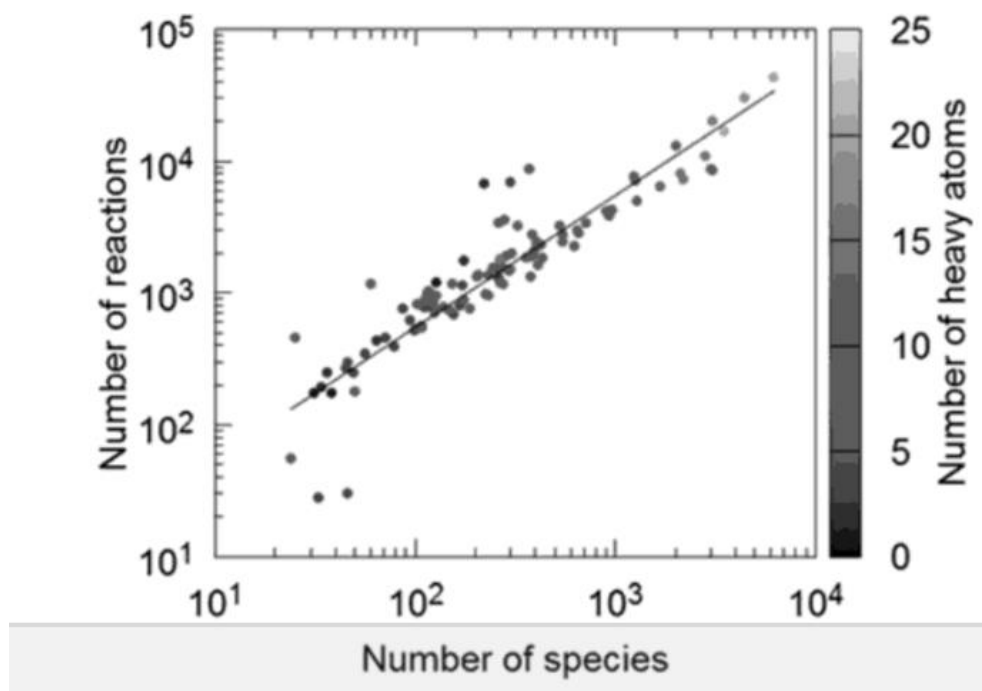
Figure 2.26: The number of reactions as a function of the number of species for gas-phase kinetic models of oxidation and combustion processes. The secondary axis is the number of heavy (non-hydrogen) atoms in the reactant molecule(s) [140].

Practical fuels, such as gasoline, are complex mixtures of hundreds of different hydrocarbons, additives and blending agents. The chemical composition of commercial gasoline varies significantly, depending on the source of the crude oil used, the refinery processes implemented, the additives tailored for optimised drivability depending on the season, the overall balance of product demand and the product specifications. A typical gasoline comprises C_4 to C_{10} n- and *iso*-paraffins (alkanes), olefins (alkenes), naphthenes and aromatics in varying proportions as shown in Figure 2.27 along with their corresponding structures. To enhance the performance and stability of gasoline, additives and blending agents, such as anti-knock agents, anti-oxidants, oxygenates, metal deactivators, lead scavengers, anti-rust agents, anti-icing agents, detergents, upper-cylinder lubricants, dyes and others, are commonly added to the hydrocarbon mixture [7, 141].
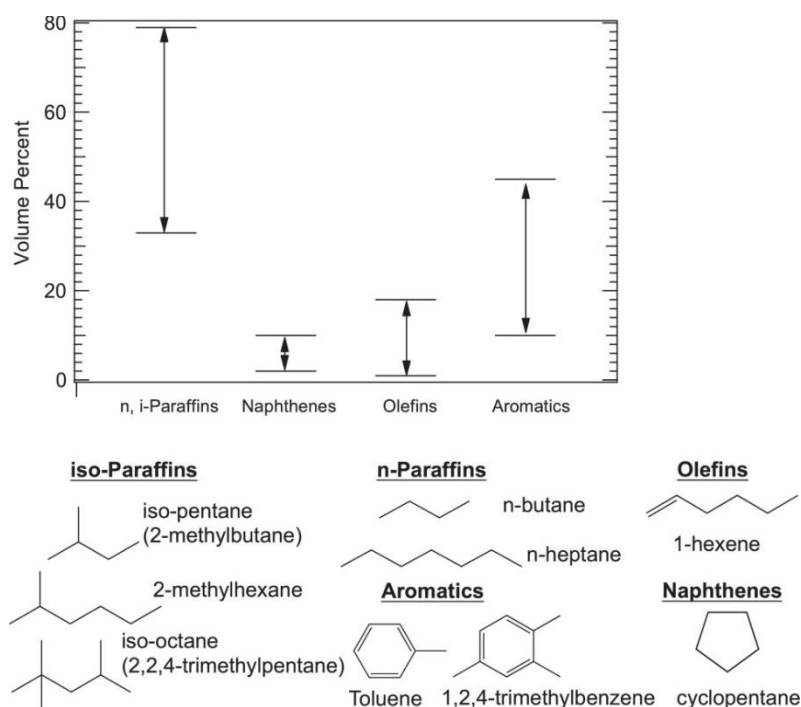
Figure 2.27: Ranges of hydrocarbon classes found in U.S. gasoline along with the representative molecular structures in gasoline fuels [7].

This nature of gasoline mixtures makes it practically exceedingly challenging to model exactly the chemistry of each individual component. Therefore, it is required to reduce the chemical and physical complexity of the simulation through the representation of gasoline with a simplified surrogate fuel. Surrogate fuels consist of reduced numbers of selected neat constituents blended together to emulate a real gasoline's target combustion characteristics. There can be either chemical (e.g. auto-ignition characteristics) or/and physical characteristics (e.g. viscosity, distillation curve). These fuels present a fixed datum for experimental studies, which in contrast to real gasoline is invariant with the season and location. The suite of species produced during the combustion is also quite substantially decreased due to the limited number of components in the surrogate fuel. The behaviours of such fuels are more elaborate compared to that of singular fuels since intermediate species from one component can interact with species from another component or with the radical pool [7, 141, 142]. However, detailed chemical kinetic mechanisms have been developed for these more complex mixtures, as recently reviewed by Sarathy et al. [7], employing conventional methods that couple the sub-mechanisms of singular constituents used to formulate the surrogate.

The original gasoline surrogate consisted of primary reference fuels (PRFs), *iso*-octane and *n*-heptane, has dominated fuel ratings in spark ignition engines especially due to their relationship to RON and MON [143]. However, they are unable to match some targets,

in particular the hydrogen to carbon (H/C) ratio and Octane Sensitivity, exposing a need for more sophisticated surrogate formulations. This motivated the research of ternary surrogate mixtures, such as toluene reference fuels (TRFs), which are mixtures of *iso*-octane, *n*-heptane and toluene as studied by Chaos et al. [144] in a variable flow reactor and Gauthier et al. [145] comparing ignition delay predictions with those obtained from gasoline shock tube experiments. In addition, the PRF surrogate has been expanded to also involve olefins as studied by Vanhove et al. [146], who used a ternary blend of *iso*-octane, 1-hexene and toluene. Kukkadapu et al. [147] also studied the TRF surrogate and a four-component mixture that involved the addition of olefin (2-pentene) to the first mixture. The composition of their surrogate fuel was targeted to replicate the relative content of alkanes, alkenes and aromatics in the studied gasoline, as well as its RON and MON values [147]. Using an RCM, the authors showed that the four-component surrogate fuel mimics the behaviour of the real gasoline relatively well. However, this is debatable as the model failed to accurately predict the NTC behaviour, which could be due to fidelity of the reaction mechanism or the adequacy the surrogate formulation. Puduppakkam et al. [148] by employing Reaction Design's Surrogate Blend Optimizer formulated gasoline surrogates based on the distillation curve, H/C ratio, and estimated RON and MON values, which showed adequate performances in replicating combustion behaviour of engine experiments and modelling them with CFD numerical tools, apart from a few exceptions.

The gasoline surrogate model by Mehl et al. [143] is an important contribution that using conventional methods combined the kinetic models of *iso*-octane, *n*-heptane, toluene and 1-hexene into a single mechanism. The model was validated against an extensive experimental dataset including ignition delays, laminar flame speeds and species concentration profiles from a JSR. This model later has shown adequate performance in replicating ignition delay data as presented in [43, 149, 150]. A different method was used by Dooley et al. [151, 152] who applied group additivity theory [153] to formulate surrogate fuels based on composition of molecular functional groups instead of hydrocarbon classes. The authors implemented this approach and developed their surrogates by targeting a real jet fuel's average molecular weight, H/C ratio, derived cetane number and threshold sooting index, which showed satisfactory performance under a broad range of fundamental combustion experiments. Despite the effectiveness of the method and surrogate fuel performance, it still relies on accurate modelling of individual compounds that involve the functional groups for the surrogate formulation

[154]. Complex surrogate fuels containing up to six component [155, 156] and seven component [141] mixtures have also been proposed to represent gasoline. For such complex surrogates, the size of the kinetic scheme becomes significant and the collective uncertainty of kinetic and thermodynamical parameters grows drastically [144].

Similarly to the earlier discussion, the number of chemical compounds in the surrogate fuel would impact the accuracy of the model and the efficiency of the computations. Therefore, a compromise has to be made between the number of components, hence the possible accuracy with respect to the gasoline chemistry, and the time required for both chemical modelling and experiments. All these chemical compounds vary in oxidation chemistry and when mixed together for practical use, can interact considerably during the oxidation [154]. Despite the complexity of these fuels' chemical interactions, they are rarely assessed. The chemical interactions between oxygenated additives, such as ethanol and butanol, and other surrogate fuel hydrocarbon components are particularly sophisticated processes. Also, the effect of addition of such oxygenated compounds to the surrogate mixture on combustion characteristics such as ignition delay times is especially intricate due to the complexity of the chemical kinetics involved. This was demonstrated by recent studies that found extremely non-linear blending behaviour in the octane number of ethanol/hydrocarbon fuel mixtures [157, 158], in which super-linear (synergistic) octane number of ethanol/paraffins mixtures was found in contrast to extremely non-linear (antagonistic) blending for ethanol/aromatic mixtures. Whereas correlations have been recommended to assess these non-linear blending behaviours [159, 160], the chemistry producing such blending behaviour has not been fully understood.

Agbro et al. [41] examined the ability of a pure TRF and n-butanol/TRF mixtures to replicate the behaviour of gasoline and n-butanol/gasoline blends and demonstrated a relatively good agreement between these fuels. Ignition delay times of the TRF mixture displayed similar trends to that of gasoline. However, they were consistently longer than those of gasoline. This can be potentially attributed to the recent requirement of addition of ethanol to conventional gasoline mixtures. Agbro et al. [42] complemented this study with further experimental and modelling investigations of knock onsets of this surrogate fuel and its blend with n-butanol in a strongly supercharged SI engine. They showed that similar to previous results of ignition delay times Agbro et al. [41], the simulated engine onsets were consistently higher than the measured data. The authors highlighted the importance of the low and intermediate temperature chemistry, and accurate representation of LTHR and ITHR within SI engines in influencing the high-temperature

heat release and consequently the overall knock onset. This behaviour is not however, currently fully understood.

This therefore motivated the study of the effects of *n*-butanol addition to TRF and a representative gasoline on the auto-ignition characteristics in this work as described in Chapter 5, and the heat release analysis as detailed in Chapter 6. Based on the literature review on surrogate fuels the mixture of Agbro et al. [41] has been proposed to numerically study the behaviour and ignition characteristic of real gasoline and butanol/gasoline mixtures. Also the chemistry driving these processes and the performance of a kinetic model to simulate the oxidation of the fuels studied is assessed in this work.

2.2.14 Methods for kinetic model assessment

As mentioned above, the detailed chemical reaction mechanisms of hydrocarbon oxidation may comprise several thousands of elementary reactions. As the reaction mechanism increases in size and complexity, the topic of sensitivity analysis and reaction pathway analysis becomes more and more crucial [81]. Uncertainties in reaction rate parameters, transport coefficients, thermodynamic properties, initial and boundary conditions, and other kinetic model characteristics may raise uncertainties in modelled results and affect the accuracy and performance of the predictive capability of the reaction mechanism [81]. During the detailed chemical reaction mechanism development process, a series of elementary reactions are compiled, whose reaction rate parameters may be established from individual rate measurements, reaction rate theory, or a combination of both. For large hydrocarbon fuels, large number of reaction pathways as well as rates has to be calculated based on the extrapolation of knowledge of smaller species reactions, which introduce further uncertainties [161]. Moreover, some of the rate constants are frequently tuned within their uncertainty limits for satisfactory model prediction accuracy [162]. Therefore, the impact of these cumulative uncertainties on chemical accuracy is questionable, as well as whether useful predictions of the intricate nature of the combustion phenomenon can be made. The model uncertainties could also originate from incomplete physics and missing reaction pathways within the model [161]. Sensitivity analysis and reaction pathway analysis provide the means of assessing the reaction progress of the species and help to determine the main input parameters that drive uncertainties in model prediction [117]. Sensitivity analysis determines the rate-limiting or rate controlling reaction steps, while reaction pathways analysis identifies the dominant reaction paths.

2.2.15 Sensitivity analysis

Sensitivity analysis describes mathematical methods that can be used to examine the relationships between the values of input parameters of a model and its predictions [117, 163]. Sensitivity analysis reveals which are the dominant control parameters in the model, which are the indirect impacts of parameter changes and generates knowledge about the structure of the model, so that the important parameters can be prioritised for model improvement. Sensitivity analysis can also be used for mechanism reduction, in other words, evaluating the reactions in the mechanism and identifying a smaller mechanism that depicts almost identical results for particular variables (e.g., species concentrations and temperature) [164]. Within combustion science, sensitivity analysis can be used to examine how the changes in rate parameters or thermodynamic data impact the performance of the model in predicting the main target parameters such as ignition delay times, flame speeds or species concentration profiles to provide kinetic insights into model and its strengths and weaknesses with respect to experimental measurements [163].

A first-order local sensitivity analysis determines the derivative of a model output with respect to model parameters [79, 161]. The change in the model output (e.g. concentration) in time for spatially homogeneous (zero-dimensional) reaction systems can be determined by the following ODE [117, 163]:

$$\frac{dY}{dt} = f(Y, x), \quad Y(t_0) = Y_0 \tag{2.57}$$

where the parameter vector x having m elements may involve any physically definable input parameters of interest, such as rate constants, Arrhenius parameters, thermodynamic data etc. The species concentration Y is the dependent variable, time t is the independent variable and Y_0 is the initial concentration. The effect of changes in parameter set x on the modelled concentrations Y at a given time can be introduced by a Taylor series expansion [117, 163]:

$$Y_i(t, x + \Delta x) = Y_i(t, x)$$
$$+ \sum_{j=1}^{m} \frac{\partial Y_i}{\partial x_j} \Delta x_j + \frac{1}{2} \sum_{k=1}^{m} \sum_{j=1}^{m} \frac{\partial^2 Y_i}{\partial x_k \partial x_j} \Delta x_k \Delta x_j + \cdots \tag{2.58}$$

where the partial derivative $\frac{\partial Y_i}{\partial x_j}$ is the first-order local sensitivity coefficient, $\frac{\partial^2 Y_i}{\partial x_k \partial x_j}$ is the second-order local sensitivity derivative, etc. The local sensitivity coefficients demonstrate the change in the model output Y_i owing to a small change in input parameter

x_j compared to its nominal value by keeping all other parameters unchanged. The sensitivity matrix $S = \left\{\frac{\partial Y_i}{\partial x_j}\right\}$, which elements are the local sensitivity coefficients, therefore represents the linear approximation of the impacts of parameter changes on the model prediction of the solution. In order to account for differences in units of parameters and the various output quantities of a model, the sensitivity coefficients are often normalised forming a normalised sensitivity matrix $S = \left\{\frac{x_j}{Y_i}\right\}\left\{\frac{\partial Y_i}{\partial x_j}\right\}$, where normalised sensitivity coefficients represent a fractional change in concentration Y_i caused by a fractional change of parameter x_j [117, 163, 164].

Several approaches to calculate the local sensitivities have been developed over the years, including the brute-force method [164], the Greens function method [165] and the decoupled-direct method [166]. The simplest method is the brute-force method, where each input parameter is perturbed in turn by a small percentage around the nominal value, re-running the model and then calculating the sensitivities of the selected results to the change by comparing the outputs to a reference or baseline case [117, 163, 164]. When the model output undergoes significant changes as the parameter is modified, the sensitivity to that parameter is high. The results can be ranked accordingly to measure the importance for each parameter with respect to important targets in the scheme. For combustion problems, when rate parameters are under investigation, the rate constants of elementary reactions with high sensitivities would have a great influence on the outputs of mathematical modelling, such as ignition delay times, and hence the rate constants for these reactions would require accurate evaluation. To calculate the sensitivity matrix using this method, *m+1* simulations have to be executed, one for the baseline case and one for the perturbation of every parameter [163]. The brute-force method becomes exceedingly expensive as the number of species, zones and parameters grows [81]. However, for zero-dimensional models such as jet stirred reactors this can be viable even for complex mechanisms, because the simulation times would be relatively small [163].

2.2.16 Reaction pathway analysis

Reaction pathway analysis is a useful tool in investigating complex chemical reaction mechanisms, which provides the means to quantify the activity of species such as the flow of conserved property from one species to another in a reaction mechanism. Element flux diagrams portray the dominant reaction pathways and underline the major and minor channels within a scheme by characterising the intensity of fluxes through arrow thickness. This can be used for the simplification and reduction of mechanisms. Also the

reaction pathway analysis can be used to analyse the reaction chain that shows how other species contribute to the formation of a specific species under examination [117].

These diagrams can illustrate different features of the flux, such as the total net reaction rate along a pathway, or the flux of a specific element associated with the reaction. They may also be time specific or show integrated fluxes over a selected modelled extent of time, hence an appropriate description of the figure and its exact meaning has to be provided in order to interpret these figures [117]. A local reaction flow analysis examines the formation and consumption of species locally, thus at specific times in time-dependent problems (e.g. ignition processes) or at specific locations in steady spatially dependent processes (e.g. laminar flame). An integrated reaction flow analysis takes into account the total formation or consumption of species, so that the results for homogeneous time-dependent systems are integrated over the entire or selected time period, while results from steady spatially dependent systems are integrated over the reaction zone [79]. An example of a C-atom element flux diagram of a local reaction flow analysis is given in Figure 2.28 for methane combustion.
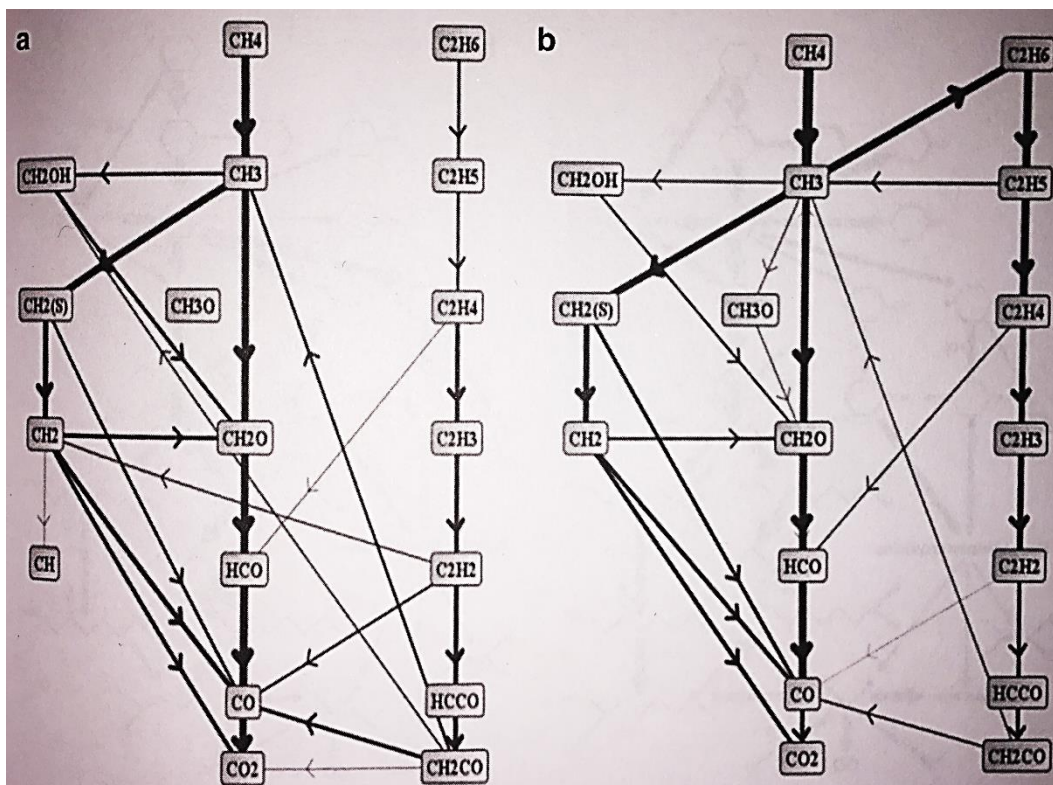
Figure 2.28: Carbon atom element flux diagram for an atmospheric freely propagating CH_4/air flame, at the location where the temperature is (a) 1500 K, (b) 1805 K [117].

In a closed chemical reacting system, the amount of the element in moles is one of the conserved properties. The instantaneous element flux of element A atom from species j to species k through reaction step i can be calculated by:

$$A_{ijk} = \frac{n_{A,j} n_{A,k} r_i}{N_{A,i}} \qquad (2.59)$$

where $n_{A,j}$ and $n_{A,k}$ are the number of atoms A in species j and k, respectively, and $N_{A,i}$ is the sum of numbers of atoms A on either side of reaction step i in all species, while r_i is the instantaneous rate of reaction i (mol/s) [117].

The total instantaneous flux between species j and k, taking into the account all viable reaction steps that contribute to transformation process, can be then calculated by adding all of the element fluxes at a given time t together:

$$A_{jk}(t) = \sum_{i}^{N_R} A_{ijk}(t) \qquad (2.60)$$

where N_R is the number of reactions in whom these species participate as reactants or products. The atomic fluxes for particular elements (C, H, O, and N) are calculated based on reaction rates at each time step using the above equations (2.59) and (2.60) and arranged in descending order; active source-sink pairs can be determined by setting a cut-off value on the atomic flux [167]. Since the ignition processes of hydrocarbons are studied in the present work, hydrogen element flux analysis is used, where the active species are determined setting a cut-off on the hydrogen flux.

2.3 Alternative fuels

2.3.1 Natural Gas

Natural gas has drawn growing attention as a way to reduce the dependence on crude oil and attempts to tackle environmental concerns. Predominantly consisting of methane, CH_4, natural gas is a combustible colourless and odourless mixture of hydrocarbons in its pure form derived from oil or gas fields and coal mines, but commonly containing varying amounts of other higher alkanes such as ethane (C_2H_6), propane (C_3H_8), butane (C_4H_{10}), pentane (C_5H_{12}), and sometimes smaller proportions of carbon dioxide, nitrogen, hydrogen sulphide or helium. Contrary to other fossil fuels, its reserves are relatively uniformly spread across the world providing energy market security and access to a

plentiful energy resources for oil-deficient countries with the current total global gas reserves of approximately 187 trillion m^3 [168]. It continues to be the fuel of choice for the electric power and industrial sectors in many regions partially due to its low carbon intensity compared to coal or oil. Moreover, it is an appealing fuel for new power station plants because of its relatively low capital costs and the beneficial heat rates for natural gas generation [30]. The accessible domestic resources, well-established re-fuelling and distribution infrastructure, supporting governmental policies encourage the increased integration of natural gas vehicles into the transport sector, particularly for heavy duty vehicles [169].

Natural gas is classified by soot-free combustion when utilised in ICEs [169]. Its high octane rating favours its use in SI engines rather than CI engines. The short carbon chain, simple and stable molecular structure encompassing only carbon-hydrogen bonds, all facilitates effective fuel resistance to the knocking phenomenon [170]. A better anti-knock quality of natural gas SI engines facilitates higher compression ratios and hence higher thermal efficiencies compared to their gasoline counterparts [171]. Vehicles can be designed to run only on natural gas with dedicated soot-free SI or be 'bi-fuel', capable of running on both natural gas and conventional fuels which would have higher soot emissions [8, 169]. Some countries such China, Iran, Pakistan, Argentina and Brazil commonly use natural gas in passenger vehicles, with approximately 24 million natural gas vehicles on the road globally today, although its share of global transport energy is less than 1% [8].

Being a primary compound of natural gas, methane has the highest hydrogen to carbon ratio among all hydrocarbons, which manifests in natural gas engines having low specific CO_2, UHCs and CO emissions compared to conventional gasoline [171]. By replacing gasoline by natural gas, it is possible to achieve 30-35%, 20-30% and 30% reduction in emissions of UHCs, CO and CO_2 respectively, in combination with downsizing, increased compression ratios, appropriate exhaust gas recirculation (EGR) use and careful optimisation [171, 172]. Moreover, natural gas engines display lower particulate matter emissions compared to diesel engines, since they do not include aromatic compounds such as benzene, as well as reduced amounts of impurities (e.g. sulphur) compared to petroleum fuels [173]. However, if operated at stoichiometric conditions, the high flame temperature of natural gas could cause elevated NOx emissions. Hence, lean burn technologies or appropriate exhaust after treatment strategies are preferable to meet emissions regulations with careful monitoring of fugitive and tailpipe methane emissions

which is a key weakness of dual fuel engines [171]. Methane emissions from unburnt methane from natural gas vehicles are more severe GHG emissions and have a much higher global warming potential than CO_2, although not currently regulated. Notwithstanding natural gas is often regarded as a temporary fix to environmental issues, since it is still a fossil fuel with just comparatively lower CO_2 emissions. On the other hand, sustainably produced renewable natural gas from biomass generated by the anaerobic digestion or through the thermal gasification, can potentially offer a greater GHG benefits compared to fossil fuel based natural gas.

Despite having a higher energy density on a mass basis, the energy density of natural gas on a volume basis is lower compared to gasoline or diesel. At atmospheric pressures and temperatures, a litre of natural gas has approximately 800 times less energy density than a litre of gasoline [8]. Therefore, it is generally compressed or liquefied to achieve higher molecular weights and hence energy that is stored in a restricted volume of the fuel tank in the form of gaseous compressed natural gas (CNG) under 20 MPa or liquefied natural gas (LNG) under extra low temperature (-435 K) at atmospheric pressure. While the CNG concept is suitable for urban transport systems with an easy access to the refuelling infrastructure, the LNG concept is an especially attractive alternative fuel in commercial transport applications such as long-haul fleets, heavy duty vehicles, rail and marine, where there are few alternatives available to conventional gasoline and diesel due to the driving range requirements, reliability and cost. The higher cost of LNG infrastructure can be easily recovered through savings in the fuel cost and larger fuel consumption in such long haul transport applications. However, reliability concerns associated with natural gas engines in terms of vehicle range, lowered by up to 40% due to the limited fuel tank size for CNG vehicles, and overall engine durability that increases the downtime and maintenance costs continue to favour their diesel fuelled counterparts [8, 169]. Stringent emission legislation may alter the balance towards the implementation of natural gas fuel.

2.3.1.1 *Modelling methane oxidation*

Methane is a major constituent of natural gas, comprising more than 90% by weight. It is also one of the simplest hydrocarbon fuels with relatively simple oxidation processes compared with those of heavier hydrocarbons. Therefore, the chemical kinetics of methane is relatively well established and provides generally a satisfactory description of oxidation chemistry over the broad range of thermodynamic conditions. Indeed, with an increase in the complexity of the fuel, the complexity and the uncertainty in the predictive

capability of the reaction mechanism also increases, which could be attributed to the numerous degrees of freedom and reaction pathways that a detailed kinetic scheme has to take for the comprehensive illustration in the combustion of the specific fuel, especially at low temperatures and high pressures [174].

There is a vast number of kinetic mechanisms describing methane oxidation available in the literature, which are usually set to replicate combustion phenomenon at specific conditions. Typically, the range of effectiveness of these mechanisms, in terms of initial fuel concentration, operating environment and chemically reacting systems varies broadly, usually with each novel mechanism offering improved capabilities in predicting combustion phenomenon over the years [175].

Initial chemical reaction mechanisms for methane oxidation developed between 1958 and 1978 (e.g. [176-178]) contained a limited amount of species and reactions, and were commonly advanced through the addition of chemical species and representative reactions for hydrogen and carbon monoxide oxidation. Successive methane mechanisms consisted of larger numbers of species to account for molecular growth reactions wherein radicals derived from methane could recombine to form larger hydrocarbons (e.g. C_2H_6, C_2H_4 etc.) especially under rich conditions [175]. Advances in reaction rate constant measurements and calculations over the years led to improved detailed chemical kinetic models, with a plethora of methane oxidation models with broadly varying rate parameters published since 1995. This is potentially due to uncertainties in the measurements/calculations and due to the requirements to simulate different global combustion data, such as ignition delay times, speciation profiles, laminar flame speeds, flame extinction and ignition, flame structure, etc. In order to tackle problems related to uncertainty, GRI-Mech carried out a mathematical optimisation to fit reaction rate constant parameters against a variety of experimental measurements that culminated in the generation of GRI-Mech, one of the most popular methane oxidation mechanisms to date [85, 175].

One of the benefits of GRI-Mech can be attributed not just to the extensive range of its validated applicability, but due to the fact that it was one of the first to be made freely available on the internet. More recently, there were several detailed chemical kinetic mechanisms developed, such as San Diego Mech [179], USC Mech II [180] and JetSurf [181] in addition to the CRECK mechanism from the Politecnico di Milano [182], AramcoMech [183-186] from NUI Galway, Glarborg Mech [187] and Leeds mechanism

[188] from the University of Leeds, which all facilitate numerical modelling studies of the oxidation of small hydrocarbon systems. All of these mechanisms have emerged from fairly distinctive, but at the same time very much alike, versions of an identical mechanism comprising analogous reactions but with different rate constants [85]. Thus, it is imperative to know the corresponding predictive range of the mechanism in order to achieve the required degree of the accuracy and obtain reliable results.

Owing to the simplicity, vast availability of chemical reaction mechanisms and relatively good understanding of its oxidation chemistry, methane has been selected for the initial numerical work in this PhD project and details of this study are provided in Chapter 4. Furthermore, the high octane number of methane makes it an interesting fuel to study from the view of its anti-knocking potential to assess its detonation propensity and thus make comparisons to that of other fuels. This can aid understanding of the characteristics that drive the transition from harmless auto-ignition to undesirable knocking combustion. This, in turn, can help in the development of SI technologies.

2.3.2 Biofuels

Biofuels are fuels predominantly produced from biomass material - organic matter that can be used as fuels in the transport sector or an energy source in industrial applications [5, 31]. They can be used directly as solid fuels (e.g. charcoal or wood pellets) or converted into liquid fuels (e.g. alcohols and biodiesel) or gaseous fuels (e.g. methane), so that the chemical energy encompassed within the biological material is converted into useful energy via combustion processes [5]. This chemical reaction enables the release of the binding energy that keeps electrons to a nucleus in the biological molecules to produce work or heat [5]. If produced sustainably, biofuels can offer reductions in carbon footprint by the growth of feedstocks used through the photosynthesis in terrestrial biomass, because plants absorb the CO_2 emitted to the atmosphere during combustion processes or via decomposition of vegetation of biological waste. Therefore, they usually are considered to be carbon neutral. Carbon neutrality is attained if CO_2 emissions sequestered and subsequently released are balanced [5, 31]. This highly depends on the location where the feedstock grows, land and cropping management practices, modes of transportation and conversion techniques used [189].

Biofuels are believed to be one of the most promising and strategically important fuel sources in short-term solutions to reduce dependence on fossil fuel, contribute to decarbonisation of the transport sector, diversify the energy mix, provide energy security

and meet rural development goals owing to their market maturity compared to other alternative fuels [13, 190]. Biofuels are an especially attractive choice of fuel in aviation, shipping and heavy goods vehicles, where there are few alternatives to conventional fossil fuels available [31]. However, failure of their sustainable production can lead to serious negative environmental and social impacts, such as over-intensive use of resources, increased water usage, reduction in food security, deforestation, loss of biodiversity, life-cycle GHG emissions, soil pollution, land usage change [13].

2.3.2.1 *Classification of biofuels*

Biofuels can be diverted from various biomass feedstocks, such as biodegradable agricultural, forestry or fishery products, wastes or residues, or biodegradable industrial or municipal waste through different conversion processes such as fermentation, Fisher-Tropsch, transesterification, hydrolysis, hydrocracking, hydrogenation, pyrolysis and gasification among many others [31, 190]. They can be distinguished according to their raw material sourcing, conversion technologies and technical specification of the fuel. Biofuels can generally be divided into primary biofuels, the fuels used in their unprocessed form, and secondary biofuels, the ones produced from biomass. Secondary biofuels can be further categorised into "generations" and "conventional or advanced biofuels" [31, 190]. Biofuels classification according to their feedstock type, as well as their potential benefits and sustainability challenges associated with their production and use, are summarised in Figure 2.29.

First generation biofuels are commonly referred as "conventional biofuels" as their production technologies and processes are mature and well established, such as fermentation, distillation and transesterification [31]. These fuels are derived from dedicated cultivation of bioenergy crops, otherwise used for food production or animal feed, such as sugar- or starch- based crops and vegetable oils (e.g. wheat, corn, sugar cane, sugar beet, palm oil, soybean, rapeseed etc.) [191]. Since first generation biofuels compete with agricultural lands, there are several sustainability challenges associated with the expansion of first generation biofuel production, such as upward pressure on food commodity prices, the risks of increase in GHG emissions through direct and indirect land use change from production of biofuel feedstock and production system emission of pollutants, environmental degradation of land, forests and ecosystems, including biodiversity losses owing to land clearing of biodiverse systems, diversion of agricultural land into fuel production, as well as depletion of water resources [31, 192]. Moreover, an increasing agricultural demand subsequently creates risks associated with

further deforestation and use of land with high biodiversity value to accommodate this demand, in addition to related use of freshwater, fertilisers and pesticides with the negative impact on the environment [31]. These concerns can potentially be addressed by employing the second generation biofuels and hence encouraging the use of non-edible biomass for the production of biofuels.
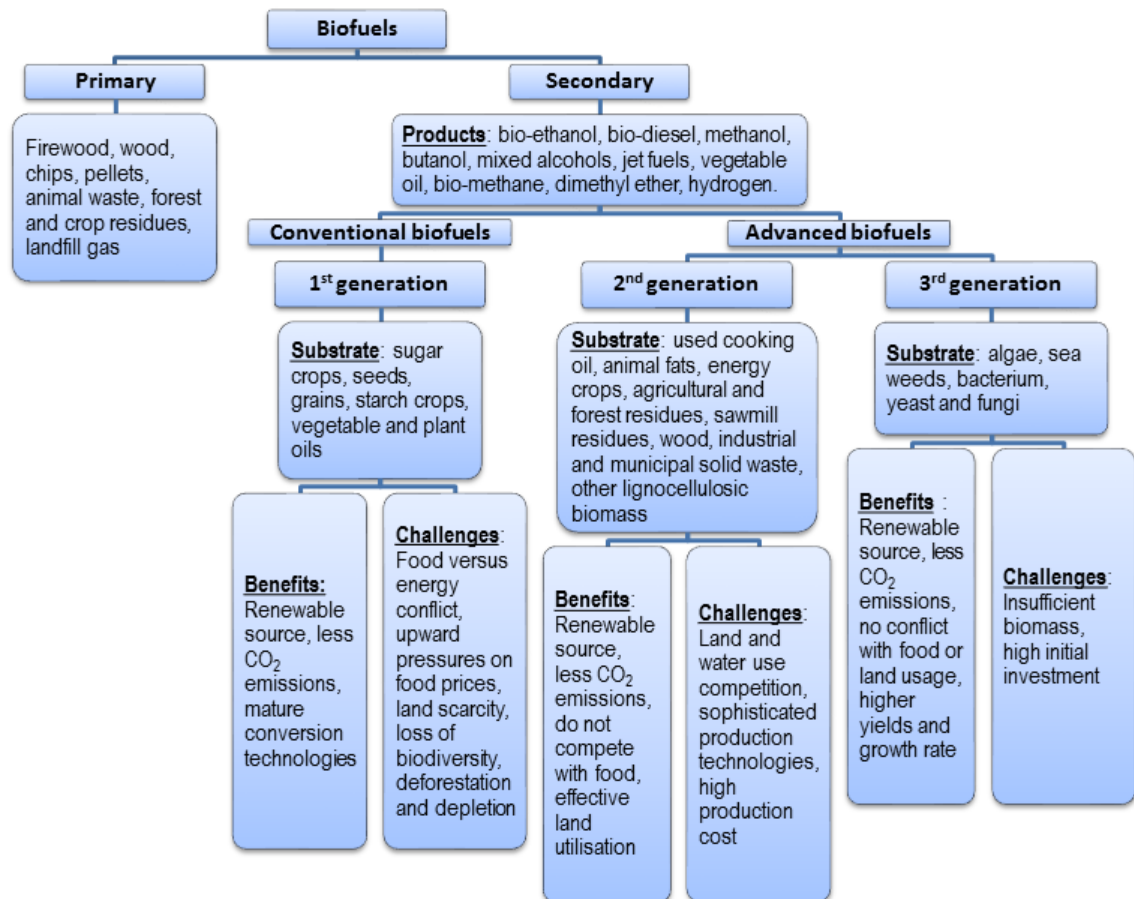
Figure 2.29: Biofuels classification based on feedstock type, as well as associated potential benefits and challenges. This diagram was based on information from [31, 190].

Second generation biofuels are bio-based products which are obtained from non-food feedstocks. These are non-food cellulosic and lignocellulosic plant biomasses containing cellulose, hemicellulose and lignin, such as agricultural residues, forest and sawmill residues, wood wastes, dedicated energy crops (e.g. switchgrass, short rotation coppice and many others) and other waste materials (e.g. herbaceous, industrial and municipal solid waste) [31]. A crucial feature is that these feedstocks cannot be used for food or feed, and therefore they remove any concerns associated with food production of the first generation biofuels. However, unless the feedstock (e.g. Jatropha, Croton) has capability to grow on non-arable land, introducing efficient land exploitation, there is still a potential

conflict of land usage for feedstock grow of energy crops otherwise suitable for food production [31, 191, 193].

Generally, the average carbon footprint of second generation biofuels is significantly smaller when compared to traditional fossil fuels. Lignocellulosic biofuels from agricultural and forest residues show lower emissions than that of energy crops, since the N_2O emissions during the cultivation of energy crops associated with pesticides and fertilisers are withdrawn in the case of residues [31]. However, the production of second generation biofuels has proved to have lower efficiency due to low yield production and involves complicated process technologies, hence more investment per unit of production and larger facilities are required to accommodate the capital costs [190]. Also, due to low conventional fuel prices, the economic feasibility of some of these biofuels is questionable in the present economical environment [31].

Despite the negative values of GHG emissions for some of second generation biofuels, their capacity to significantly lower the carbon footprint of transport fuels at the national level is relatively small at the current blending mandate of 5% (E5) in Europe. Thus, if 5% of bioethanol is blended to all conventional gasoline used annually in the UK, it will result in 0.35% reduction of GHG emissions on average per year [194]. In order to tackle the problem of climate change and comply with the EU binding targets on renewable energy share for transport sector, the much higher blends are required to achieve substantial reductions in GHG emissions from transport.

As introduced in Section 1.1, under the original RED (2009/28/EC), each EU member state is mandated to produce 20% of its energy share through renewable sources by 2020 [24]. As part of this effort, a binding minimum target of 10% renewable energy for the transport sector by 2020 has been set for each member state [24]. A new RED (2018/2001/EU) sets a new legally binding target of 32% renewables in its energy mix by 2030. It reserves the right to adjust this target in 2023 (if required). At the same time, there is a binding minimum target of 14% of the energy consumed in road and rail transport by 2030 as renewable energy (RED II) [24, 26]. Within this target sits sub-targets expressly for advanced biofuels: a minimum of 0.2% by 2022, and 3.5% by 2030. Hence, biofuels are expected to play a prominent role in achieving these binding targets. This will be partly achieved by introducing higher blending ratios of alternative fuels within fossil fuels. Current EU legislation that limits the blending of biofuels with petrol to 5% is being revised to enable higher blending ratios [190]. However, issues associated

with compatibility of some older vehicles with higher blend ratios of ethanol stall an introduction of E10 in some countries (e.g. Ireland) [195]. Thus, the introduction of higher blend ratios of alternative fuels within conventional fossil fuels is bounded by their compatibility within existing or new engine technologies. An improved understanding of their combustion characteristics under blending can help in assessing and selecting the optimum alternative fuel, as well as the optimum blending ratio, for their use within engine technologies. This is one of the important driving forces in this research.

Third generation biofuels are derived from aquatic cultivated feedstocks (e.g. algae) [191]. One of the advantages of third generation biofuels is their easily accessible and available feedstocks, solving the problems associated with their predecessors [193]. Microalgal production systems, including open ponds and closed photobioreactors, have a potential to overcome some of the challenges of first generation biofuels, such as issues of food versus fuel competition and land usage, because microalgae can be grown on non-arable land or in wastewater systems and industrial CO_2 sources, as well as in saline and brackish water. They can be grown very fast offering higher biomass yields than terrestrial crops per unit area, and hence facilitating water remediation and decreasing CO_2 emissions [192]. However, the production of biofuels from microalgae requires high energy inputs that can counter any CO_2 savings and remains economically unfeasible at present [31]. More advanced technologies are required for the sustainable production of biofuels from algae that are currently less effective in the exploitation of resources than the less competitive alternative biofuels [191, 193].

Second and third generation biofuels are commonly referred to as "advanced biofuels" since their production techniques and pathways are still within the research and development, pilot or demonstration stage [31].

2.3.2.2 *History of biofuels*

Biofuels have a long history and have been employed since the beginning of the automotive industry. Ethanol and turpentine mixtures were first tested as an ICE fuel in a boat by inventor Samuel Morley in 1826, while Nicolaus August Otto developed another ICE that ran on an ethanol fuel blend in 1860, preceding the launch of commercial production of gasoline in 1913 [31, 196]. The inventor of the diesel engine, Rudolph Diesel, selected peanut oil as the fuel for his first engine after pulverised coal was proven to be ineffective. Later, industrialist Henry Ford designed the Model T car powered by ethanol [31, 196]. Until the Second World War, biofuels were regarded as feasible

transport fuels with bioethanol-gasoline blends such as 'Agrol' and 'Monopolin' competing with gasoline in the USA, Europe and other regions [31, 197]. However, with the new discovery of cheap extensive reserves of crude oil, increased supply of petroleum, expensive fermentation processes of ethanol and high cost of feedstock, further development of biofuels has diminished [31, 197].

A resurgence of interest in alternative fuels and the commercial production of biofuels was sparked by the oil crisis in the 1970s. Nonetheless, only Brazil commenced a commercial production of ethanol and mandated blending of sugarcane ethanol in gasoline throughout the country with a strong governmental support of neat ethanol-fuelled 'flex fuel' vehicles, as well as associated storage and distribution infrastructure [31, 197]. These flex fuel engines are capable of operating on gasoline, ethanol or a mixture of these two fuels in any blending ratios.

The increase in crude oil prices, concerns over energy security and dependence on foreign oil prompted the USA and many countries in Europe to provide strong political and economic incentives for the implementation of policies advocating national domestically produced biofuel industries in the late 1990s. In the last decade, an increased awareness of climate change and subsequent governmental policies and strategies encouraging reduction of GHG emissions in mobility sector and diversification of the energy mix have further strengthen the interest in biofuels. Over 60 countries have since implemented initiatives and set targets for adding biofuels into their fuel pools boosting the demand for biofuels [31]. For the EU, a binding minimum target of 10% and 14% renewable energy for transport sector has been mandated for each member state, by 2020 and 2030, respectively [24, 26]. The RED II includes specific sustainability requirements for fuel suppliers to include biofuels in the mix that they offer. The share of first generation biofuels is capped at 7% EU-wide. On the other hand, the use of advanced (non-food based) biofuels is strongly encouraged with a minimum of 3.5% their use by 2030 [26]. This later target demonstrates the RED II's wider objective to phase-out crop-based biofuels.

The global production of biofuels has seen a rapid increase in demand in the recent years. For instance, bioethanol production increased from 20.5 billion litres in 2000 to 123.4 billion litres in 2017 – a tremendous 500 percent rise after a modest 12.5 percent increase between 1990 and 2000 [196, 198]. First generation biofuels are currently the only alternative liquid fuel that can be produced on an industrial scale and economically

compete with fossil fuels, due to the very high share of feedstock cost of other biofuels in overall production cost [13, 199]. The most prevalently produced biofuels are conventional ethanol derived from sugarcane, corn, wheat and sugar beet and biodiesel diverted from vegetable oils, typically from rapeseed, soybean and palm [13].

2.3.2.3 Alcohol fuels

The similar physical and thermodynamic properties of alcohol fuels compared to fossil fuels make them viable lower carbon fuel components in spark ignition (SI) engines with little or no engine modifications required at low blending ratios [57, 200, 201]. Moreover, some alcohols have similar or higher octane numbers than conventional fuels, and therefore compression ratios can be increased in the ICE, enabling more power to be produced efficiently and economically [57].

For a compression ignition (CI) engine, the addition of an alcohol compound to diesel fuel enhances oxidation during the combustion process and provides the oxygen required to form CO_2 instead of carbon rich particles, therefore subsequently substantially reducing PM formation [202]. On the other hand, for SI engines, the addition of alcohol compounds to gasoline can significantly reduce knock tendency, carbon monoxide (CO) and soot, whereas unburned hydrocarbons (UHC) and nitrogen oxides (NO_x) may either increase or decrease depending on operating conditions [203, 204]. These changes in emissions can be attributed to the larger latent heat of vaporisation values of alcohols compared to petroleum fuels, leading to lower flame temperatures that subsequently influences the ignition chemistry and final emission products [205]. While a better knock resistance of alcohols has been predominantly related to the distinct nature of the alcohol fuel auto-ignition chemistry and the better charge cooling abilities which leads to increased charge density and thus higher volumetric efficiency due to their larger latent heats of vaporisation [206]. Milpied et al. [207] showed that addition of ethanol to conventional gasoline can increase knock resistance up to 60%. Fuels with higher knock resistance enable earlier spark timing at high loads, which increases engine efficiency.

2.3.2.4 Ethanol

Ethanol, a biodegradable colourless transparent liquid, is an alcohol fuel and if it is derived from renewable biomass, it is called bio-ethanol [208]. Ethanol is the most popular choice of biofuel whether used by itself as a neat fuel within modified SI engines or blended with gasoline or diesel as an extender and octane enhancer, attributing to more than 90% of the world's total biofuel usage [209]. Bio-ethanol can be seen as clean,

renewable and green combustible fuel alternative to gasoline due to its oxygen content, high octane rating, high heat of vaporisation, and low vapour pressure. Moreover, ethanol is easy to blend with gasoline and is employed as the oxygenated portion in gasoline for less emissions of CO, UHC and carcinogens owing to the presence of oxygen in its molecular structure, as well as in order to increase octane rating of the blend [210]. It has the capacity to replace gasoline in internal combustion engines; nevertheless, its production cost remains considerably higher than the production cost of gasoline [211]. The competitiveness of biofuels has been drastically affected by the low cost oil climate since 2014. Although, there are still some economically favourable environments persistent for biofuels where they are protected by mandates and supportive policies and few, with Brazilian ethanol among others, are competitive [13].

Presently, ethanol is mostly produced through first generation methods and predominantly derived from sugar containing raw materials (i.e. sugar-cane) and starch grains (i.e. corn, wheat and cassava), which is objectionable because of their food and feed value [212]. In 2017, the main ethanol producer was the USA, with the production volume of 71.8 billion litres or 58% share of global production, mostly derived from corn. Brazil was the second largest ethanol producer with 32.1 billion litres or 26% share of the global production, primarily derived from sugarcane. Europe produced 6.4 billion litres of ethanol or 5% of the global production. Its ethanol was predominantly made from wheat and sugar beet. China produced 4.0 billion litres or 3% of the global production and Canada produced 2.0 billion litres or 2% of the global production [196, 198]. In China, the primary bioethanol feedstock are corn, wheat and cassava, while in Canada, they are corn and wheat [196].

Brazil is currently the principal country on exploiting ethanol in ICE with 25-27.5% ethanol by volume mixed in standard gasoline sold at the pump, accounting for 40% automobile fuel demand for cars, lories and busses within the country [190, 213]. The Brazilian sugarcane network is a successful example of a policy, cooperation of institution and technological innovation [199]. Its unique superior edge over the majority of other biofuels from oil seeds and energy crops can be attributed to 70% reduction in CO_2 emissions when substituting the gasoline, that ultimately qualifies Brazilian ethanol as 'advanced biofuel' according to the USA government categorisation [199].

Meanwhile, the leading producer of the ethanol, the USA, has also seen some success in recent years. Its annual bio-ethanol consumption rate accounted for 65.5 billion litres in

2017, replacing slightly more than 10 percent of the USA gasoline demand with ethanol and hence exceeding a so called 'blend wall' for the second year in a row [198]. The slower success of North America's corn-based ethanol is potentially due to a lower-yield feedstock of approximately 0.374 litres per square metre. This is 50% less of what can be produced from water sugarcane or 90% less than using algae. Moreover, due to increased bio-fuel requirements and its usage in recent years, the U.S. stopped exporting corn. This has had a drastic effect on world food supplies, causing shortages in low income countries such as Guatemala, which reported increases in hunger as the price of corn has risen because of the demand for ethanol [214].

Ethanol production through second generation methods from lignocellulosic biomasses such as agriculture residues, woody biomass, and algae, industrial and municipal solid waste are more appealing options. They are not only renewable, but also relatively cheap, plentiful and sustainable. For mass production of bio-ethanol through second generation methods, there are readily accessible large quantities of biomasses from the major agricultural residues, such as rice straw, wheat straw, corn straw and sugarcane bagasse; while starchy industrial biomasses, such as waste from starch processing factories and potato food factories, offering favourable feedstock for high yield production especially in equatorial countries [212]. These advanced biofuels hold more promise however would still struggle to compete with fossil fuels without introduction of carbon pricing or technological breakthroughs in future [13].

Despite a drawback of bio-ethanol current large-scale production from food sources raw materials and its potential solution of bio-ethanol large-scale production from lignocellulosic biomasses, there are other problems associated with ethanol. One major disadvantage of ethanol is that above 20% ethanol concentration in gasoline blends, complex modifications to conventional SI engines are mandatory to avoid engine corrosion [208, 215]. This usually entails modifications to the carburettor, fuel injection system and often compression ratio, which can cost up to £550 to the end consumer [13, 208]. In Europe, a 5% (E5) mixture of ethanol is a standard, that is 5% ethanol and conventional gasoline blend, while in the USA 10% ethanol blend (E10) is quite popular [157, 215]. In the USA approximately 97% of the gasoline contains ethanol that extends the gasoline supply, increases the octane rating and adds clean burning properties of oxygenates [216].

In Brazil, ethanol has been used extensively as neat fuel in flex fuel engines and in other regions such as North America and Sweden it is used at as high concentrations as 85% (E85) by employing bi-fuel vehicles specially designed to operate at this fixed volumetric blend [208, 215, 217]. On the other hand, flex fuel vehicles are able to operate on various blends of ethanol and gasoline ranging from 100% gasoline to 85% ethanol, although they operate the best at an E85 blend [208]. The variation of fuels and blend ratios in flex fuel vehicles is achieved through the implementation of electronic technology that controls the fuel injection and ignition point. In the flex fuel engine, sensors detect the ethanol-gasoline ratio of the fuel and inform an electronic injection system, which subsequently adjusts the engine parameters such as ignition timing, the fuel injection timing, the air-fuel ratio, the opening and closing of the valves according to the fuel blend used and operating conditions [218]. These engines are generally more efficient compared to modified conventional gasoline engines for alcohol-gasoline blend operation [208].

One major disadvantage of ethanol is that it has a significantly lower calorific value. Therefore, high addition of ethanol to gasoline would have an unfavourable effect on the fuel economy of vehicles. There are also problems associated with ethanol nature of being hygroscopic and fully miscible in both gasoline and water. These include a high tendency of ethanol water absorption, difficulties in storage and transportation of ethanol through existing gasoline pipelines, and formation of uniform and homogeneous water/ethanol blend [219].

2.3.2.5 *Butanol*

Butanol is a four carbon atom alcohol (C_4H_9OH), containing more hydrogen and carbon compared to ethanol and hence it is easier to blend with gasoline and other hydrocarbon products. It can be produced from the same feedstocks as ethanol, however its yield is approximately half of that of ethanol [190, 220]. Increased hydrogen and carbon content also means that a molecule of butanol has a higher volumetric energy content - energy density than ethanol, which is defined as the amount of energy stored in a system per unit volume, representing 25% increase in harvestable energy, and therefore will have a less negative effect on vehicle fuel economy and better mileage when compared with ethanol, especially at higher blend ratios, due to a smaller ratio of oxygen to carbon in the fuel [219, 221, 222]. This, combined with the higher stoichiometric air-fuel ratio, enables higher blend ratios of butanol in gasoline up to 85% without changing regulations and engine control systems [223]. Currently, in the USA, blends of up to 16% vol butanol in

gasoline (Bu16) are permitted as a legal fuel equivalent to 10% vol ethanol in gasoline (E10) [89, 224].

The volatility of alcohols decreases with an increase of carbon content, which means the tendency to vaporisation decreases. Therefore, butanol has a significantly lower vapour pressure than ethanol, minimising the evaporative (volatile organic compound) emissions and the likelihood of detonation, reducing cavitation and vapour lock problems, although making evaporation more difficult. It has a lower latent heat of vaporisation and higher flash point than ethanol, potentially decreasing issues with fuel atomisation and combustion during cold start of engine, commonly associated with alcohol fuels. In addition, butanol is considerably less hygroscopic compared to ethanol, and therefore less prone to water contamination. Being less corrosive to materials, enables butanol be transported and distributed through the existing fuel supply infrastructure [219, 221]. The properties of gasoline, ethanol and butanol are summarised in Table 2.2.

Table 2.2: A comparisons of fuel properties of gasoline, ethanol and *n*-butanol [216].

Parameter	Gasoline	Ethanol	*n*-butanol
Chemical formula	C_4-C_{12}	C_2H_5OH	C_4H_9OH
Energy density (MJ/l)	32	19.6	29.2
Lower heating value (MJ/kg)	42.7	26.8	33.1
Density (g/ml) at 293 K	0.72-0.78	0.79	0.808
Boiling temperature (K)	298-488	351	391
Latent heat of vaporisation (kJ/kg) at 298 K	380-500	904	582
Auto-ignition temperature (K)	~573	707	658
Stoichiometric air-fuel ratio	14.7	9.0	11.2
Saturation pressure (kPa) at 311 K	31.01	13.8	2.27
Flash point (K) at closed cup	228-235	281	308
Cetane number	0-10	8	25
RON	88-98	109	98
MON	80-88	90	85
Octane number (RON+MON)/2	80-99	108	96

There are several butanol isomers with viable production pathways from biomass, each with different branching degrees and OH positions. *N*-butanol has been the most prominent to date. As it has been mentioned in Section 2.1.7 and 2.1.11, usually straight-chain molecules have shorter ignition delay times compared to branched isomers,

101

resulting in *tert*-butanol being the least reactive and *n*-butanol the most reactive butanol isomer [225-227]. Alternatively, the OH group position impacts the strength of C-H bonds, as discussed by Gu et al. [228] which could lead to various distributions of probability of H-abstraction from other species or free radicals (major pathway controlling the low-to- intermediate temperature chemistry of hydrocarbons [57]). The combined effect of branching and OH group position can result in unforeseen combustion behaviour of these fuels when blended with other hydrocarbons, as has been shown in several studies [229-232]. For example, *tert*-butanol and diesel blends have shown shorter ignition delay times compared to *n*-butanol and diesel blends.

The longer hydrocarbon chains of butanol, its lower oxygen content and higher heating value compared to ethanol make its characteristics quite similar to conventional gasoline, including its octane rating. The corollary of a lower octane number than ethanol is a higher cetane number, suggesting that *n*-butanol could be a possible blending component for diesel as well as for gasoline. While *n*-butanol has a higher energy density than ethanol, it has a lower octane rating and therefore the potential octane enhancing benefits of *n*-butanol addition are unclear, since the lower octane number value can potentially decrease the efficiency of the engine. This can be addressed by advancing the spark timing. According to Merola et al. [233], there are no negative effects on engine performance for blends up to 40% *n*-butanol in gasoline.

Nevertheless, when blended with gasoline it is important to determine its impact on the potential knocking characteristics of the blend. This is particularly important because, although it has a similar Research Octane Number (RON) to gasoline, it has a lower Motor Octane Number (MON). Therefore, it has a higher octane sensitivity, which could be beneficial in modern downsized boosted engines [234, 235]. Relevant conditions relating to the anti-knock quality of fuel blends within engines are the temperature and pressure conditions experienced by the unburnt end gas, which in modern engines tends to be at lower temperatures than those in the RON test. Hence, the most appropriate way to describe the octane appetite is neither RON nor MON, but an extrapolation of RON/MON values to cooler conditions [236].

Despite these few distinctive advantages of butanol over ethanol, there is one major drawback – the cost of production. At the moment, the cost of butanol production is substantially higher compared to ethanol, preventing butanol from becoming a mainstream fuel [237]. This is due to its very low production yield through its traditional

acetone-butanol-ethanol (ABE) fermentation, which uses bacterial fermentation to produce acetone, butanol and ethanol from carbohydrates through anaerobic conversion. The yield of butanol varies depending on the type of biomass and bacteria used. However, even though the theoretical butanol yield is approximately 20% less than that of ethanol, its energy value is approximately 32% higher than that of ethanol [220].

There are several bio-technology companies, including Butyl Fuel, Cathay Industrial Biotech, Cobalt Biofuels, Green Biologics, Metabolic Explorer, Tetravitae Bioscience, and others around the world committed to providing strains and process solutions for ABE fermentation for industrial customers. In general, the yeast of the ethanol fermentation process has a 10-30 times higher production rate compared to that of the yeast of butanol production [221]. Continued research by Busche and Allen [238] and Ezeji et al. [239, 240] into butanol production through fermentation of agricultural feedstock decreasing butanol toxicity to the fermentation culture and boosting product recovery via pervaporation and gas stripping has the capacity to considerably cut down the production cost of butanol. However, attaining profitability for n-butanol production as bio-fuel remains challenging, despite its attractiveness for chemical markets that offers higher revenues [216]. The comparisons of ethanol, n-butanol and sugar prices in the international market in 2016 are reported in Table 2.3. The further development of novel technologies and processes in the production of n-butanol can bring it to commercial scale and enable it to economically compete against gasoline and ethanol. Therefore, n-butanol can offer many attractive features for transportation fuel and it is vital to consider it as a potential alternative fuel in near future.

Table 2.3: Comparisons of prices for ethanol, n-butanol and sugar in 2016 international market [216].

Commodity	Price (US $)
Sugar cane	27.26 $ per tonne
Sugar	0.48 $ per kg
Ethanol	0.66 $ per l
n-butanol (chemical)	1.34 $ per l
n-butanol (biofuel)	0.83 $ per l

2.3.2.6 Ignition studies of butanol

As aforementioned, *n*-butanol is a promising renewable fuel that has a potential to overcome the drawbacks introduced by the ethanol combustion in ICEs, while improved methods have increased the yield of *n*-butanol. On the other hand, some factors, such as uncertainty in oil prices, greenhouse emissions, the need for increased energy security and diversity, promote the research and development of biofuels. Also, the development and implementation of advanced engine technologies, combined with the broader penetration and use of biofuels and their blends with gasoline in SI engines necessitates a thorough understanding of auto-ignition phenomenon. Since biofuels are more likely to be blended with conventional fuels rather than entirely replace them, at least in short term [5], it is paramount to study the effects on the auto-ignition characteristics of butanol addition to gasoline at different blending ratios. Thus several studies on butanol auto-ignition behaviour have been carried out in well-controlled fundamental combustion systems such as shock tubes [43, 225, 227, 231, 241-248] and RCMs [40, 226, 230, 249, 250].
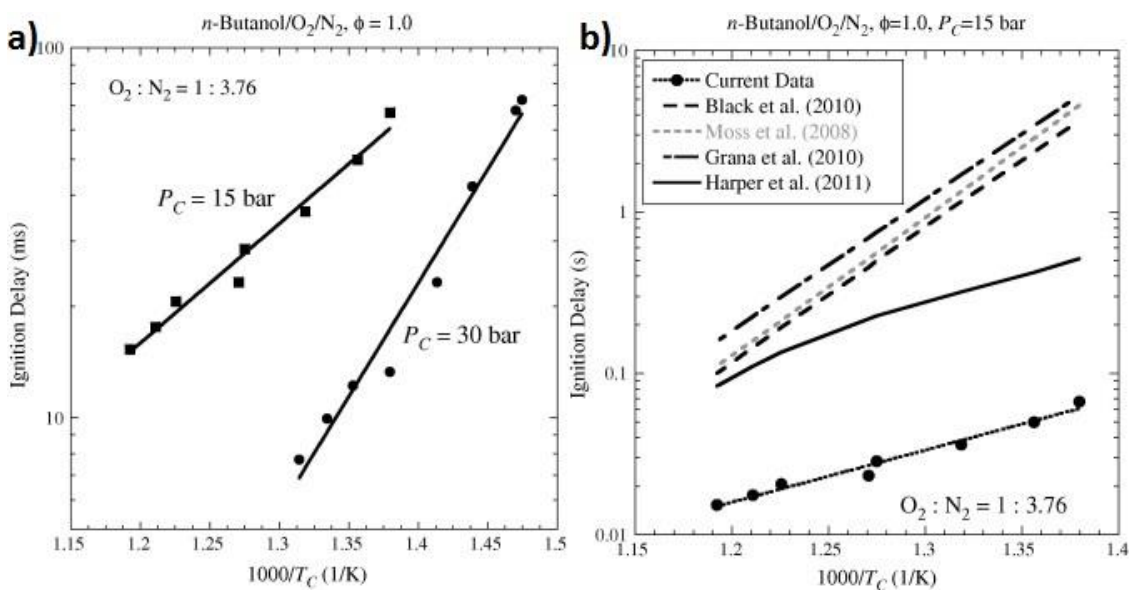
Figure 2.30: a) Comparisons of experimental ignition delay measurements at *P*=1.5 MPa and 3.0 MPa and *φ*=1.0. b) Comparisons of simulated ignition delay times with RCM experimental measurements at *P*=1.5 MPa and *φ*=1.0. Lines through the experiments are least squares fits to the data. Adopted from [250].

Weber et al. [250] investigated auto-ignition of *n*-butanol at pressures of 1.5-3 MPa and temperatures of 675-925 K in an RCM. They showed a systematic reduction of ignition delay times over these conditions as temperature was raised, as illustrated in Figure 2.30 (a). Also, the auto-ignition response exhibited single-stage characteristics. Weber et al.

[250] also compared measurements with the predictions from simulations, which had a relatively poor agreement as shown in Figure 2.30 (b). They attributed these discrepancies to uncertainties in the rate constants of the parent fuel decomposition reactions.

Moss et al. [225] studied the high temperature ignition characteristics of all four isomers of butanol: *n*-butanol, 2-butanol, *iso*-butanol and *tert*-butanol, at pressures of 0.1 and 0.4 MPa and temperatures of 1200-1800 K in a shock tube. A detailed reaction mechanism describing the oxidation of butanol isomers was developed and validated against experimental measurements. Results of their work concluded that *n*-butanol is primarily consumed by H-abstraction by H atoms and OH radicals yielding radicals, the decomposition of which results in the formation of highly reactive radicals, such as chain branching agents, H atoms and OH radicals. They also concluded that *tert*-butanol is the least reactive, while *n*-butanol is the most reactive isomer as demonstrated in Figure 2.31. These observations were later verified and expanded to broader ranges of pressures, temperatures and equivalence ratios [227, 231, 245, 248].
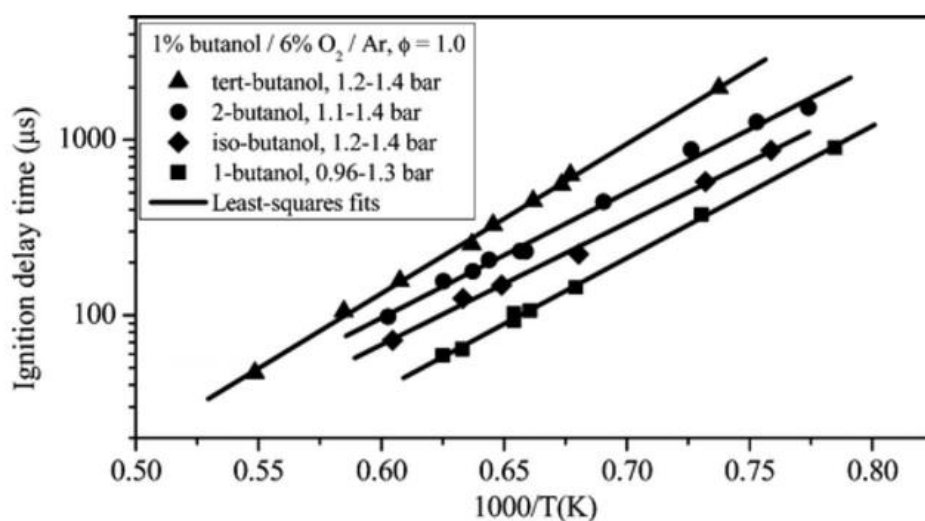
Figure 2.31: Comparisons of experimental ignition delay measurements of four butanol isomers for a mixture composition of 1% butanol/ 6% O_2/ 93% Ar, φ=1 and P=~0.1 MPa. Adopted from [225].

Black et al. [248] studied the auto-ignition of *n*-butanol at pressures of 1, 2.6 and 8 atm at temperatures from 1100 to 1800K. They also developed a detailed chemical model and validated it against the measured ignition delay data. Although, the modelled ignition delay times showed reasonable agreement with the measured data, at the lower temperatures the model over-predicted ignition delays. Results highlighted H-abstraction

to be the primary route of consumption of butanol, where the abstraction from the α-site prevails, succeeded by the γ-, β- and δ-sites, while abstraction from the hydroxyl group suggested of being less important (see Figure 2.32), as detailed in Section 2.1.11.
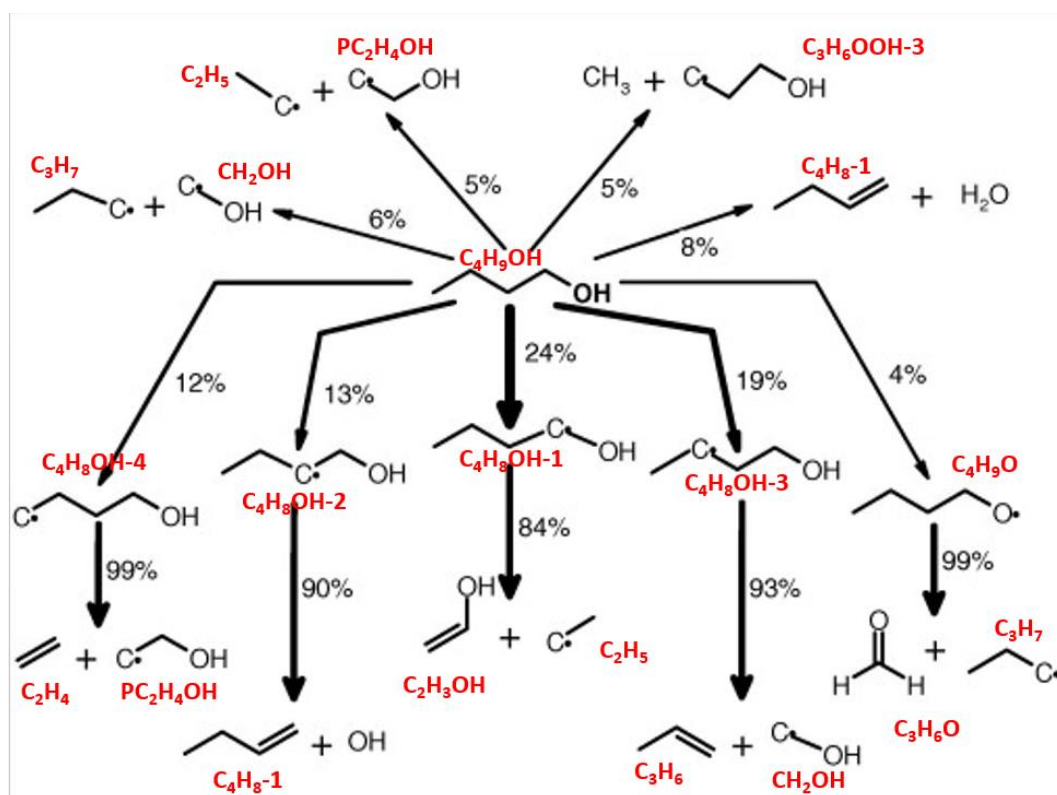
Figure 2.32: Reaction path analysis for *n*-butanol in the shock tube, $\varphi=1$, $T=1450$ K, $P=1$ atm, 20% consumption. To ease interpretation, chemical formulas of structures have been written out. Adapted from [248]

Heufer et al. [247] measured ignition delay times at high pressures of 1-4.2 MPa and temperatures of 770-1250 K of stoichiometric *n*-butanol-air blends. Their results showed that experimental ignition delays deviate from Arrhenius behaviour at lower temperatures (below 1000K) compared to isochoric simulations (see Figure 2.33). The authors attributed this unusual auto-ignition behaviour to pressure and temperature gradients, which are caused by shock attenuation. They also suggested that experimental data might have been affected by pre-ignition. Without the impact of chemistry, both effects result in higher pressures and temperatures compared to that of constant reactor (constant energy and volume) behind the reflected shock, hence shorter ignition delay times. The authors highlighted that a fuel $+HO_2$ reaction is the most important reaction for ignition delay times, in particular at lower temperatures. In their further study Vranckx et al. [246], authors measured ignition delay times in the temperature range of 795-1200 K and pressure range between 6.1 and 9.2 MPa. This study illustrated also non-Arrhenius

behaviour at elevated pressures, with this behaviour amplified as the pressures increased (see Figure 2.34). The authors noted that, due to the large inner diameter and the longer driven section of the shock tube used in their study, the facility effects would have a negligible influence on the experimental data. However, for longer resistance time (above 3 ms), these effects still can be quite significant. Therefore, in their simulations, the authors incorporated the measured pressure gradients. Their detailed chemical model showed a good agreement with experimental data and the literature.
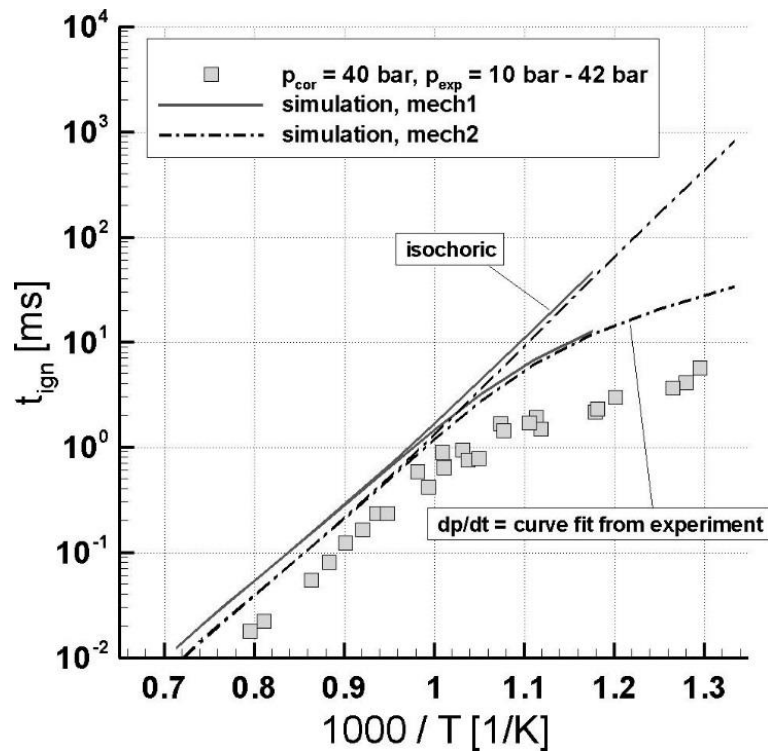
Figure 2.33: Modelled and experimental ignition delay times for *n*-butanol, φ=1, *P*=4 MPa. Adopted from [247].
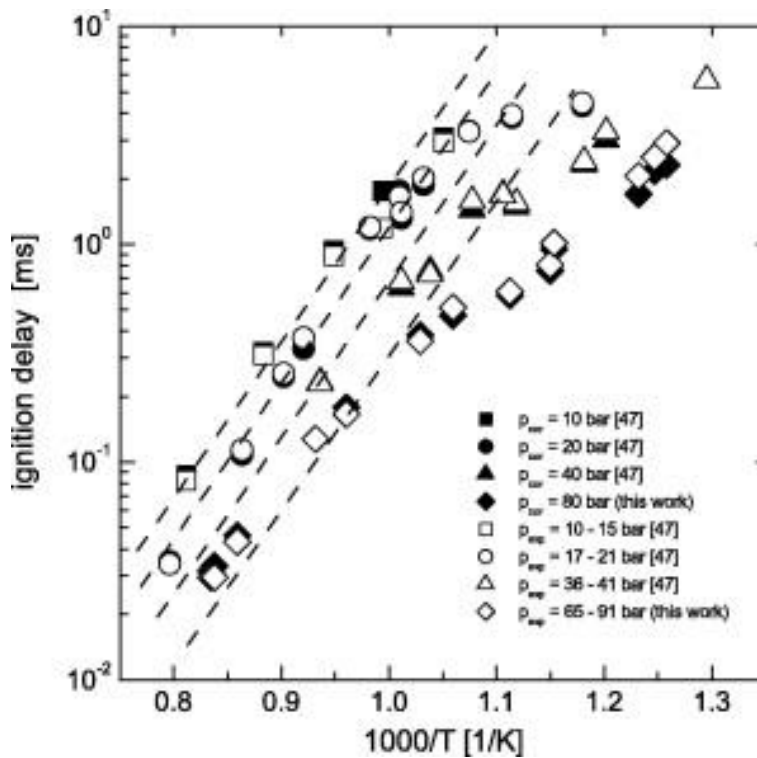
Figure 2.34: Pressure dependence of experimental ignition delay times for *n*-butanol, *φ*=1. The dashed lines represent high temperature Arrhenius behaviour. Adopted from [246].

Zhu et al. [245] also studied *n*-butanol auto-ignition behaviour in a shock tube using both conventional operation and constrained-reaction-volume method (CRV) at pressures of 20 and 40atm, at temperatures of 716-1121 K and at equivalence ratios of 0.5, 1.0, and 2.0. The authors demonstrated that ignition delay times with strong pre-ignition pressure in conventional operation were substantially shorter compared to those using CRV strategy (see Figure 2.35). Their reported ignition delay measurements did not show NTC behaviour at the conditions of the study. However, their CRV results did not cover the temperature range at which Vranckx et al. [246] simulations showed NTC behaviour (770-820 K) at a pressure of 20 atm. Therefore, the NTC behaviour of this alcohol is still not well established and controversy exists between different research groups.
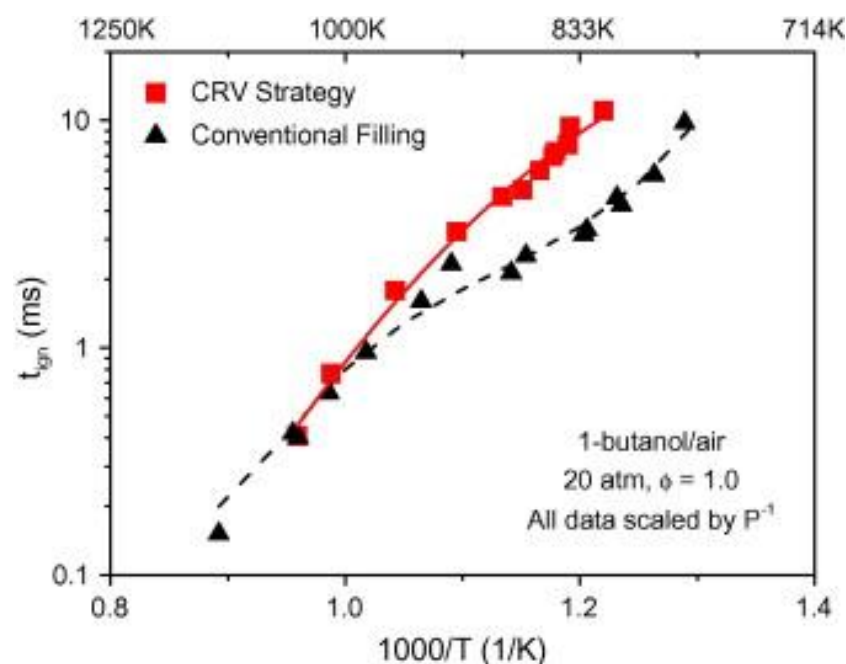
Figure 2.35: Comparisons of ignition delay time measurements using conventional method and CRV strategy of *n*-butanol, φ=1, *P*=20 atm. Adopted from [245].

Karwat et al. [249] reported the speciation data on *n*-heptane and *n*-butanol blends at 700K and at 9 atm, stoichiometric conditions and at two blend ratios, 80%/20% and 50%/50% by mole of *n*-heptane and *n*-butanol, respectively. They showed that ignition delay times increase with the *n*-butanol concentration. The main limitation of their study was that only one temperature was tested. A much wider study on ignition delay times for *n*-butanol/*n*-heptane fuel was presented by Yang et al. [251], who measured ignition delay times in an RCM in the temperature range 650-830 K and pressures of 1.5, 2.0 and 3.0 MPa, at blending ratios of 20%, 40% and 60% in moles of *n*-butanol in *n*-heptane. They confirmed that ignition delay times distinctively increase with the *n*-butanol concentration in the blend as illustrated in Figure 2.36. Results demonstrated clear two-stage ignition behaviour with a characteristic NTC at the lower temperatures, which disappeared as temperature increased resulting in a single-staged ignition. This suggests that the low temperature chain branching that propagates the first stage of auto-ignition curtails at higher temperatures. This study was complemented by the group's further investigation [230] of *n*-butanol/*n*-heptane blends in an RCM at different blending ratios. Results showed consistency with their previous study [251]. Only 50% *n*-butanol/*n*-heptane blend ignition delay times exhibited marginally longer values than the 60% blend, thus the non-linear correlation between the blend ratio and ignition delay time can be speculated at this temperature range.
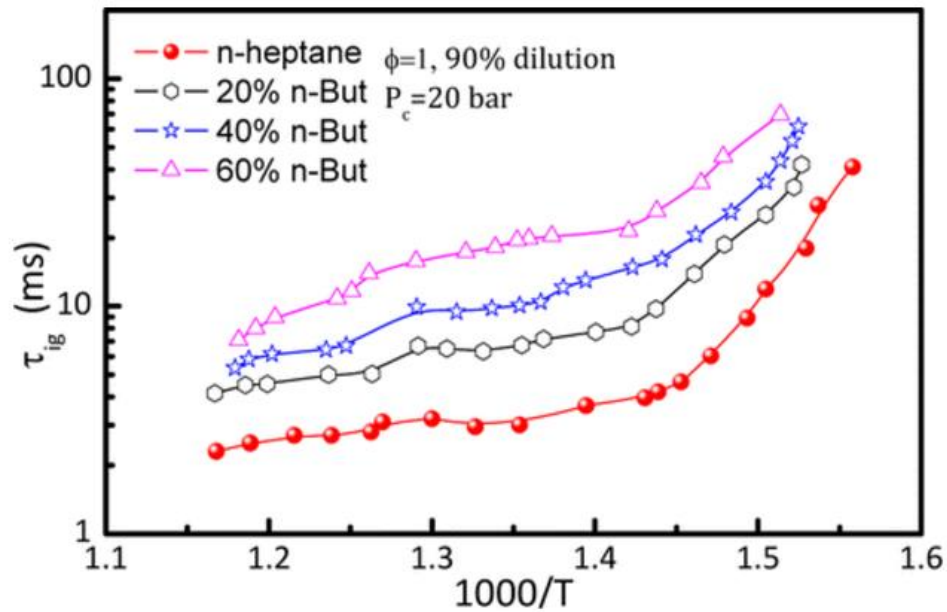
Figure 2.36: Ignition delay times for pure *n*-heptane and 20%, 40% and 60% (in mole fractions) *n*-butanol/ *n*-heptane blends at *P*=2 MPa, *φ*=1. Adopted from [251].

Kumar et al. [40] studied the influence on ignition delay times of *n*-butanol addition to *n*-heptane and *iso*-octane at temperatures of 613-979K and pressures of 2 MPa using the RCM. They found that *n*-butanol addition to *n*-heptane decrease the overall reactivity exhibited by increased ignition delay times, as demonstrated in Figure 2.37 (a). An addition of *n*-butanol to *iso*-octane gave shorter ignition delay times for lean fuel (φ = 0.4) as shown in Figure 2.37 (b). For *n*-heptane blends, results for both first and second-stage ignition delay showed positive correlations between ignition delay times and *n*-butanol concentration, while, for *iso*-octane blends, the second-stage ignition delay times decreased with the increase in *n*-butanol concentration. This suggests possible non-linear behaviour since one stage can change at a faster rate compared to another with respect to *n*-butanol blend. They also compared the improved detail kinetic mechanism against the measurements of ignition delay times, which reasonably well predicted the general trend. However, it failed to predict the trend for the *n*-butanol/*iso*-octane mixture.
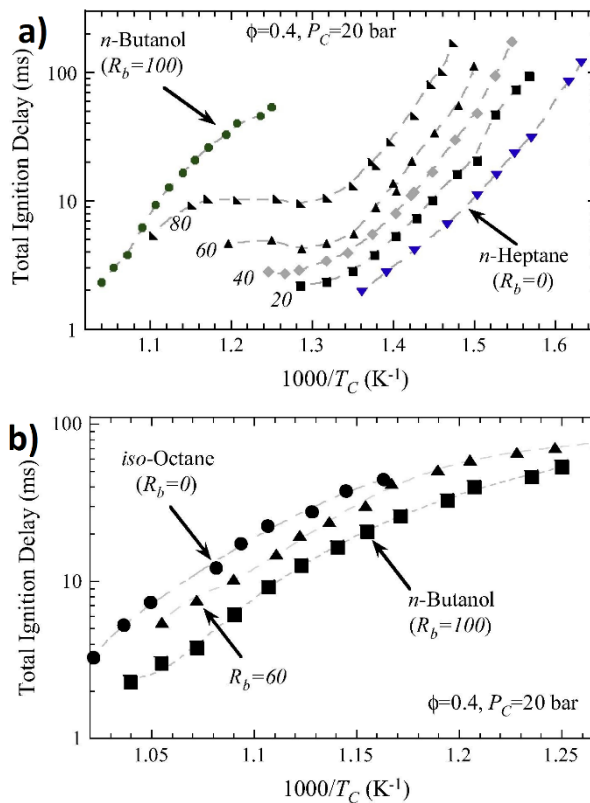
Figure 2.37: Ignition delay times for a) *n*-butanol/ *n*-heptane blends and b) *n*-butanol/*iso*-octane blends at P=2 MPa, φ=0.4. Adopted from [40].

In contrast, AlRamadan et al. [43] investigated mixed butanol (68.8% of 2-butanol and 31.2% of *tert*-butanol by volume) at 10% and 20% volume addition to two different TRF fuels in a shock tube at pressures of 2-4 MPa and temperatures of 800-1200 K. They showed that addition of mixed butanol isomers to TRFs can either reduce or raise the reactivity, depending on the temperature range. Below 850 K, the ignition delay times increased in magnitude, while above this temperature the addition of *n*-butanol caused a decrease in the ignition delay times. This cross-over temperature varied slightly between the TRFs, with one laying around 850 K and another around 870 K (see Figure 2.38). Also they developed a new chemical kinetic model that demonstrated a good agreement with experimental data. It showed that addition of mixed butanol isomers at 10% and 20% blending ratios to pure toluene always speeds up the reactions, while the addition to pure *iso*-octane shows the same trend as addition to TRFs where crossover occurred at 770 K. Figure 2.39 (a) illustrates that addition of mixed butanol isomers to pure toluene reduces the reactivity of the system resulting in shorter ignition delay times. On the other hand, from Figure 2.39 (b) it can be seen that below 770 K an addition of mixed butanol isomers to *iso*-octane increases the fuel mixture resistance to auto-ignition, whereas below this

111

temperature the mixture's behaviour is reversed. Hence, the mixed butanol isomers act as an octane enhancer below 770 K and as an octane retarder above 770 K.
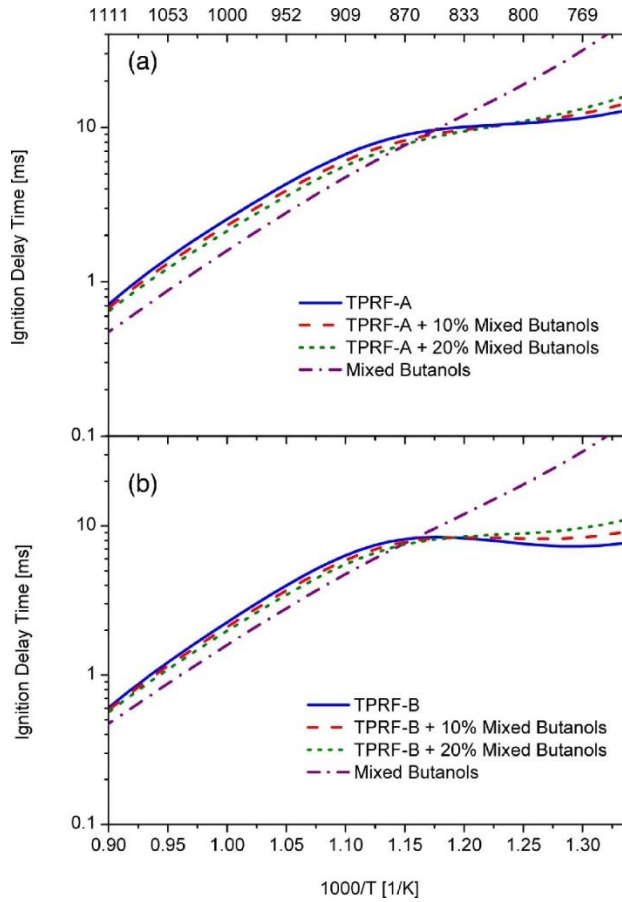
Figure 2.38: Modelled ignition delay times pure and mixed butanol isomers (68.8% of 2-butanol and 31.2% of *tert*-butanol by volume) with toluene reverence fuel mixtures at *P*=2 MPa, *φ*=1, a) TPRF-A and b) TPRF-B. Adopted from [43].
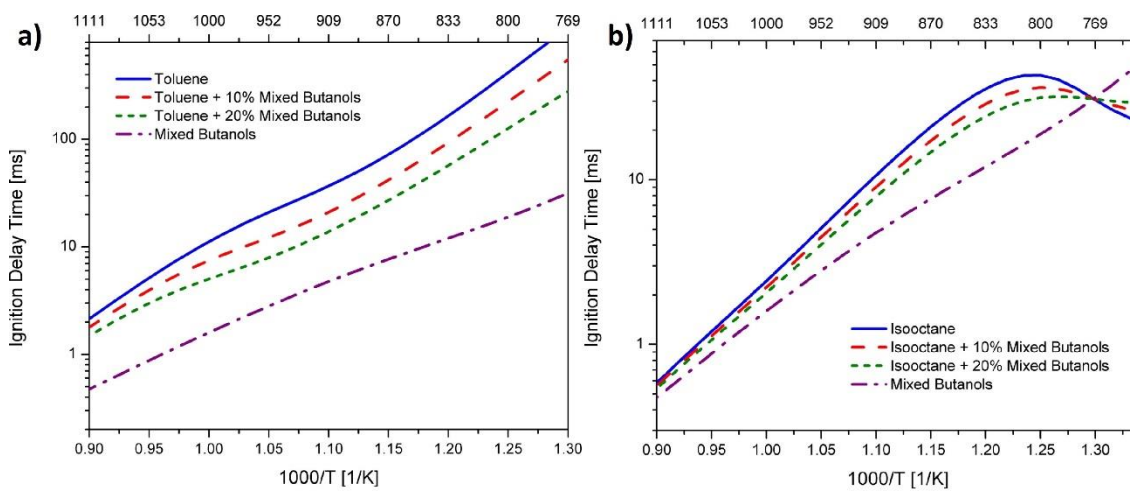
Figure 2.39: Modelled ignition delay times pure of a) toluene and toluene/mixed butanol isomers and b) *iso*-octane and *iso*-octane/mixed butanol isomers at 10% and 20% blending ratios, *P*=2 MPa, *φ*=1. Adopted from [43].

Agbro et al.[41] studied the influence of *n*-butanol at 20% by volume mixed with reference gasoline/ TRF on ignition delay times in an RCM at a pressure of 2 MPa and in the temperature range 678-858 K. The ignition delay times were shown to lie between the trends of the unblended fuels as illustrated in Figure 2.40. Results concluded that H-abstraction by OH from *n*-butanol appeared to be key in predicting the effect of blending and highlighted the importance of collecting accurate site specific abstraction rates from α- and γ-site. Also they suggested that further studies with a wider range of blending ratios are required to explore potential non-linearity in the anti-knock behaviour of *n*-butanol/TRF and *n*-butanol/gasoline blends. This study was extended to complementary chemical kinetic modelling and experimental study on impact of *n*-butanol blending at the same 20% concentration on auto-ignition and knock characteristics of gasoline under conditions of a strongly supercharged SI engine in Agbro et al. [42]. Their results emphasised the importance of the chemical model to accurately represent low temperature heat release chemistry in order to accurately model overall knock onset and analyse combustion phenomenon in the engine. They showed that *n*-butanol addition suppresses the NTC behaviour compared to TRF and has an inhibiting impact on the cool flame heat release of TRF due to scavenging OH radicals, but it disappears at higher spark advance where the end gas temperature is higher.
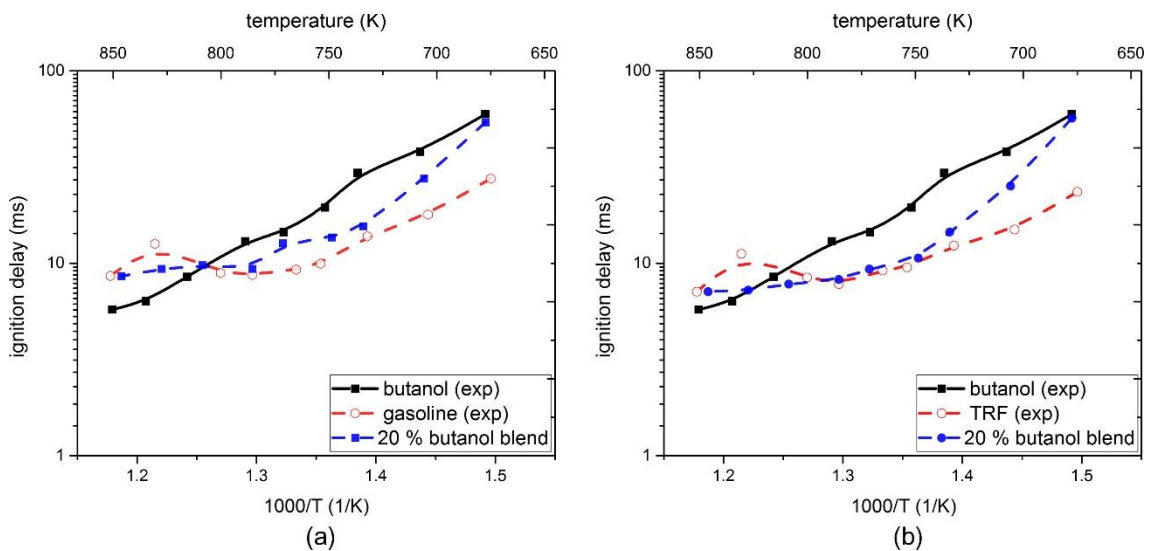
Figure 2.40: Measured ignition delay times for a) gasoline and b) TRF on blending with *n*-butanol by volume. *P*=2 MPa, *φ*=1. Adopted from [41].

It can be seen from the literature review, despite this recent progress, there is a clear need for further experimental and numerical studies on *n*-butanol addition to gasoline and its surrogate mixture to understand the underlying chemistry controlling auto-ignition and

related phenomenon, especially for high pressure and low temperature environments. Also, direct comparisons of the experimental ignition delay times using *n*-butanol/surrogate blends with those predicted by the corresponding chemical reaction mechanism would help to evaluate the fidelity of the surrogate model, as well as provide valuable information for the model refinement. Therefore, changes on the auto-ignition behaviour caused by progressive addition of *n*-butanol with commercial gasoline and its surrogate mixture have been studied as part of this PhD project, presented in Chapter 5.

3. Experimental, Modelling and Analysis Procedures

3.1 Overall methodology

Environmental concerns endorse a search of an "optimal" alternative fuel within the transportation sector. Blending these alternative fuels requires a detailed understanding of their combustion behaviour for their effective use within conventional and advanced engine technologies. Advanced technology development is currently constrained by inhomogeneous and abnormal combustion behaviours, such as knock and super-knock. Therefore, this dissertation aims to provide a better understanding of auto-ignition phenomena and conditions that drive these processes. It also investigates the effects of the addition of an alcohol fuel to gasoline and its representative surrogate mixture on key fundamental properties, such as ignition delay time, heat release rate and excitation time. This is crucial for new fuels' safe, optimised and effective use within low temperature advanced combustion technologies. Furthermore, the fuel chemistry that drives these abnormal combustion processes is studied, a deeper understanding of which can be used to improve modern combustion strategies using conventional or alternative fuels to attain higher efficiency and lower emissions.

In this work, such understanding is achieved through experimental and detailed chemical modelling work with accompanying theoretical analysis. Ignition delay times are commonly used to assess engine knock. For the experimental study presented in this thesis, the University of Leeds rapid compression machine (RCM) was employed. Section 3.2 presents an overview of this experimental apparatus and details the experimental procedure employed here. Ignition delay time measurements were performed at low temperature, high pressure conditions relevant to advanced combustion strategies. This enabled a study on the effects of addition of an alcohol fuel constituent, *n*-butanol, to a conventional fuel, gasoline, on auto-ignition response. The acquired experimental data not only provided an opportunity to study the auto-ignition performance of fuels but also offered the basis and targets for detailed chemical kinetics model validation and performance assessment.

A well validated kinetic model offers the means for accurate simulations of reacting systems under conditions that may not be possible otherwise, as well as insights into the effect of fuel composition on combustion processes such auto-ignition. Through chemical kinetic modelling work, the performance of a detailed kinetic mechanism was initially

assessed against experimental results. Owing to the chemical complexities associated with modelling a real gasoline due to the large number of hydrocarbon components involved, it is common to use a representative gasoline surrogate which mimics the important properties of the studied fuel. Hence, here the auto-ignition behaviour of a representative gasoline surrogate mixture was also investigated, as well its performance in replicating auto-ignition behaviour when blended with *n*-butanol at different blending ratios. The computational methodology employed in this work is explained in Section 3.3.

As introduced in Sections 2.1.12 and 2.1.13, auto-ignition phenomena can result in different auto-ignition modes, including developing detonations. Therefore, the ignition behaviour in the RCM was further analysed and characterised using the detonation peninsula framework proposed by Bradley et al. and co-workers [91, 96], within which detonations could develop. Details on the methodology used are provided in Section 3.4.2. Severe detonations are linked to intense heat release rates during excitation times which are short enough to reinforce the pressure wave. Therefore, excitation times were modelled to enable assessment of the fuels and conditions studied in terms of the detonation peninsula.

On the other hand, low temperature heat release, LTHR, is also vital in describing auto-ignition phenomena, whereas high temperature heat release, HTHR, is a critical parameter in determining the excitation time, and subsequently the uncontrolled auto-ignition during active ignition processes, e.g. knock, pre-ignition, detonation and super-knock. In order to facilitate a study on heat release, analyses on preliminary exothermicity as well as the main hot ignition were performed. This has been achieved through the methodology proposed by Goldsborough et al. [252], which is based on the energy conservation equation and adiabatic core assumptions. Details on this approach are provided in Section 3.4.1.

Finally, through the use of brute-force sensitivity analysis, the chemistry controlling the auto-ignition processes, heat release rates, HRRs and excitation times was investigated to determine the main reactions which influence τ_i, τ_e and HHRs at selected conditions.

3.2 Apparatus and experimental methods

Ignition delay measurements were performed in the Leeds RCM, which is used to simulate an ideal single compression stroke of an internal combustion engine. An RCM is designed to enable the study of auto-ignition phenomena in a more ideal, constant and

controllable environment compared to that in a reciprocating engine. Auto-ignition is achieved by rapidly compressing a fuel-oxidiser mixture by a piston assembly to a higher temperature and pressure. The reactor piston is brought to rest and fixed at the end of compression. A detailed description of the University of Leeds RCM used in the experimental study can be found in previous literature [75, 78, 253] and only a brief description is given here.

3.2.1 University of Leeds RCM

The University of Leeds RCM was originally developed in 1968 at Shell Thornton Research Centre, then commissioned by Prof. J. Griffiths from the Chemistry Department at the University of Leeds in the 1970's and later transferred to the School of Mechanical Engineering at Leeds. The apparatus is based on one half of a dual opposed, pneumatically driven and hydraulically damped piston design, where the twin piston is simultaneously triggered to decrease the compression time and achieve mechanical balance, as originally proposed by Affleck and Thomas [254]. The Affleck and Thomas [254] design has been significantly improved in terms of higher post-compression pressure, damping characteristics, and data acquisition, at the University of Leeds. The operating parameters of this RCM are given in Table 3.1, while a labelled photograph of its setup along with its schematic diagram are provided in Figure 3.1.

Table 3.1: A summary of operating parameters for the University of Leeds Rapid Compression Machine. Source: RCM Experimental Protocol and Materego [75].

Operating Parameter	Value
Maximum pneumatic driving pressure	2.0 MPa
Maximum hydraulic locking pressure	5.0 MPa
Maximum mixing chamber pressure	0.4 MPa (absolute)
Maximum post compression pressure	2.7 MPa
Maximum initial combustion chamber pressure	0.15 MPa
Maximum initial combustion chamber temperature	473 K
Temperature at the end of compression range	600-1000 K
Compression ratio used	11:1
Compression time	20 ms
Laser measurement range	30 mm
Average piston speed	12.7 m/s
Piston Radius	23 mm
Cylinder Volume	412.3 mm^3
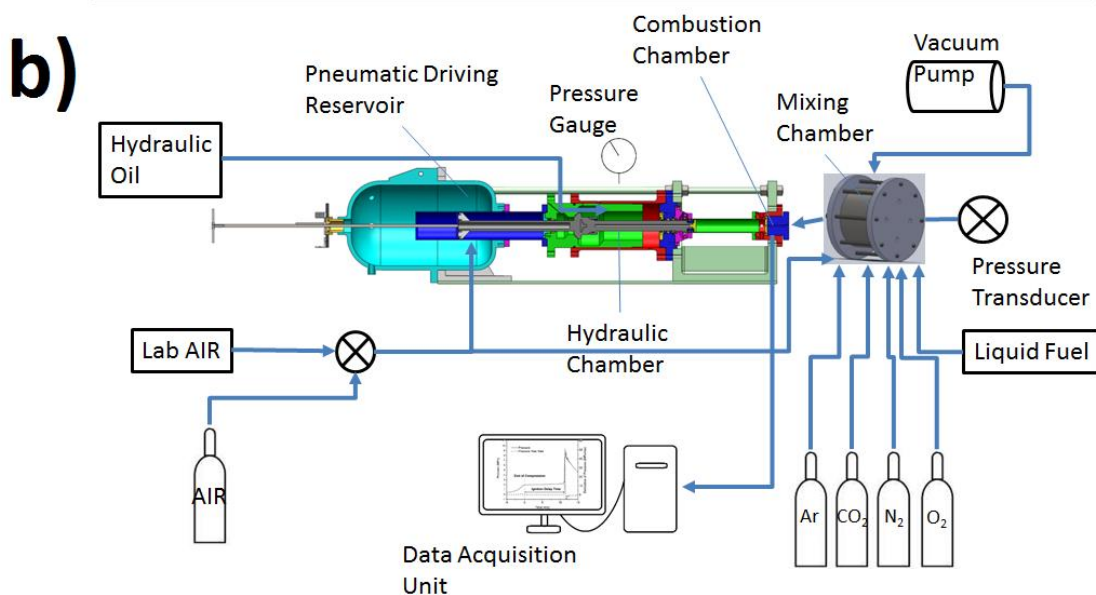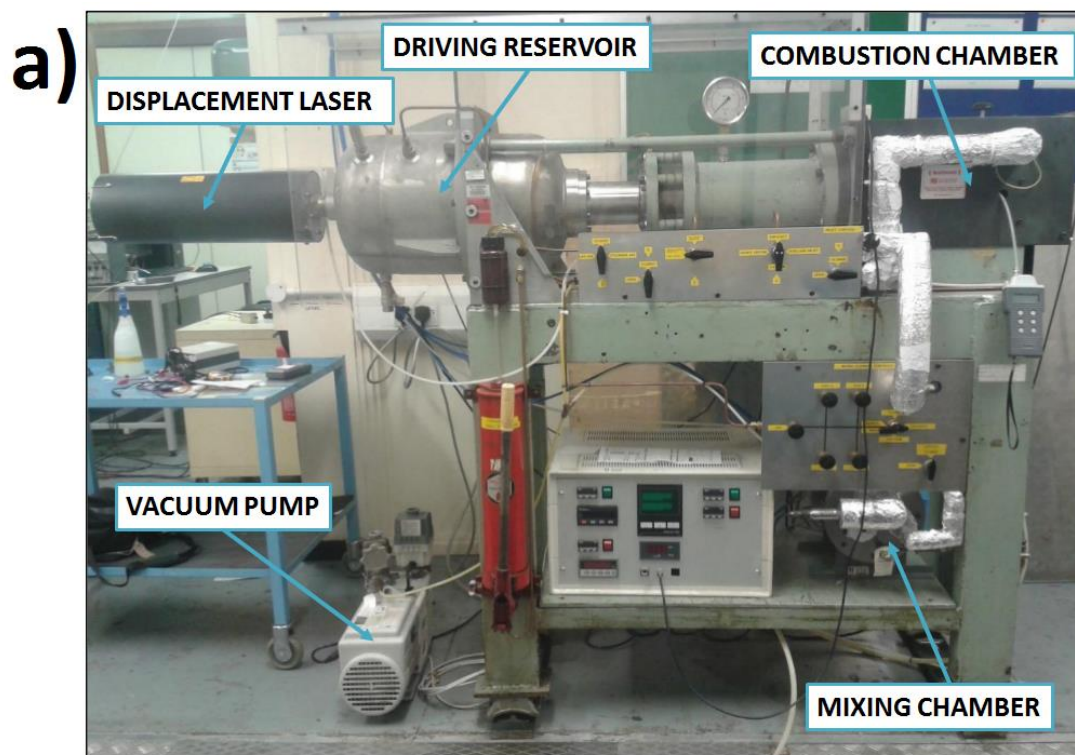
Figure 3.1: a) Labelled photograph of the University of Leeds RCM b) Schematic diagram of the University of Leeds RCM.

The University of Leeds RCM consists of four main sections, namely a pneumatic driving reservoir, a hydraulic locking and damping section, a combustion chamber and a mixing chamber. To constrain major heat losses and limit considerable reactivity before the end of compression, the reactor piston has to travel extremely quickly. This is accomplished by driving a piston pneumatically by compressed air from the driving reservoir. For the present setup, the reservoir is able to manage pressures up to 2 MPa, but in practice a

driving pressure of 1.32 MPa was used. The higher pressures can exceed the piston holding force and cause the piston to misfire.

Another key feature of the Leeds RCM is the hydraulic locking and damping mechanism, which is used to hold the piston in place before firing, as well as to decelerate and stop the piston by controlled venting of hydraulic oil. The piston is decelerated using a stopping ring and groove mechanism, where a small amount of pressurised oil is trapped between the damping ring and groove. The created pressure in the hydraulic oil acts as the kinetic energy transfer from the travelling piston rod and ensures a fast and uniform deceleration of the piston at the end of compression. This is required to minimise the vibrations and changes in the volume of the reactor which can dramatically deteriorate the quality of the acquired data and potentially damage the equipment.

The combustion chamber of the University of Leeds RCM is designed to withstand high pressures and temperatures formed during combustion. The end plug of the combustion chamber has a cartridge type heating element, whereas the pipework feeding the mixture from the mixing chamber to the cylinder has a semi-conductive wire heating element, under dense insulation to facilitate a uniform temperature distribution. Also to ensure temperature uniformity and homogeneity of the mixture, the liquid fuel is pre-vaporised and blended with oxidiser and inert gases in the mixing chamber before its delivery to the combustion chamber. This increases the performance of the apparatus and improves the control over the mixture preparation procedure.

There are other instruments and apparatus incorporated in the rig to enable the control and measurement of various parameters. The temperatures of the mixing chamber, combustion chamber, mixture feeding pipelines and combustion chamber inlet line are controlled separately by a proportional integral derivative temperature unit and measured by K-type thermocouples. This is incorporated to ensure that the fuel-oxidiser mixture remains vaporised and as homogeneous as possible throughout the experiment. Also it stops the accumulation of potential condensation within the pipework, which can impair the accuracy of data. The pressure changes during the operation of the RCM in the combustion chamber are measured by a Kistler 6045A dynamic pressure transducer, while the pressure of the mixing chamber is measured by a Duck static pressure transducer. A Keyence LK-G32 linear displacement laser is employed to measure the movement of the piston within a 30 mm distance of the compression stroke, to facilitate monitoring the damping characteristic of the apparatus and piston rebound. Two $\pm 10v$

analogue signals for piston linear displacement and dynamic pressure transducer are processed by a National Instruments data acquisition card, NI PCI-6110, whereas a LabView virtual instrument (VI) interprets these signals and graphically displays and records both the pressure-time histories and piston displacement at a sampling frequency up to 50 kHz.

This design of the RCM defines the performance of the machine and ensures quite reliable data acquisition, however there are some limitations in the current setup. Despite the fact that the pneumatically driven piston of the University of Leeds RCM travels fairly fast at average speed of 12.7 m/s, the compression is still not instantaneous and heat losses are inevitable, making the pressure and temperature at the end of compression lower than predicted by the adiabatic assumption. This is a limiting factor for the RCM, especially for measuring long ignition delay times (above 120 ms), where the accuracy of the acquired data will be compromised due to the onset of chemical reactions and non-uniformity within temperatures and pressures at the end of compression during the delay time. This can even prevent mixtures from igniting in some cases [75].

3.2.2 Experimental procedure

3.2.2.1 Mixture preparation

Each test charge is made up in batch quantities in a separate preheated stainless steel tank with a volume of 1.7671×10^{-3} m^3 and a maximum working pressure of 0.5 MPa. This can typically provide the capacity for 15-25 subsequent mixture runs for experimentation, dependant on fuel mixture, equivalence ratio, temperature and the initial pressure conditions within both the combustion and mixing chambers.

The mixture tank was initially evacuated and heated to a target temperature for a minimum of 2 hours to ensure temperature uniformity. Prior to mixture preparation, the tank was purged with laboratory air and then dry air up to 0.2 MPa pressure and evacuated to less than 0.002 MPa. This process was repeated several times to ensure there was less than 0.01% residual gas from previous experiments. This procedure was required in order to prevent any potential mixture contamination. Liquid fuels were then injected into the vessel using syringes via a gas chromatograph valve with luer-lock fittings so that no air entered the mixing chamber and the pressure was allowed to equilibrate. A different syringe and needle was used for each liquid fuel to allow optimum volume and precision, as well as to minimise cross-contamination of fuels.

The temperature within the mixing chamber and volume of injected liquid fuel was pre-determined by measurements of the relative partial pressure of each mixture component. To enable complete vaporisation of the fuel, it was ensured that the partial pressure of each major component was less than its saturation pressure corresponding to the set initial preheat temperature. Once the liquid fuel was injected, the partial pressure of each mixture component was recorded, and typically found to be within +/- 0.0001 MPa of that predicted by partial calculations. Then the gaseous components, comprising typically 21% O_2 and a 79% composite of varying proportions of inert components (N_2, CO_2, Ar) were carefully administered into the mixing chamber using high precision needle valves.

The initial temperature, pressure and composition of diluent gases (N_2, CO_2, Ar) were adjusted to vary the compressed temperature (T_c) of the premixed fuel and oxidiser gas mixture at a constant compressed pressure. This enabled the achievement of a range of compressed gas temperatures (678 - 916 K) with a fixed compression ratio of the apparatus, CR=11:1, owing to associated variations of specific heats, thermal conductivities and diffusivities of associated inert gases, hence variations in overall heat capacities of the test mixtures. This is further discussed in Section 3.2.3.

Following the addition of each gaseous constituent, the temperature and pressure of the test charge was left to equilibrate for approximately 3 minutes prior to recording the pressure and addition of the next gaseous portion. Then the test charge was left to mix diffusively for a minimum of 45 minutes before use in order to promote complete evaporation and homogeneity. No apparent change in ignition delay time measurements for the studied conditions was observed when this waiting time was extended to 1-1.5 hours. However, for lower initial pressures, initial temperatures or less volatile fuels, longer mixing times might be required to ensure full evaporation and homogeneity.

3.2.2.2 Operating technique

Prior to any operation of the RCM, a check was made to ensure that the piston was reset to its start of compression position. Also the combustion chamber was inspected to ensure that there were no soot build ups which could be removed with acetone. Consistent with the mixture preparation procedure described above, the combustion chamber and its delivery pipelines were sufficiently heated to their predetermined initial pre-compression temperature for at least 2 hours to allow temperature to equilibrate.

The combustion chamber was then evacuated to 0.002 MPa and purged of any potential exhaust gas residuals from previous experiments several times through filling it with

initially laboratory air and then dry air to 0.2 MPa. This ensured that any gaseous residuals were less than 0.1%. The transfer lines were similarly purged and evacuated before starting the series of experiments. The required quantity of the pre-heated test mixture was then slowly metered to the targeted initial pressure from the mixing chamber into the combustion chamber via a high precision needle valve. This quantity was calculated based on partial pressures. Both the mixing chamber and the combustion chamber were then closed and the test charge was left to equilibrate for approximately 3 minutes to promote mixture homogeneity and uniformity. Then the piston was hydraulically locked under the maximum safe working pressure of 0.4 MPa using the hydraulic hand pump. Next the driving reservoir was filled with laboratory compressed air, limited to 0.7 MPa line pressure, and then with dry cylinder air up to the pressure of 1.36 MPa.

Once the mixture in the combustion chamber was stabilised, and once the pressure of the hydraulic system and driving reservoir dropped to 0.4 MPa and 1.32 MPa, respectively, the RCM was triggered to initiate the rapid compression of the test charge via the firing button. This button was electrically connected to the solenoid valve in the hydraulic oil chamber. The triggering was attained by venting the hydraulic oil back into the hand pump, which subsequently broke the force balance and caused the driving force to exceed the hydraulic oil holding force.

After firing, all the collected and recorded data of the pressure-time histories and piston displacement data was saved to a file. The combustion product gases were then evacuated to the main exhaust line and the piston was reset via pressurising the combustion chamber with laboratory air. The combustion chamber was then purged and evacuated as described above in order to prepare the apparatus for the subsequent test runs.

3.2.3   Calculating the final compression temperature and pressure

Direct measurement of temperature in RCMs is challenging and there are uncertainties involved contributing to errors in estimating the true temperature at the end of compression (T_c). Any internal temperature probe can promote complex aerodynamic effects within the combustion chamber that would affect the adiabatic core region assumption. Moreover, due to repeated extreme conditions inside the combustion chamber during the auto-ignition event, it is questionable whether a temperature probe with sufficient response rate would have the required structural integrity to withstand such adverse conditions. On the other hand, optical temperature measurements are found to be subjected to timely calibration issues due to RCM vibration. Therefore, to estimate the

compression temperature, the adiabatic core hypothesis, proposed by Mittal et al. [255], and proven by a number of RCM researchers, was adopted herein to indirectly deduce temperature measurements from the experimental pressure traces.

This hypothesis assumes an ideal core gas region where there is no heat exchange with surrounding areas such as chamber walls or heat loss during the compression stroke, so that it has temperature uniformity. Despite compression processes not being completely adiabatic, this core gas region is considered to be compressed isentropically. For isentropic compression the relationship between temperature and pressure is expressed as:

$$\int_{T_i}^{T_{ad}} \frac{1}{\gamma - 1}\left(\frac{dT}{T}\right) = \ln(CR) \tag{3.1}$$

where T_{ad} is adiabatic temperature, T_i the initial mixture temperature before compression begins, CR the volumetric (geometric) compression ratio and γ the time-varying, temperature dependent ratio of specific heat capacities.

However, as discussed earlier, compression in the RCM is not truly adiabatic owing to heat loss across the gas core. The actual experimental temperatures and pressures at the end of compression are systematically lower than those predicted for isentropic compression. To account for the heat transfer to the wall during compression, Desgroux et al. [256] and Griffiths et al. [257] have demonstrated that it is reasonable to assume an isentropically compressed core gas region with the effective compression ratio. Based on the adiabatic core hypothesis, the temperature at the end of compression, T_c, can be estimated by incorporating the actual pressure at the end of compression, P_c, which is experimentally measured by a pressure transducer. Hence, using this hypothesis, T_c is computed using the equation:

$$\int_{T_i}^{T_c} \frac{1}{\gamma - 1}\left(\frac{dT}{T}\right) = \ln\left(\frac{P_c}{P_i}\right) \tag{3.2}$$

where P_i is the initial pressure and the other variables are the same as in Equation (3.1). The discrepancy between the calculated T_c and T_{ad} for truly adiabatic conditions reveals the extent to which the compression deviates from the truly isentropic case [258]. Since for the current experimental setup the CR is fixed at 11:1, the required pressure at the end of compression of 2.0 MPa and a range of the studied end of compression temperatures

was attained by varying the initial pressure, P_i, initial temperature, T_i, and specific heat ratio, γ, of the mixtures. Variations in the specific heat ratio were obtained by changing the type of diluent with the individual specific heats of the constituents (N_2, CO_2, Ar) and/or their corresponding concentrations in the initial mixture composition.

Variations in the diluent gas composition impose different chemical kinetic effects on ignition behaviour. This in turn can alter the heat loss profiles of different test mixtures, due to differences in their thermal diffusivities [258]. Generally, species with high thermal diffusivities exhibit more significant heat losses. Sung and Curran [258] showed that reductions in post-compression pressure, temperature and associated heat losses are more significant in experiments for Ar, whereas N_2 exhibited compression more similar to a truly isentropic compression. Wagnon [259] demonstrated that the diluent gas composition has an especially significant effect on the total ignition delay time in the NTC region, with Ar decreasing and CO_2 increasing ignition delays compared to N_2. Nevertheless, in the case of the first-stage ignition delay times, the composition of the diluent gases had less profound effects on ignition delay times relative to N_2. Wagnon [259] also showed that the effects of diluent gas composition on heat release are amplified at shorter ignition delays, higher pressures or higher levels of dilution. At these conditions, three-body reactions (e.g. H_2O_2 decomposition) and their corresponding collision efficiencies have a more substantial impact on overall ignition delay times. Ignition delay times are also affected by the uncertainties in the collision efficiencies of various diluent gases. Therefore, particular care must be taken when analysing data acquired in the NTC region from different experimental facilities (that may have used different diluent gasses). In the present study, the precise diluent gas and mixture composition was modelled. Different chemical effects were treated in the model through their differing assumed third body efficiencies. Molar fractions of the mixture composition at each tested condition are provided in Table 3.5 to Table 3.7.

The thermodynamic data required for the adiabatic compression calculations were obtained from [260]. The molar heat capacity at constant pressure (C_p) in $Jmol^{-1}K^{-1}$ was estimated from:

$$C_p = cp_a + cp_b + cp_c T^2 + cp_d T^3 + cp_e T^4 \qquad (3.3)$$

where cp_a, cp_b, cp_c, cp_d and cp_e are regression coefficients for chemical constituents of the mixture from [260]. The regression coefficient, cp_a, for a test charge was determined

124

by performing a weighted sum of the cp_a values of each individual constituent based on the blend fraction for each of the chemicals in the blend. Hence, each regression coefficient for the test charge was estimated in turn, and then applied in Equation (3.3) to determine the total molar heat capacity of the test charge at constant pressure. Then the molar heat capacities at constant volume (C_v) were estimated:

$$C_v = C_p + R \tag{3.4}$$

where R is the universal gas constant, of value 8.3143 $Jmol^{-1}K^{-1}$.

The pressure rise was then estimated over incremental steps of 1 mm using the following equation:

$$P_{n+1} = P_n + CR_n^{\gamma_n} \tag{3.5}$$

where P_{n+1} and P_n are the corresponding pressure at the end and start of each incremental rise in the piston position, n, respectively. The initial pressure, P_i, prior to compression is equal to zero, $P_n=0$, and was estimated from partial pressures of the fuel-oxidiser individual constituents. Whereas CR_n is the compression ratio at the start of the each incremental rise given by:

$$CR_n = \frac{V_i}{V_i + (\pi r^2 l_n)} \tag{3.6}$$

where V_i is the initial volume of the chamber, l_n is overall distance travelled by piston after each incremental rise.

Since the maximum distance that the piston can travel is 230 mm for the University of Leeds RCM configuration, the pressure was calculated for each incremental rise, where its final position corresponded to the compression pressure P_c. Similarly, the transient temperature during the piston compression was estimated for each incremental rise, where the final piston position represents the end of compression temperature T_c:

$$T_{n+1} = T_n \left(\frac{P_{n+1}}{P_n}\right)^{\frac{\gamma_n-1}{\gamma_n}} \tag{3.7}$$

3.2.4 Experimental conditions

Auto-ignition measurements were conducted for 10%, 40% and 85% by liquid volume of *n*-butanol mixed with gasoline or the surrogate fuel for temperatures of 678-916 K at 2 MPa pressure and an equivalence ratio (φ) of 1. Initial conditions were chosen based on their applicability to ICE operating conditions, previous experimental RCM data, operating parameters and the design of the University of Leeds RCM. The motivation behind the study of *n*-butanol/TRF blends was detailed in previous Chapters along with the reasons for choosing this particular TRF surrogate composition. The reference gasoline, *iso*-octane (UN1262), *n*-heptane (UN1206) and toluene (UN1294) were supplied by Shell Global Solutions, and high purity *n*-butanol by Fischer Scientific. Details on the composition and properties of the reference gasoline and surrogate mixture are provided in Table 3.2. Note, the gasoline contains the oxygenated compound (ethanol) while the TRF does not. The composition of *n*-butanol/TRF blends based on volumetric and molar fraction percentages of individual fuel components and their corresponding properties are outlined in Table 3.3 and Table 3.4, respectively. The fuel/oxidiser/diluent compositions expressed in molar fractions along with the experimental initial thermodynamic conditions and target temperature at the end of compression, T_c (based on Equation (3.7)), are presented in Table 3.5 - Table 3.7.

Table 3.2: Summary of the composition and combustion characteristics of the reference gasoline and formulated Toluene Reference Fuel (TRF) surrogate [41].

Gasoline Component	PR5801 (vol%)	TRF Component	TRF (vol%)	TRF (mole%)
Paraffins	47.1[a]	*Iso*-octane	65.63[b]	57.50[b]
		N-heptane	11.40[b]	11.25[b]
Olefins	7.9[a]			
Naphthenes	8.2[a]			
Aromatics	26.0[a]	Toluene	22.97[b]	31.25[b]
Oxygenated (ethanol)	4.7[a]			
RON	95[a] ($\pm$0.6)		95	
MON	86.6[a] ($\pm$0.8)		89.8[b]	
H/C	1.934		1.934	
S=RON-MON	8.4		5.2	
AKI=(RON-MON)/2	90.8		92.4	

[a]Values are taken from analysis supplied by Shell Global Solutions.
[b]Values are calculated based on a linear blending law and component properties list in Table 3.4.

Table 3.3: Estimated volumetric and molar fractions% of *n*-butanol/TRF blends for 10%, 40% and 85% by liquid volume of *n*-butanol mixed with the surrogate fuel, referred to as B10, B20, B40 and B85 respectively here.

Mixture Component	B10		B40		B85	
	% mole	% vol	% mole	% vol	% mole	% vol
N-butanol	14.90	10.00	51.23	40.00	89.93	85.00
Toluene	26.37	20.67	15.11	13.78	3.12	3.44
Iso-octane	49.25	59.07	28.22	39.38	5.83	19.85
N-heptane	9.48	10.26	5.44	6.84	1.12	1.71

Table 3.4: Properties of individual mixture constituents used in this work from [78, 156, 261].

Mixture Component	RON	MON	Molar weight (g/mol)	Density at 298K (kg/m^3)	Lower heating value (kJ/kg)
N-butanol	96	78	74.12	810	33100
Toluene	120	103.5	92.1	867	40589
Iso-octane	100	100	114.2	692	44310
N-heptane	0	0	100.2	684	44566

Table 3.5: Summary of 10% vol *n*-butanol blend in TRF compositions (mole fractions) and their initial and compressed conditions.

				10% vol *n*-butanol							
Mixture	P_i (MPa)	T_i (K)	T_c (K) using Equation (3.7)	*N*-butanol	Toluene	*Iso*-octane	*N*-heptane	O_2	N_2	CO_2	Ar
1	0.0870	353	678	0.00292	0.00517	0.00966	0.00186	0.20530	0.30306	0.47202	
2	0.0840	353	702	0.00292	0.00518	0.00967	0.00186	0.20545	0.42949	0.34542	
3	0.0745	323	727	0.00293	0.00519	0.00968	0.00187	0.20583	0.74099	0.03352	
4	0.0737	327	745	0.00293	0.00519	0.00969	0.00187	0.20587	0.77446		
5	0.0741	338	765	0.00293	0.00519	0.00969	0.00187	0.20587	0.77446		
6	0.0746	347	782	0.00293	0.00519	0.00969	0.00187	0.20587	0.77446		
7	0.0734	353	809	0.00293	0.00519	0.00969	0.00187	0.20587	0.69604		0.07842
8	0.0718	353	831	0.00293	0.00519	0.00969	0.00187	0.20587	0.59310		0.18136
9	0.0700	353	855	0.00293	0.00519	0.00969	0.00187	0.20587	0.49507		0.27939
10	0.0657	353	916	0.00293	0.00519	0.00969	0.00187	0.20587	0.28136		0.49310

Table 3.6: Summary of 40% vol *n*-butanol blend in TRF compositions (mole fractions) and their initial and compressed conditions.

Mixture	P_i (MPa)	T_i (K)	T_c (K) using Equation (3.7)	N-butanol	Toluene	Iso-octane	N-heptane	O_2	N_2	CO_2	Ar
					40% vol *n*-butanol						
1	0.0870	353	678	0.01223	0.00361	0.00674	0.00130	0.20442	0.31150	0.46021	
2	0.0840	353	702	0.01224	0.00361	0.00675	0.00130	0.20457	0.43837	0.33316	
3	0.0745	323	727	0.01227	0.00362	0.00676	0.00130	0.20494	0.74854	0.02258	
4	0.0740	329	745	0.01227	0.00362	0.00676	0.00130	0.20497	0.77108		
5	0.0745	340	765	0.01227	0.00362	0.00676	0.00130	0.20497	0.77108		
6	0.0748	349	782	0.01227	0.00362	0.00676	0.00130	0.20497	0.77108		
7	0.0735	353	809	0.01227	0.00362	0.00676	0.00130	0.20497	0.67348		0.09760
8	0.0718	353	831	0.01227	0.00362	0.00676	0.00130	0.20497	0.57100		0.20009
9	0.0700	353	855	0.01227	0.00362	0.00676	0.00130	0.20497	0.47144		0.29964
10	0.0657	353	916	0.01227	0.00362	0.00676	0.00130	0.20497	0.25866		0.51242

Table 3.7: Summary of 85% vol *n*-butanol blend in TRF compositions (mole fractions) and their initial and compressed conditions.

				85% vol *n*-butanol							
Mixture	P_i (MPa)	T_i (K)	T_c (K) using Equation (3.7)	*N*-butanol	Toluene	*Iso*-octane	*N*-heptane	O_2	N_2	CO_2	Ar
1	0.0870	353	678	0.02795	0.00097	0.00181	0.00035	0.20293	0.32372	0.44227	
2	0.0840	353	702	0.02797	0.00097	0.00181	0.00035	0.20308	0.44968	0.31614	
3	0.0747	324	727	0.02802	0.00097	0.00182	0.00035	0.20344	0.75565	0.00974	
4	0.0747	332	745	0.02802	0.00097	0.00182	0.00035	0.20345	0.76538		
5	0.0752	343	765	0.02802	0.00097	0.00182	0.00035	0.20345	0.76538		
6	0.0756	352	782	0.02802	0.00097	0.00182	0.00035	0.20345	0.76538		
7	0.0735	353	809	0.02802	0.00097	0.00182	0.00035	0.20346	0.63459		0.13079
8	0.0718	353	831	0.02802	0.00097	0.00182	0.00035	0.20346	0.53286		0.23252
9	0.0700	353	855	0.02802	0.00097	0.00182	0.00035	0.20346	0.43404		0.33134
10	0.0658	353	916	0.02803	0.00097	0.00182	0.00035	0.20346	0.21993		0.54545

3.2.5 Measurement of auto-ignition delay times

The ignition delay is obtained by measuring the pressure changes in the combustion chamber. From the start of compression, the pressure-time trace is monitored up to the time when pressure rapidly increases. At the end of compression the pressure stops increasing reaching a local maximum, which indicates the end of compression. After a short period of time a further rapid increase in pressure was observed for reactive mixtures, indicating the auto-ignition of the fuel-air mixture and the end of the ignition delay time. Therefore, from the pressure traces, the total ignition delay time, τ_i, is defined as the time difference between the point of ignition, where the maximum rate of pressure rise is observed (max dP/dt), and the end of the compression at top dead centre (TDC), where the piston displacement is zero, as illustrated in Figure 3.2.
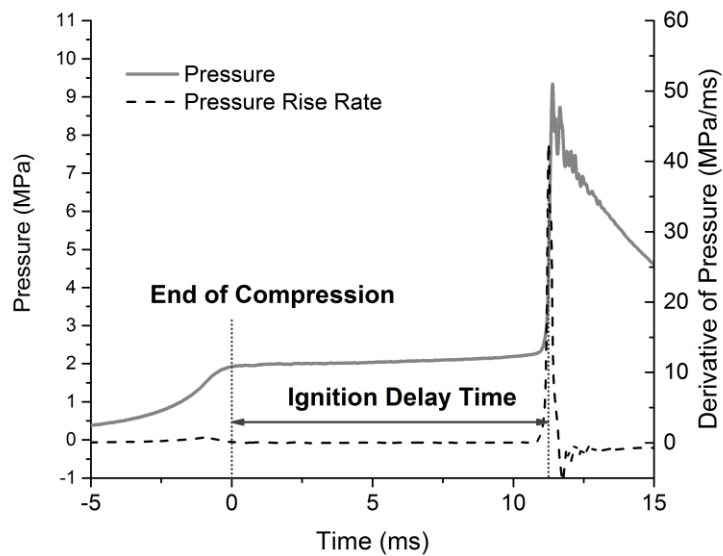
Figure 3.2: Typical experimental pressure trace defining the ignition delay time, τ_i, presented in this study. 40% vol *n*-butanol blend with TRF at *T*=831 K, *P*=2 MPa and φ=1.

Figure 3.3 depicts a representative RCM pressure trace of two-stage auto-ignition behaviour, where there are two noticeable pressure increases detected in the post-compression process. The initial rise in pressure appears due to the fuel-oxidiser compression; the second and third rises correspond to first- and second-stage ignition, respectively. Two-stage auto-ignition is characterised by a cool flame of LTHR preceding the auto-ignition event, the hot stage ignition. Based on this, the first-stage ignition delay

131

time, τ_1, duration is defined as the time from the end of compression at TDC, to the local maximum in the LTHR deduced from the experimental pressure trace as detailed in Section 3.4 and corresponding to the local dP/dt maximum as shown in Figure 3.3. The subsequent time interval from τ_1 to the hot ignition, where the maximum dP/dt is evident, is referred to as the second-stage ignition delay time, τ_2. Hence, in the two-stage ignition processes examined in this thesis, the total ignition delay time, τ_i, is the sum of τ_1 and τ_2.
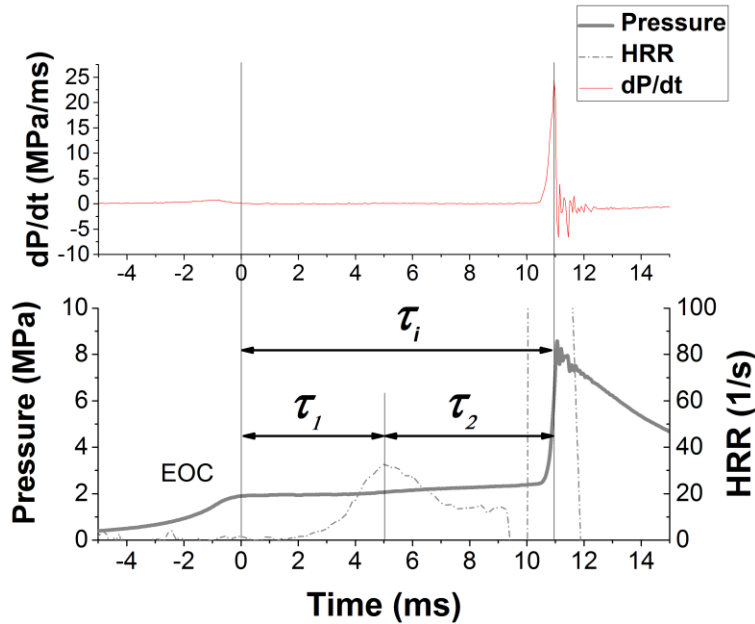
Figure 3.3: The definition of first-stage ignition delay, τ_1, second-stage ignition delay, τ_2, and total ignition delay time, τ_i, where EOC is the end of compression and HRR is the heat release rate. 10% vol n-butanol blend with TRF at T=745 K, P=2 MPa and φ=1.

Reported ignition delay times are the averages of 4-6 runs made at each test condition with a standard deviation of less than 10% of the mean in every case, as an indication of reproducibility. Moreover, both the first- and second-stage ignition delay times align very well for all the repeated experiments as demonstrated later in this work in Figure 5.1. The steep pressure rise at the end of the second-stage ignition or hot ignition essentially implies the uniformity of the reacting mixture and homogenous ignition. Similar to Zhang et al. [262], three pure dry air experiments were performed after each run, in order to limit the effect of soot deposits, and to enable good repeatability. For each reactive experiment, the corresponding, nearly-identical, non-reactive run was conducted by replacing the oxygen fraction in the test mixture with nitrogen while maintaining the same mixture concentration, since the thermal conductivity and the heat capacity of these two gases are quite similar. The volume profiles calculated from pressure traces obtained in these inert

experiments were used for variable volume simulations to better account for heat losses and any reactions taking place during compression. The compressed temperatures (T_c) were taken as the reference for presenting ignition delay data, and were obtained using an adiabatic core hypothesis [41], using the experimentally measured pressure at the end of compression (P_c), as detailed in Section 3.2.3. Potential errors in the measured initial pressure, the measured initial temperature and the measured compressed pressure, are perhaps some of the major factors that contribute to the overall error or uncertainty in calculated T_c.

3.3 Computational framework

As discussed in Chapter 2, chemical kinetic modelling has become an important approach in the analysis of combustion systems and prediction of the different fuel behaviours commonly used in fundamental combustion research. In this thesis computational work was carried out using the CANTERA suite of software (version 2.4, x64) [126] with Python 2.7 with supporting packages and assuming a closed, zero-dimensional homogeneous batch reactor under either adiabatic constant volume or variable volume conditions. A constant volume approach, where the effects of compression processes on predictive capability of the auto-ignition delay times are assumed to be negligible, was used in the study of methane-air auto-ignition processes, as detailed in Chapter 4. Both a constant volume approach and a variable volume approach, which accounts for any heat losses and any exo- and endo-thermicity prior to ignition, were applied in the study of the auto-ignition behaviour of n-butanol/TRF blends presented in Chapters 5 and 6. This enabled comparisons between these two approaches as discussed in Section 5.6. Also the relevance and validity of the constant volume approach, which is seen to be a more computationally cost-effective approach in complex simulations, was assessed. Details on the computational framework used in these studies are provided in the following sections, Section 3.3.5 and 3.3.6.

3.3.1 Constant volume simulations

A constant volume approach imitates an adiabatic chamber where the reactor physics, associated facility effects due to the compression stroke, and heat losses from the core region to the walls of the reaction chamber are not considered. This approach assumes that all reactions take place after the piston has reached its TDC position under a constant volume environment through a homogenous reactor model. A homogeneous reactor model represents an RCM reaction chamber by employing a single zone with uniform

conditions. The initial mixture composition is predetermined using the calculation method described in Section 3.2.3. This is used to achieve the desired thermodynamic conditions at the end of compression of T_c and P_c. These values are then used in constant volume simulations to predict ignition delay times at each condition without simulating the compression stroke and considering the system as adiabatic.

3.3.2 Variable volume simulations

While an ultimate goal is to have an RCM design as close as possible to an ideal homogeneous reactor, and there are numerous precautions taken to conduct measurements in a homogeneous reaction environment, there are still non-ideal effects that require treatment from a computational modelling standpoint. Therefore, to account for facility effects, including heat losses to the chamber walls and heat release from chemical reactions in the RCM experiments during a piston compression stroke, a variable volume approach with imposed specific "effective" volume histories can be used. These volume histories are calculated from experimental pressure traces of the representative non-reactive experiments as detailed in Mittal and Sung [263].

In this approach, the modelled pressure is matched with experimental pressure at TDC, based on the non-reactive experiments. For the compression phase, the effective volume approach is a relationship that incorporates an additional volume to the actual time-dependent geometric volume of the reaction chamber. This is called a time-dependent "effective volume" of the core gas region. After TDC is attained, the volume expansion is specified in terms of a polynomial fit to estimate effective volume according to the adiabatic core assumption. Alternatively, the effective volume can be calculated based on Equation (3.8) and reported in tabular format:

$$V(t) = V_i \left(\frac{P(t)}{P_i}\right)^{\frac{1}{\gamma}} \tag{3.8}$$

where $V(t)$ is the time varying effective volume, $P(t)$ is the measured non-reactive pressure, P_i is the initial pressure and γ is the specific heat ratio.

Figure 3.4 shows that the experimentally measured pressure traces match precisely with the computed pressure-time histories using the variable volume approach for both reactive and non-reactive cases. Here, an example for the 40% vol n-butanol blend with TRF at $T=831$ K, $P=2$ MPa and $\varphi=1$ is provided. The pre-ignition heat loss between reactive and non-nonreactive mixtures, as well as between experimentally measured and

computed profiles were found to be nearly identical. This consistent behaviour between experimental and computed, reactive and non-reactive mixtures was evident for all fuel blends and thermodynamic conditions tested in this study. Therefore, the approach of using variable volume for simulating RCM experiments is computationally validated and is deemed as adequate for chemical kinetic analysis.
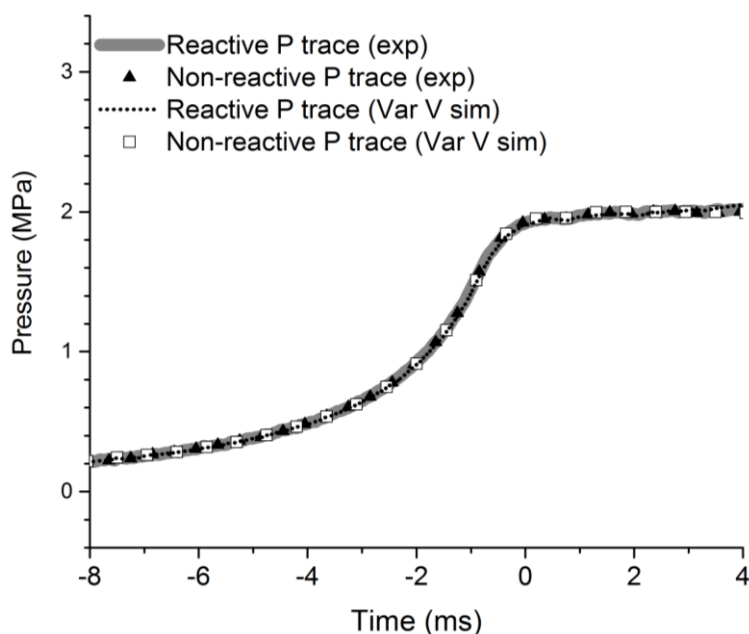
Figure 3.4: Comparisons of experimental reactive and non-reactive pressure histories with computed reactive and non-reactive pressure-time profiles using a variable volume approach for 40% vol n-butanol blend with TRF at T=831 K, P=2 MPa and φ=1. Pressure traces are aligned at end of compression where time is zero.

The experimental non-reactive pressure history can be immediately transformed into a volume history using the mixture temperature-dependent specific heat ratio and the isentropic core relations. Herein, a python-based sub programme acquired from the GitHub account of Weber [264] was applied together with an in-house Cantera RCM code. The produced volume histories were employed in Cantera simulations at each time step, during which the state of the RCM reactor is progressed. While this methodology is quite simple and produces a relatively accurate representation of experimental pressure profiles, it doubles the number of tests required for the experimental work, as for every chosen reactive run its equivalent non-reactive counterpart is required. Also, computations using a variable volume approach require experimental input and as such necessitate a longer modelling timeframe. For example, the computation for B10 at 727 K using a constant volume approach was 39.8 seconds long, whereas the same

computation using a variable volume approach took 136.2 seconds to compute. Hence, in this case, a variable volume simulations was 3.4 times longer compared to constant volume simulations. In case of B85 at 727 K, a variable volume simulation was 19.3 times longer compared to the equivalent computations using a constant volume approach, with respective values of 807.6 seconds and 41.8 seconds. Hence, the computations using a variable volume approach are more computationally expensive compared to computations using a constant volume approach.

3.3.3 Ignition delay time simulations

Consistent with the experiments, the computed τ_i is based on variable volume approach were defined as the time from the end of compression, determined from experimentally non-reactive runs, to the point of the maximum pressure derivative and reported at T_c determined from experimentally measured P_c (Equation (3.7) as described earlier). For the constant volume simulations, these were defined from the start of the simulations to the maximum pressure derivative, and reported at computed T_c based on Equation (3.7). Also similarly to experiments, the modelled first-stage ignition delay times, τ_1, were defined from the end of compression, determined from experimentally non-reactive runs, to the time of local maximum in the LTHR. The computed second-stage ignition delays, τ_2, were defined as the induction time from the end of τ_1 to the maximum dP/dt.

3.3.4 Excitation time simulations

Following Lutz et al. [36], the excitation time, τ_e, was defined as the time from the point where the heat release rate was 5% of the maximum heat release rate to the instant where that maximum value was attained. No experimental validation of the computed values of τ_e is possible, as it is not possible to measure either compositional or temperature changes on such a small time scale. This implies a degree of uncertainty in the controlling chemistry and its applications. To ensure high accuracy of the computed heat release at this lower bound, the value of the heat release was interpolated using cubic splines in time.

3.3.5 Modelling ignition delay times and excitation times for methane

The study of the auto-ignition of CH_4/air detailed in Chapter 4 employed the Cantera software toolkit under the Python programming language and the detailed chemical kinetic mechanism for CH_4/air, Mech_56.54, of Burke et al. [186]. This is based on the AramcoMech1.3 mechanism [183]. Mech_56.54 [186] was developed in 2015, covering 113 species and 710 reactions. For convenience, for each set of conditions, the reactions were numbered consecutively in order of increasing endothermicity. The mechanism has

been broadly validated against measurements in flow reactors, jet stirred reactors, and shock tubes for predictions of ignition delay times, burning velocities, and flame speciations for pressures, P, between 0.71 and 4.15 MPa over a range of temperatures, T, between 600 and 1600 K, at values of equivalence ratio, ϕ, from 0.3 to 2.0 [186].

For comparison, the present simulations of τ_i were also performed with the widely used GRI Mech3.0 mechanism [265], developed earlier in 1999. This comprises 325 elementary chemical reactions, with related reaction rate constants and thermodynamic parameters of 53 species. GRI Mech3.0 [265] has improved kinetics and broader target data when compared to the earlier versions of this mechanism. It has been optimised against CH_4 and natural gas flame speeds and shock tube measurements between 0.001-1.01 MPa and 1000-2500 K [266].

The simulations were zero dimensional, adiabatic, and at constant volume. The time steps were adaptive, dependent upon P and T, with sufficiently small time meshes of 1.0×10^{-7} -1.0×10^{-10} s for, τ_i, and of $1.0 \times 10^{-12} - 1.0 \times 10^{-14}$ s for τ_e, to ensure grid independent solutions.

3.3.6 Modelling n-butanol/gasoline surrogate auto-ignition in the Leeds RCM

Simulations of τ_i for all fuels and conditions investigated in Chapters 5 and 6 were conducted using Cantera for a single-zone, zero-dimensional variable volume reactor model with imposed specific volume histories determined from measured pressure traces of the non-reactive counterparts to account for RCM facility effects such as heat losses and reactions taking place during compression. Non-reactive experimental volume profiles of n-butanol/TRF blends are provided in the Supplementary Materials of [267]. The detailed chemical kinetic mechanism employed here comprises the LLNL gasoline surrogate mechanism of Mehl et al. [143] combined with the n-butanol scheme of Sarathy et al. [57] with several updated rate constants. Firstly, rates for the H-abstraction from n-butanol by OH were updated according to the study of McGillen et al. [268] as used in [41]. In addition, based on the sensitivity analysis conducted in [41], which highlighted the importance of the reaction: phenol+CH_3↔toluene+OH, this rate has been updated according to Seta et al.[269] which was the source of other toluene+OH rate coefficients within the mechanism. The mechanism has been combined and has been updated by Agbro [78]. It comprises 529 species and 4439 reactions and is provided in the Supplementary Materials of [267].

For comparison, the computations of τ_i and τ_e were also conducted using the upgraded Politecnico di Milano (POLIMI) kinetic mechanism [89], in which the low temperature chemistry for alcohol fuels was recently updated. The initial global POLIMI mechanism contains approximately 500 species and 20 000 reactions and has been extensively validated for pure TRF constituents, specifically *n*-heptane, *iso*-octane and toluene as well as their blends [270-272]. The updated POLIMI mechanism [89] employed in this study uses a lumped description of the primary propagation reactions of larger species and primary intermediates [273], alongside the structural analogies and similarities within different classes. This enabled maintaining a lower number of species within the kinetic mechanism (459 species, 12 687 reactions). Cross reactions present in the POLIMI scheme are not featured in the primary mechanism used in this study, the KAUST/LLNL mechanism. The importance of cross reactions is debatable. Hence, the use of the POLIMI scheme allowed a study of the effects of cross reaction addition and comparisons between the two mechanisms as detailed in Section 5.7. Moreover, this also enabled investigation of τ_e dependence on the mechanism, since as mentioned previously it is extremely difficult to validate τ_e experimentally. Details on this study and its main findings are provided in Section 6.3.

3.3.7 Sensitivity analysis of chemical kinetic models

In order to explore and assess the chemistry controlling the auto-ignition processes of the fuels studied in this thesis, and to determine the main reactions that effect ignition delays, excitation times and heat release rates, brute-force local sensitivity analyses were carried out.

3.3.7.1 *Methane/air auto-ignition*

For the study of methane/air auto-ignition discussed in Chapter 4, brute-force sensitivity analyses were performed at four temperatures of 1000 K, 1200 K, 1500 K and 1800 K at a pressure 0.1 MPa, and 700 K, 1000 K, 1200 K and 1500 K at a pressure of 10 MPa for τ_i and τ_e. The A-factors of all reactions were increased by 10% from their nominal values in a sequential manner, while all other parameters were held at their base values, and the influences on important reaction ignition delay times or excitation times were measured by performing a new simulation for each parameter change. The ignition delay time or excitation time sensitivity to each reaction i in the mechanism was estimated as:

$$S_i = \frac{(\tau_0 - \tau_1)}{\tau_0} \tag{3.9}$$

where S_i is the sensitivity coefficient of reaction i, τ_0 is the ignition delay time or excitation time computed with the original kinetic scheme without any changes to A-factors, τ_1 is the ignition delay or excitation time modelled when one of reaction rates A-factors has been perturbed.

Therefore, a positive S_i coefficient indicates the reaction which promotes reactivity thus decreasing τ_i or τ_e, whereas a negative S_i signifies a reaction which inhibits reactivity thus increasing τ_i or τ_e. The S_i values for each temperature and pressure were normalised by the maximum value at each temperature and pressure, hence the reaction with the largest effect on the predicted output target has a sensitivity index of 1.

3.3.7.2   n-butanol/TRF blends auto-ignition

For the study of n-butanol/TRF auto-ignition detailed in Chapters 5 and 6, brute-force sensitivity analyses were executed using predicted τ_i, τ_e, accumulated heat release, peak low, intermediate and high temperature heat release values as the target output for pure n-butanol, TRF and their fuel blends tested at $\varphi = 1$, $P = 2$ MPa and various temperatures using constant volume simulations. Constant volume conditions were used in order to achieve the shortest run times since thousands of simulations are required for a brute-force study where the sensitivity of the output to each reaction in the mechanism was computed by increasing each reaction rate A-factor by 50% for τ_i, and 10% for all other tested parameters from their nominal values in turn. These increases in reaction rate A-factor magnitudes were found to be sufficient to assess the effect of change of model parameters in close proximity to its nominal value on model response. As shown in Table 5.1 to Table 5.3, T_c predicted by adiabatic core relations and temperature dependent mixture specific heat ratios, have uncertainties in temperature estimation of ~9 K compared to T_c calculated using measured P_c. However, it was confirmed that the constant volume simulations did not deviate significantly from those using variable volume histories, with examples shown Figure 5.19. The small differences were shown to not affect the sensitivities greatly.

Similarly to the methane/air auto-ignition study, the τ_i, τ_e, peak values of LRHR, ITHR, HTHR and low temperature aHR sensitivity to each reaction in the kinetic mechanism was calculated using Equation (3.9), where S_i is the sensitivity coefficient, τ_0 is the parameter simulated with the original kinetic model and τ_1 the parameter computed when one of reaction rates has been perturbed. Consequently, a positive S_i signifies a reaction which decreases τ_i, τ_e, aHR and peak values of heat releases, whilst a negative S_i signifies

139

a reaction which increases τ_i, τ_e, aHR and peak values of heat releases. Again, the S_i values for each blend were normalised by the maximum sensitivity at each temperature, thus the reaction with the highest effect on the predicted τ_i has a sensitivity index of 1.

3.4 Analyses of heat release and knock potential

3.4.1 Heat release analysis

The acquired experimental RCM pressure-time histories of *n*-butanol/TRF blends at a compressed pressure of 2.0 MPa, a temperature range of 678-916 K and stoichiometric conditions presented in Chapter 5 were post-processed to assess the extents of preliminary heat release, as detailed in Chapter 6. The heat release analyses provided fundamental data on auto-ignition behaviour and associated multi-stage auto-ignition phenomena. Also, this allowed a further investigation into the effects of *n*-butanol addition on the LTHR, aHR, ITHR and HTHR of the blends.

3.4.1.1 Multi-stage ignition

As discussed in Section 2.3.2.6, *n*-butanol exhibits a more Arrhenius-like behaviour. The TRF surrogate consists of aromatic and paraffinic fuels. Similarly to alcohols, aromatics do not show a clear NTC behaviour, and exhibit a single-stage ignition. On the other hand, the two paraffinic TRF components, namely *iso*-octane and *n*-heptane, have an apparent LTHR. They are known to display NTC behaviour at low temperatures. This consequently results in a two-stage ignition, or in some cases three or more stage ignition processes. Sarathy et al. [274] recently showed *n*-heptane exhibits three-stage ignition behaviour in their RCM measurements. However, it is not clear how the addition of an *n*-butanol constituent to the mixture affects this multi-stage behaviour. Hence, heat release analyses help to assess and to quantify the heat release behaviour of *n*-butanol/TRF blends under different blending ratios. They also provide further characterisation of the auto-ignition processes of these fuel blends. Examples of single-, two-, and three-stage ignition, with accompanying HRR profiles, are illustrated in Figure 3.5.

In Figure 3.5 (a), it is shown that a single-stage ignition is represented by the total ignition delay time, and does not exhibit LTHR in its corresponding HRR profile. Figure 3.5 (b) demonstrates a two-stage ignition event, where two pressure rises occur in the post-compression processes. Two-stage ignition is characterised by an apparent peak in the LTHR, which defines the end of the first-stage ignition delay time. The subsequent time interval is representative of the second-stage process. In Figure 3.5 (c), heat release and

ignition characteristics demonstrate a three-stage ignition, which can be identified from the HRR profile. Here, each ignition stage is identified by a distinct peak in the heat release. Similarly to the two-stage auto-ignition, for the three-stage auto-ignition the first-stage ignition is defined as the time from the end of compression at TDC to the local maximum in the LTHR. The second-stage ignition is the proceeding time interval to the second local maximum representative by the peak in the ITHR. The third-stage ignition is the final time lapse from the peak in the ITHR to the hot ignition, where the maximum *dP/dt* value is evident. The total ignition delay is the sum of first- and second-stage ignition delays in the two-stage process, or the sum of first-, second- and third-stage in the three-stage process. In Section 6.1, the three-stage events were represented by the two-stage ignition, where the second- and third-stage processes were combined.
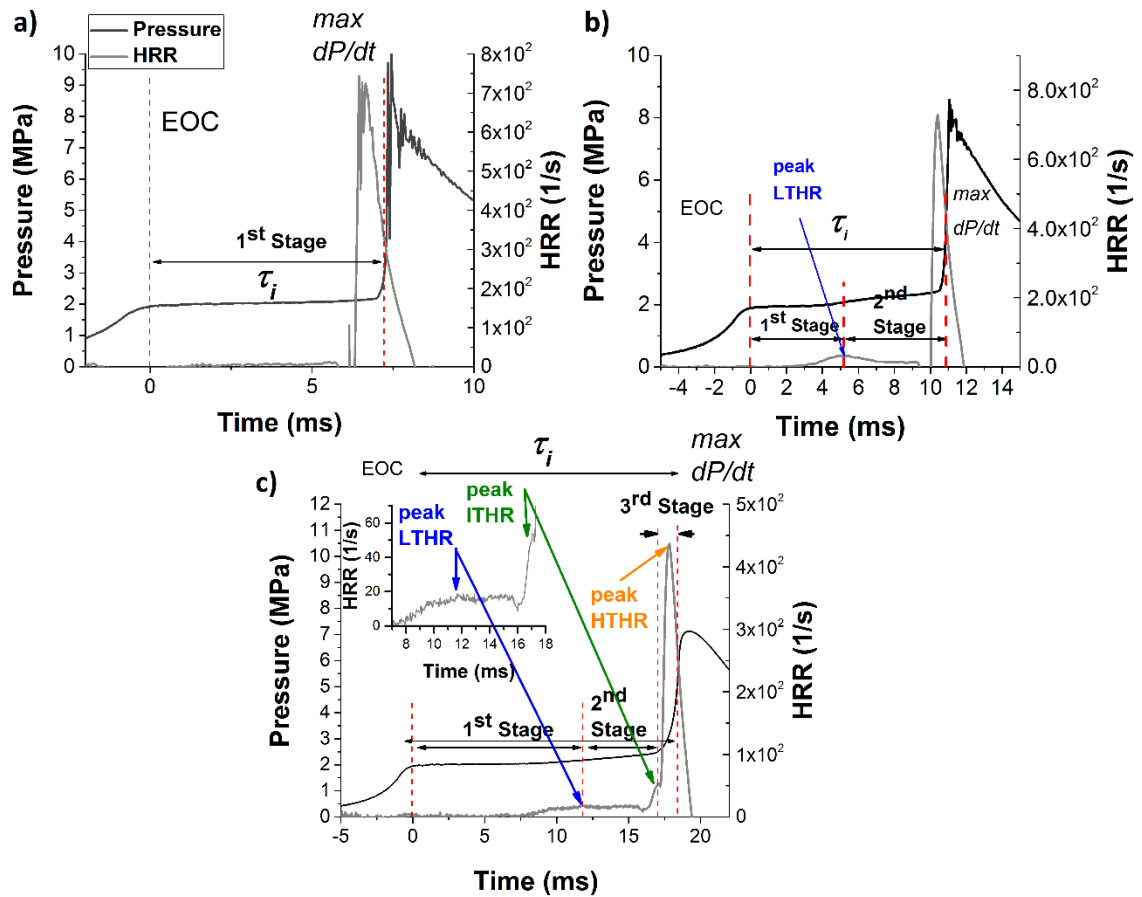
Figure 3.5: Representative experimental pressure time histories and heat release rates defining a) single-stage ignition of B85 at 855 K b) two-stage ignition of B10 at 745 K and c) three-stage ignition of B10 at 702 K. *P*=2 MPa and *φ*=1.

3.4.1.2 Data processing

The heat release rates (HRRs) and accumulated time-integrated heat releases (aHRs) were modelled using an energy balance method as described in [275], but in which the

volumetric compression and accompanying heat loss are empirically accounted for in the heat release analysis through experimentally measured non-reactive pressure traces. This method was proposed by Goldsborough et al. [252] and successfully applied in [252, 276] to extract quantitative information on preliminary exothermicity of various fuels from RCM records based on the energy conservation equation:

$$\frac{dU_s}{dt} = \dot{Q}_{chem} - \dot{Q}_{wall} - W_{piston} - \dot{H}_{out} + \dot{H}_{in} \qquad (3.10)$$

where U_s is the total sensible internal energy, $\dot{Q}_{chem}$ is the rate of heat released, $\dot{Q}_{wall}$ is the rate of heat exchange with the chamber walls, W_{piston} is the rate of work done by the piston on the gas, $\dot{H}_{out}$ and $\dot{H}_{in}$ are the rates of enthalpy flow out of and into the system, respectively. When the energy flows can be accurately monitored, the excess energy can be assigned as chemical energy [252].

Herein, an adiabatic core hypothesis as described in Section 3.2.3 was employed with a single zone consisting of both burnt and unburnt gasses, in which any reactivity in the boundary layer gas was neglected. This model assumes ideal gas behaviour with a uniform pressure distribution across the reactor. Similarly to detailed kinetic simulations with a variable volume approach detailed in Section 3.3.2, the heat loss within the reactor was accounted for empirically via measured non-reactive pressure traces.

By assuming that the piston trajectories and change in volume *dV/dt* are identical between both reactive and non-reactive experimental measurements, Equation (3.10) can be expressed as:

$$HRR = \frac{\gamma}{\gamma-1}\frac{dV}{dt}(P - P_{nr}) + \frac{1}{\gamma-1}V\left(\frac{dP}{dt} - \frac{dP}{dt}\Big|_{nr}\right)$$
$$- \frac{PV}{(\gamma-1)^2}\left(\frac{d\gamma}{dt} - \frac{d\gamma}{dt}\Big|_{nr}\right) \qquad (3.11)$$

where *HRR* is the heat release rate, γ is the ratio of specific heats, *V* is the reaction chamber volume, *P* is the pressure in the chamber and the suffix '*nr*' denotes properties of the non-reactive case.

Based on Equation (3.11) the HRR can be calculated at any point during an RCM experiment, provided the respective reactive and non-reactive pressure time traces are available. Therefore, calculations were carried out on corresponding reactive and non-reactive filtered runs where the heat capacity of the reacting mixture was evaluated in

accordance with the degree of reaction, and with the desired blend of reactants and complete products. The Cantera suit was employed to simulate the experiments using a combined mechanism of LLNL gasoline surrogate mechanism of Mehl et al. [143] with the *n*-butanol scheme of Sarathy et al. [57] with several updated rate constants as detailed in Section 3.3.6. This enabled calculations of the temperature dependent specific heat ratios in Equation (3.11) resolving the changing composition of the mixture during the experiments. The thermodynamic properties of all species for the LLNL gasoline surrogate mechanism of Mehl et al. [143] and for the *n*-butanol scheme of Sarathy et al. [57] were calculated using the THERM program developed by Ritter and Bozzeli, and by applying Benson's group additivity method [153, 277]. This method uses discrete point values for each "group" value, adds the distinct values for each temperature and then fits a polynomial to obtain the final results [278]. Generally, only a small minority of species in combustion processes can be assigned high accuracy standard enthalpies of formation. Even for small C_1-C_3 hydrocarbons with relatively small errors in the standard enthalpy of formation values, there might be relatively large uncertainty in the equilibrium constants. The values are less well-known for larger hydrocarbons, implying a higher degree of uncertainty [278]. For example, according to the Argonne Active Thermochemical Tables [279], the estimated uncertainty in the enthalpy of formation of -187.52 kJ/mol for *n*-heptane at 298.15 K is +/-0.48 kJ/mol, based on 20 contributions between 1931 and 2009. For *iso*-octane, the corresponding enthalpy of formation is -258.9 kJ/mol at 298.15 K with an uncertainty of +/-1.5 based on one contribution from 1945 [280]. There were no direct links to the sources of the thermodynamic properties in the combined KAUST/LLNL mechanism. However, in their analysis [143] utilised relevant thermodynamic properties provided in the Burcat database [278] (when the species was available). These evaluations may not always enclose the latest data or be derived from single theoretical studies. This implies a high degree of uncertainty in the enthalpy of formation for some larger species, which are less well known.

The combined KAUST/LLNL detailed chemical kinetic scheme was also used to model the HRRs detailed in Section 6.2 using a variable volume approach as outlined in Section 3.3.2. This enabled an assessment of the ability of the chemical detailed mechanism to reproduce experimentally derived HRRs and to investigate the exothermicity of fuel blends over a range of temperatures as presented in Chapter 6. Also in this study the potential links between the extent of LTHR and ignition delay times were explored.

A Kistler 6045A dynamic pressure transducer was used to acquire pressure-time histories at a frequency of 20 kHz in the University of Leeds RCM as described in Section 3.2. Recorded signals are capable of resolving both low- and high-temperature heat release processes. A higher degree of uncertainty is encountered for the high-temperature heat release processes in this thesis due to limitations of the experimental apparatus and its current setup. Since the focus of the study in Chapter 6 is primarily associated with the LTHR processes, the data were sampled at a frequency of 20 kHz providing a higher resolution for the low temperature heat release processes. A much higher frequency (~1000 kHz) is required to adequately resolve HTHR processes [252]. For this reason, the experimentally derived and modelled HTHR were not directly compared in this thesis. A higher degree of accuracy of HTHR can be achieved by incorporating a second data acquisition card, calibrated specifically for HTHR processes, as detailed in [252, 276]. The recorded pressure-time histories were aligned at the end of compression, based on piston displacement measurements at TDC. A 2nd order fit, Savitzky-Golay algorithm was applied to measured pressure traces prior to processing, with a 51 data points window of 2.55 ms for TRF and n-butanol/TRF blends, or an 11 data points window of 5.5 ms for pure n-butanol. This supplementary filtering ensured that the high frequency noise was excluded from the pressure measurements. For simplicity, all reported HRRs were normalised by the lower heating value (LHV) of the fuel blend. The LHV of the mixtures were calculated using the Cantera code.

The extent of accumulated low temperature heat release (aHR) is adopted as the time-integrated HRR from the end of compression through the peak HRR in the first-stage ignition delay, τ_1, up to the subsequent local minimum in HRR (infection point in HRR) just before the further rapid increase in HRR indicative of ITHR or HTHR of the hot ignition. This definition is illustrated in Figure 3.6 for four subsequent experimental runs and their corresponding average for B10 at 727 K, where representative reactive and non-reactive pressure traces are aligned at the point of the maximum pressure rise for the main ignition, along with accompanying HRR profile. Generally, at higher n-butanol/TRF blending ratios, it was challenging to define the exact location of the infection point in the HRRs. Here, there was no abrupt end of LTHR nor a distinctive local minimum in the HRR profiles prior to the main ignition event. Instead, a slow gradual rise in the HRR profiles was observed. This is not surprising, since this behaviour was previously shown in the chemical kinetic study by Agbro et al.[42]. However, it made the interpretation of the heat release and the definition of aHR substantially more difficult. For these cases,

the infection point in the HRRs was assumed to be the point of the smallest heat release gradient occurring prior to the main heat release event. This adopted approach implies some degree of uncertainty and results in some variability in the aHRs, but ensures consistency between all tests. The reported aHRs in Figure 6.7 and Figure 6.9 are presented as averages of 3-5 subsequent test runs, with error bars of one standard deviation as an indication of reproducibility.
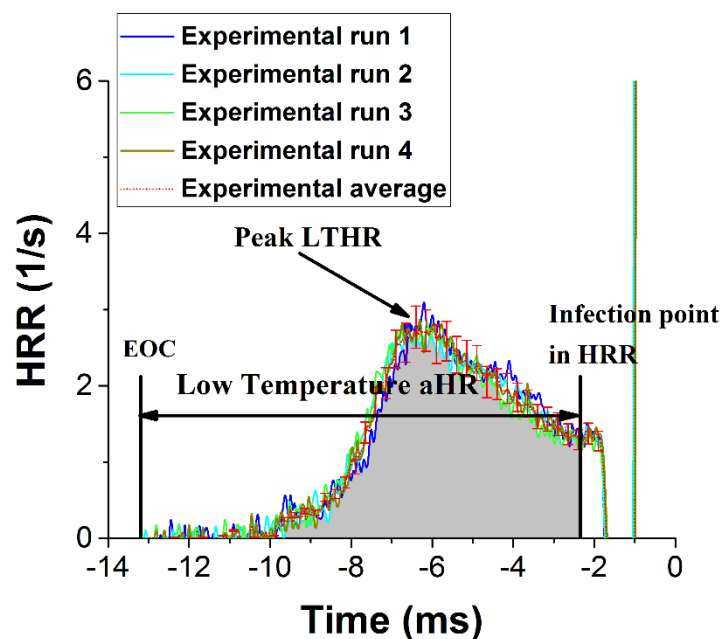
Figure 3.6: The normalised HRR curves of four experimental runs and their corresponding average for 10% vol n-butanol blend with TRF at T=727 K, P=2 MPa and φ=1, illustrating experimental repeatability and the definition of the aHR. The traces are aligned at the point of the maximum pressure rise for the main ignition. The error bars signify the uncertainty of the aHR experimental average boundary.

Uncertainties related to the RCM experiments can be quite challenging to precisely estimate [281]. The compressed pressures and temperatures are commonly calculated using the adiabatic core assumption. These uncertainties, along with the adiabatic core assumption are among the largest sources of error in heat release calculations. Heat loss is a significant factor influencing the accuracy of experimentally derived heat release profiles. During the heat release processes, there can be a heat loss that is larger than the one represented by non-reactive experiments [276]. Moreover, at some conditions heat release rates of the mixtures can be comparable to heat losses of the system. This results in further challenges regarding the estimation of the heat release calculation errors. As a result, it is challenging to distinguish the estimated heat release calculation errors from

the uncertainties in the RCM experiments. A precise assessment of these errors is outside the scope of this work.

3.4.2 Characterisation of detonation

The ignition behaviour in the RCM was further assessed and characterised following the detonation peninsula framework proposed by Bradley et al. and co-workers [91, 96], within which detonations could develop. The boundaries were defined by dimensionless parameters, $\xi = a/u_a$ (Equation (2.22)) and $\varepsilon = r_0/a\tau_e$ (Equation (2.23)), where a is the acoustic speed, u_a is the auto-ignition velocity, r_0 is the radius of a spherical hot spot and τ_e is the excitation time. Details on detonation theory and its governing equations are provided in Sections 2.1.12 and 2.1.13.

This theoretical approach aims to extend understanding of auto-ignition phenomena and to assess the anti-knock characteristics of fuels over a wide range of engine relevant conditions. The distinct regimes for hot spot auto-ignition, stretching from controlled auto-ignition towards the development of knock and super-knock phenomenon, could be detected through the values of τ_i, τ_e and $\bar{E}$ on the ε-ξ diagram, where $\bar{E}$ is defined by Equation (2.24).

For methane-air auto-ignition study detailed in Chapter 4, all parameters were based on detailed chemical computations of AramcoMech1.3 mechanism [183] using constant volume approach. On the other hand, for the n-butanol/TRF study described in Chapter 6, reported in Chapter 5 experimentally measured τ_i were employed. Cantera was used to simulate τ_e using a variable volume approach and a reduced combined mechanism for n-butanol from Sarathy et al. [57] and for the TRF surrogate from Mehl et al. [143], modified with the suggestions in [41] as described in Section 3.3.6. Values of acoustic speed, a, for every fuel/fuel blend and studied condition were also calculated using the same mechanisms in the Cantera package. The assumption of a temperature gradient value of $(\partial T/\partial r)$= -2 K/mm was chosen based on engine and other measurements [90], while a hot spot radius of 5 mm was assumed which is representative of the turbulent flow length scales and heterogeneities in SI engines. This value of a hot spot radius was also chosen by Kalghatgi et al. [282] and Rudloff et al. [283].

4. Computational Study of Methane/Air Auto-ignition Behaviour

Ignition delay times, τ_i, and excitation times, τ_e, for stoichiometric methane/air mixtures were modelled using a comprehensive chemical kinetic scheme within a pressure range of 0.1 and 10 MPa, and a temperature range of 700 and 1800 K. Methane is the major constituent of natural gas and relatively clean-burning fossil fuel. It was studied here because of its widespread distribution and usage in heating and power generation. The chemical kinetics of its oxidation are reasonably well understood, rendering predictions based on recently developed chemical mechanisms fairly reliable, when compared to many larger hydrocarbon fuels. For these reasons it has been chosen for the initial simulations and study of auto-ignition phenomena described in this Chapter, prior to the more complex fuels and fuel blends described in the Chapters 5 and 6. The present predictions are based on the widely used GRI Mech3.0 mechanism [265], with the more recently developed Mech_56.54 mechanism [186].

The purpose of this study is to provide a better understanding of conditions that lead to detonation and identification of the characteristics of the deflagrative, auto-ignitive and transitional reaction regimes. This is achieved through careful evaluations and interpretations of the key fundamental combustion characteristics, namely ignition delays and excitation times. These two times can be used for any fuel over an extensive range of pressures and temperatures and provide a fundamental approach to auto-ignition phenomena. In particular, these analyses were performed for CH_4 in this Chapter. In Chapter 6, this was extended to more complex fuels, namely TRF, *n*-butanol and their blends. It is of interest of this thesis to examine how the auto-ignition phenomena of CH_4 with Arrhenius-type behaviour compares to that of fuels with an NTC. Accurate evaluations of τ_i and τ_e make it possible to assess the propensity of CH_4 to detonate, whilst its auto-ignition loci in an engine, relative to the detonation peninsula on the ξ/ε diagram, enable its knocking propensity to be compared with those of other fuels. Also to further explore and assess the chemistry controlling the auto-ignition processes of the methane/air and to determine the main reactions that effect ignition delays and excitation times, the brute-force local sensitivity analyses were performed at four temperatures and two pressures of 0.1 MPa and 10 MPa.

4.1 Comparison of model prediction with the available experimental data in the literature

Figure 4.1 (a) and (b) compare the modelled ignition delay times, using both the Mech_56.54 and GRI Mech3.0 detailed kinetic mechanisms with available experimental data from the literature, at different T, for stoichiometric CH_4/air, at pressures of 0.1 MPa and 4 MPa, respectively. The plots suggest a near Arrhenius relationship between 1000 and 1800 K. In Figure 4.1 (a) agreement between these models and the experimental measurements of Hu et al. [284], Herzler and Naumann [285], Trevino and Mendez [286], and Zeng et al. [287] is satisfactory at the higher temperatures. However, at the lower temperatures the GRI Mech3.0 mechanism tends to over-predict reactivity presenting shorter ignition delays than reported in Trevino and Mendez [286]. This is not surprising, as this scheme has been designed and validated against the higher end of the temperature range, where it indeed has showed relatively good performances. The earlier values of Lutz et al. [36] tend to underestimate τ_i to a greater extent than GRI Mech3.0.

There is a much greater scatter in the experimental measurements at the higher pressures in Figure 4.1 (b). Both mechanisms show significant differences with the experimental measurements of Huang and Bushe [288], Kim et al. [289], Huang et al. [266] and Merhubi et al. [290]. The Mech_56.54 mechanism tends to capture the overall trend of τ_i variations better than those of the GRI Mech3.0 model, particularly at the lower temperatures. Mech_56.54 has been validated against a rather broader range of pressures and temperatures than GRI Mech3.0. GRI Mech3.0 has been optimised only up to 1.01 MPa. The Mech_56.54 mechanism was therefore employed to model τ_i and τ_e and to conduct the subsequent chemical analysis of ignition processes of methane-air mixtures. Nevertheless, a severe limitation is that the selected detailed chemistry essentially rests upon shock tube and RCM data that exhibit significant scatter implying a level of uncertainty in the predicted results. This is particularly so at the highest pressure of 10 MPa, at which there are few, if any, direct measurements of τ_i for stoichiometric CH_4/air. There can be no such practical check on the predicted values of τ_e and the only procedure for its evaluation is through the detailed chemical kinetics route.
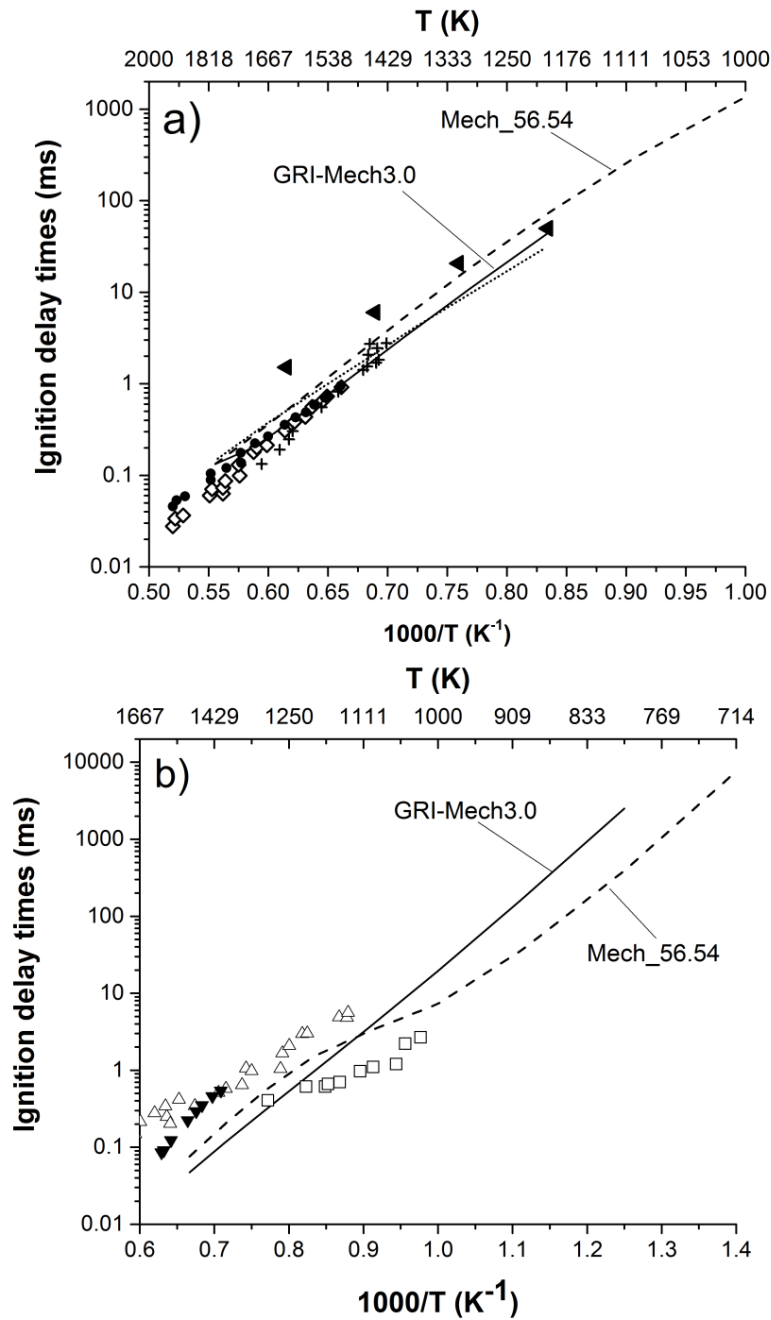
Figure 4.1: Ignition delay time predictions using both detailed schemes, GRI Mech3.0 [265] and Mech_54.54 [186], and comparison with measured values (a) at 0.1 MPa and (b) at 4 MPa. Lines represent modelled results, symbols referenced experimental data. (…) Lutz et al. [36], (◊) Hu et al. [284], (+) Herzler and Naumann [285], (◄) Trevino and Mendez [286], (•) Zeng et al. [287], (□) Huang and Bushe [288], (Δ) Kim et al. [289], (□) Huang et al. [266] and(▼) Merhubi et al. [290].

4.2 Comparisons between the comprehensive kinetic scheme and reduced global scheme

Reduced mechanisms illustrate the minimum number of chemical kinetic reactions and species that mirror, within a specified accuracy bond, the original detailed chemical kinetic scheme. Reduced schemes are extensively used in high-quality computational fluid dynamics softwares (e.g. Ansys Fluent, Ansys CFX, StarCCM++ etc.) for solving chemically reacting flow problems, which involve complex interactions of fluid mechanics. These software packages are capable of accurately predict the fluid flow behaviours and related physical phenomena by effectively solving complete systems of partial differential equations, which are greatly non-linear, stiff, prohibitively computationally expensive and very complicated. They are able to compute complex three-dimensional reactor geometries and elementary chemistry of reduced mechanisms. However, they fail to incorporate complete systems of species and reaction mechanisms, involving multi-component thermodynamic properties, transport properties, and reaction chemistry due to increased complexity of large systems. This is because the number of species in the detailed kinetic mechanism is linked to the number of solved equations in each computational cell of the mesh of reactor. This is usually limited to tens or few hundred species to avoid an excessive run time. Therefore, there is always a trade of between the efficiency of fluid mechanics and certainty of chemical kinetics of the model. The accuracy of such predictions using reduced mechanisms is debatable, and probably could be only applicable to rather specific combustion problems. Therefore, one of the initial objectives of this study was to assess the reliability of such reduced schemes.

All the work of calibrating and development of such reduced global reaction schemes, G1 and G2, as well as all its computations were conducted by Bates [291] and full details on its framework and computational procedures are given in [292] with just a brief description covered here.

The reduced global kinetic scheme employed in the present study requires just five global reactions between six active species with the appropriate selection on tuning of the global rate constants. The scheme is based on that of Schreiber et al. [293] and has a particular ability to predict τ_i for the Primary Reference Fuels, PRF, i-octane and n-heptane. The schematic details are outlined in Table 4.1. The octane number scaling factors of the original paper are omitted, allowing the model to be adapted for a fuller range of individual fuels. It is applicable to a broad range of fuels within its specified range of

150

conditions. For non PRF, mixtures, the model must be matched to the fuels by further adjustment of the global rate constants.

Table 4.1: Reduced Reaction Scheme. F: fuel, O_2: oxygen, P: product, Y: chain propagating species, X: chain branching species, I: product oxygenated radicals, molar ratio of O_2 to Fuel for desired equivalence ratio, $a = 2$ for CH_4.

Reaction Number	Reaction	Reaction Description
1 High Temperature	$F \rightarrow X$	Breakdown of fuel into branching intermediates
2 High Temperature	$X + aO_2 \rightarrow P$	Reaction of intermediates with oxygen to form products
3 Low Temperature	$F + 2O_2 \leftrightarrow I$	Reversible reaction converting between fuel and oxygen, and radical intermediate species
4 Low Temperature	$I \rightarrow 2Y$	Radicals react to form chain propagating intermediates
5 Low Temperature	$Y + 0.5F + (a\text{-}1)O_2 \rightarrow P$	Intermediates, fuel and oxygen react to form products.

An undeniable benefit of the global scheme is its computational speed, an important factor in the modelling of chemically reacting flow. The reduced global model was able to compute a single τ_i value, using Matlab's ODE15s solver for $T = 1000$ K and $P = 6$ MPa within 0.83 seconds. For the computations of τ_e, with a much reduced time mesh, this time was extended to 17.14 seconds. In contrast, the detailed kinetic scheme using Cantera software computed a value of τ_i, within 6.55 seconds and of τ_e, using advanced time step, within 199.69 seconds for the same conditions.

The resulting predictions using reduced global kinetic schemes are presented in Figure 4.2 to Figure 4.4. They have been shown to be capable of capturing the general trends of τ_i with the values similar compared to the detailed chemical kinetic predictions, as well as to the measured experimental values in the literature. Global kinetic schemes showed a slight tendency of over-predicting ignition delays at high temperatures and under-predicting them at low temperatures. However, despite the employment of sufficiently small time increments and separate calibrations of rate parameters, the reduced global scheme failed to accurately predict τ_e, under-estimating the τ_e values with several orders

of magnitude compared to those using the comprehensive scheme. These differences in τ_e predictions between two schemes also manifested in the differences in computed volumetric heat release rates. The failure to accurately predict τ_e and heat release rates for such a relatively simple fuel compared to larger hydrocarbons was one of the primary reasons for using the comprehensive kinetic modelling approach in Chapters 5 and 6. Also, in order to gain a more fundamental understanding of intricacies involved in detonation phenomenon, the detailed modelling is seen to be a more appropriate tool.
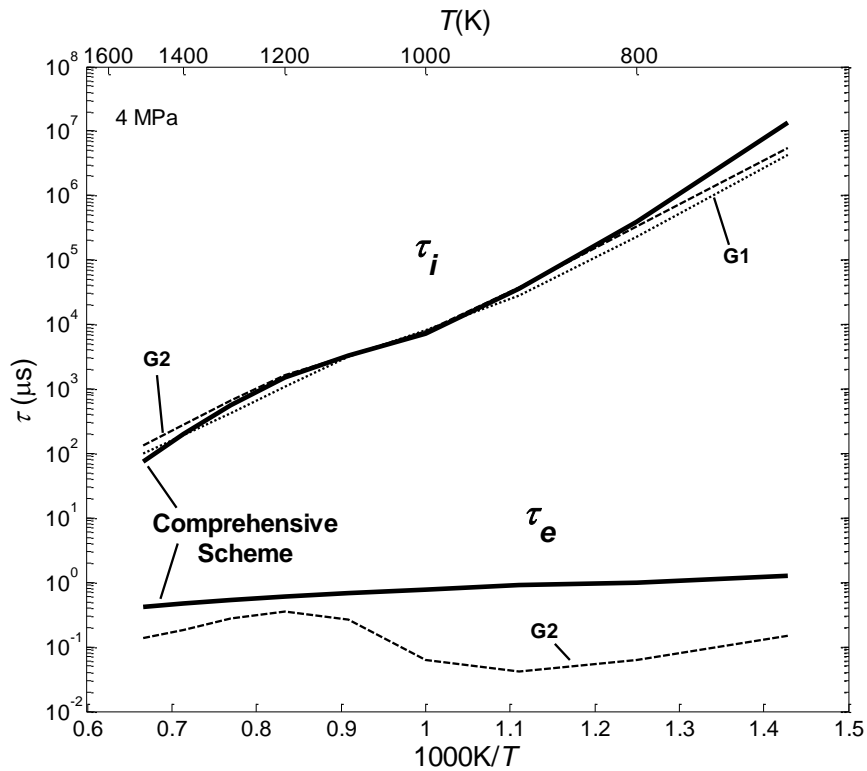
Figure 4.2: Comparison of ignition delay times, τ_i, and excitation times, τ_e, predicted by Comprehensive and Global schemes, G1 and G2, for stoichiometric CH_4/air at 4 MPa.
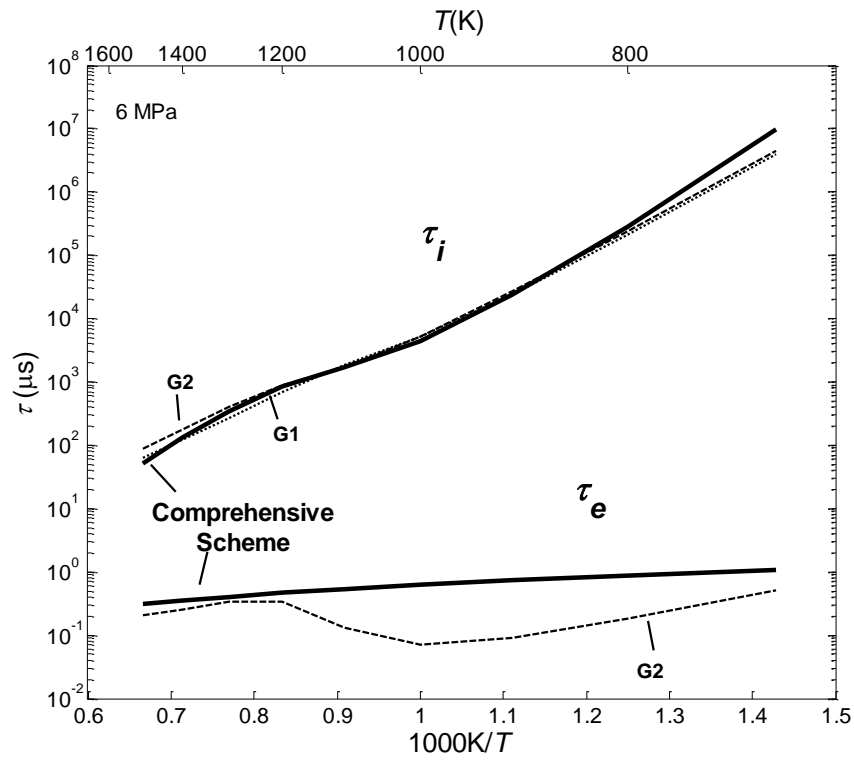
Figure 4.3: Comparison of ignition delay times, τ_i, and excitation times, τ_e, predicted by Comprehensive and Global schemes, G1 and G2, for stoichiometric CH_4/air at 6 MPa.
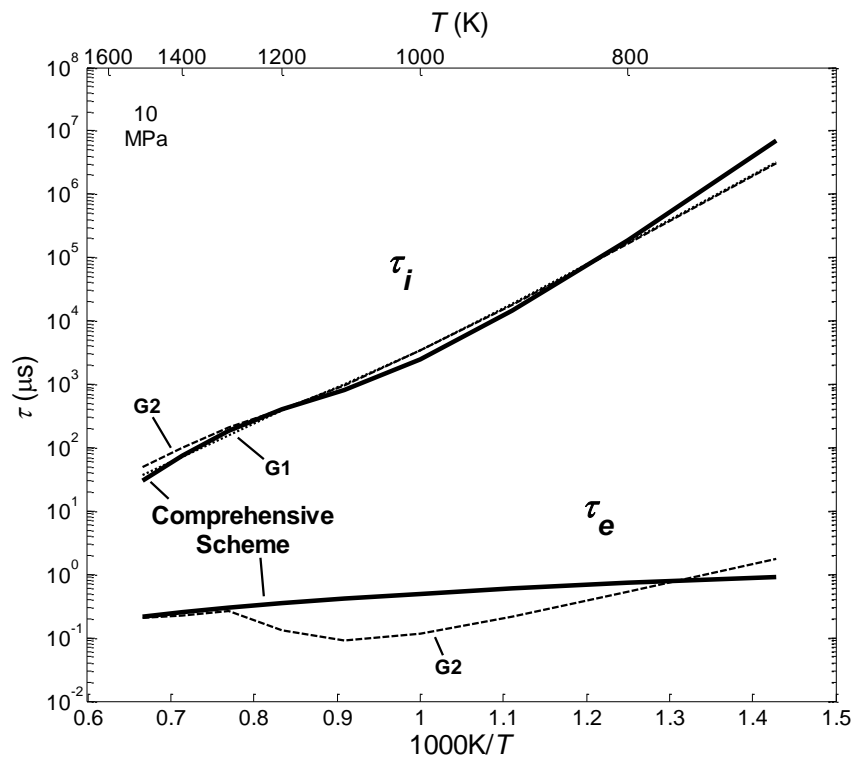
Figure 4.4: Comparison of ignition delay times, τ_i, and excitation times, τ_e, predicted by Comprehensive and Global schemes, G1 and G2, for stoichiometric CH_4/air at 10 MPa.

4.3 Computed values of ignition delay time and excitation time

Figure 4.5 presents modelled τ_i results as a function of inverse temperature for the stoichiometric methane/air at 0.1, 4, 6 and 10 MPa using the comprehensive kinetic scheme. The calculations predict that the ignition delay times decrease continuously with an increase of the initial temperature or pressure. They exhibit the Arrhenius-type behaviour, with the highest slope at the lowest pressure of 0.1 MPa. This is a typical characteristic of the methane auto-ignition behaviour (which is known to not exhibit the NTC behaviour), where the ignition delay increase with the temperature.
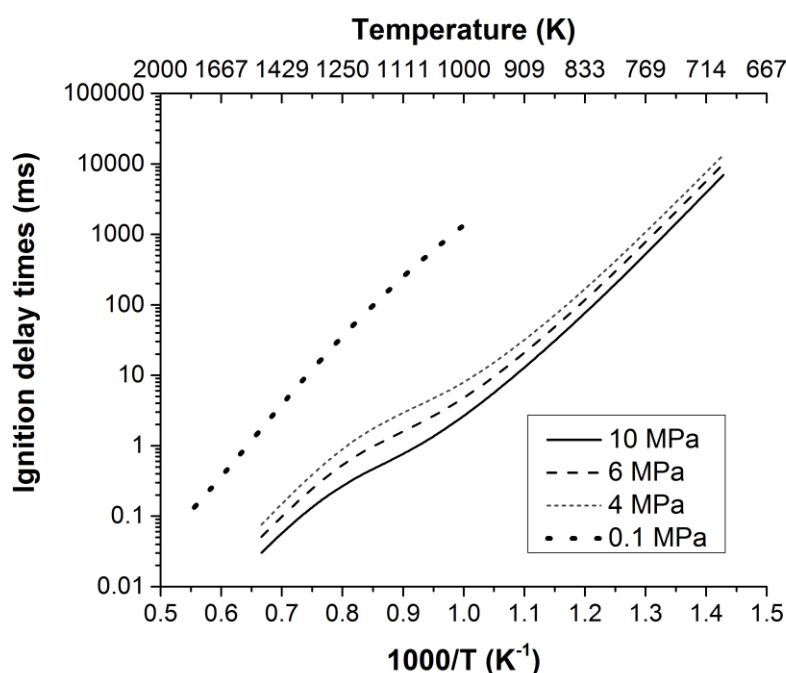
Figure 4.5: Effects of pressure on simulated ignition delay times of stoichiometric CH_4/air using Mech_56.54 [186] scheme.

Interestingly, the ignition delay trends are very similar across the high pressure conditions, showing analogous temperature dependent auto-ignition behaviour. The ignition delay times vary by about five orders of magnitude over the full range of temperature at all pressures, but by less than one order of magnitude over the pressure range of 4, 6 and 10 MPa at a fixed temperature. This distinctively differs for the lowest pressure of 0.1 MPa. Ignition delays still show a strong dependence of auto-ignition behaviour on temperature, with about five orders of magnitude change for the atmospheric pressure. There is a sharper increase in ignition delay times at 0.1 MPa compared to other pressures at a fixed temperature (about two to three orders of magnitude).

154

Predicted τ_e values for the methane-air mixture at pressures of 0.1, 4, 6 and 10 MPa were computed for the first time and are illustrated in Figure 4.6. Excitation times decrease only slightly with the increasing initial temperature (except for the 0.1 MPa case). This is consistent with the trends observed by Lutz et al. [36]. They are more sensitive to pressure change than temperature. Similarly to ignition delay time trends, 0.1 MPa has a distinctive behaviour with an increase of approximately two orders of magnitude at a fixed temperature compared to that of higher pressures. This implies that the controlling chemistry of ignition delay times and excitation times at this lowest pressure is substantially different compared to other conditions studied. This is explored later in this chapter though the assessment of the key reactions contributing to the overall heat release rate and the use of brute-force local sensitivity analyses.
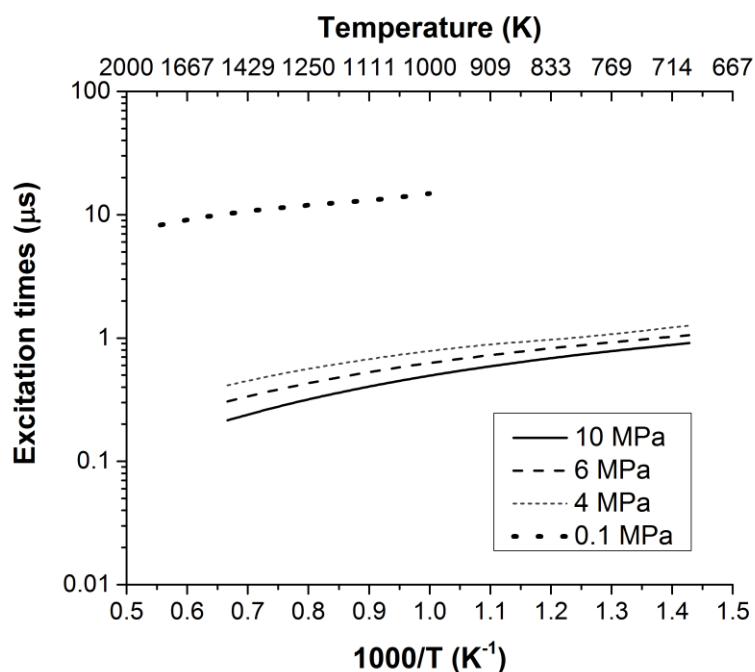
Figure 4.6: Effects of pressure on simulated excitation times of stoichiometric CH₄/air using Mech_56.54 [186] scheme.

4.4 Investigation of heat release rates

During the ignition delay time, chain branching reactions are active with small heat release, yet this period is terminated by the onset of a high heat release rate. The overall volumetric heat release rate, VHRR, is the net thermal energy release rate encompassing all 710 reactions. It has been used in calculating τ_e and has been analysed to determine the principal 23 contributory exothermic and endothermic reactions at different pressures

listed in Table 4.2. These are given for three different values of P and two of T in Table 4.2. The order in which the reactions appear approximately follows the chronology of the reactions from start to finish. They are selected on the criterion that, during the period within which the total heat release rate is more than 5% of the maximum heat release rate, the reaction should contribute more than 5% of the total. The four most endothermic reactions were selected on a similar basis, within the same regime. The bracketed figures within the Table 4.2 express the order of increasing endothermicity of the 710 reactions. Numbering is consecutive from 1 to 710, in increasing order of endothermicity. These numbers are given in brackets for each listed reaction. Percentage contributions to the maximum VHRR at the time of this maximum heat release are also given.

At 4 and 10 MPa the principal reactions contributing to the heat release rate are:

$$H + OH + M \leftrightarrow H_2O + M, \qquad\qquad R22 \qquad (4.1)$$

$$CO + OH \leftrightarrow CO_2 + H \qquad\qquad R21 \qquad (4.2)$$

or

$$H + O_2 (+ M) \leftrightarrow HO_2 (+ M) \qquad\qquad R16 \qquad (4.3)$$

with

$$HO_2 + OH \leftrightarrow H_2O + O_2 \qquad\qquad R23 \qquad (4.4)$$

And

$$H_2 + OH \leftrightarrow H + H_2O. \qquad\qquad R20 \qquad (4.5)$$

Not surprisingly, these are predominantly termination reactions, whereas previous work has shown that the time to ignition for CH_4/air mixtures is highly sensitive to chain branching routes such as R24 and R9 [138, 186, 294]:

$$CH_3 + O_2 \leftrightarrow CH_2O + OH, \text{ and} \qquad\qquad R24 \qquad (4.6)$$

$$H + O_2 \leftrightarrow OH + O. \qquad\qquad R9 \qquad (4.7)$$

Table 4.2: The 23 principal exothermic and endothermic reactions contributing to the overall Volumetric Heat Release Rate.

No.	Key Reaction	0.1 MPa 1200 K %		4 MPa 800 K %		4 MPa 1200 K %		10 MPa 1200 K %	
R1	$CH_4 + OH \leftrightarrow CH_3 + H_2O$	2.83	(12)	0.97	(21)	2.08	(18)	1.6	(20)
R2	$CH_3 + H (+M) \leftrightarrow CH_4 (+M)$	2.64	(14)	1.89	(14)	4.92	(9)	3.06	(12)
R3	$CH_3 + O \leftrightarrow CH_2O + H$	22.35	(1)	2.48	(10)	6.91	(6)	3.53	(11)
R4	$CH_2O + H \leftrightarrow H_2 + HCO$	6.66	(5)	1.22	(18)	3.00	(15)	1.96	(16)
R5	$HCO + M \leftrightarrow CO + H + M$	-10.40	(709)	-3.30	(708)	-6.61	(709)	-5.07	(709)
R6	$CH_2 + O_2 \leftrightarrow HCO + OH$	6.74	(4)	1.49	(16)	3.29	(14)	2.23	(14)
R7	$HCO + O_2 \leftrightarrow CO + HO_2$	1.79	(25)	0.31	(39)	0.59	(35)	0.40	(40)
R8	$CH_3OH (+M) \leftrightarrow CH_3 + OH (+M)$	0.52	(43)	3.01	(9)	4.19	(12)	4.53	(9)
R9	$H + O_2 \leftrightarrow O + OH$	-22.19	(710)	-14.82	(710)	-17.19	(710)	-13.68	(710)
R10	$2CH_3 (+M) \leftrightarrow C_2H_6 (+M)$	0.15	(71)	0.01	(114)	0.07	(92)	0.03	(98)
R11	$C_2H_4 + H (+M) \leftrightarrow C_2H_5 (+M)$	-0.21	(699)	-0.01	(687)	-0.07	(691)	-0.04	(690)
R12	$H + O + M \leftrightarrow OH + M$	0.09	(89)	2.40	(11)	1.73	(21)	2.18	(15)
R13	$H + HO_2 \leftrightarrow 2OH$	3.61	(10)	5.50	(7)	5.17	(8)	5.23	(7)
R14	$H_2O + O \leftrightarrow 2OH$	-0.99	(707)	-4.54	(709)	-2.67	(708)	-3.15	(708)
R15	$H + HCO \leftrightarrow CO + H_2$	5.73	(6)	0.43	(34)	1.21	(27)	0.57	(33)
R16	$H + O_2 (+M) \leftrightarrow HO_2 (+M)$	0.23	(63)	18.00	(2)	10.10	(2)	14.53	(2)
R17	$2HO_2 \leftrightarrow H_2O_2 + O_2$	0.03	(121)	0.39	(35)	0.25	(53)	0.58	(31)
R18	$HCCO + O_2 \rightarrow CO + CO_2 + H$	0.99	(31)	0.55	(29)	0.71	(32)	0.59	(30)
R19	$HCCO + OH \rightarrow 2CO + H_2$	7.97	(3)	5.51	(6)	7.40	(5)	5.60	(6)
R20	$H_2 + OH \leftrightarrow H + H_2O$	12.08	(2)	6.98	(5)	8.81	(3)	7.28	(5)
R21	$CO + OH \leftrightarrow CO_2 + H$	4.56	(6)	14.61	(3)	7.85	(4)	8.93	(4)
R22	$H + OH + M \leftrightarrow H_2O + M$	0.59	(39)	23.20	(1)	13.77	(1)	20.82	(1)
R23	$HO_2 + OH \leftrightarrow H_2O + O_2$	2.34	(18)	10.95	(4)	6.55	(7)	8.97	(3)

However, Nagy et al. [295] noted a high degree of uncertainty concerning R22, especially at high temperatures [296]. Experimental data points in support of a particular value of rate coefficient are sparse. Potential inconsistencies also occur in the data for R23, in that Burke et al. [297] suggested a temperature dependence different from that in [296]. In addition, R23 has been shown by Burke et al. [186] to have a weak sensitivity for the simulation of CH_4 ignition delays at high pressure, and to inhibit ignition, as does R16.

Along with R21, R20 is an important exothermic contributor at the lower pressure of 0.1 MPa and 1200 K, as shown in Figure 4.7. Here it can be seen that the principal contributor to the heat release rate is:

$$CH_3 + O \leftrightarrow CH_2O + H. \qquad\qquad R3 \qquad (4.8)$$
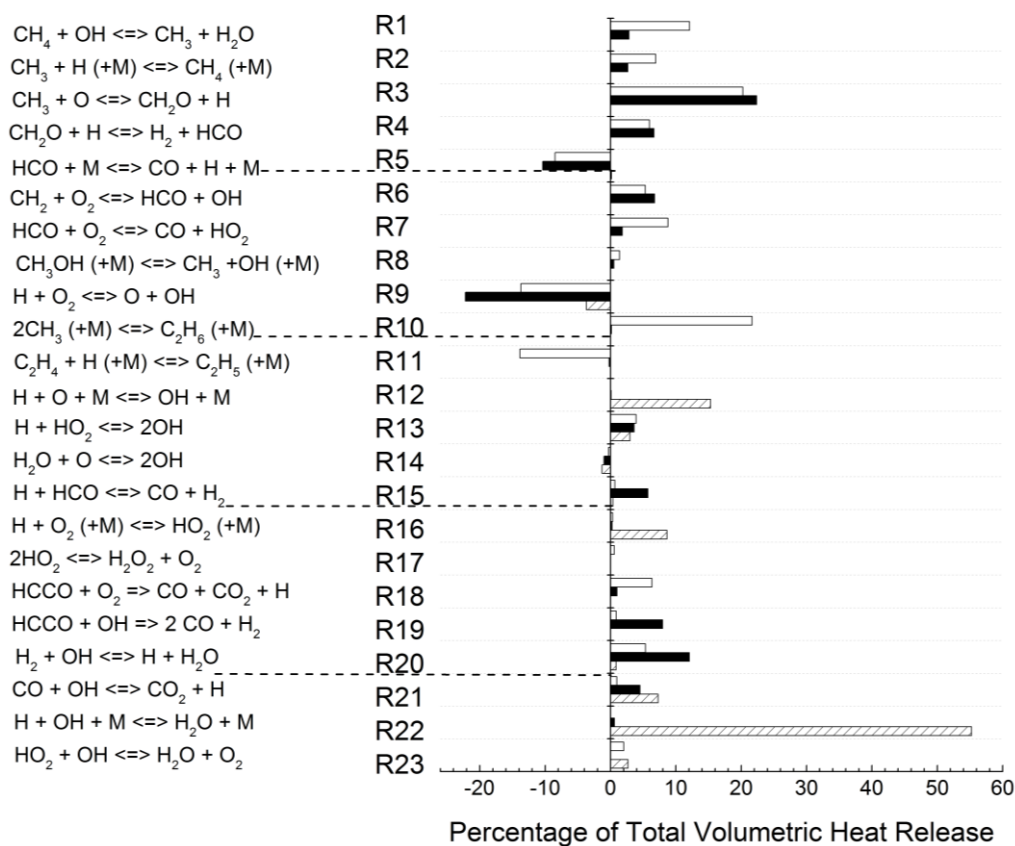
Figure 4.7: Principal reactions contributing to volumetric heat release rate, VHRR, with Mech 56.54 [186], P=0.1 MPa and T=1200 K. Black fill indicates VHRR of the reaction at the point of maximum total VHRR. No fill indicates contribution at a VHRR of the reaction that is 5% of this maximum, during the increase in VHRR. Shaded fill indicates contribution at a VHRR that is 5% of the maximum total VHRR, during the decrease of VHRR.

At this lower pressure, R22 and R16 seem to be unimportant, contributing less than 1% of the overall heat release compared to higher pressure conditions. This is because the rates of these reactions increase with pressure due to third body effects. The principal contributors are now R3 and R20. According to Nagy et al. [295] R20 also has a high sensitivity to the calculated burning velocities for hydrogen and syngas systems at fuel lean conditions. Varga et al. [296] optimised the rate coefficients for this reaction and showed very small uncertainty in the predictions of this reaction, which are very close to the experimental data. Consequently, there is a high degree of confidence in the value of the rate coefficient in this reaction. We might therefore anticipate a higher degree of uncertainty in predicting heat release rates at high pressures than at low pressures.

The contributions of each of the principal reactions to the overall VHRR are compared in Figure 4.7 and Figure 4.8. These are, respectively, for 0.1 and 10 MPa, the lowest and highest pressures studied. An unshaded rectangle is indicative of this percentage at the time for the first 5% of the maximum total VHRR, a black rectangle at the time of the maximum total VHRR, and a shaded rectangle at the time of the last 5% of the maximum total VHRR.
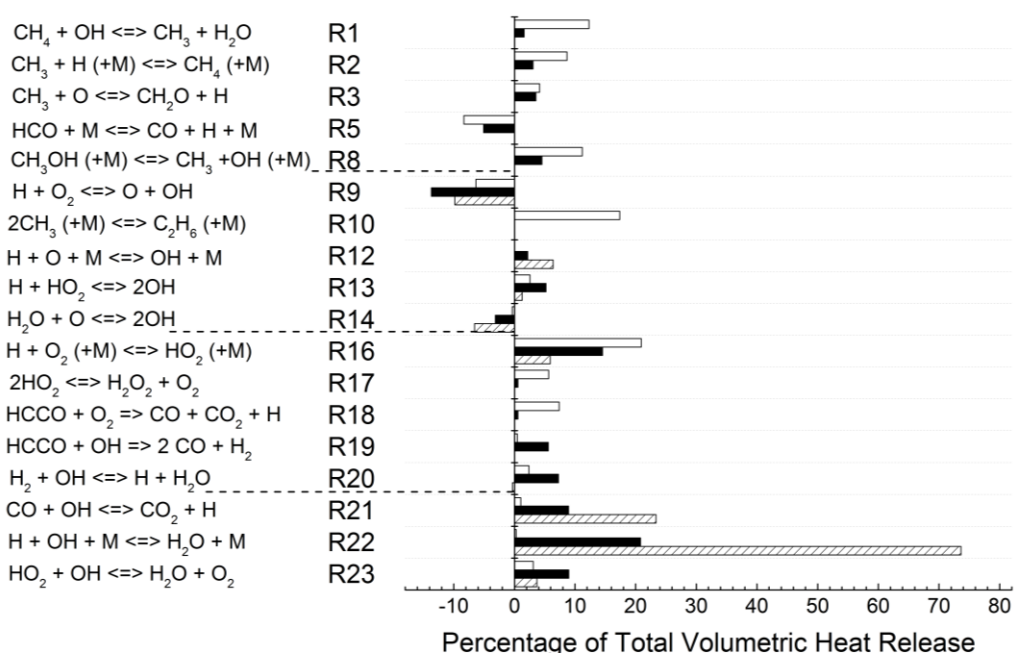
Figure 4.8: Principal reactions contributing to volumetric heat release rate, VHRR, for Mech 56.54 [186] at P=10 MPa and T=1200 K. See Figure 4.7 caption for key to rectangle fills.

More detailed temporal distributions, of the volumetric total VHRR, at initial pressures of 0.1, 4 and 10 MPa, are shown by the bold dashed curves in Figure 4.9 to Figure 4.12.

Other profiles on these figures are for the four principal exothermic and one endothermic reaction that contribute to this overall rate. In these cases the profiles are only shown at some selected instants. Figure 4.10 also shows the typically good correspondence that was found to exist between the volumetric heat release rate and the pressure gradient.
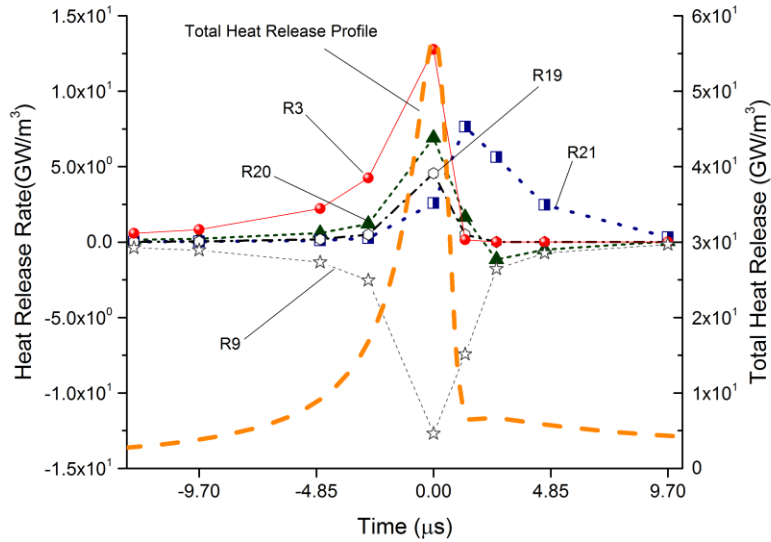
Figure 4.9: Mech 56.54 [186] heat release profiles for largest contributing reactions to total heat release at P=0.1 MPa and T=1200 K.
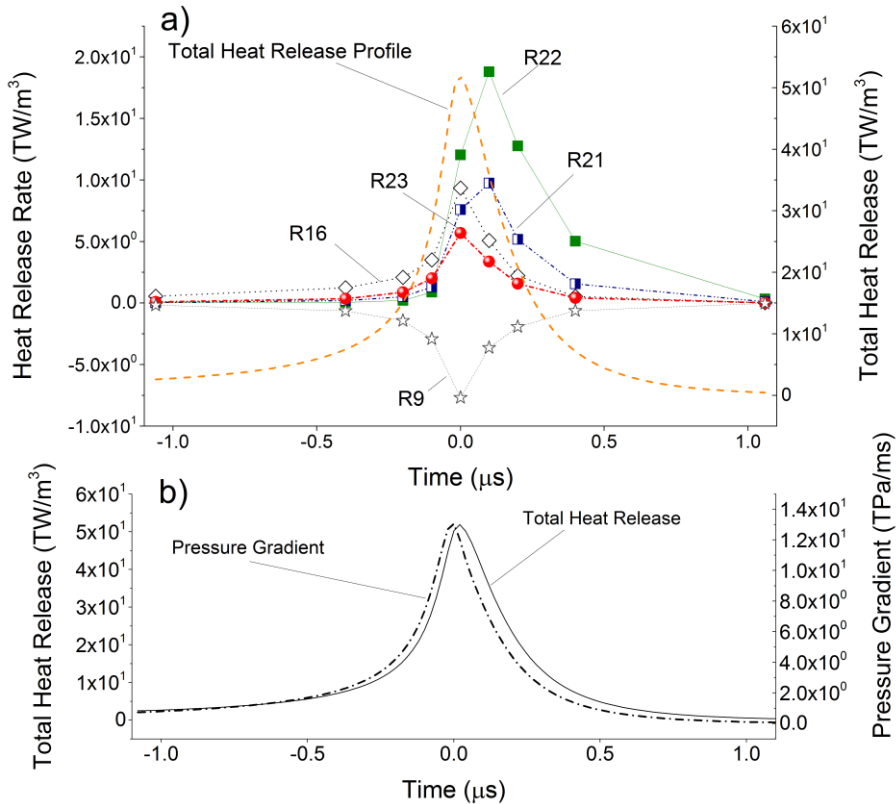
Figure 4.10: a) Mech 56.54 [186] heat release profiles for largest contributing reactions to total heat release at P=4 MPa and T= 800 K and b) the pressure gradient.
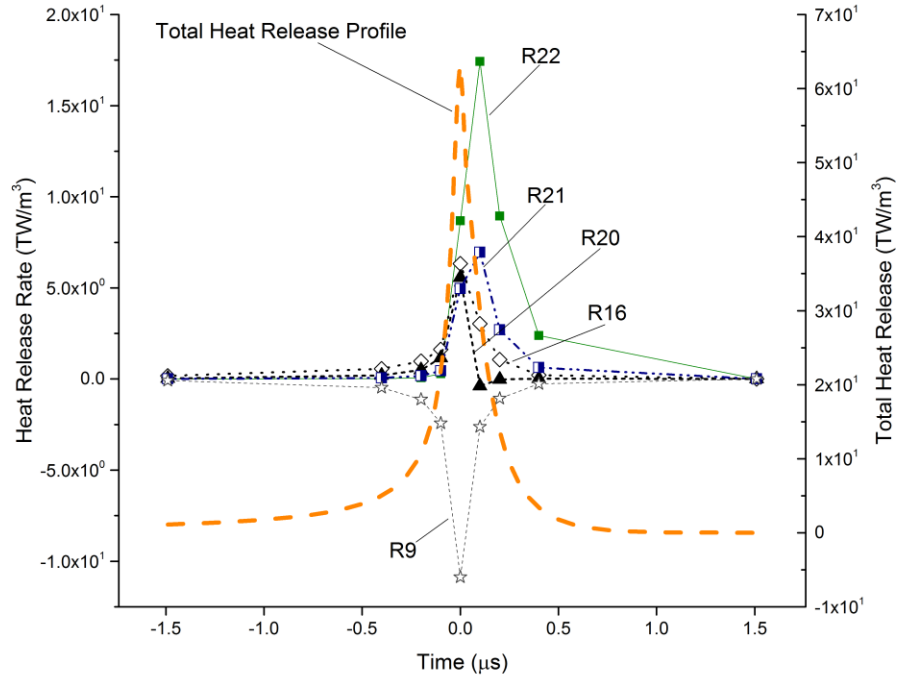
Figure 4.11: Mech 56.54 [186] heat release profiles for largest contributing reactions to total heat release at P=4 MPa and T=1200 K.
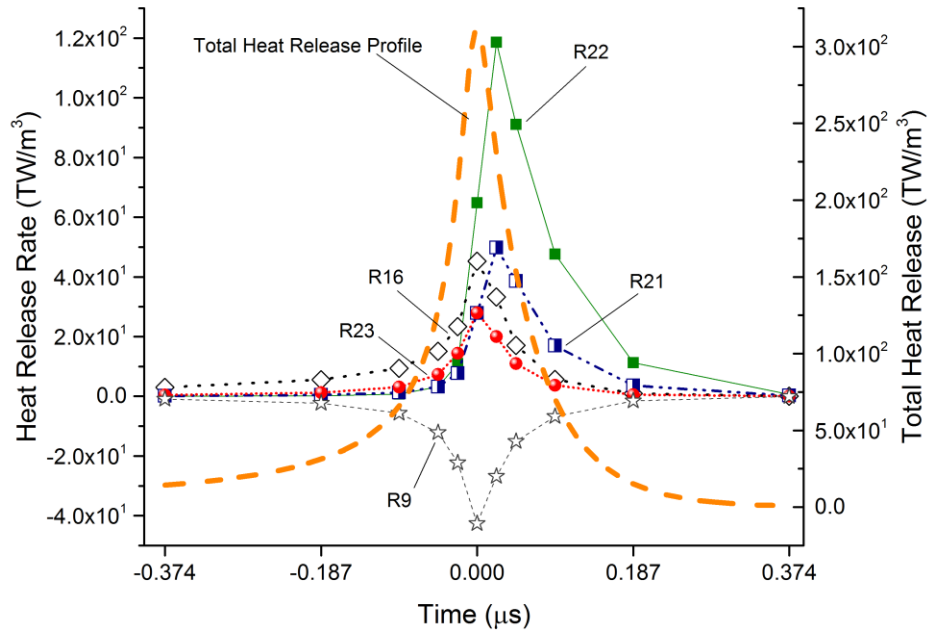
Figure 4.12: Mech 56.54 [186] heat release profiles for largest contributing reactions to total heat release P=10 MPa and T=1200 K.

The key reactions that influence the prediction of heat release rate at the time of maximum VHHR are more dependent on pressure than temperate. Interestingly, immediately after the time at which the heat release rate is a maximum, the principal contributors to the overall heat release rate are the same for all the four conditions studied, but in slightly

161

varying orders of magnitude, R22, R21, R16 and R12. The high pressure conditions of 4 and 10 MPa produce large contributions from the three body exothermic reactions R22 and R16 during the excitation time. This follows from the stronger dependence of the maximum VHRR on pressure. Since the rate of these reactions cannot attain that of the rapid chain branching at higher temperatures, they peak after the instant of peak VHRR. For the low pressure condition of 0.1 MPa, the exothermic reactions R3 and R20 contribute most to the energy release. Since excitation time is essentially based on the prediction of the overall VHHR, these differences in the level of significance, ranking and effects of key reactions contributing to overall VHRR, as well as their stronger dependence on pressure could be a possible explanation of the significant jump of approximately two orders of magnitude in excitation time value for the lowest pressure of 0.1 MPa at a fixed temperature compared to the excitation times at higher pressures investigated here. Of all the conditions tested, reaction R9 appears to be the main endothermic reaction. The branching reaction, R9, $H + O_2$, is known to be the principal reaction in combustion.

As it has been highlighted in this work earlier, the heat release is one of the principal characteristics of combustion processes Moreover, the time it takes for the heat release to be fed into and strengthen the pressure pulse is crucial the detonation phenomena and is represented here by excitation time. The temporal profiles of the VHRR, at 4MPa and 1200K, are employed in Figure 4.13, to demonstrate the defined value of τ_e, extending from 5% of the maximum heat release rate to the maximum value [36]. The heat release rate profile also suggests a possible alternative definition of τ_e, as the period of time during which the heat release rate is more than, say, 20% of the maximum, as also indicated on Figure 4.13. This definition might be a better choice of τ_e, since during this time the most intense heat release is fed into the acoustic wave. Furthermore, the heat release during the cool flame is fundamental for the auto-ignition processes. A more detailed discussion on the importance of the heat release is presented in Chapter 6.
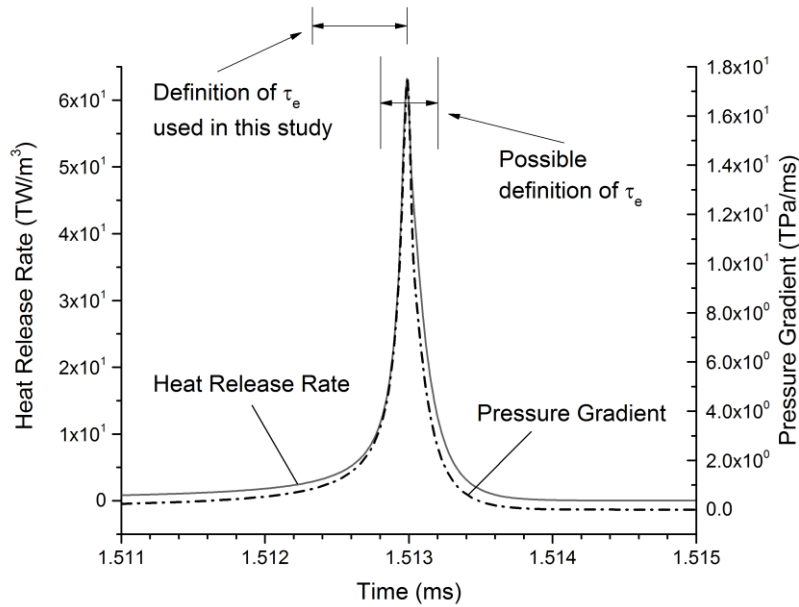
Figure 4.13: Volumetric heat release rates, at times after the instantaneous compression of a stoichiometric CH_4/air mixture at initial $P = 4$ MPa and $T = 1200$

4.5 Brute-force local sensitivity analysis

4.5.1 Ignition delay times

Figure 4.14 portrays the results of the normalised brute-force sensitivity analyses of the stoichiometric methane/air ignition delay times for the 8 and 6 most influential reaction sensitivities at each of the four temperatures for pressures of a) 0.1 MPa and b) 10 MPa, respectively.
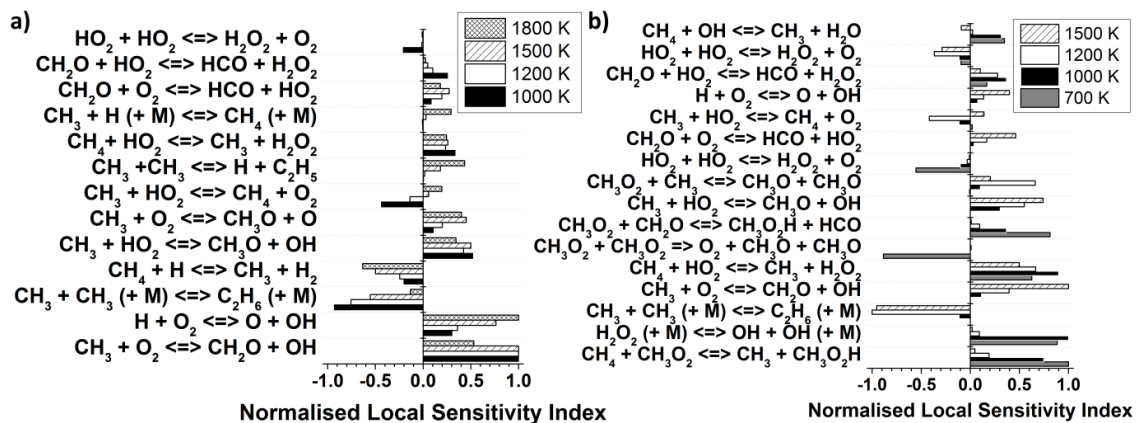
Figure 4.14: Normalised brute-force local sensitivity indices for the ignition delay times of stoichiometric methane/air fuel at four temperatures and pressures of a) 0.1 MPa and b) 10MPa. Duplicate entries for the reaction $HO_2 + HO_2$ express a double Arrhenius expression for this reaction.

Figure 4.14 a) shows that for the low pressure of 0.1 MPa the chain branching reactions $CH_3 + O_2 \leftrightarrow CH_2O + OH$ (R24) and $H + O_2 \leftrightarrow O + OH$ (R9) dominate the chemistry of the ignition delay times. This is consistent with previous studies [138, 186, 294]. These reactions have a promoting effect, decreasing ignition delay times. The sensitivity of reaction R9 is seen to increase with an increase in temperature. This leads to the acceleration of chain branching efficiency [298], which can explain the temperature dependence of the ignition delay times. Ignition delays are found to increase by five orders of magnitude as temperature decreases. These promoting reactions are competing with the inhibiting reactions $2CH_3$ (+M) $\leftrightarrow C_2H_6$ (+M) (R10) (that consumes methyl radicals to form ethane) and $CH_4 + H \leftrightarrow CH_3 + H_2$ (R25) (that suppresses the reactivity because it consumes H atoms). An increase in the temperature causes the sensitivity of R10 to reduce, hence reducing the inhibiting effect of this reaction on ignition delay times. This is another probable cause of the temperature dependence of ignition delays.

At the lowest pressure, the methane reactivity is predominantly controlled by methyl radicals. The increase in reaction rates of $CH_3 + O_2 \leftrightarrow CH_2O + OH$ (R24) and $CH_3 + O_2 \leftrightarrow CH_3O + O$ (R26) increases the reactivity of the system, and thus decreases ignition delay times. The competition between these two product channels of $CH_3 + O_2$ also has an effect on pressure dependence. Improved estimates or measurements of these reaction rate constants would enable an improved estimate of the contribution of these reactions to the ignition delay times.

Figure 4.14 b) shows that at 10 MPa the controlling chemistry does indeed slightly differ from 0.1 MPa. The chemistry is governed primarily by promoting reactions. HO_2 and H_2O_2 radicals become more important. The decomposition of H_2O_2 into two OH radicals (reaction H_2O_2 (+M) $\leftrightarrow OH + OH$ (+M) (R27)) has the highest sensitivity at 1000 K. Consequently, this reaction increases the concentration of OH radicals and has a promoting effect on the system. Also, the reaction $CH_4 + CH_3O_2 \leftrightarrow CH_3 + CH_3O_2H$ (R28) plays a key role in promoting ignition at low temperatures. However, similarly to low pressures, R10 and R24 are dominant at higher temperatures.

4.5.2 Excitation times

Sensitivity analyses for the excitation times of the stoichiometric methane/air fuel for the 6 and 7 most dominant reactions at each of the four temperatures and pressures of a) 0.1 MPa and b) 10 MPa, respectively, are given in Figure 4.15. Reaction $H + O_2$ (R9) has the highest sensitivity coefficient for both pressures and at all temperatures studied here. This
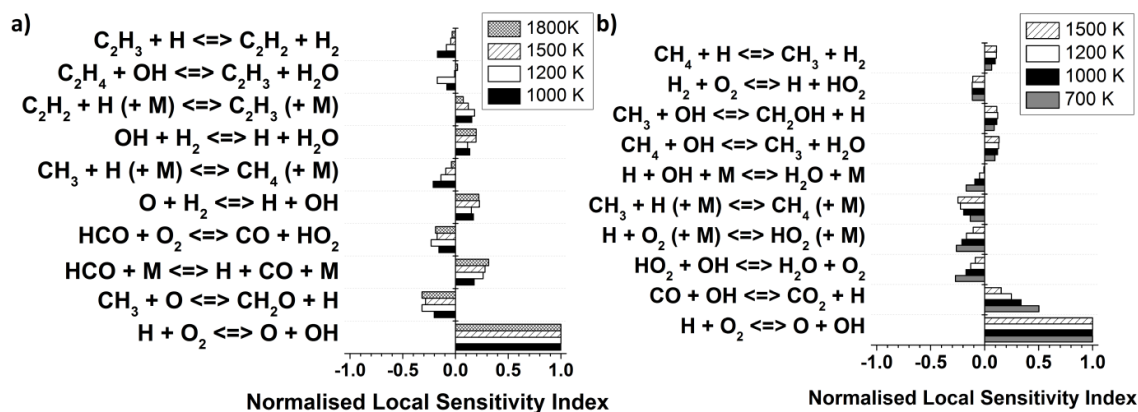
Figure 4.15: Normalised brute-force local sensitivity indices for the excitation times of stoichiometric methane/air fuel at four temperatures and pressures of a) 0.1 MPa and b) 10MPa.

reaction has also been highlighted as the main endothermic reaction in the VHHR analyses. It has a promoting effect, therby reducing excitation time values. Moreover, R9 is the principal reaction at 916 K for all other fuels studied (pure *n*-butanol, the TRF and their blends at different blending ratios), as highlighted in Chapter 6. This suggests a little dependence of the excitation time on the fuel, its chemical composition or the chemical kinetic scheme. However, as reported in Chapter 6, small differences in the predicted excitation times are apparent at lower temperatures. This is investigated later in this thesis. The substantial dominance of R9 in methane/air sensitivity analyses across the whole temperature region can explain the sensitivity of the excitation times to temperature. Griffiths and co-workers [299, 300] suggested that the development of knock is related to the competition between R16 and R9 near the point of main heat release, with R9 resulting in knock. The rapidity and severity of the onset of high temperature ignition may be attributed to the onset of vigorous O atom chain branching. The non-knocking reactions are restrained to the conditions where the HO_2 chemistry is able to survive to the later stage. The production of HO_2 is favoured at lower temperature conditions. The larger pressure dependence of this reaction indicates the HO_2 propagation route is sustained to higher temperatures when higher pressures prevail [82].

Based on sensitivity analyses, there are some pressure effects on the controlling chemistry of excitation times when comparing the predictions at 0.1 MPa to those at 10 MPa. There are also apparent differences in excitation time trends in Figure 4.6, when comparing results at 0.1 MPa to those at 10 MPa. To recall, an exothermic reaction $CH_3 + O \leftrightarrow CH_2O + H$ (R3) was found to be the main contributor to heat release in VHHR analysis.

This reaction is also highlighted in τ_e sensitivities for methane/air simulations at 0.1 MPa, followed by HCO decomposition reactions $HCO + M \leftrightarrow H + CO + M$ (R5) and $HCO + O_2 \leftrightarrow CO + HO_2$ (R7). Interestingly, despite ranking relatively high in the VHHR analysis as an exothermic reaction, $CO + OH \leftrightarrow CO_2 + H$ (R21) is not featured in the sensitivity analysis at atmospheric pressure. However, this reaction is highlighted in the sensitivity analyses of excitation times for n-butanol, TRF fuel and their blends. It is found to be a key promoting reaction for pure TRF at low and intermediate temperatures, as well as at low blending ratios of n-butanol with TRF at low temperatures, as demonstrated in Chapter 6.

An inhibiting reaction $HO_2 + OH \leftrightarrow H_2O + O_2$ (R23) is illustrated in the sensitivity analyses in Figure 4.15 (b), but it is absent in τ_e sensitivities for methane/air at atmospheric pressure. However, R23 is featured in the sensitivities of excitation times for n-butanol and TRF, as well as their blends, at 2 MPa. Reactions involving hydroperoxyl radicals (HO_2) are known to be more sensitive at higher pressures, which could explain its supremacy at these conditions.

Figure 4.15 (b) shows that the pressure dependent reactions involving the third body (+M) are important at these conditions. This may explain the trends evident in Figure 4.6, where 0.1 MPa excitation time predictions are approximately two orders of magnitude larger at a fixed temperature compared to those of other pressures. Finally, the heightened sensitivity of excitation times on hydrogen, carbon monoxide and small hydrocarbon kinetics, suggests that there is no major fundamental difference between the kinetics of methane and that of the other complex hydrocarbons.

4.6 Pathway analysis of methane/air auto-ignition

To further investigate important reaction pathways in methane/air oxidation processes, reaction pathway flux analyses of the H atom were conducted. These analyses produced the ratio of H-atom flux through different reaction pathways for methane/air oxidation at a temperature of 1200 K and two pressures of 0.1 MPa and 10 MPa (illustrated in Figure 4.16 and Figure 4.17, respectively). The numbers shown in these figures represent the fractions of hydrogen flux through various pathways. The cut-off time for these analyses is the time when the temperature has increased by 25 K from its initial value. After the initiation reaction of CH_4 to form methyl radical, there are three major reaction pathways of CH_3 at a low pressure of 0.1 MPa and four at 10 MPa.
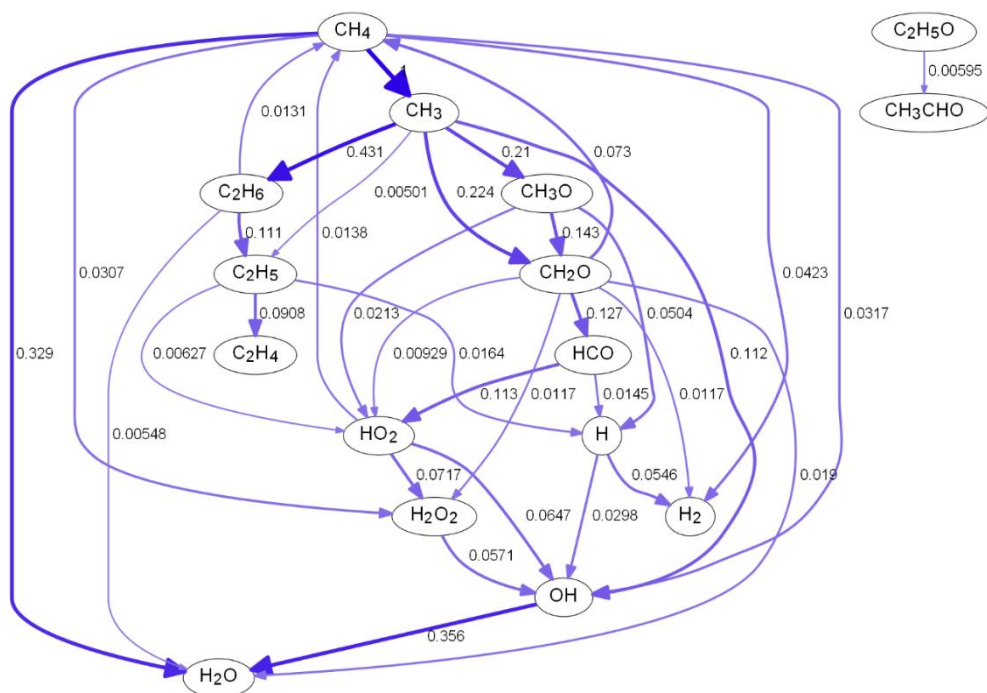
Figure 4.16: Reaction pathway flux analysis of H atom for stoichiometric methane/air fuel at 1200 K and pressures of 0.1 MPa. The numbers indicate the fractions of H flux through various pathways.
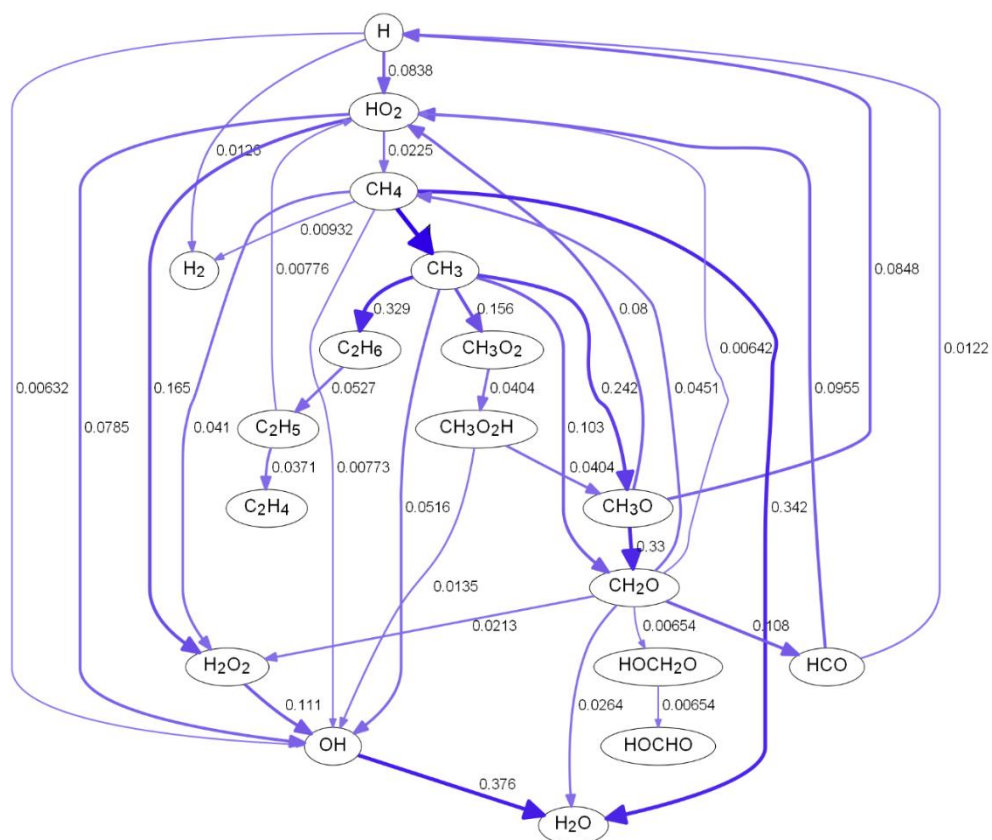
Figure 4.17: Reaction pathway flux analysis of H atom for stoichiometric methane/air fuel at 1200 K and pressures of 10 MPa. The numbers indicate the fractions of H flux through various pathways.

The recombination reaction pathway of CH_3 to form ethane (C_2H_6) is found to be the most important reaction pathway of CH_3, with a flux fraction of 0.431 at 0.1 MPa and 0.329 at 10 MPa. Another major channel highlighted at two pressures is the CH_3 oxidation to form CH_3O, with H atom flux fractions of 0.21 at 0.1 MPa and 0.242 at 10 MPa. On the other hand, the $CH_3 \rightarrow CH_2O$ pathway is found to be more significant at a lower pressure of 0.1 MPa than the $CH_3 \rightarrow CH_3O$ pathway, with a fraction of 0.224. At 10 MPa the $CH_3 \rightarrow CH_2O$ pathway has a fraction of 0.103, which is two times smaller compared to that at 0.1 MPa. The CH_3 oxidation reaction to form formaldehyde is seen to dominate the sensitivity analyses for ignition delay times at this low pressure. At a pressure of 10 MPa, another pathway ($CH_3 \rightarrow CH_3O_2$) becomes more important. This pathway promotes auto-ignition and is seen to be competing with three other channels.

4.7   Assessment of the anti-knock properties of methane/air

The excitation time is featured in the present work because of the growing awareness of its importance in the transition to detonation and also the stability of detonation waves [45, 301]. It features in an assessment of the knocking tendencies of different fuels as have been shown in Section 2.1.13 and is illustrated in Figure 4.18, from an earlier study of auto-ignition in engines [94]. Figure 4.18 features a detonation peninsula, which defines the bounds of the region within which detonations can develop. Different auto-ignition modes, specifically thermal explosion, subsonic auto-ignition, developing detonations, and non-auto-ignitive deflagration, can be located relative to a detonation peninsula. In a detonation peninsula, there are two non-dimensional parameters, namely the ratio of acoustic to auto-ignitive velocity, ξ, and the reactivity parameter, ε. The latter represents the resistance time for the acoustic wave to move through the hot spot radius (r_0/a), to excitation time, τ_e [90, 96, 97, 302]. It is a measure of the energy transferred into the acoustic front [90]. Further details on detonation theory and its governing equations were given in Sections 2.1.12, 2.1.13 and 3.4.2.

The detonation peninsula theory can be successfully applied to study knock and super-knock phenomena in engines [45, 282, 283, 303]. For example, Robert et al. [304] demonstrated how increasing spark advance and accompanying severity of knock, cause the representative engine cycle loci to enter the detonation peninsula. In Figure 4.18, loci of engine compressions for six different fuel/air mixtures, including CH_4/air, at different equivalence ratios, ϕ, are shown. Compressions of the mixtures are downwards toward the peninsula, first with an increasing propensity to engine knock, and, within the

peninsula, increasing knock severity. This increases with increasing penetration into the toe of the peninsula and increasing ε. It decreases in the thermal explosion regime [110].
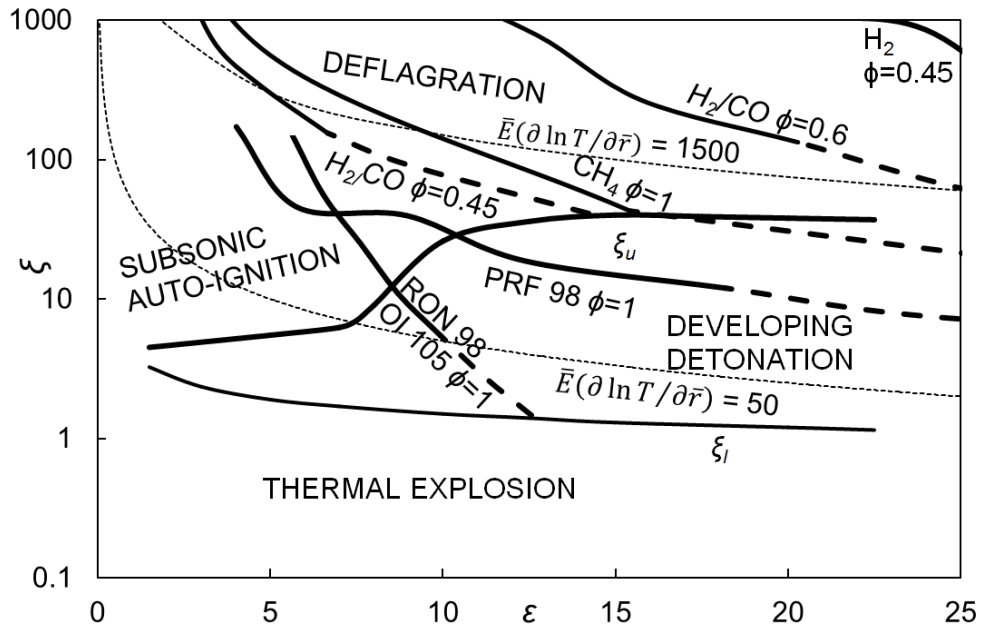
Figure 4.18: Developing detonation peninsula in terms of resonance parameter, ξ, and reactivity parameter, ε. Isentropic compression curves for different fuels showing propensity for detonation. Solid curves indicate compression from 800 K to 1000 K at $\approx$10 MPa. Broken curves show continuation of this compression to 1100 K at 15 MPa, relevant to turbo charged engines.

The solid line isentropes are compressions to 800 K and 10 MPa. The continuing dashed isentropes are compressions to 15 MPa and 1100 K, representing conditions that might occur in turbocharged engines. The H_2 and H_2/CO isentropes do not cross the upper limit of the detonation peninsula and there is no detonation. Those for the two gasolines, one with a Research Octane Number, RON, of 98, the other a Primary Reference Fuel, PRF98, enter the peninsula in the first compression stage. There they remain and detonate at hot spots, with increasingly severe engine knock as the curves penetrate further into the peninsula.

The CH_4/air ϕ=1.0, isentrope does not even enter the detonation peninsula during the first stage of compression to 10 MPa. This only occurs during the subsequent compression to 15 MPa. Then, it only skirts along the upper limit of the peninsula, indicating the relatively strong resistance to knock of CH_4/air. The CH_4/air mixtures are characterised by relatively high values of both E/R and τ_i/τ_e, while the gasoline fuels are associated with lower values of E/R.

169

The ξ/ε diagram in Figure 4.18 also shows contours of $\bar{E}(\delta lnT/\delta\bar{r})$, which is equal to the product ($\xi\,\varepsilon$) [4]. Values of $\bar{E}(\delta lnT/\delta\bar{r})$ equal to 50 and 1500 are shown by the dotted curves in Figure 4.18. Values approach 10 at the strong ignition limit and are conducive to stable detonations, with a uniform reaction zone strongly coupled with the shock wave [45]. Low values of $\bar{E}$ ln(T/T_o) are associated with the most stable detonations [45, 293]. High values, above a threshold of about 1500, were tentatively suggested in [90] as a regime of increasing deflagration.

4.8 Auto-ignitive and deflagrative flame front propagation regimes

In the region close to $\bar{E}(\delta lnT/\delta\bar{r}) = 1500$, direct numerical simulations, DNS, [305], experimental analysis, [306], and engine performance [94] show both modes of reaction propagation from hot spots can coexist, sometimes in about equal measure. For stoichiometric CH_4/air, values of $\bar{E}$ were calculated at 0.1, 4, 6 and 10 MPa for different temperatures using the computer codes and the data in Figure 4.1 to Figure 4.6. The probable values of $(\delta lnT/\delta\bar{r})$ will be distributed and, consequently, less definite. The experimental RCM studies of Mansfield and Wooldridge [307] of the propagation of reaction in syngas mixtures, with $\phi = 0.5$, showed it became predominantly deflagrative with dT/dr -5 K/mm. More recently, Mansfield et al. [33] employed the Sankaran criterion [305], that defines the auto-ignitve regime as that in which the auto-ignitive propagation velocity is greater than the laminar burning velocity, and showed values of dT/dr of between -5 and -10 K/mm to be in excellent agreement with the measured transitions between the two regimes.

The engine experiments of Kalghatgi et al. [38] suggest a most probable engine temperature gradient of about -2 K/mm. Combined with an often assumed hot spot radius, r_o, of 5 mm, this was used, along with the and the calculated values of $\bar{E}$ to give $\bar{E}(\delta lnT/\delta\bar{r})$ for stoichiometric CH_4/air. These values are employed as a function of temperature for the isobars of 0.1, 4, 6 and 10 MPa in Figure 4.19. However, there is no clear boundary between the auto-ignitive and deflagrative regimes, which can coexist within a transition regime, in which there is also uncertainty about the details of hot spot structures. The two distinctive regimes are indicated in the figure, with the hatched transition regime between them. It can be seen that auto-ignition is favoured by higher pressures and temperatures. As will be shown, experimental evidence suggests a transition regime extending over the hatched limits in Figure 4.19.
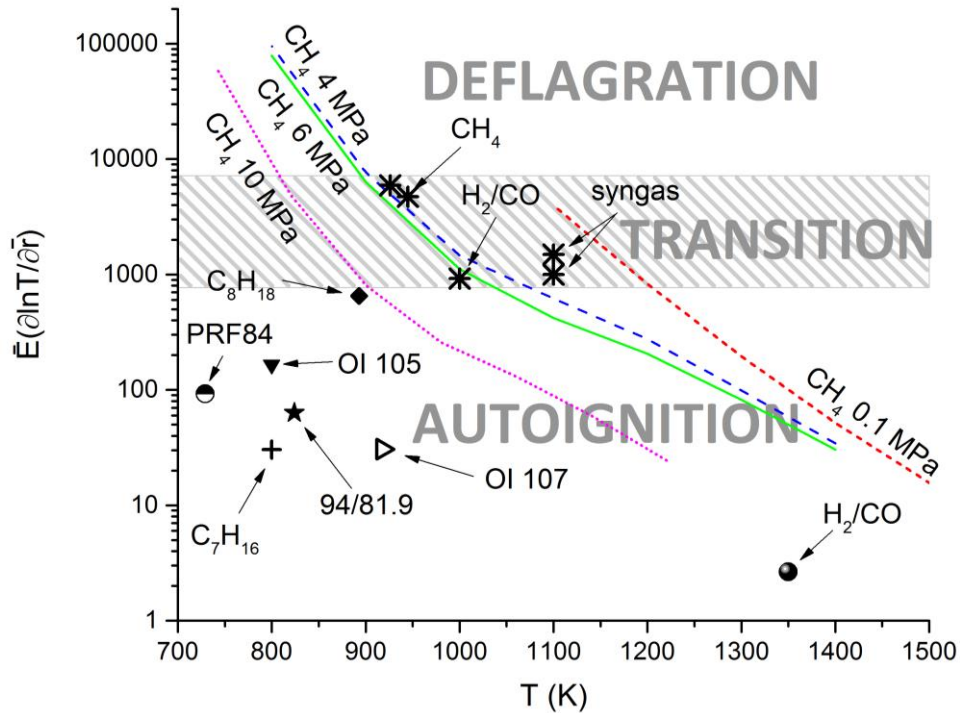
Figure 4.19: (a) $\bar{E}(\delta lnT/\delta \bar{r})$ as a function of T and P for stoichiometric CH4/air. (b) Asterisks indicating experimental and computed values of $\bar{E}(\delta lnT/\delta \bar{r})$, at given T in the transition regime. (c) Engine operational data of different fuels. Details in Table 4.3. (d) Three regimes of reaction propagation.

The extent of the transition regime for stoichiometric CH4/air has been studied experimentally by Strozzi et al. [306] at pressures close to 4 MPa in an RCM. They employed both chemiluminescence and planar laser induced fluorescence to visualise the structure of the reacting mixture after compression. It was fond that auto-ignition was associated with a very rapid rate of pressure rise, that was significantly reduced, with increased deflagrative burning, and an increase in the apparent value of τ_i when the temperature was decreased from 945 K to 926 K. The changes at these temperatures are marked by the two asterisked CH4 points on Figure 4.19 with respective values of $\bar{E}(\delta lnT/\delta \bar{r})$ of 4729 and 5927.

The transition regime studied by Mansfield and Wooldridge [307] employed syngas/air mixtures, see Table 6, with $\phi = 0.5$, became predominantly deflagrative when dT/dr -5 K/mm. With this gradient and assumed values of $r_o = 3$ mm and $\bar{E} = 1.1 \times 10^5$ at 1100 K [4], $\bar{E}(\delta lnT/\delta \bar{r})$ was found to be 1490. With the present assumed hot spot characteristics this value becomes 996. Both these estimated transition points are shown by the syngas asterisks on Figure 4.19.

Another mixed regime coordinate is provided by the computed τ_i and τ_e data derived in the DNS studies of hot spot auto-ignitions in (0.5 CO +0.5 H$_2$)/air mixtures in [91]. For this, the conditions were $\phi = 0.6$, T=1000 K, and $P = 5.066$ MPa. With the present assumed hot spot conditions this gives $\bar{E}(\delta lnT/\delta\bar{r}) = 919$, marked by the H$_2$/CO asterisk in Figure 4.19. This same study provided another H$_2$/CO theoretical point is provided in the Figure 4.19, for 1350 K, $P = 5.066$ MPa and $\phi =1.0$, this time in the auto-ignition regime, well within the detonation peninsula, with $\bar{E}(\delta lnT/\delta\bar{r}) = 2.64$. The upper and lower asterisk points in Figure 4.19 are tentatively taken as indicators of the limits of the transition regime.

The data points on Figure 4.19 have been extended by the inclusion of existing engine operational data. These are predominantly engine operational points and are in the auto-ignitive regime. PRF84 was an engine running on a very lean mixture in the auto-ignitive mode. The different mixtures, of course, would have different isobars. Values of ϕ, P, T, $\bar{E}$, and other details for these points are given in Table 4.3. The presently assumed hot spot conditions were employed in deriving $\bar{E}(\delta lnT/\delta\bar{r})$. All these data, predominantly based on Primary Reference Fuels and their blends are, not surprisingly, in the auto-ignitive regime, below the $\bar{E}(\delta lnT/\delta\bar{r}) = 1500$ line.

The engine heavy knocking regime is at about $\bar{E}(\delta lnT/\delta\bar{r}) = 31$, extending from about 910 to 950 K. It is of interest to note that, while engine operation is impaired by low values of $\bar{E}(\delta lnT/\delta\bar{r})$, measurements of τ_i in RCMs are impaired by high values of this parameter. Values greater than 1500 might result in hot spot initiated auto-ignitions, from which a laminar flame propagates. This can create erratic apparent values of τ_i, that are inaccurate and usually excessively high.

Table 4.3: Data for plots of $\bar{E}(\delta lnT/\delta\bar{r})$ against temperature at different pressures.

Fuel	Conditions and References	ϕ	P (MPa)	T (K)	$10^{-3}\,\overline{E}$
CH_4	Present computations RCM [90]	1.0	4.0	926	551.78
	Present computations RCM [90]	1.0	4.0	945	449.31
Syngas 0.59H_2/0.41 CO/H_2/air	RCM [307]	0.5	0.8	1100	110
.5 H_2 + 0.5 CO	Present computations [91]	0.6	5.066	1000	92.34
	Present computations [91]	1.0	5.066	1350	0.358
94RON/81.9MON	Turbocharged engine [90]	1.0	10.45	824	5229
PRF84	Engine running in auto-ignitive mode [90]	0.25	6.52	729	6.799
OI 107 98 RON/ 89 MON	Turbocharged engine [90]	1.0	13.3	918	2822
OI 105 0.62 i-octane/0.29 toluene/0.09 n-heptane 95 RON/ 85 MON	Turbocharged engine, light auto-ignition [90]	1.0	7.0	800	13.269
C_8H_{18}	Theoretical [90]			893	58.700
C_7H_{16}	Theoretical [90]			800	2.450

4.9   Conclusions

Ignition delay times and excitation times for a stoichiometric methane/air mixture have been simulated using the detailed chemical kinetics Mech_56.54 mechanism at different pressures and temperatures. It has been shown that the reduced global scheme model of Bates [291] has shown adequate performances probably within the uncertainty of experimental error in modelling ignition delay times for complex flow 3D problems at reduced computational cost. Simulations of both τ_i and τ_e were approximately 10 times faster with the reduced global mechanism compared to detailed kinetic modelling. However, reduced global scheme was unable to accurately predict τ_e, with an under-estimation within an order of the magnitude. For the fundamental analysis of the detonation phenomena, as well as to understand the chemistry controlling these phenomena, all subsequent work was performed using the detailed kinetic scheme.

The four reactions that contribute the most to the overall heat release rate have been identified for different values of P and T, along with the two principal endothermic

173

reactions. These are rather different at atmospheric pressure compared to higher pressures. The brute-force sensitivity analyses have shown that the dominant reactions affecting τ_i also differ between the high pressure conditions and low pressure conditions. These differences in controlling chemistry could be a possible explanation in the sudden increase of τ_i at atmospheric pressure. However, τ_i have been proven to be more temperature dependent with a five orders of magnitude increase across the temperature region studied.

On the other hand, excitation times have shown little temperature dependence and are more sensitive to pressure changes. The brute-force sensitivity analyses for excitation times have shown that the third body reactions are more sensitive at higher pressures and could be a reason for the observed trends in excitation times. There is a greater degree of uncertainty in the reaction rates at the highest pressure. Also, an important reaction in combustion R9 has the highest sensitivity for the excitation times across the whole temperature and pressure region studied here. This reaction, together with R23, is also featured in the sensitivity analyses for the excitation times of n-butanol and TRF blends (as discussed in Chapter 6). The hydrogen, carbon monoxide and small hydrocarbon dominance in these sensitivities suggests that there is a little (if any) fundamental difference between the kinetics of methane and other gaseous and liquid fuels.

The very good antiknock properties of stoichiometric CH_4/air under turbocharged engine running conditions in comparison with those of other fuels have been demonstrated on the ξ/ε diagram. The modelled τ_i and τ_e, combined with data available in the literature, have been used to assess the proximity of the deflagrative and auto-ignitive regimes and the possible transition regime between those, in terms of the $\bar{E}(\delta lnT/\delta \bar{r})$ parameter. It was concluded that rapid compression machines should operate within the auto-ignitive regime.

5. Experimental and Modelling Study of the Impacts of *n*-Butanol Blending on the Auto-Ignition Behaviour of Gasoline and its Surrogate Mixture at Low Temperatures

The objective of this study is to provide an improved understanding of the impacts of *n*-butanol addition to gasoline (RON 95 and MON 86.6) on its auto-ignition properties at various blending ratios (10%, 20%, 40% and 85% vol *n*-butanol, referred to as B10, B20, B40 and B85 respectively here), as well as to a gasoline surrogate mixture, in order to facilitate the evaluation of a recent chemical mechanism describing the combustion of the blends. In particular, the study investigates the ignition delay times (τ_i) in a Rapid Compression Machine (RCM), through experimental measurements and numerical modelling for the low temperature region 678-916 K at a pressure of 2 MPa under stoichiometric conditions.

Since the kinetics of gasoline combustion is extremely complex due to the large number of hydrocarbon components present, typical kinetic models attempting to represent gasoline combustion comprise simpler surrogate mixtures which are developed to mimic the important properties of the gasoline under investigation. In this study, a 3-component toluene reference fuel (TRF) surrogate has been employed, comprising toluene (22.97% vol), *iso*-octane (65.64% vol) and *n*-heptane (11.4% vol) as detailed in Agbro et al. [41]. The performance of this TRF surrogate in representing the ignition delay behaviour of the reference gasoline on its own, and when blended with *n*-butanol, is investigated first experimentally, and subsequently used to assess the ability of an existing model representing *n*-butanol/TRF blends to predict τ_i in the RCM for the temperature range under investigation. Furthermore, through the use of brute-force sensitivity analysis, the chemistry controlling the auto-ignition of the *n*-butanol/TRF blends was investigated to determine the main reactions which influence τ_i at selected conditions and blending ratios.

5.1 Experimental pressure traces and reproducibility

Table 5.1 - Table 5.3 summarise the initial and compressed conditions, ignition delay times in this study measured using a Rapid Compression Machine in the Thermo Fluid Laboratory at the University of Leeds, as well as computed variable volume ignition delay times presented for 10%, 40% and 85% by liquid volume of *n*-butanol with TRF or gasoline. Ignition delay times are reported as the averages of 4-6 runs made at each test

condition, with uncertainty of error based on one standard deviation (1σ). It can be inferred from these tables that the largest errors are apparent at low temperature conditions where the ignition delay times are relatively long. This is potentially due to the fact that for long ignition delay times, pressure and temperature after the end of compression and during the ignition delay itself, tend to decrease due to associated heat losses that have more profound effects at these longer ignition delay times. Also the effects of possible temperature and species inhomogeneities are increased, such as undesirable combustion mode.

Figure 5.1 illustrates typical pressure-time histories of the auto-ignition of a stoichiometric 10% vol *n*-butanol blend in TRF for four subsequent test runs of a) single-stage ignition at 831 K and b) two-stage ignition at 745 K for a compressed pressure of 2 MPa indicating experimental reproducibility. The repeatability was to some degree less for LTHR cases, but still satisfactory. Here, pressure traces are aligned at the end of compression, as determined by piston displacement measurements, such that the end of compression is equivalent to piston top dead centre. The pressure traces have identical characteristics related to the compression phase, heat loses, heat release and the distinct and steep increases of pressure due to auto-ignition. The apparent gradual first increase in pressure is due to mixture compression, while second and third increases correspond to first-stage and second-stage ignition, respectively.
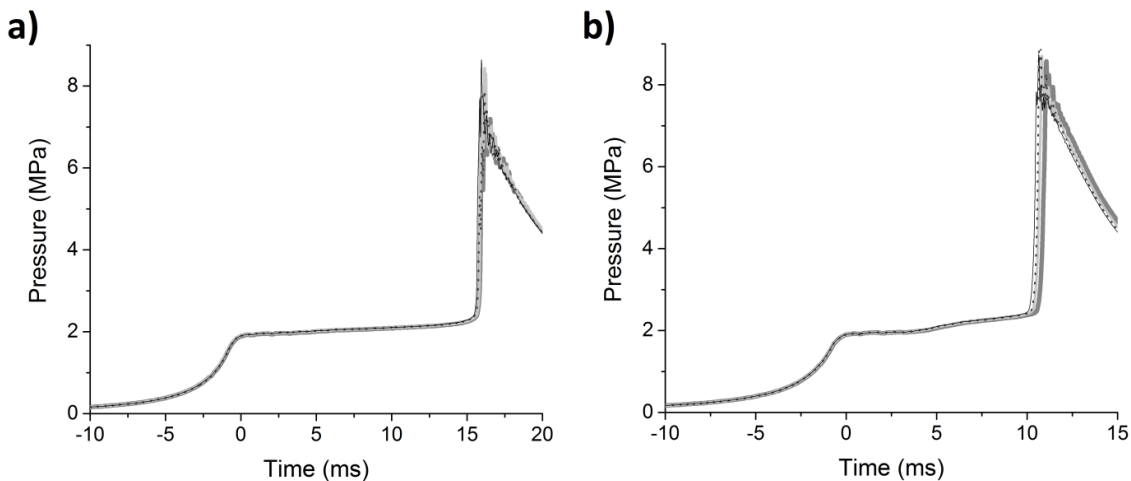
Figure 5.1: Pressure traces for a stoichiometric 10% vol *n*-butanol blend in TRF of 4 sequential test runs illustrating experimental reproducibility for a) single-stage ignition delay time at 831 K and b) two-stage ignition delay time at 745 K at 2 MPa.

Table 5.1: Summary of experimental and simulated ignition delay times for 10% vol *n*-butanol blend in TRF or gasoline and their initial and compressed conditions.

				10% vol *n*-butanol				
						10% vol *n*-butanol in TRF exp average τ_i (ms)		
P_0 (MPa)	Estimated T_c at end of compression (K) using modelled P_c	Estimated T_c at end of compression (K) using measured P_c	$1000/T_c$ K^{-1}	10% vol *n*-butanol in gasoline exp average τ_i (ms)	1σ of 4-6 runs for blends with gasoline (ms)		1σ of 4-6 runs for blends with TRF (ms)	Sim var vol reactor τ_i (ms)
0.0870	678	669	1.4957	35.41	4.1607	36.89	0.7319	38.70
0.0840	702	692	1.4451	19.33	0.6813	18.59	0.2250	21.50
0.0745	727	717	1.3945	10.83	0.6589	13.51	0.2485	13.45
0.0737	745	731	1.3679	9.44	0.4942	10.70	0.2345	11.40
0.0741	765	752	1.3296	8.36	0.4200	13.85	0.1658	9.65
0.0746	782	771	1.2969	13.83	0.1988	13.69	0.2162	9.10
0.0734	809	796	1.2561	15.46	0.0894	14.03	0.2080	9.50
0.0718	831	815	1.2275	9.97	0.5500	15.89	0.0250	10.05
0.0700	855	841	1.1893	7.10	0.6500	13.97	0.3511	9.60
0.0657	916	904	1.1068	3.65	0.0900	7.06	0.2329	5.90

Table 5.2: Summary of experimental and simulated ignition delay times for 40% vol n-butanol blend in TRF or gasoline and their initial and compressed conditions.

				40% vol n-butanol				
P_0 (MPa)	Estimated T_c at end of compression (K) using modelled P_c	Estimated T_c at end of compression (K) using measured P_c	$1000/T_c$ K^{-1}	40% vol n-butanol in gasoline exp average τ_i (ms)	1σ of 4-6 runs for blends with gasoline (ms)	40% vol n-butanol in TRF exp average τ_i (ms)	1σ of 4-6 runs for blends with TRF (ms)	Sim var vol reactor τ_i (ms)
0.0870	678	674	1.4841	47.03	2.3045	108.68	9.3735	66.51
0.0840	702	703	1.4231	24.03	0.4735	30.80	0.6874	26.87
0.0745	727	718	1.3926	11.68	0.7331	28.29	0.5749	19.44
0.0740	745	734	1.3624	10.46	0.7352	21.05	0.6093	14.98
0.0745	765	757	1.3212	8.79	0.5498	17.45	0.2828	11.06
0.0748	782	770	1.2992	13.30	0.2450	15.89	0.2462	10.30
0.0735	809	796	1.2568	13.67	0.2885	12.25	0.4108	8.99
0.0718	831	819	1.2212	8.11	0.6088	11.22	0.1483	7.82
0.0700	855	841	1.1885	5.26	0.2016	10.71	0.3092	6.99
0.0657	916	905	1.1050	2.58	0.1848	5.36	0.1025	3.73

Table 5.3: Summary of experimental and simulated ignition delay times for 85% vol *n*-butanol blend in TRF or gasoline and their initial and compressed conditions.

				85% vol *n*-butanol				
P_0 (MPa)	Estimated T_c at end of compression (K) using modelled P_c	Estimated T_c at end of compression (K) using measured P_c	$1000/T_c$ K^{-1}	85% vol *n*-butanol in gasoline exp average τ_i (ms)	1σ of 4-6 runs for blends with gasoline (ms)	85% vol *n*-butanol in TRF exp average τ_i (ms)	1σ of 4-6 runs for blends with TRF (ms)	Sim var vol reactor τ_i (ms)
0.0870	678	672	1.4892	147.43	9.9195	145.17	1.7750	152.20
0.0840	702	697	1.4351	37.30	1.4669	40.20	0.9010	56.29
0.0747	727	722	1.3860	24.97	1.1930	32.33	2.3200	27.52
0.0747	745	737	1.3565	17.98	1.0563	22.83	0.8410	19.60
0.0752	765	756	1.3234	8.46	0.3959	23.80	0.4223	14.69
0.0756	782	772	1.2947	16.81	0.0479	17.07	0.3055	11.86
0.0735	809	804	1.2436	11.05	1.4760	12.23	0.2887	8.05
0.0718	831	824	1.2140	9.44	0.3543	8.31	0.2212	6.84
0.0700	855	848	1.1788	8.06	0.4230	7.46	0.4131	5.19
0.0658	916	911	1.0983	1.80	0.2916	2.98	0.1323	2.65

5.2 Characterisation of experimental pressure traces

Occurrence of severe knock and super-knock phenomena is one of the principal constrains in the development of advanced ICE technologies. Therefore, improved knowledge of auto-ignition characteristics is paramount for understanding of the fuel performance in engines. Under practical engine conditions, auto-ignition characteristics of hydrocarbon fuels can display a single-stage or a multi-stage ignition behaviour. Low temperature auto-ignition is an extremely complex phenomenon, which can be very sensitive to the smallest change in the fuel structure and thermodynamic conditions [308]. To better understand auto-ignition processes, initial assessment and characterisation of collected experimental pressure records is performed.

Figures 5.2 – 5.7 show aligned representative pressure-time histories for the individual experimental test runs. These correspond to the ignition delay times that are closest to the reported averages presented in the subsequent figures. Here, the pressure-time histories are reported for stoichiometric 10%, 40% and 85% by liquid volume of n-butanol blends with TRF or gasoline at a pressure of 2 MPa and different compression temperatures. The presented pressure evolution of the RCM pressure-time histories can be compared to the supper-knock traces detected in SI engines [309, 310]. There are three distinctive events observed from these pressure-time histories. Initially, a gradual pressure increase is detected after the end of compression. Next, a strong pressure discontinuity and rise is observed. Finally, subsequent maximum pressure rise and either a smooth pressure decrease or strong pressure oscillations are observed. A smooth pressure decrease indicates a mild ignition (conventional knock in gasoline engine), whereas strong pressure oscillations are attributed to strong ignition events (detonation/super-knock in gasoline engine). The later then gradually attenuates with the entire combustion process being terminated.

Wang et al. [65] previously quantified the knock intensity of the RCM experiments by the amplitude of the maximum pressure oscillation. Tanaka et al. [311] related the intensity of the knock to the amplitude of high frequency oscillations of the RCM experiments. In SI engines, these oscillations are believed to be caused by shock waves produced by auto-ignition of the "end gas" which lead to the "ringing" noise of the metal cylinder detected by the pressure transducer. During the HCCI combustion this mechanism for producing significant pressure gradients in the gas is not present, and it is more likely to be related to the high impulsive load produced directly by the explosion of

the mixture [311]. This interpretation and assessment of the pressure time histories is adopted in this work. However, it is arguable whether reliable data from pressure oscillations can be extracted as transducer goes into shock and appropriate system calibration has to be implemented.
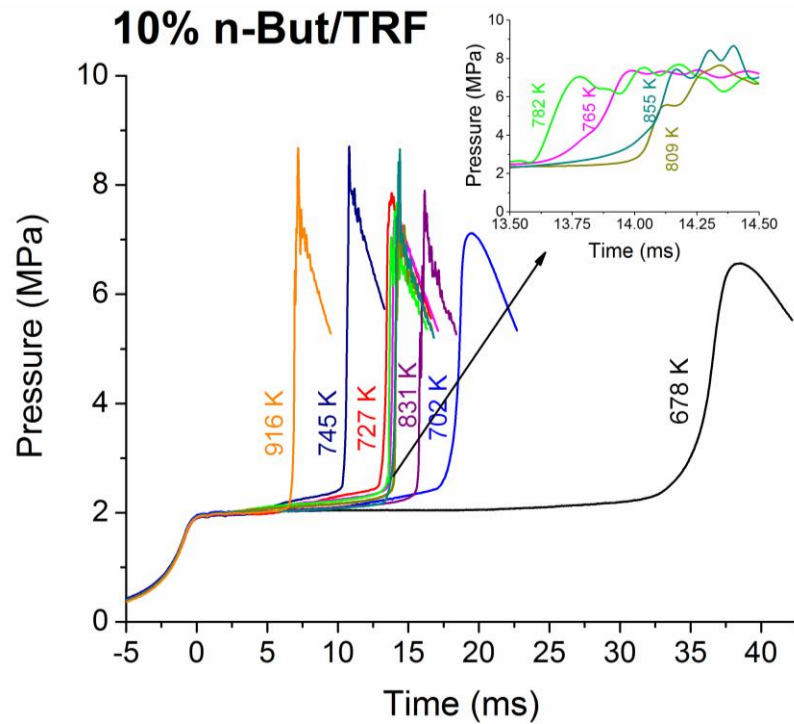
Figure 5.2: Pressure records for stoichiometric fuels at 2 MPa and various compression temperatures for 10% vol *n*-butanol blend in TRF.
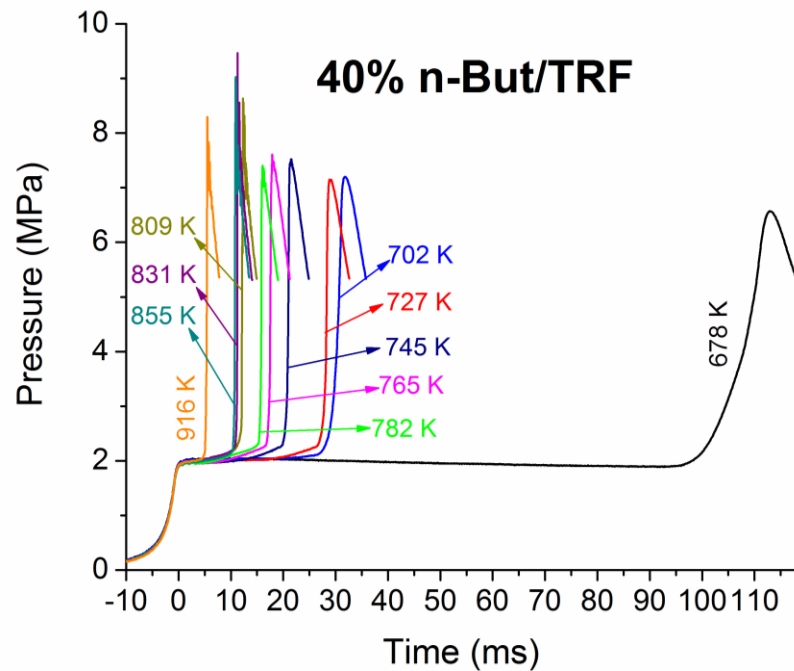
Figure 5.3: Pressure records for stoichiometric fuels at 2 MPa and various compression temperatures for 40% vol *n*-butanol blend in TRF.
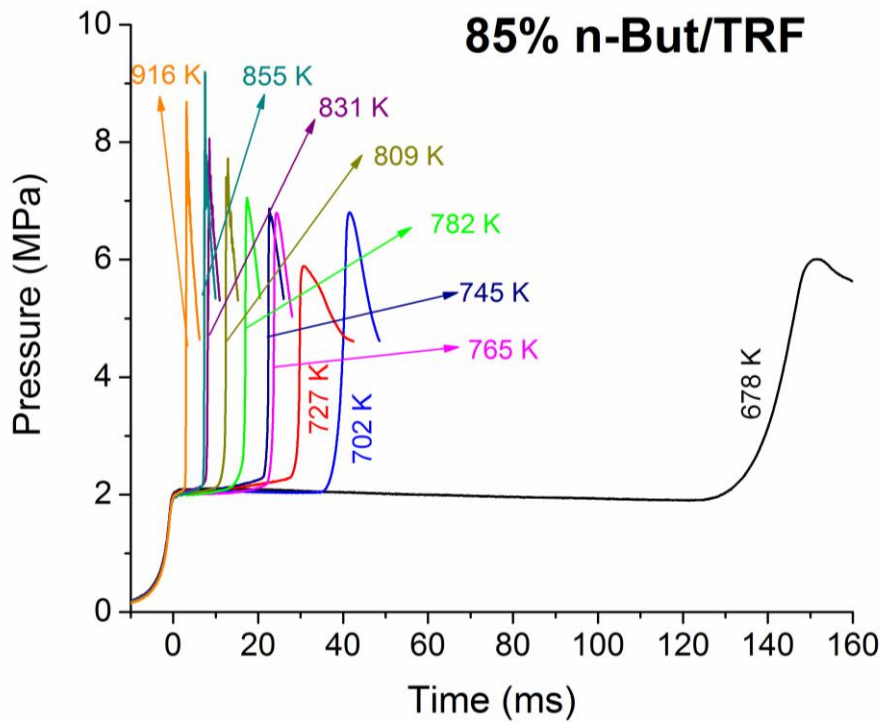
Figure 5.4: Pressure records for stoichiometric fuels at 2 MPa and various compression temperatures for 85% vol *n*-butanol blend in TRF.
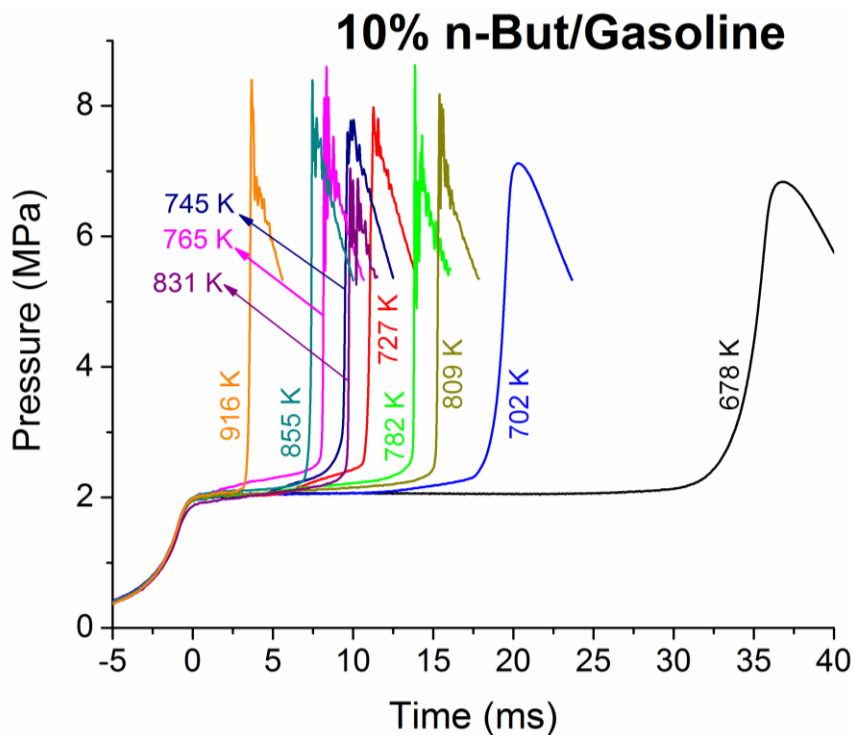
Figure 5.5: Pressure records for stoichiometric fuels at 2 MPa and various compression temperatures for 10% vol *n*-butanol blend in gasoline.
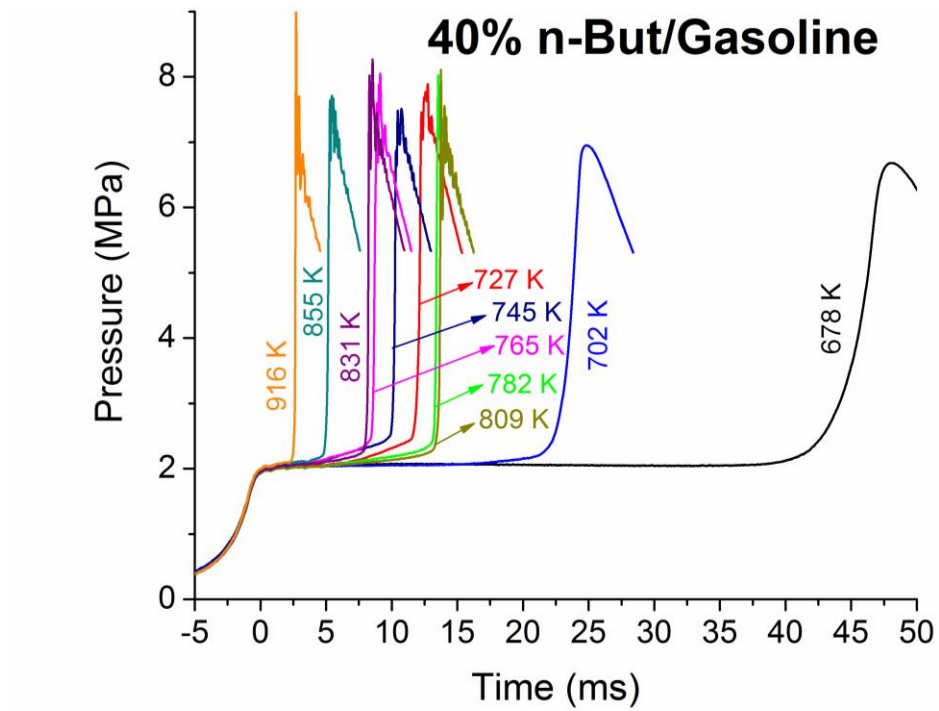
Figure 5.6: Pressure records for stoichiometric fuels at 2 MPa and various compression temperatures for 40% vol *n*-butanol blend in gasoline.
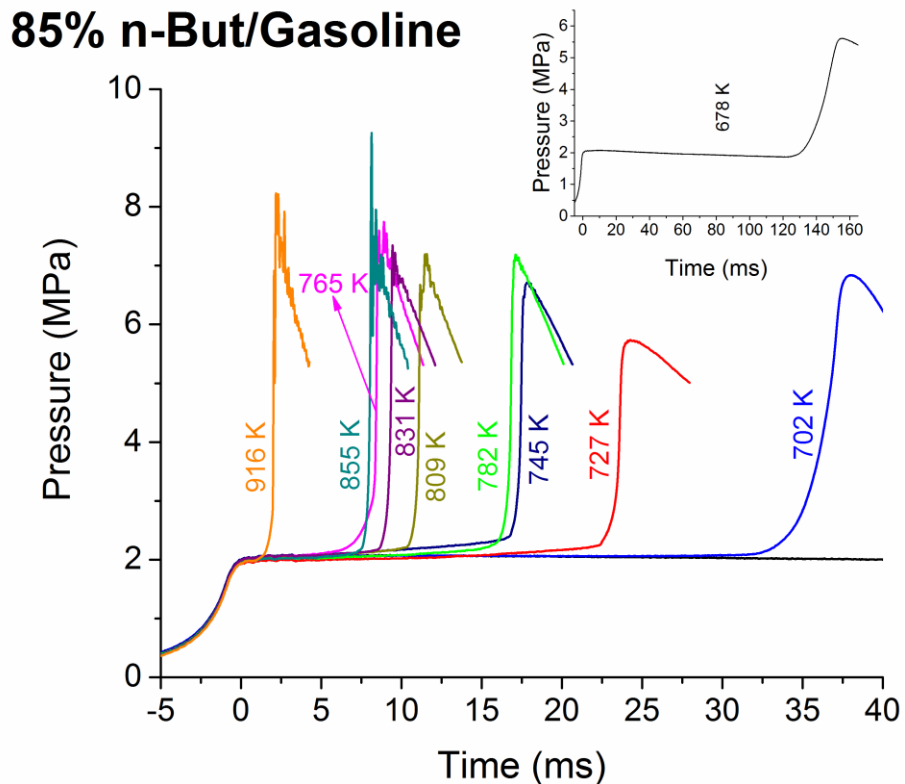
Figure 5.7: Pressure records for stoichiometric fuels at 2 MPa and various compression temperatures for 85% vol *n*-butanol blend in gasoline.

From Figures 5.2 – 5.7 it can be seen that at low temperatures of 678 K and 702 K the smooth gradual pressure increase is apparent with smaller values of the maximum pressure rise, the relatively slow burn rates and practically no pressure oscillations for all tested mixtures. Generally, a decrease in burn rate corresponds to an increase in ignition delay time magnitude indicating a mild ignition event of weak two-stage ignition or complete single-stage ignition and less steep pressure rise. Here, the majority of the mixture can potentially already be consumed hence this process can be representative of mild ignition and deflagration similar to the single-stage ignition behaviour rather than actual strong auto-ignition. This would be further explored in Chapter 6.

Also at temperatures of 678 K – 727 K, an increase in n-butanol concentration increases the resilience to auto-ignition and hence results in appreciably longer ignition delays. This is detected by examining a pressure trace of an individual temperature and comparing its magnitude between Figures 5.2 - 5.4 for n-butanol/TRF blends and Figures 5.5 - 5.7 for n-butanol/gasoline blends. This, in turn, highlights the octane enhancing capabilities of n-butanol at these conditions. In the high temperature region the opposite trend is seen when comparing pressure traces and an increase in n-butanol leads to shorter ignition delay times owing to shorter ignition delay times of pure n-butanol. At intermediate temperatures, there is a distinct pressure rise prior to the main ignition event. This is representative of a two-stage ignition behaviour. From Figures 5.2 – 5.7 the distinct two-stage ignition behaviour is evident for blends with TRF and gasoline fuels translating in the NTC behaviour. Here the first-stage is related to the occurrence of cool flames and the second-stage to the main ignition event, as discussed in Section 2.1.9. The implication of the two-stage ignition and the NTC behaviour on different auto-ignition modes, abnormal combustion and engine knock will be examined in the Chapter 6.

5.3 Examination of the robustness of the TRF surrogate in representing the auto-ignition behaviour of studied n-butanol/gasoline blends

Figures 5.8 – 5.11 show the comparisons of τ_i measured in the current RCM experiments, in addition to those reported in [41] for 20% blends in order to cover a wide range of blending conditions for n-butanol with TRF and gasoline. Ignition delay times are presented as the averages of 4-6 runs made at each test condition, with errors based on one standard deviation (1σ). Lines are B-spline fits indicating trends of ignition delays for each fuel or fuel blend. The results show that for the pure fuels, TRF exhibits similar

temperature dependent behaviour to gasoline with both showing a shallow NTC (negative temperature coefficient) regime at intermediate temperatures. In contrast, *n*-butanol demonstrates a more Arrhenius like behaviour with a slight drop in slope in the lower temperature region. The lack of NTC for *n*-butanol means that over the whole temperature region studied, it shows a higher slope than the gasoline or TRF.
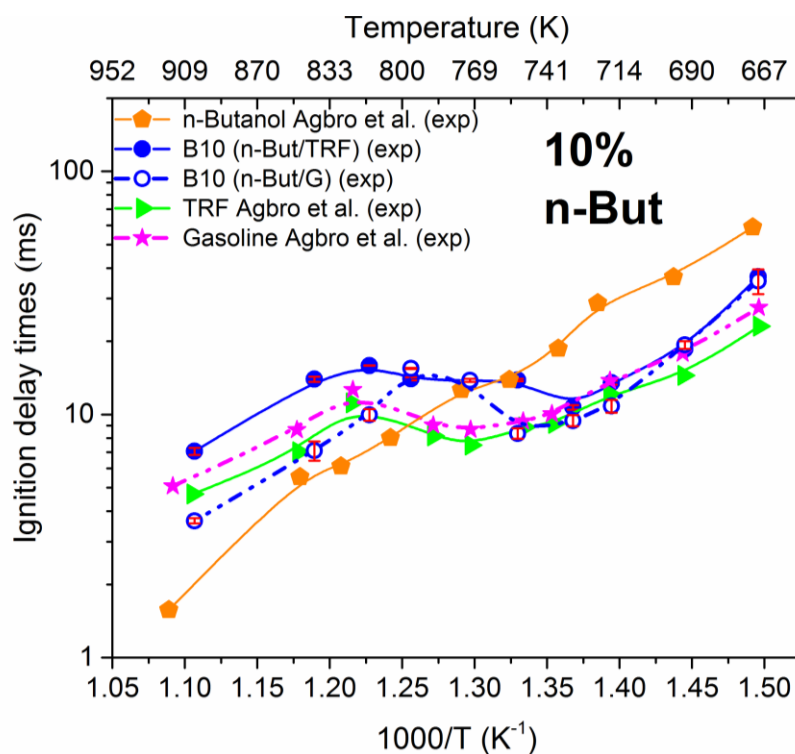
Figure 5.8: Experimental ignition delays from this study and that reported in Agbro et al. [41] for 10% vol *n*-butanol blends with TRF and gasoline, as well as neat fuels, at stoichiometric conditions and a pressure of 2 MPa.
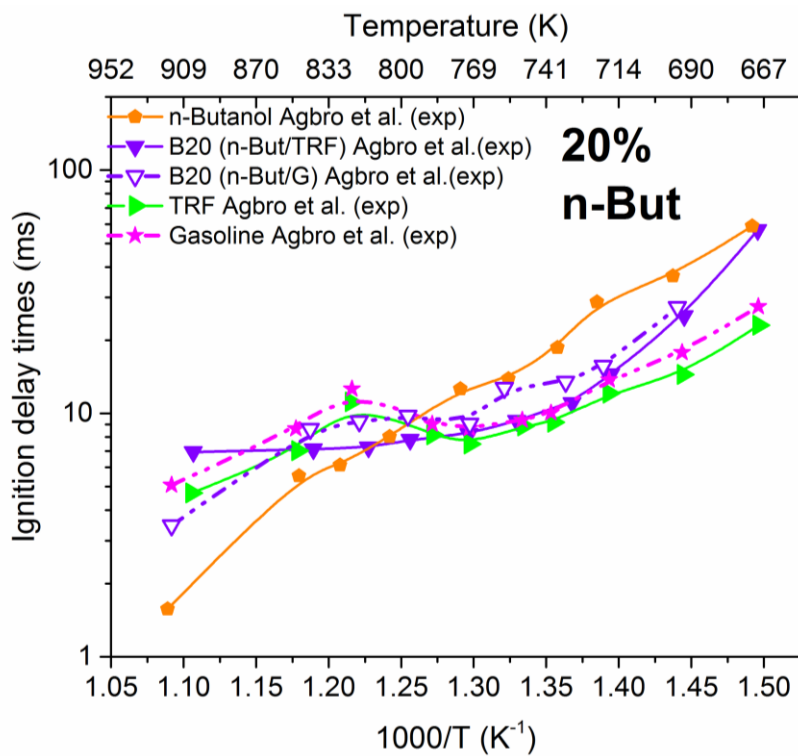
Figure 5.9: Experimental ignition delays from this study and that reported in Agbro et al. [41] for 20% vol *n*-butanol blends with TRF and gasoline, as well as neat fuels, at stoichiometric conditions and a pressure of 2 MPa.
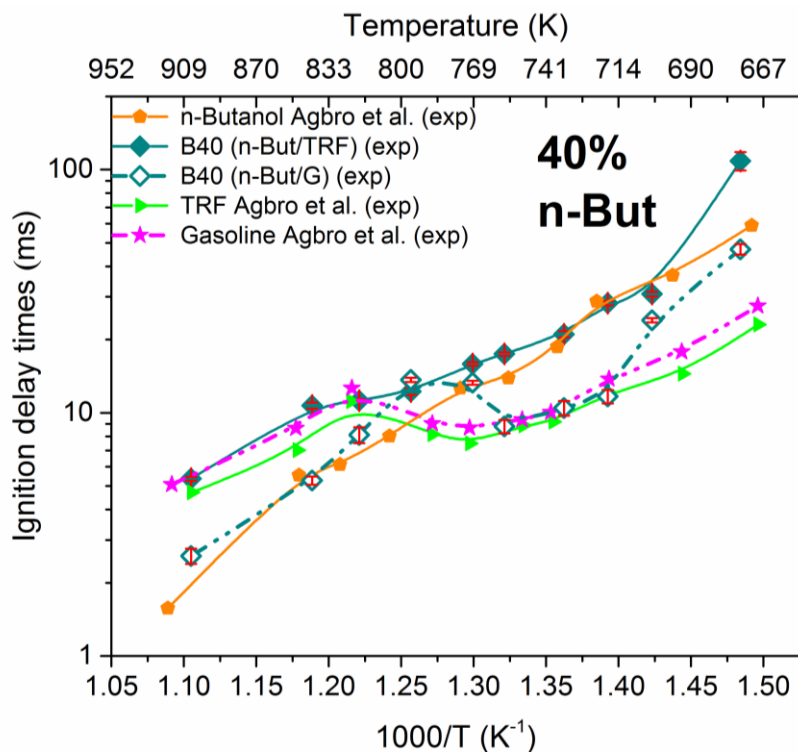
Figure 5.10: Experimental ignition delays from this study and that reported in Agbro et al. [41] for 40% vol *n*-butanol blends with TRF and gasoline, as well as neat fuels, at stoichiometric conditions and a pressure of 2 MPa.
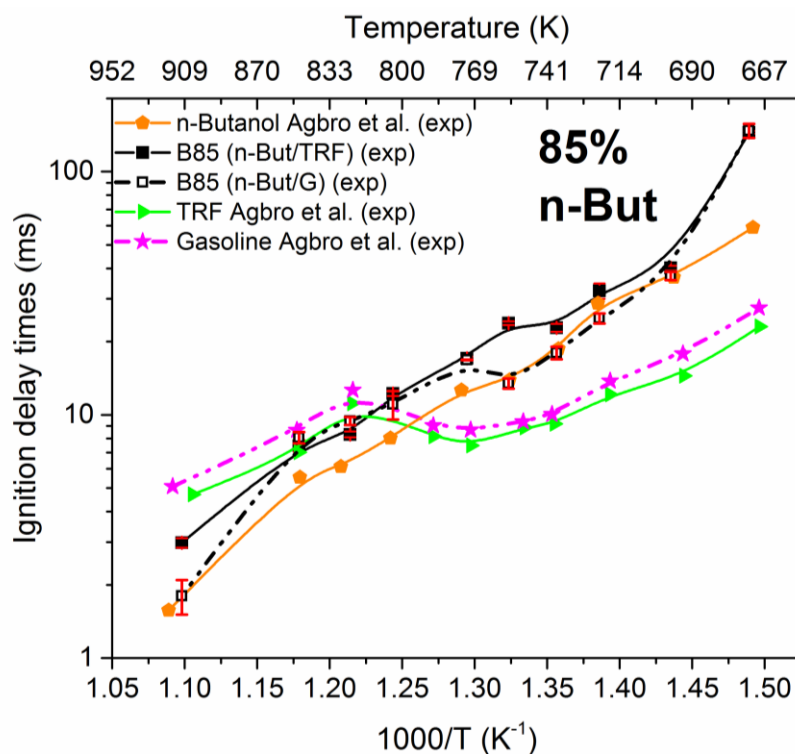
Figure 5.11: Experimental ignition delays from this study and that reported in Agbro et al. [41] for 85% vol *n*-butanol blends with TRF and gasoline, as well as neat fuels, at stoichiometric conditions and a pressure of 2 MPa.

In general, at lower temperatures, the agreement between experimentally measured delays using TRF and gasoline are in good agreement for all of the blends except for B40 at the lowest temperature. However, for B10, where a significant NTC still exists, the agreement between the TRF and gasoline blend is poorer in the NTC regime than at lower temperatures, showing a higher degree of non-linear blending behaviour of mixtures. During the study, additional repeats for these conditions (including 6 sequential runs, as well as repeats on separate days) were performed, which showed consistency and reproducibility. Table 5.1 indicates a standard error between repeats for these conditions of < 0.3 ms. These results highlight the kinetic complexities as well as the need for further research into the formulation of appropriate surrogates as briefly discussed in Section 5.5 of this Chapter. The agreement improves with blending ratio and at 85% the good agreement between the TRF and gasoline blends can be attributed to the large alcohol concentration within these blends. Whilst intuitively, we might expect the gasoline or surrogate chemistry to dominate for B10 and the *n*-butanol chemistry to dominate at B85, this will be explored via the sensitivity analysis in the following sections.

187

5.4 Effects of *n*-butanol addition on the auto-ignition behaviour in an RCM

The influence of *n*-butanol blending on the experimental ignition delay times of gasoline and its surrogate mixture are presented in Figure 5.12. Consistent with earlier, symbols represent ignition delay times as the averages of 4-6 runs made at each test condition, with errors based on one standard deviation. Lines are the best linear fits illustrating trends of ignition delay times for each compressed temperature. At a fixed molar pressure and constant temperature at the end of the compression, at lower temperatures (678 K -745 K) increasing the *n*-butanol concentration within the blends with TRF or gasoline makes the mixtures more resistant to auto-ignition (Figure 5.12 (a) and Figure 5.12 (b), respectively) than pure TRF and for higher blending ratios of B40 and B85 even than pure *n*-butanol. In the higher temperature region (809 K – 916 K), this auto-ignition behaviour is almost reversed with ignition delay times becoming shorter as the *n*-butanol fraction increases within the blends. This is more evident for blends with gasoline fuel. In the temperature range 745 K - 809 K, the strongest variation in ignition delay times is noticed with uncertain and continuously changing trends in the auto-ignition response of the tested fuel blends. Here, cool flame and low temperature chemistry have a significant effect on ignition delay times. Hence, the different reactivities of fuels and their components can make the kinetics of the mixtures more susceptible to temperature and compositional changes and not directly proportional to *n*-butanol fraction within the blend.
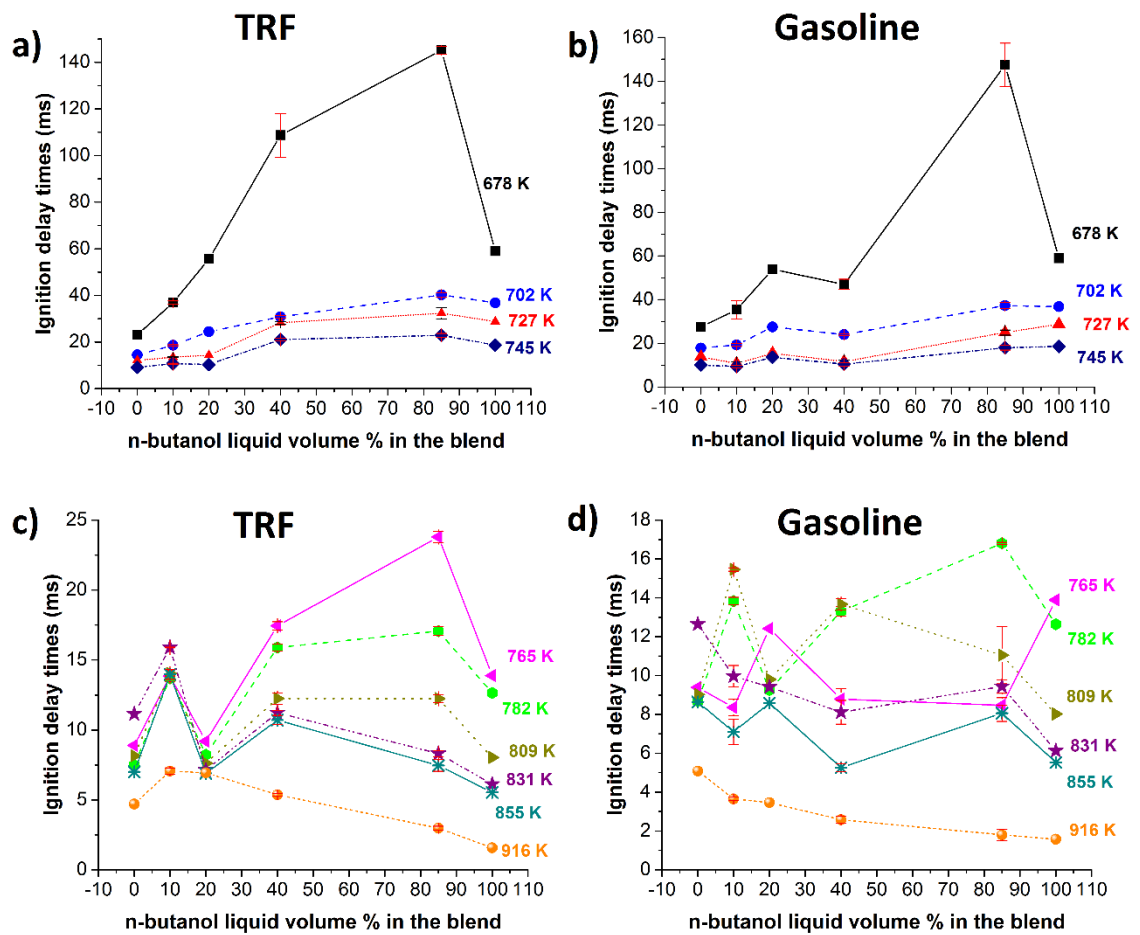
Figure 5.12: Change of ignition delay times with the proportion of *n*-butanol in the blend a) and c) mixtures with TRF surrogate fuel; b) and d) mixtures with gasoline in the temperature range 678 K -916 K. *P*=2 MPa , *φ*=1.0.

From Figures 5.8 -5.11 it can be noted that there is a cross-over of τ_i for *n*-butanol and its blends when compared to the reference gasoline and TRF i.e. at lower temperatures the addition of *n*-butanol increases τ_i, whereas at higher temperatures it tends to decrease τ_i. The effects of *n*-butanol addition at different blending ratios to TRF and gasoline on ignition delay times are directly compared in Figure 5.13 (a) and Figure 5.13 (b), respectively.

189
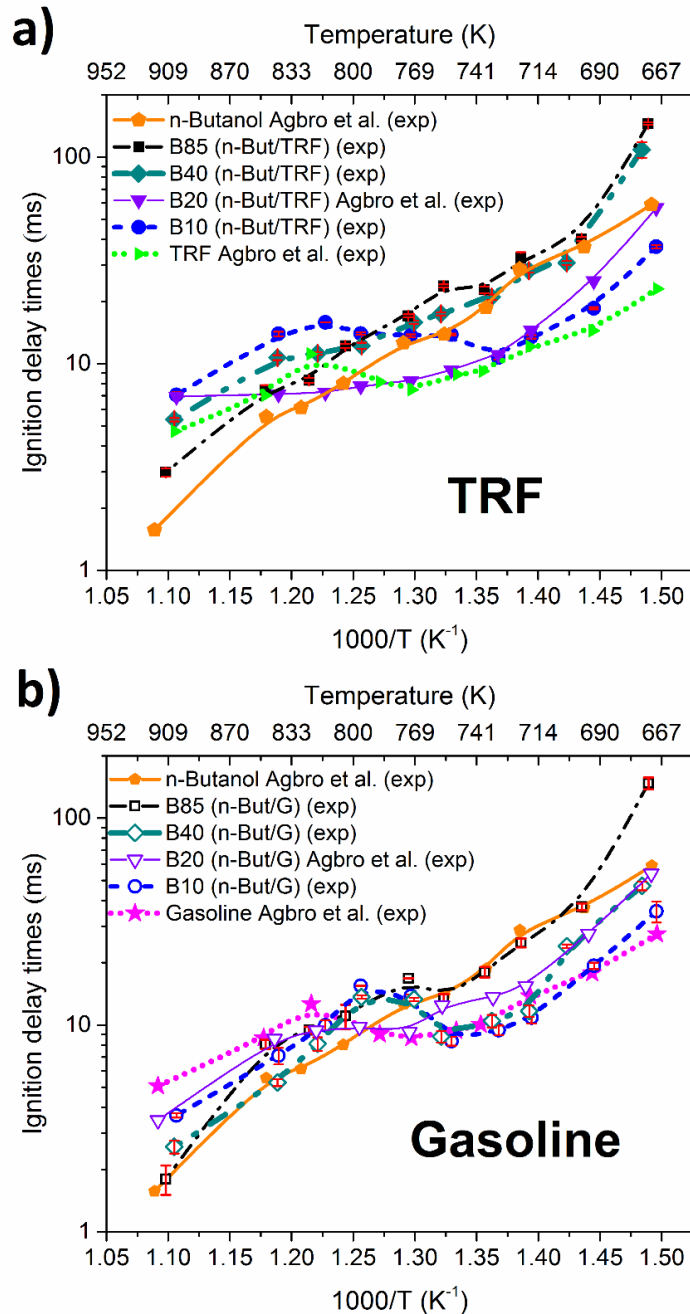
Figure 5.13: The effects on auto-ignition response of *n*-butanol addition at different blending ratios of 10%, 20%, 40% and 85% vol with a) TRF and b) gasoline compared to pure fuels under stoichiometric conditions and at a pressure of 2 MPa.

The NTC response is seen to flatten with increasing *n*-butanol for both TRF and gasoline blends, almost disappearing at the highest blend tested of 85% which exhibits a more Arrhenius like temperature dependency. For the gasoline, each of the blends exhibits a shorter τ_i at the higher temperatures and a longer τ_i at the lower temperatures than the reference gasoline, although the temperature at which the curves cross varies with the blending ratio with a range of 792-812 K. For the TRF, only the highest blends exhibit

shorter τ_i than the TRF, with a range of cross over temperatures from 780-849 K, and in this sense the surrogate fails to capture the intricacies of the impact of blending on the NTC region. This would have consequences for engine simulations where a wide temperature regime would be accessed, and hence whilst the surrogate used captures the general trends when compared to the gasoline, small discrepancies in predicted τ_i could be significant when trying to predict knocking regimes for different spark timings for example.

In general within the lower temperature region, the addition of n-butanol supresses the reactivity of the blend and therefore the n-butanol is acting as an octane booster by delaying ignition. This feature is more pronounced for the TRF surrogate than for the reference gasoline, because it has a more pronounced low temperature heat release (LTHR). Differences in the octane sensitivity (S) and MON of the surrogate (S=5.2 and MON=89.8) compared to the gasoline (S=8.4 and MON=86.6), will affect changes in the fuel reactivity due to changes in pressure and temperature [41, 312]. These effects may amplify with the addition of n-butanol and can be an indication of different octane number response when blended with alcohol fuels as previously reported in AlRamadan et al. [43].

For the n-butanol/TRF blends of B10 and B40, the ignition delay times lie outside the bounds of the unblended fuels in the higher temperature region (765-916 K) with the lowest blend ratio of B10 acting as more of octane booster compared to any other blend ratios tested in this temperature region. The highest blend tested of B85 also shows enhanced octane boosting characteristics compared to n-butanol in the lower temperature region (678-765 K) for both TRF and gasoline blends. According to a linear blending law, both of these blends would be expected to lie between the trends of the pure fuels. Also, in the lower temperature region, the B40/TRF blend exhibits very similar auto-ignition behaviour to the B85/TRF blend, suggesting little influence of increased concentration of n-butanol above 40% blends. The results indicate that linear blending rules based on volume would fail to capture the true temperature sensitivity of ignition delays for fuels when an alcohol compound, in this case n-butanol, is added to the test mixture. Surrogates are more commonly developed using linear-by-mole blending rules [41, 156, 313] and Anderson et al. also suggest that such an approach can be used for blending ethanol and methanol with gasoline [313]. However, the cross over of measured ignition delays for the n-butanol blends with those for pure n-butanol at the lowest temperatures suggests non-linear effects do exist for the blends studied here, even when considered on a molar basis.

A similar non-linear synergistic blending behaviour has been reported in [314] when *n*-butanol at 5%, 10% and 20% vol percentage was added to base fuels, namely Fuels for Advanced Combustion Engines (FACE gasolines) FACE I (RON=70.2, MON=69.5, *S*=0.7) and FACE J (RON=73.8, MON=70.1, *S*=3.7) and also PRF 70, in CFR engine experiments of HCCI combustion mode. The authors used HCCI fuel number to report octane rating similar to RON and MON in SI engines. They showed that an increse of the *n*-butanol concentration within the blend does not necesssarily result in a linear increase of HCCI number. Moreover the blending HCCI octane number had a lower value for the blend with the FACE J gasoline, which is known to have 30% more aromatics and higher octane sensitivity, than the FACE I gasoline. Also mixtures containing FACE J base fuel were less succeptible to the change with respect to either an increase in *n*-butanol content or operating conditions. The 10% vol *n*-butanol blend with FACE I gasoline was reported to have the highest blending HCCI octane number of 170 at lean HCCI operating conditions of high air intake temperature (422 K) and low engine speed (600 rpm) than any other *n*-butanol/base fuel mixture or at any other experimental conditions. Similarly, in the present study the B10 *n*-butanol/TRF blend exhibited peculiar behaviour, acting as more of an octane enhancer than any other tested fuel blend in the temperature region above 782 K. This subsequently indicates the importance of chemical and physical properties for determining the blending behaviour of octane boosters.

5.5 Further investigation of surrogate fuel mixtures effectiveness in representing reference gasoline

Using three components, two of the gasoline properties can be matched and the surrogate used here was based on matching the RON (95) and H/C ratio (1.934) of the reference gasoline with slight differences in MON and octane sensitivity (*S*) noted in [41]. These differences contribute to small discrepancies in the two-stage ignition and the NTC slope between the *n*-butanol/TRF and *n*-butanol/gasoline blends, as illustrated in Figures 5.8-5.11. Better representation may be obtained by matching both RON and MON or by increasing the number of surrogate components, using for example naphthenes and olefins, in the formulation of the model. According to Sarathy et. al [7], a surrogate should match both RON and MON of the target gasoline in order to accurately mimic gasoline auto-ignition response in engines running under premixed conditions. To assess a surrogate fuel that has identical octane numbers (RON and MON) with gasoline performances in capturing auto-ignition behaviour of gasoline on its own and when blended with *n*-butanol the following modelling study has been conducted.

A new three component surrogate fuel (referred to as TRF2) for the tested gasoline was formulated based on the correlations developed by Kalghatgi et al. [315]. These correlations calculate the TRF surrogate composition required to emulate the RON and sensitivity of the target fuel. Javed et al. [150] used this approach in developing surrogate fuels and showed that the estimated RON and MON values using correlations from [315] are in close agreement with the measured RON and MON values in a CFR engine thus further encourage the applicability of this method. Moreover, based on a modified second-order response surface model for RON and MON, the octane number values were confirmed [316]. The properties and the composition of the new formulated surrogate fuel (TRF2) developed based on [315] are listed in Table 5.4. Note that this surrogate model severely undervalues the H/C ratio and suggests a high proportion of aromatic content within the mixture. This will have kinetic consequences due to differences in the chemistry and kinetic interactions between different fuel constituents.

Table 5.4: Summary of the composition and combustion characteristics of the reference gasoline [41] and the new TRF2 surrogate developed based on [315].

Gasoline Component	PR5801 (vol%)	TRF Component	TRF2 (vol%)	TRF2 (mole%)
Paraffins	47.1	*Iso*-octane	34.3465	26.81
		N-heptane	15.8606	13.73
Olefins	7.9			
Naphthenes	8.2			
Aromatics	26.0	Toluene	49.7929	59.47
Oxygenated (ethanol)	4.7			
RON	95		95	
MON	86.6		86.6	
H/C	1.934		1.6206	
S=RON-MON	8.4		8.4	
AKI=(RON-MON)/2	90.8		90.8	
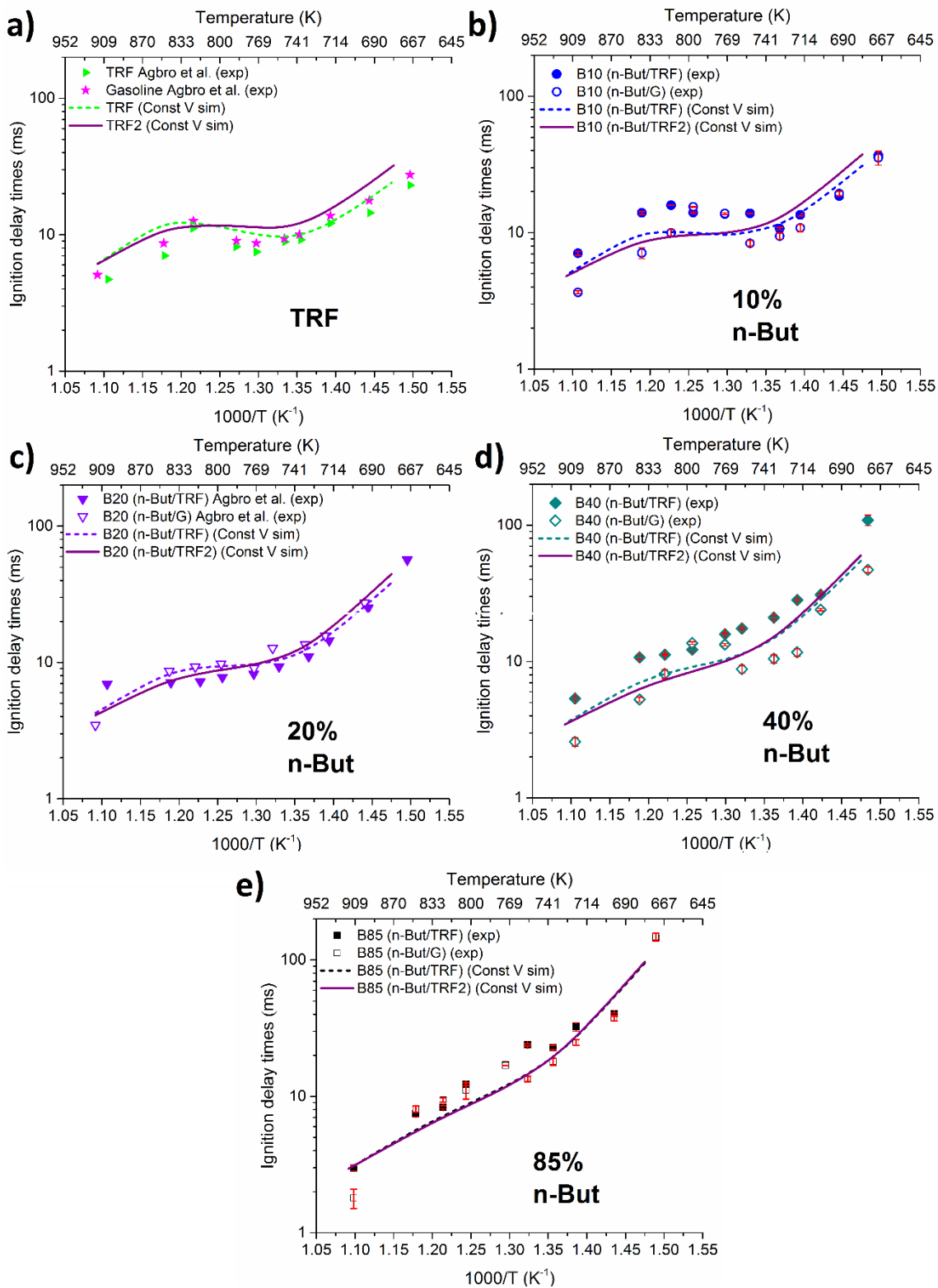
Figure 5.14: Simulations of the auto-ignition response of different TRF surrogate mixtures and their performance in replicating the ignition delay times of a RON95 gasoline a) pure fuels; b) 10%; c) 20%; d) 40% and e) 85% vol *n*-butanol in TRF or gasoline blend, φ=1 and *P*=2 MPa. Symbols represent measured data collected in this work and that of Agbro et al. [41] and lines the simulated results.

Comparison of the constant volume modelled ignition delay responses of the new surrogate fuel, TRF2, for stoichiometric mixtures at 2 MPa and at different blending ratios with n-butanol are shown in Figure 5.14. It illustrates similar trends to the original surrogate fuel, TRF, with the higher blending ratios showing progressively increased analogy due to the stronger influences of n-butanol chemistry. This could be also related to the fact that at these blending ratios, single-stage ignition behaviour is more prevalent, controlled primarily by the hot ignition chemistry, resulting in adequate performances of both surrogates. Therefore, this again highlights the complexity and significance of the low temperature chemistry and cool flames in auto-ignition phenomenon.

In the low temperature region, the TRF2 surrogate tends to over-predict the auto-ignition response of pure gasoline and the B10 blend, which is likely due to the high content of toluene within the mixtures. The original surrogate fuel (TRF, S=5.2) has lower sensitivity than the new surrogate (TRF2, S=8.4), subsequently indicating that large reactivity differences at low temperatures are primarily driven by the non-paraffinic constituent in these fuels. Thus, at low temperatures, the octane dependence of surrogate fuels is more important for high sensitivity surrogate fuels, which is consistent with observations reported in [150, 317]. In the high temperature region, TRF2 slightly better captures the auto-ignition response of the pure gasoline and n-butanol/gasoline blends compared to the original TRF.

There is little or no change of the new surrogate performance in replicating the auto-ignition response in the NTC regime at intermediate temperatures auto-ignition trends in this region. Mehl et al. [312, 318] have previously shown that ignition delay times in the NTC region correspond well with the RON values of fuels, which are identical for both surrogates and gasoline in this study. This can potentially explain the similar NTC behaviour for both surrogate fuels. Also, the surrogate fails to accurately capture the auto-ignition response of the addition on n-butanol to gasoline, even though both RON and MON are matched. Therefore, matching octane numbers of a surrogate fuel with the tested gasoline did not result in significant improvement in its performance in representing the auto-ignition behaviour of gasoline. An additional surrogate component in the current TRF fuel could potentially result in enhanced performance of the surrogate fuel and would allow both octane numbers and the H/C to be matched precisely. However, particular care must be taken in selecting appropriate target properties of the real fuel to ensure success and adequacy of the surrogate fuel model rather than unnecessary complexities associated with an increased number of constituents from both numerical

and experimental standpoint. Hence, further investigation of other surrogate formulations under blending is desirable.

At the present, there is a continuing debate of the best surrogate fuel formulation strategies and the critical target fuel properties [7, 151, 319, 320]. The relative trade-off around how precisely physical and kinetic properties of real gasoline need to be imitated remain unclear [320]. Average molecular weight of the fuel primarily controls physical property imitation, while chemical structure of the fuel governs chemical kinetic imitation. Hence, it is extremely challenging to define the number of surrogate components and the required mixture composition to replicate both physical and chemical kinetic properties at the same time [320]. In addition, for the detailed kinetic modelling, the entailed complexities in representing mixtures of structures of different molecular weights and classes are especially challenging. A brief discussion of the important target fuel properties is provided next.

The H/C ratio of the fuel defines the ratio of CO_2 to H_2O produced from the combustion and hence dictates the amount of heat released during combustion [152]. The H/C ratio of a fuel also represents the molecular diversity of the fuel, as it is a result of relative composition of paraffins, aromatics, naphthenes and olefins [319]. It also effects the overall radical population in a reacting flow [152]. Therefore, H/C is deemed as an important target property for surrogate formulation of real fuels. Note, since modern gasoline often contains oxygenated compounds, it is important to consider H/C/O ratio, as presented by Pera and Knop [156]. Also, the average molecular weight of the fuel is an important target property to regulate gas phase fuel diffusive properties, which are paramount in many transport dominated combustion processes [319].

Overall chemical kinetic reactivity measure, in particular the derived cetane number (DCN), of the target fuel is another important parameter to be considered during surrogate formulation. This parameter reflects the reactivity potential of the particular fuel to that of multi-component mixtures of defined surrogate fuel components [152]. The DCN arise from relationship of the absolute ignition delay as measured by an Ignition Quality Tester with cetane scale [152]. The fuel blends of the specific surrogated fuel components are made by mass measurement to define the effect of each individual component on the mixture DCN [152]. The DCN replicates the degree of LTHR for both petroleum-derived and jet fuels and helps to relate the ignition quality of a fuel with its molecular structure [152, 320]. The H/C ratio and DCN are crucial constraints in defining the kinetic

196

behaviour. At the same time, as discussed earlier, Octane numbers of the target gasoline are important properties for auto-ignition characteristics emulation of gasoline fuels.

For a surrogate fuel to replicate the combustion processes of any real fuel, it should encompass the identical chemical group composition, rather than the molecular class composition, of the target real fuel [320]. Therefore, numerous different molecular class compositions can lead to very analogous chemical group distributions. Several studies [152, 319-321] demonstrated that atom types/chemical functionalities have shown to be an adequate basis set as important descriptors for surrogate fuel formulation. For example, it was demonstrated that DCN has resilient constraining potential to outline the measure of CH_2 functional group and additive configurations formed with it as the base unit, which determines the reactivity of both high- and low-temperature kinetics [320]. The chemical function group approach combined with quantitative structure property relationship (QSPR) regression analysis as a low-dimensional descriptor has shown the high fidelity of the approach to predict reflected shock ignition delay times of fuel mixtures [320].

5.6 Analysis of the robustness of the scheme and chemical kinetic detection of main reactions which influence the predicted ignition delay times

RCM simulations, including the compression phase and associated heat loss effects during compression and post-compression events, were performed in order to evaluate the performances of the combined KAUST/LLNL scheme. This scheme comprises of LLNL gasoline surrogate mechanism of Mehl et al. [143] and *n*-butanol scheme of Sarathy et al. [57] with several updated rate constants. As described in Section 3.3.2, the heat loss characteristics during the compression and post compression were modelled using variable volume approach and inferred from the non-reacting experimental counterparts. Here, non-reacting runs were taken by replacing O_2 with N_2 in the reactive experiments thus maintaining almost fixed specific heat ratio. Further details on the modelling approach are provided in Chapter 3.
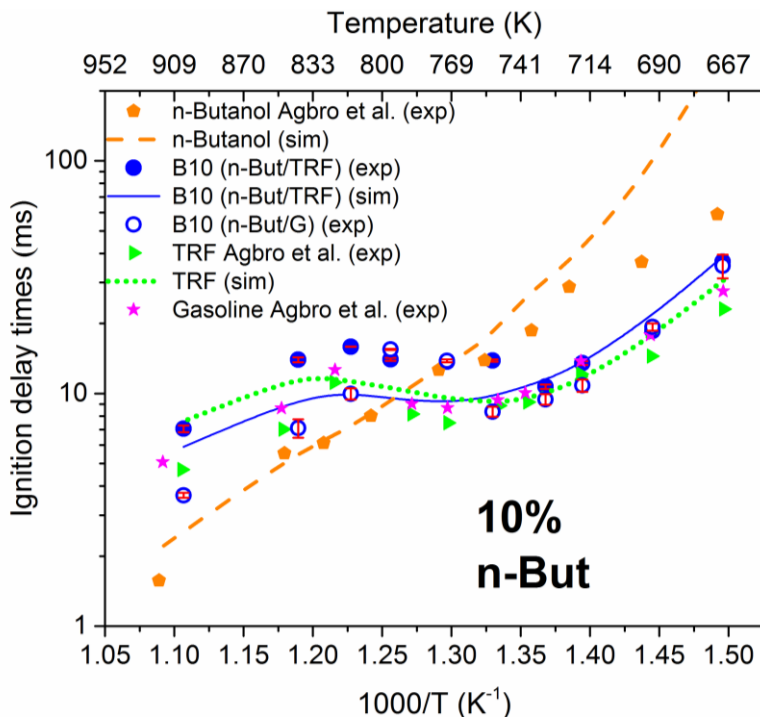
Figure 5.15: Comparison of simulated, and experimental ignition delays from this study and that reported in Agbro et al. [41] for 10% vol *n*-butanol blends with TRF and gasoline, as well as neat fuels, at stoichiometric conditions and a pressure of 2 MPa.
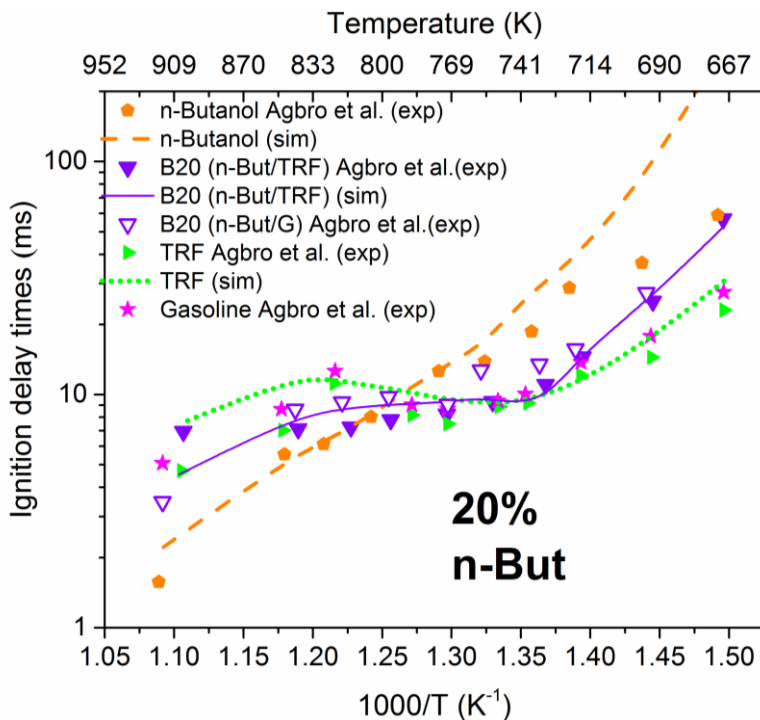
Figure 5.16: Comparison of simulated, and experimental ignition delays from this study and that reported in Agbro et al. [41] for 20% vol *n*-butanol blends with TRF and gasoline, as well as neat fuels, at stoichiometric conditions and a pressure of 2 MPa.
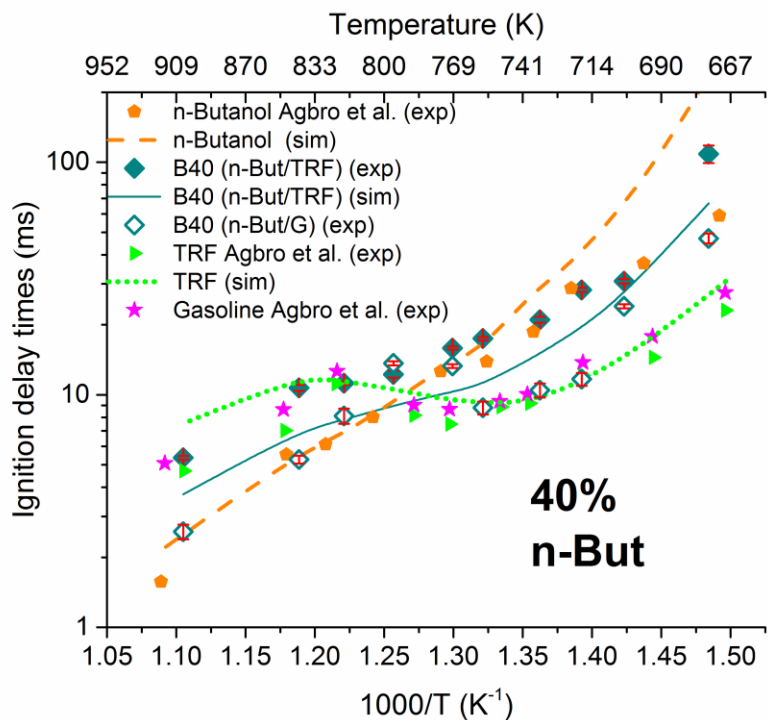
Figure 5.17: Comparison of simulated, and experimental ignition delays from this study and that reported in Agbro et al. [41] for 40% vol *n*-butanol blends with TRF and gasoline, as well as neat fuels, at stoichiometric conditions and a pressure of 2 MPa.
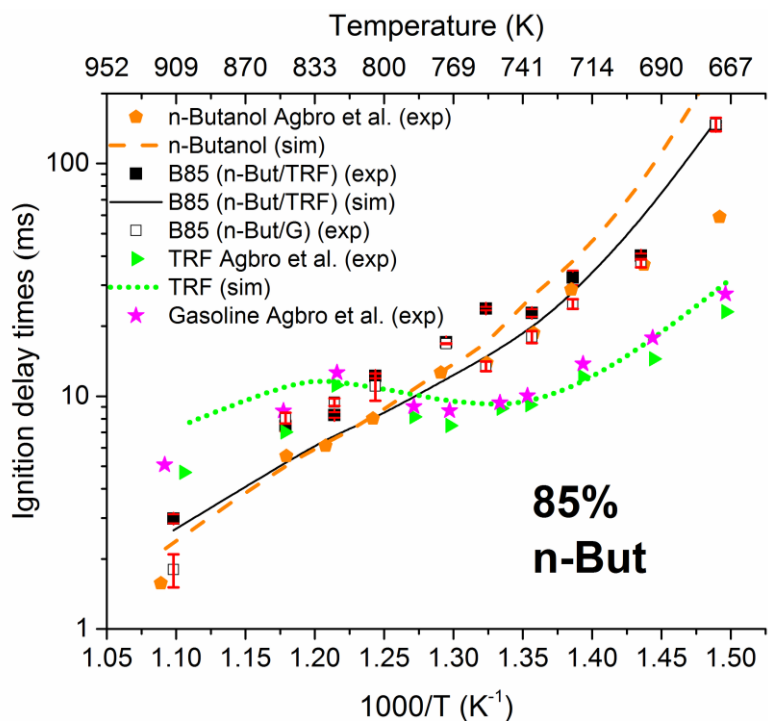
Figure 5.18: Comparison of simulated, and experimental ignition delays from this study and that reported in Agbro et al. [41] for 85% vol *n*-butanol blends with TRF and gasoline, as well as neat fuels, at stoichiometric conditions and a pressure of 2 MPa.

Figures 5.15-5.18 illustrate the comparison of the experimental and simulated ignition delay times for the pure fuels (*n*-butanol, TRF) and blends of 10%, 20%, 40% and 85% by volume of *n*-butanol with TRF as a function of inverse temperature. Experimental ignition delay times are indicated by symbols and were measured in the current RCM experiments, in addition to those presented in [41] for 20% blends in order to examine an extensive range of blending conditions for *n*-butanol with TRF and gasoline. Lines represent simulated ignition delay times in Figures 5.15-5.18. Generally, the modelled ignition delay times demonstrate reasonable agreement with the experimental data for tested conditions, capturing the overall trends of ignition delay times. At low temperatures, the simulations successfully capture the octane enhancing quality of *n*-butanol. Here, the addition of *n*-butanol supresses the reactivity of the blend resulting in appreciably longer ignition delay times. This behaviour will be later explored by sensitivity analysis.

For the pure fuels, Figures 5.15 – 5.18 show that the simulations provide a reasonable representation of the temperature dependent behaviour, except for some discrepancies for the *n*-butanol predictions at the very lowest temperatures and for TRF at the highest temperatures. On blending, the agreement actually improves and the mechanism captures the general trend of the ignition delay times across the whole temperature range quite well, with some underestimation of τ_i in the NTC region. This is especially evident for B10 blend, where a significant NTC exists. With an increase in *n*-butanol concertation within the blend, the mechanism performance in representing the NTC behaviour improves. Also, the NTC response is seen to be flattened with an increase of *n*-butanol concentration, disappearing at B85. These trends are also successfully captured by the scheme. In the NTC region the fuel oxidation route and chain branching processes are controlled by two different mechanisms as detailed in Sections 2.1.9 and 2.1.11. These depend on the type of intermediate species produced in the combustion process that can either accelerate or retard reactions. There is a larger number of reactions that control the NTC auto-ignition behaviour, which results in larger uncertainties in modelled results.

To achieve the shortest test runs during brute-force sensitivity analysis, constant volume adiabatic simulations have been implemented. Constant volume simulations do not capture the effect of the compression stroke and post-compression heat losses. However they facilitate the direct analysis of the kinetic mechanism. Since there is no significant reactivity and, hence, significant heat release during the compression stroke, the errors in predicting pressure and temperature at the end of compression are relatively small and do not affect the sensitivities greatly. The applicability of this approach is demonstrated in

Figure 5.19, where comparisons between variable and constant volume simulations of auto-ignition responses for 10%, 40% and 85% *n*-butanol blends with TRF, show a relatively good agreement between the two adopted modelling approaches in predicting ignition delay times. The constant volume assumption is seen to slightly underestimate the longest ignition delay time studied here for the 85% vol *n*-butanol blend with TRF at the lowest temperature of 678 K, potentially due to heat effects. Therefore, the constant volume reactor model has been deemed a viable tool for brute-force sensitivity analysis.
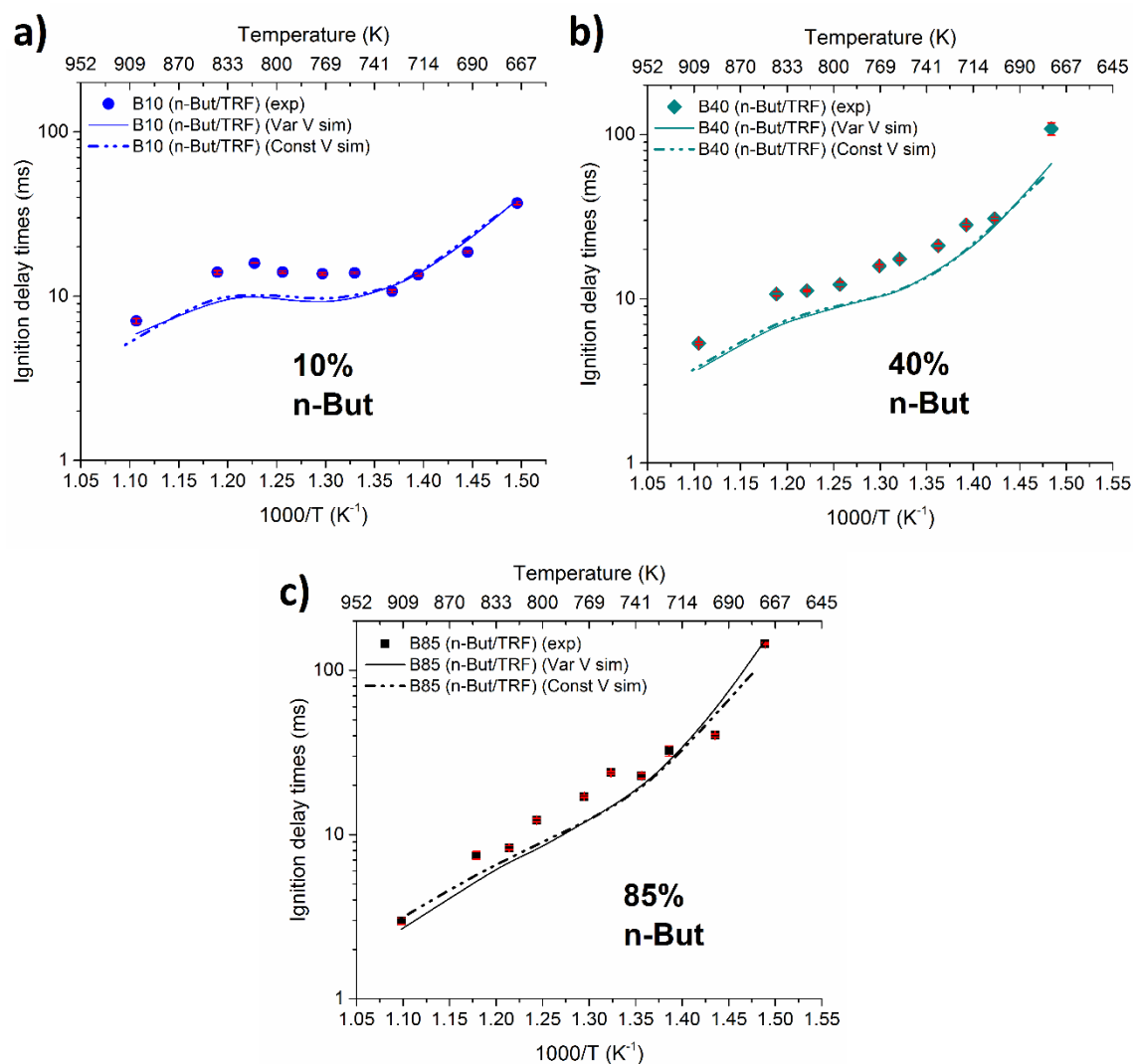
Figure 5.19: Comparisons of experimental and simulated ignition delay times using a constant and variable volume reactor model for a) 10%, b) 40% and c) 85% vol *n*-butanol blend with TRF. P=2 MPa, φ=1.0.
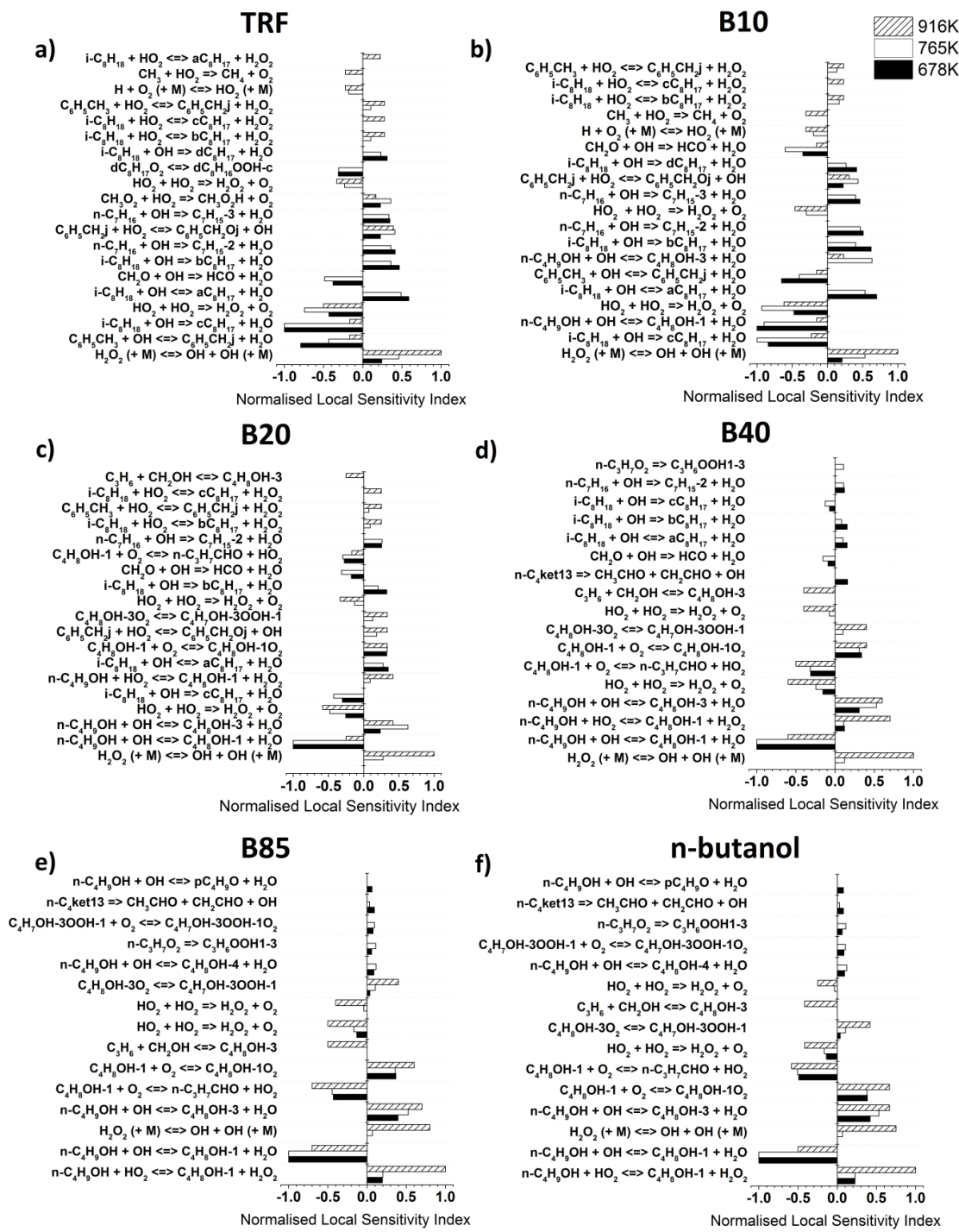
Figure 5.20: Normalised brute-force local sensitivity indices for ignition delay time for a) pure TRF surrogate mixture; b) 10% vol *n*-butanol +TRF blend; c) 20% vol *n*-butanol +TRF blend; d) 40% vol *n*-butanol +TRF blend; e) 85% vol *n*-butanol +TRF blends and f) pure *n*-butanol fuel at 3 temperatures, $\varphi=1$ and $P=2$ MPa. Duplicate entries for the reaction HO_2+HO_2 indicate a double Arrhenius expression for this reaction.

Figure 5.20 depicts the results of the normalised brute-force sensitivity analysis for the 10 most dominant reaction sensitivities at each of the three temperatures studied for all

the fuels and fuel blends tested in this work in order to assess the dominant chemistry at the chosen blending ratios. Perhaps the most striking feature of the sensitivity indices in Figure 5.20 (b) is that, at the lowest temperature, it is an *n*-butanol reaction that ranks the highest in terms of its impact on predicted τ_i despite butanol forming only 10% of the mixture by volume. H abstraction via OH from the α-carbon site $(nC_4H_9OH+OH \leftrightarrow C_4H_8OH-1+H_2O)$ has an inhibiting role, leading primarily to the direct elimination of HO_2 forming butanal as discussed in Welz et al. [322]. Other reactions inhibiting ignition at low temperatures include H abstraction from toluene $(C_6H_5CH_3+OH \leftrightarrow C_6H_5CH_2j+H_2O)$ as well as from the tertiary site of *iso*-octane. A Rate of Production (ROP) analysis showed that for this blend, the toluene reaction had the highest rate throughout the ignition, although τ_i was not as sensitive to changes in its rate. The main reactions promoting ignition at this low temperature relate to H abstraction from *n*-heptane and from the primary and secondary sites of *iso*-octane. Therefore, at low temperatures, the inhibiting role of $nC_4H_9OH+OH \leftrightarrow C_4H_8OH-1+H_2O$ is in competition with chain branching reactions from the surrogate gasoline, and in fact for B10, only a small increase in τ_i was observed compared to pure gasoline/TRF as shown in Figures 5.8 - 5.11 and Figures 5.15 – 5.18.

As *n*-butanol increases to 20%, 40% and 85% by volume, the OH from the α-carbon site dominates the sensitivities at both the low and intermediate temperatures, and in this case is competing against the alkane-like chain branching route initiated by abstraction from the γ-site of *n*-butanol similarly to pure *n*-butanol, and consistent with studies for pure *n*-butanol in [323] and for B20 in [89]. The importance of H abstraction by OH from the α-site at low temperatures leads to the octane enhancing influence of *n*-butanol under these conditions as seen in Figures 5.8 -5.11 and Figure 5.13. This differs from previous studies for ethanol/PRF blends where H abstraction by HO_2 (rather than by OH as seen here) leading to acetaldehyde and H_2O_2 was suggested to be a factor in slowing the production of reactive radicals [324]. However, at higher temperatures, abstraction from the α-site by HO_2 is the dominant reaction for the 85% blend studied here similarly to the pure *n*-butanol, and in this case promotes reactivity since at these temperatures the H_2O_2 formed, reacts to form 2 OH radicals. Thus at these higher temperatures, high blends of *n*-butanol reduce ignition delay times and butanol does not act as an octane enhancer in this situation.

Figures 5.15 – 5.18 show that the mechanism fails to properly capture the slope of ignition delays at the lowest temperatures, although as shown in Tables 5.1-5.3, this is where the largest experimental uncertainties lie. This may possibly be due to the over dominance of

H abstraction from the α-channel in this temperature region. As noted in [323], the prediction of τ_i is not highly sensitive to the overall rate of OH+n-butanol, but rather to the branching ratios for the different abstraction sites. McGillen et al. [268] suggest higher uncertainties for the site specific channel for the γ-site compared to the α-site and there are no site specific experimental data for temperatures of relevance in combustion. A second possible source of discrepancy is the lack of inclusion in the mechanism of possible cross reactions between the blend components. Cross reactions used in other schemes include different product channels for benzyl+n-butanol, benzyl+butanal or benzyl+1-butene. Sensitivity of ignition delay predictions to their inclusion was therefore tested here using rate coefficients and thermodynamic properties from the mechanism discussed in Pelucchi et al. [89] and the summary of findings is presented in Section 5.7.

At the highest temperature of 916 K, for all fuels, $H_2O_2(+M) \leftrightarrow OH+OH(+M)$ plays a key role in forming OH radicals and promoting ignition [150, 325], with the reaction of HO_2 with itself playing an inhibiting role. For B10, abstraction from the γ site, which promotes reactivity, has a low sensitivity. Hence even at high temperatures, this blend shows longer ignition delay times than TRF despite a small promoting role for H abstraction from toluene and iso-octane by HO_2. For B85, H abstraction by OH from the γ-site becomes more important in promoting ignition and the ignition delay times become shorter than for TRF.

The intermediate temperatures in the NTC region for gasoline posed the largest challenges in terms of the ability of the surrogate to mimic gasoline under blending, as well as for the chemical mechanism employed. At the intermediate temperature of 765 K, we see a mixture of reactions contributing to the sensitivities, particularly for B10, including H abstraction by both OH and HO_2 from the primary fuel molecules, as well as the reactions of HO_2 and H_2O_2. The contribution of a higher number of reactions to the overall uncertainty in predicting ignition delays creates challenges for the chemical mechanism within the NTC region where there is a low gradient of τ_i with respect to temperature. The main inhibiting reactions eventually leading to HO_2 formation are $iC_8H_{18}+OH \leftrightarrow cC_8H_{17}+H_2O$ and $nC_4H_9OH+OH \leftrightarrow C_4H_8OH-1+H_2O$ [150] but these are competing against a larger number of significant chain branching routes than at lower and higher temperatures. This feature, of larger uncertainties within the NTC region, was also noted by Hébrard et al. [326] for n-butane oxidation, and suggests the need for highly accurate estimates of site specific abstraction rates by both OH and HO_2 for the main fuel molecules.

5.7 Effects of addition of cross reactions

The deficiency of the mechanism in accurately predicting the slope of ignition delays at the lowest temperatures and NTC behaviour could perhaps be attributed to the lack of the cross-reactivity and reactions between *n*-butanol and TRF species in the mechanism. Hence, the following reactions (adopted from POLIMI mechanism [89]) have been added to the mechanism:

benzyl + *n*-butanol

$n\text{-}C_4H_9OH + C_6H_5CH_2j \rightarrow C_4H_8OH\text{-}4 + C_6H_5CH_3$ [4.060e+04, 2.0, 19525.57]

$n\text{-}C_4H_9OH + C_6H_5CH_2j \rightarrow C_4H_8OH\text{-}3 + C_6H_5CH_3$ [2.707e+04, 2.0, 16157.33]

$n\text{-}C_4H_9OH + C_6H_5CH_2j \rightarrow C_4H_8OH\text{-}2 + C_6H_5CH_3$ [2.707e+04, 2.0, 16157.33]

$n\text{-}C_4H_9OH + C_6H_5CH_2j \rightarrow C_4H_8OH\text{-}1 + C_6H_5CH_3$ [4.060e+04, 2.0, 16157.33]

benzyl + butanal

$n\text{-}C_3H_7CHO + C_6H_5CH_2j \rightarrow 0.6\ CH_2O + 0.4\ HCO + 0.4\ C_3H_6 + 0.6\ C_3H_5\text{-}a + C_6H_5CH_3$ [4.872e+04, 2.0, 16157.33]

$n\text{-}C_3H_7CHO + C_6H_5CH_2j \rightarrow 0.75\ CH_3 + 0.25\ C_2H_4 + 0.25\ CH_2CHO + 0.75\ C_2H_3CHO + C_6H_5CH_3$ [1.624e+04, 2.0, 16157.33]

$n\text{-}C_3H_7CHO + C_6H_5CH_2j \rightarrow C_2H_4 + CH_3CO + C_6H_5CH_3$ [1.624e+04, 2.0, 16157.33]

$n\text{-}C_3H_7CHO + C_6H_5CH_2j \rightarrow CO + n\text{-}C_3H_7 + C_6H_5CH_3$ [9.473e+04, 2.0, 14112.33]

benzyl + 1-butene

$C_4H_8\text{-}1 + C_6H_5CH_2j \rightarrow C_4H_71\text{-}3 + C_6H_5CH_3$ [8.120e+04, 2.0, 16157.33]

$C_4H_8\text{-}1 + C_6H_5CH_2j \rightarrow C_4H_71\text{-}4 + C_6H_5CH_3$ [4.060e+04, 2.0, 19525.57]

$C_4H_8\text{-}2 + C_6H_5CH_2j \rightarrow 0.02\ CH_3 + 0.02\ C_3H_4\text{-}p + 0.98\ C_4H_71\text{-}3 + C_6H_5CH_3$ [8.120e+04, 2.0, 16157.33]

Here, the numbers in the brackets indicate input parameters (pre-exponential factor, *A*, temperature exponent, *n*, activation energy, *E*, (cal/mol)) of the modified Arrhenius equation (2.7) for rate coefficients calculations.

205

As seen from Figure 5.21, the addition of selected cross reactions to the mechanism makes almost no difference in the simulated ignition delay times with a change of less than 0.1 ms across the whole temperature range.
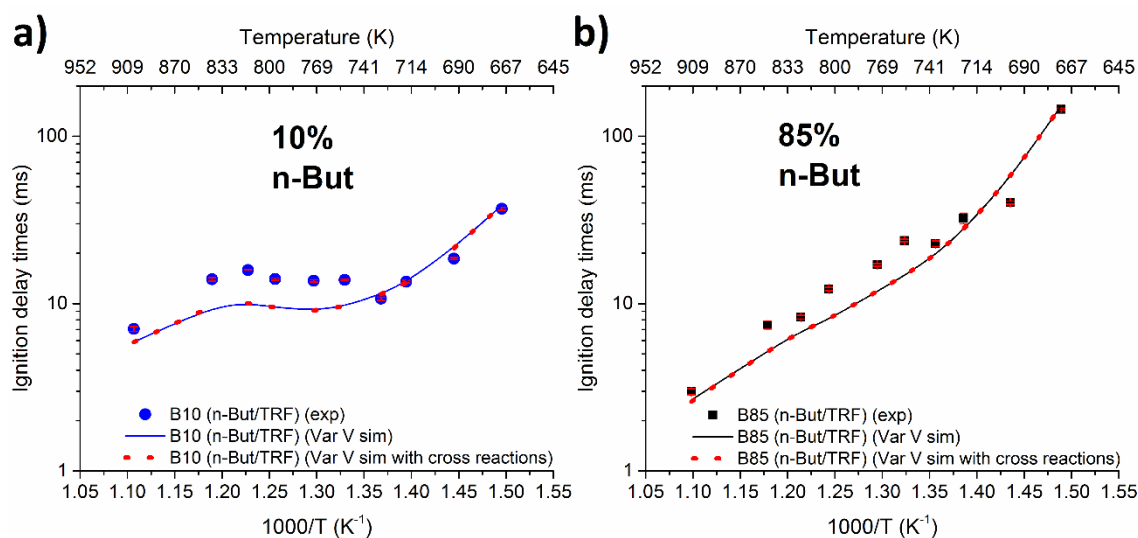
Figure 5.21: Effects on the simulated ignition delay times of the addition of cross reactions benzyl + *n*-butanol, benzyl + butanal or benzyl + 1-butene to the mechanism for a) 10% and b) 85% vol *n*-butanol blend with TRF. *P*=2 MPa, *φ*=1.0.

It is noteworthy to say that POLIMI mechanism [89] contains the aforementioned benzyl cross reactions but also exhibits a higher slope at lower temperatures (see Figure 5.22 and Figure 5.23), although in general its predicted ignition delay times lie closer to the experimental data for the higher *n*-butanol blend B85. The POLIMI mechanism shows better performance in capturing the auto-ignition response of pure *n*-butanol compared to the KAUST/LLNL scheme. On the other hand, POLIMI predictions of ignition delay times for pure TRF and the lowest *n*-butanol/TRF blend B10 have a considerably higher slope at low temperatures compared to the KAUST/LLNL mechanism or the experimental data with a noticeable underestimation in the NTC region. This can be related to a possible deficiency of the POLIMI mechanism in accurately representing the chemistry of the primary reference fuel components, *iso*-octane or *n*-heptane.
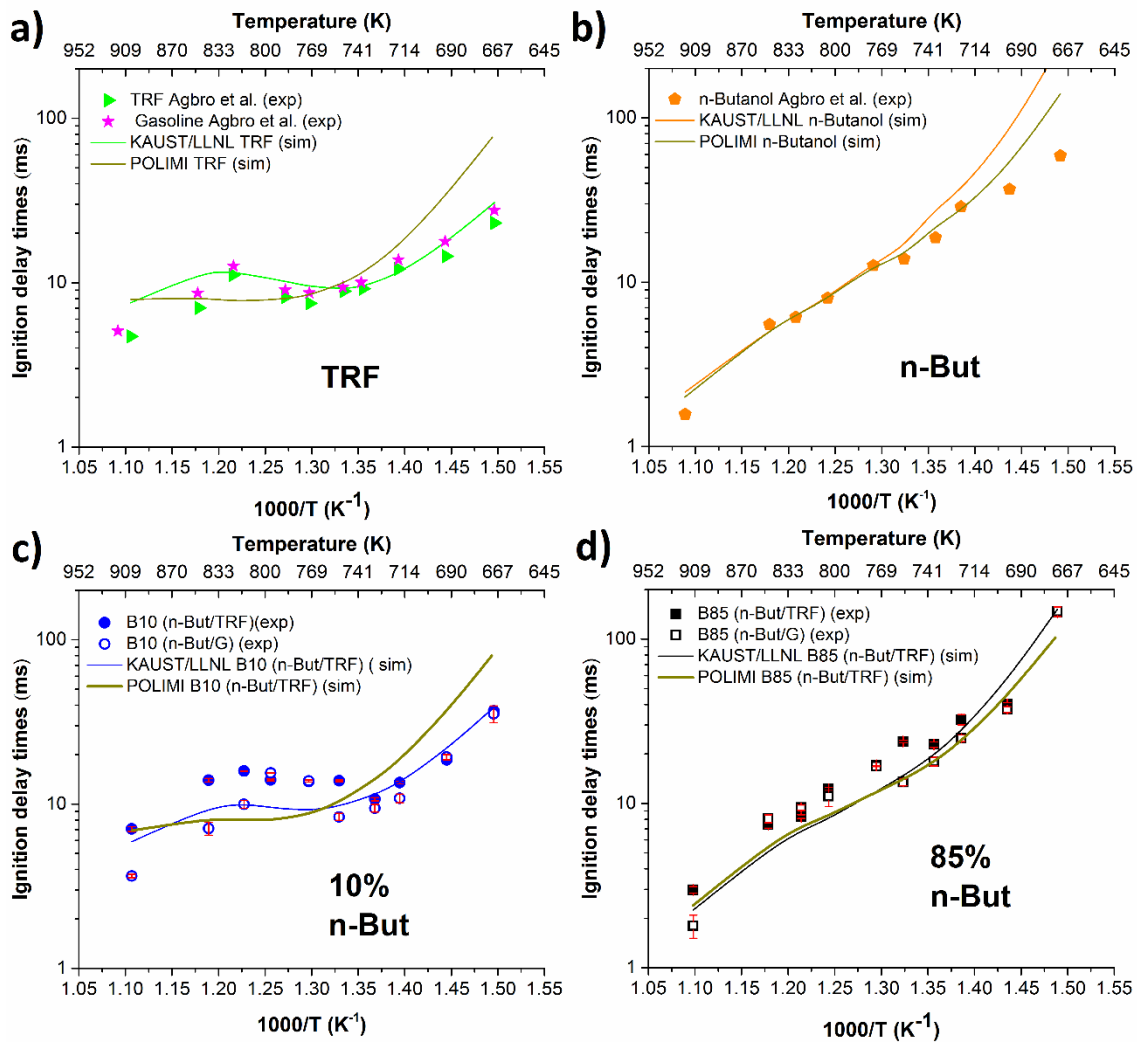
Figure 5.22: Comparison of experimental data from this study and that reported in Agbro et al. [41] and simulated ignition delay times using the KAUST/LLNL mechanism with predictions of the POLIMI mechanism [89] for a) pure TRF; b) pure *n*-butanol; c) 10% vol *n*-butanol +TRF blends and d) 85% vol *n*-butanol +TRF blends at stoichiometric conditions and a pressure of 2 MPa.
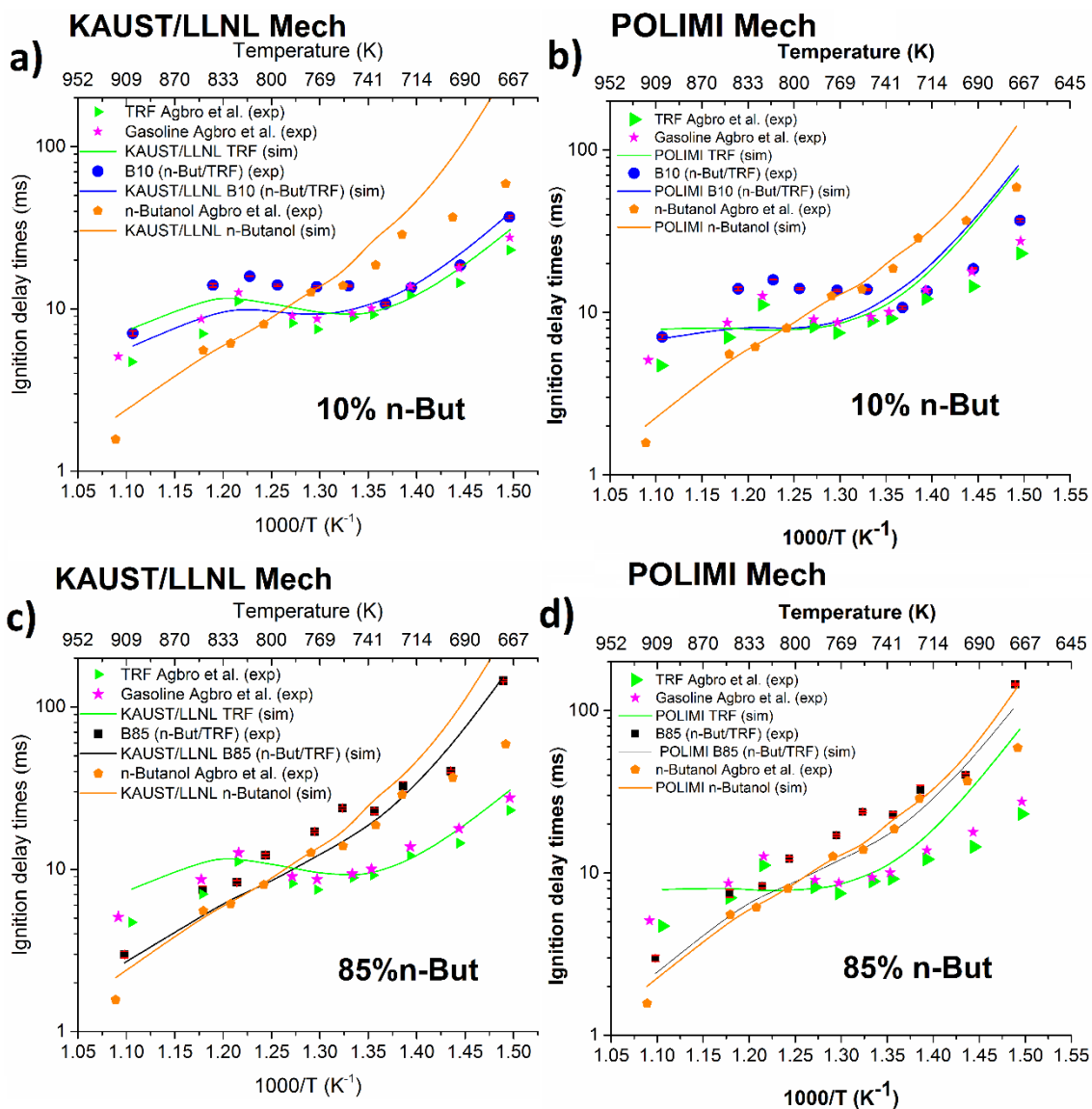
Figure 5.23: Comparisons of predictive capabilities of effects of *n*-butanol addition to TRF on auto-ignition response using the KAUST/LLNL mechanism and the POLIMI mechanism [89] for pure fuels and 10% and 85% vol *n*-butanol +TRF blends of experimental measurements presented in this work and that reported in Agbro et al. [41]. *P*=2 MPa, *φ*=1.0.

Figure 5.24 illustrates results from constant volume simulations for pure *iso*-octane and *n*-heptane using the POLIMI and KAUST/LLNL schemes. The predicted ignition delay times are compared with the RCM experimental measurements of Materego et al. [75] for pure *iso*-octane and for pure *n*-heptane from shock tube experiments of Gauthier at al. [145] at stoichiometric conditions and a pressure of 2 MPa. It is apparent that both mechanisms show adequate performances in modelling *n*-heptane chemistry capturing

the overall trend of its auto-ignition response. On the contrary, there are some substantial differences in the predictions of *iso*-octane ignition delay times between two mechanisms. The KAUST/LLNL mechanism successfully replicates the overall trend of the *iso*-octane experimental data, slightly overestimating ignition delay times which can be potentially attributed to the constant volume approach. It is recognised that this explanation is speculative, but this cannot be tested due to lack of volume histories from Materego et al. [75]. The POLIMI mechanism shows adequate performance at higher temperatures but fails to capture the NTC behaviour of *iso*-octane or the slope of ignition delays at low temperatures, pointing out the weakness of the POLIMI mechanism in representing *iso*-octane chemistry at these temperatures. This, in fact, results in the observed deficiencies of the POLIMI mechanism in predicting the auto-ignition responses of the TRF surrogate fuel and *n*-butanol/TRF mixtures at lower blend ratios revealed in Figure 5.22 and Figure 5.23.
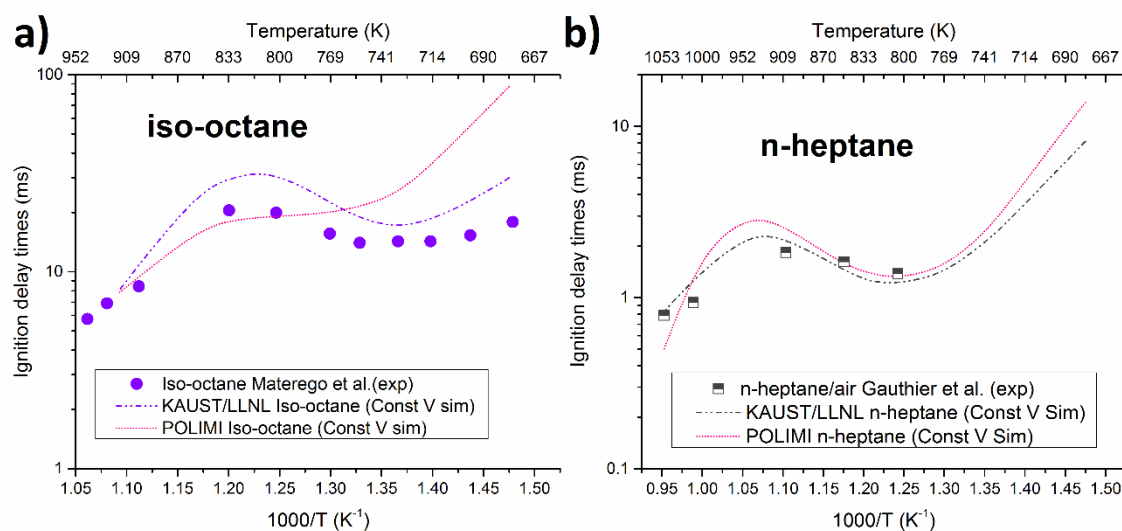
Figure 5.24: Comparisons of simulated ignition delay times using KAUST/LLNL mechanism and POLIMI mechanism [89] with experimental measurements for a) pure *iso*-octane from Materego et al. [75] and b) pure *n*-heptane from Gauthier et al. [145]. *P*=2 MPa, φ=1.0.

One possible reason for this disparity is perhaps differences in the low temperature and NTC pathways of *iso*-octane between the two mechanisms. It is also noted that the POLIMI scheme is a lumped mechanism with isomers being lumped together for individual reactions according to a minimisation procedure. The different low

temperature paths are distinguished at later stage in the POLIMI mechanism during *iso*-octylperoxy radicals internal isomerisation reactions.

Despite the total reaction rates of H abstraction reactions by OH and HO$_2$ from *iso*-octane being in a good agreement between the two schemes across the temperature region tested, the discrepancies in *iso*-octane auto-ignition behaviour can be attributed to the differences in reaction rates of reactions at the stage of internal isomerisation between alkylperoxy radicals and alkylhydroperoxide radicals (ROO→QOOH) and perhaps the successive second addition to O$_2$. For the POLIMI mechanism the low temperature pathways are differentiated by distinguishing channels between those leading to low temperature branching (through IC8-QOOH) and channels inhibiting it (from IC8T-QOOH). It seems that the propagation route (ROO→IC8T-QOOH) which is primarily responsible for the formation of the cyclic ethers from tertiary radicals is favoured over the chain branching route (ROO→IC8-QOOH) which results in the formation of keto-hydroperoxides. Thus, this subsequently results in the production of less OH radicals from keto-hydroperoxides, leading to less fuel consumption, hence less alkylperoxy radicals and alkylhydroperoxide radicals, and therefore very low radical profiles. The CRECK modelling group is currently revising the POLIMI mechanism for *iso*-alkane chemistry.

Figure 5.25 compares sensitivity coefficients for the 10 most sensitive reactions at each temperature tested for 10% and 85% vol *n*-butanol blend with TRF using the POLIMI mechanism. At high temperatures, ignition is primary controlled by the thermal chain branching of H$_2$O$_2$ to produce two OH radicals via reaction H$_2$O$_2$(+M)↔2OH(+M) for both blends, while for the KAUST/LLNL mechanism at the highest blending ratio of B85 the H abstraction by HO$_2$ from α-site of *n*-butanol dominated the sensitivities at 916 K. In general a better agreement between the two mechanisms is observed for the highest blend (B85) than for B10. Consistent with the KAUST/LLNL scheme, H abstraction from the α-site of *n*-butanol at low and intermediate temperatures dominates the sensitivities for the B85 blend decreasing the reactivity of the system, and competes with H abstraction from the γ-site.
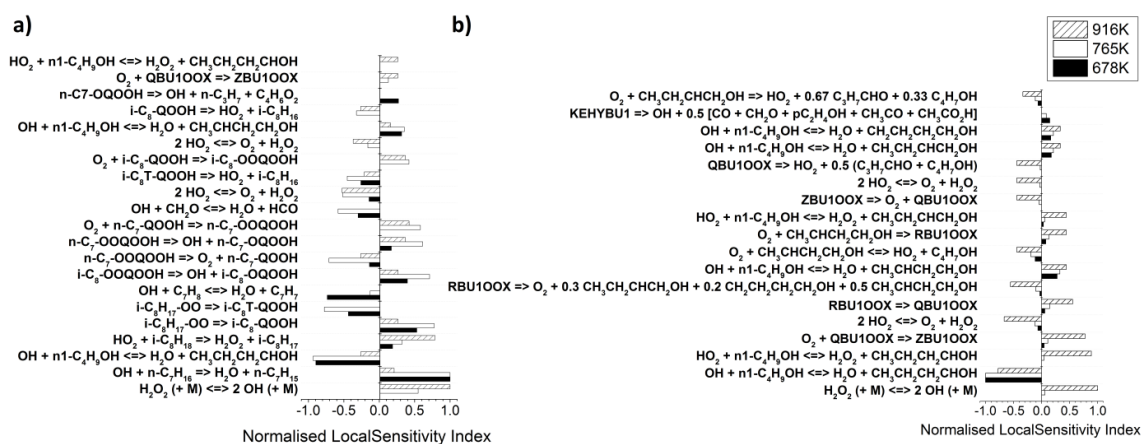
Figure 5.25: As predicted by the POLIMI mechanism. Normalised brute-force local sensitivity indices for ignition delay time for a) 10% vol *n*-butanol +TRF blend and b) 85% vol *n*-butanol +TRF blends at 3 temperatures, φ=1 and *P*=2 MPa.

For the 10% vol *n*-butanol blend with TRF, some differences are seen between the two schemes. For the POLIMI mechanism the most important reaction is the *n*-heptane reaction at low and intermediate temperatures that is not featured in the KAUST/LLNL sensitivity analysis. Also there are some apparent differences in *iso*-octane chemistry and ranking of its reactions. The KAUST/LLNL mechanism accentuates the site specificity of *iso*-octane with OH reactions, whereas in the POLIMI mechanism these different low temperature paths are featured at the later stage during *iso*-octylperoxy radicals internal isomerisation reactions, specifically i-C$_8$H$_{17}$-OO→i-C$_8$-QOOH which leads to the formation of hydroperoxy *iso*-octyl radicals, subsequently facilitating chain branching reactions and i-C$_8$H$_{17}$-OO→i-C$_8$T-QOOH that predominately results in conversion to cyclic ethers and OH radicals, thus acting as OH radical scavenger. However, the H-abstraction from the α-site of *n*-butanol (inhibiting reaction) is seen to be important and competes with the chain branching reactions of TRF chemistry. It is worth noting that the previously mentioned benzyl cross reactions do not feature in the sensitivity analysis for the POLIMI scheme.

5.8 Conclusions

This study improves our understanding of the effects of *n*-butanol addition to a reference gasoline (RON 95, MON 86.6) and a gasoline surrogate on auto-ignition response at various blending ratios. Ignition delay times from an RCM were reported for 10%, 20%, 40% and 85% vol *n*-butanol blends with a TRF surrogate and reference gasoline for temperatures of 678-916 K and a pressure of 2MPa under stoichiometric conditions. The TRF surrogate was capable to quite accurately emulate the auto-ignition behaviour of the

target gasoline, including the NTC behaviour. Generally, the TRF surrogate showed adequate performance in replicating the ignition response of gasoline for all conditions tested, with the closest agreement for the 85% blends. The results show that with the addition of *n*-butanol even at 10%, the TRF was unable to match gasoline well. Some discrepancies existed within the NTC region, suggesting that better matching of both RON and MON or another surrogate fuel formulation method may be required. However, a modelling study on a new TRF surrogate with identical RON and MON values to the reference gasoline did not show a significant improvement in performance in replicating the auto-ignition response in the NTC regime at intermediate temperature and failed to accurately capture the slope of ignition delay times at low temperatures. Hence, the matching RON and MON values in the surrogate formulation is insufficient. Additional components within the surrogate may be required in order to adequately represent the chosen gasoline. However, the sensitivity analysis suggested that a larger number of reactions control the ignition within the NTC region, and hence the addition of further surrogate components may also increase the level of uncertainty within the chemical mechanism representing the surrogate within numerical simulations.

At low temperatures, increasing the *n*-butanol concentration led to increases in ignition delay times, showing that *n*-butanol acts as an octane enhancer in this region even at low concentrations, with marginal additional effects for blends above 40%. At higher temperatures, the behaviour reverses as the chain branching routes from H abstraction from the γ-site of *n*-butanol become more dominant. For the lower blends, the largest discrepancies between the simulations and experiments were seen in the NTC region where a large number of reactions contribute to the uncertainty in predicting τ_i. For the higher blends, the largest discrepancies were noted in the low temperature region, indicating that uncertainties within the low temperature *n*-butanol chemistry need to be resolved. Accurate, temperature dependent reaction rates for site specific H abstraction by both OH and HO_2 for each of the fuel blend components are necessary in order to improve the agreement between numerical simulations and experimental data.

The inclusion of a limited set of specific benzyl cross reactions within the KAUST/LLNL mechanism did not lead to the significant improvement in predictive capability of the chemical kinetic scheme. Moreover these reactions did not feature in the sensitivity analysis for the POLIMI scheme which showed less satisfactory performance in capturing the NTC behaviour of pure TRF and low *n*-butanol/TRF blends compared to the KAUST/LLNL mechanism. Sensitivity analysis using the POLIMI scheme showed that

the chemistry driving the auto-ignition is very similar to the KAUST/LLNL scheme for the highest *n*-butanol/TRF blend B85, while substantial differences existed in the chemistry of the lowest *n*-butanol/TRF blend B10. Also, the numerical modelling work highlighted the weakness of the POLIMI scheme in replicating *iso*-octane chemistry, which is currently under revision.

6. Characterisation of Auto-ignition Phenomenon and Heat Release Analysis

Since auto-ignition of the larger hydrocarbon fuels, such as *n*-heptane and *iso*-octane, follows multiple reactions and pathways, multiple-stage ignition can be observed especially at low temperatures. This is generally characterised by low temperature chemistry and is also related to the phenomenon of cool flames and the pressure of an NTC. As introduced in Chapter 2, first-stage ignition delays and associated low temperature heat releases are paramount in the design and operation of advanced engine technologies, such as HCCI. An accurate representation of the first-stage ignition delay is seen as a prerequisite in defining the total ignition delay time. Exothermic reactions can limit spontaneous ignition by shifting the equilibrium backwards, increasing the delay between ignition stages. Hence, it is important to accurately determine the first-stage ignition delay and the associated low temperature heat release for accurate prediction of total ignition delay times. Moreover, the low temperature heat release from experimental measurements in RCMs provides an additional necessary refinement in the development of chemical kinetic mechanisms. A crucial aspect is the principal heat release rate that plays a leading role in the definition of excitation times. This parameter plays an important role in defining conditions that lead to engine knock and super-knock. The objective of this study is to experimentally and computationally further characterise the full auto-ignition phenomena of *n*-butanol/ TRF blends studied in Chapter 5.

6.1 Investigation of two stage auto-ignition

Research of Kim et al. [327] and Westbrook et al. [101] shows that Octane Sensitivity of the fuel is strongly correlated with the low temperature reactivity, which can be shown as a two-stage heat release behaviour during auto-ignition. Also, Yao et al. [63] indicate that the octane number of the fuels relates to low temperature heat release (LTHR). Specifically, for higher octane numbers, the fuel's auto-ignition reaction becomes suppressed at low temperatures. This is in line with the present study observation where experimental ignition delay times for the pure *n*-butanol and the highest blend B85 *n*-butanol by liquid volume in the TRF mixture exhibited a more Arrhenius type of auto-ignition behaviour as reported in Chapter 5. In these cases, only a small amount of heat is released during the first-stage ignition, leading to a single-stage fuel ignition. Therefore, no distinct multi-stage ignition behaviour is detected for any of these fuels.

In Chapter 5, RCM pressure profiles indicate the presence of two-stage ignition characteristics for pure TRF fuel, and lower *n*-butanol/TRF blends at low and intermediate temperatures, a typical feature of most transport fuels. The apparent first-stage ignition helps to raise the temperature of the systems and to establish radical pools, which can substantially accelerate the main ignition. Figure 6.1 summarises both measured and computed first-stage, second-stage and total ignition delay times as functions of the inverse compressed temperature for pure TRF, 10% and 40% by liquid volume of *n*-butanol with TRF in the low temperature region, 678-916 K, at a pressure of 2 MPa under stoichiometric conditions. The first- and second-stage ignition delay times are presented as the averages of 3-5 runs made at each test condition with errors based on one standard deviation. The first-stage ignition delay time, τ_1, is defined as the time interval from the end of compression at TDC to the local maximum in the experimentally derived LTHR, which corresponds to the local *dP/dt* maximum. The subsequent time interval from the end of τ_1 to the main ignition event is the second-stage ignition delay time, τ_2. The sum of these two times, τ_1 and τ_2, is the total ignition delay time, τ_i. The definitions for τ_1, τ_2, and τ_i are illustrated in Figure 3.3. For more details on the methodology of the multiple-stage ignition, the reader is referred to Section 3.2.5.
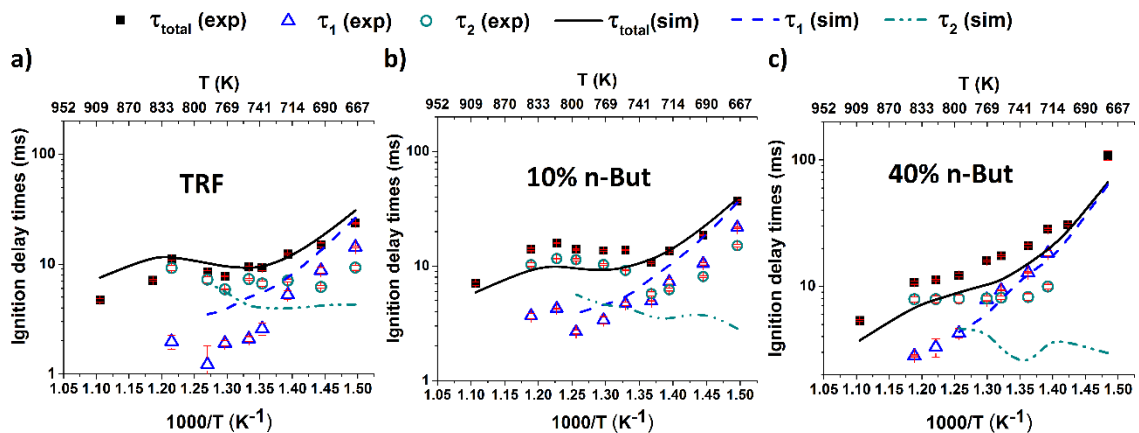
Figure 6.1: RCM measured and simulated first stage, second stage and total ignition delay times from this study and that reported in Agbro et al. [41] for a) pure TRF b) 10% and c) 40% vol blends with TRF at stoichiometric conditions and a pressure of 2 MPa. Experimental first- and second-stage ignition delays are indicated by open symbols. Lines represent simulated data.

The experimental first-stage ignition delay times are captured across the entire temperature range studied here except at 916 K for all three fuels. For B40, at the two lowest temperatures (678 K and 702 K) covered in this study, it is difficult to detect first-

stage ignition, since the LTHR and HTHR events merge, in accordance with known low temperature behaviour. Such distinctively merged LTHR and HTHR behaviour is illustrated in Figure 6.2 (b) for B40 at 678 K. Figure 6.2 (a) demonstrates a representative pressure trace for two-stage ignition with associated experimentally derived HRRs profile for B10 at 727 K. Here, a distinct LTHR event is apparent and followed by a distinct HTHR event. Generally, experimental first-stage ignition delays are found to monotonically decrease with an increase in the compressed temperature. However, at 831 K for both B10 and TRF mixtures the experimental first-stage ignition delay times, indicated by blue triangles in Figure 6.1, are seen to slightly increase in magnitude. This first-stage ignition behaviour, combined with the increased values of second-stage ignition delay times, result in the longest total ignition delay times at these temperatures compared to the other blends tested.
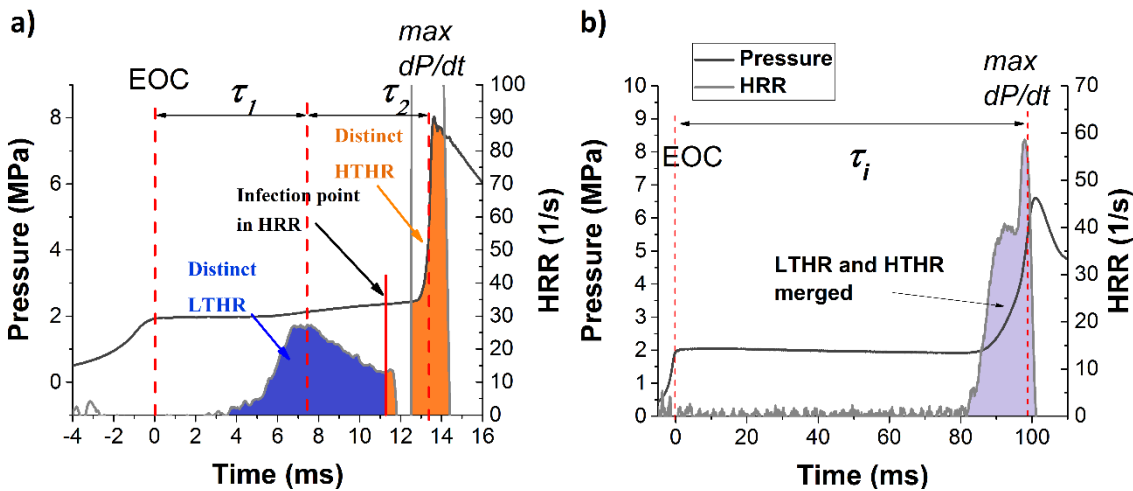
Figure 6.2: Representative experimental pressure trace and experimentally derived normalised HRRs for a) B10 at 727 K illustrating the distinct LTHR and HTHR stages and b) B40 at 678 K demonstrating merged LTHR and HTHR events. $P=2$ MPa, $\varphi=1.0$.

Within the NTC region, an increase in the experimental total ignition delay time is primarily related to an increase in the magnitude of the second-stage ignition delay. A compressed temperature of 727 K is found to indicate a crossover temperature where first-stage ignition delay times become increasingly important in defining total ignition delay times. Below this crossover temperature, both experimental first- and second-stage ignition delay times increase with a decrease in the compressed temperature. Here, the first-stage ignition delays are becoming longer compared to the second ignition delay times, indicating an increasing importance of the first-stage ignition delay time on the total ignition delay time at low temperature region.

In this low temperature region an addition and subsequent increase in *n*-butanol concentration within the TRF mixtures results in increased first-stage ignition delay times. It the intermediate temperature region, first-stage ignition delay times are seen initially to increase in value, with a 10% *n*-butanol addition to TRF, and then decrease for B40. Interestingly, second-stage ignition delay is found to mimic the NTC behaviour and the trends of total ignition delay times. Similarly to first-stage ignition delays, they are seen first to increase in magnitude for the lowest blend, and then decrease for B40. Typically, in cases of very similar magnitude total ignition delay times, and the same initial conditions such as at 727 K temperature for pure TRF and B10, the longer first-stage ignition delay time for B10 allows the accumulation of more radicals and intermediates. These subsequently result in shorter second stage ignition delay times.

The detailed chemical model did not illustrate a two-stage ignition behaviour for these fuels at temperatures above 809 K, which differs from the experimental observations. The model over-estimates the first-stage ignition delay values for the lowest blend, B10, as well as for pure TRF fuel. On the other hand, for the higher blend, B40, the model captures the first-stage ignition delay times quite well. These observations are consistent with the trends of the total ignition delay times presented in Chapter 5, showing an improved performance in the detailed chemical mechanism with an increase in *n*-butanol content within the mixture. This implies that a potential deficiency in the detailed chemical model to capture accurately the first-stage ignition delay times, and consequently the low temperature heat release for B10, results in the observed discrepancies of the total ignition delay times between experimental and modelled results for this fuel.

It is interesting to see that, for *n*-butanol/TRF blends, the detailed chemical kinetic model predicts first-stage ignition relatively well, yet the second-stage ignition delay time is substantially under-predicted. This is especially so for *n*-butanol/TRF blends. This can potentially be attributed to a higher pressure rise during first-stage ignition, predicted by the model, compared to the experiments for these blends. An example of experimental and modelled pressure profiles and their associated normalised HRRs is given in Figure 6.3. A higher pressure rise from the first-stage ignition would shorten the total ignition delay time, and hence the subsequent second-stage ignition delay time. This is because the total ignition delay time is influenced by heat release during the first-stage ignition. This leads to higher gas temperatures that accelerate the onset of hot ignition, as demonstrated by Tanaka et al. [311]. This is also consistent with the interpretation of Ribaucour et al. [328] and Westbrook [329], that the onset of hot ignition is determined

by a critical temperature at which H_2O_2 decomposes rapidly. Moreover, this theory was also recently confirmed by Wilson et al. [330], who showed that the amount of heat released during the first-stage of ignition influences the onset of the main ignition event. Min et al. [331] have re-affirmed that the reaction rate and kinetic pathways of second-stage ignition delay times are strongly affected by the inter-stage temperature between the first- and second-stage ignition delays, due to heat release during the first-stage ignition.
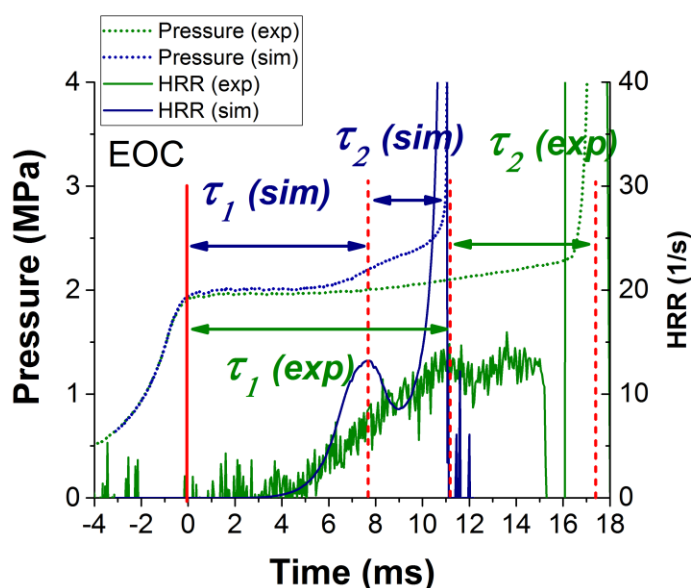
Figure 6.3: Representative experimental/experimentally derived and simulated pressure and heat release profiles for 40% vol *n*-butanol/TRF blend at 765 K stoichiometric conditions and a pressure of 2 MPa.

According to Sarathy et al. [274] reactions that are generally highlighted as important during the first-stage ignition are those that describe the low temperature chemistry of alkanes, as discussed in Chapter 2. The hydrogen abstraction reactions from parent fuel molecules by OH radicals and the isomerization reactions of alkylperoxy radicals (RO_2) are major reaction classes that control first-stage ignition delay times. On the other hand, concerted elimination reactions of alkylperoxy radicals and β-scission reactions leading to the production of the less reactive HO_2 and olefins, compete with chain-branching low temperature reactions, and subsequently result in an apparent fall in the overall heat release rate [149, 274, 300]. Interestingly, the rate constant for dissociation of hydrogen peroxide (H_2O_2) is known to be crucial in defining the total ignition delay time, but not the first-stage ignition time. Hydrogen peroxide begins to accumulate around the time of the first-stage ignition, and then rapidly dissociates to form two highly reactive OH

radicals when the temperature reaches approximately 1000 K, thereby promoting auto-ignition [329]. This reaction and other hydrogen-related chemistry of auto-ignition are critical in defining the evolution of the second-stage ignition delay time and subsequent acceleration in the pressure rise [274, 300, 332]. The controlling chemistry of first-stage ignition delay and subsequently low temperature heat release is further investigated in the following sections.

6.2 Heat release analysis

The presence of multiple-stage behaviour in the SI engine has serious consequences on engine operation, leading to an increased likelihood and intensity of engine knock. Hydrocarbon fuels typically display two-stage ignition processes, but these fuels can also exhibit auto-ignition phenomena with more than two distinct stages of heat release, e. g. the three-stage process [274, 333-335]. Three-stages of oxidation are revealed by from the heat release profile. Each ignition stage is signified by a distinct peak in the heat release, corresponding to a low temperature heat release (LTHR), an intermediate temperature heat release (ITHR) and, ultimately, a high temperature heat release (HTHR). An example of this for experimentally derived HRR and computed HRR profile for B10 at 702 K is demonstrated in Figure 6.4 (a) and (b), respectively. Further details on the HRR analysis is provided in Section 3.4.1.
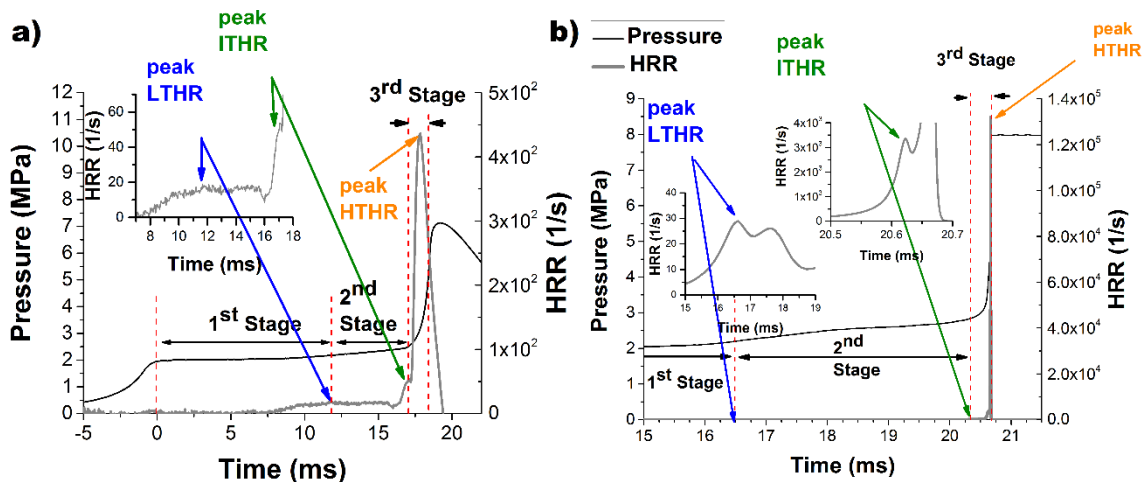
Figure 6.4: Three-stage ignition and normalised heat release rates (HRRs) for a) experimentally derived HRRs, and b) computed HRRs for 10% volume *n*-butanol/TRF blend at 702 K stoichiometric conditions and a pressure of 2 MPa. The magnified insets illustrate heat release profiles.

When considering multiple-stage ignition it is necessary to examine the fuel's low temperature oxidation processes and associated low temperature heat release (LTHR) and intermediate temperature heat release (ITHR). Goldsborough et al. [252] recently presented a methodology for assessing and quantifying the evolution and trends of preliminary exothermicity, in particular LTHR, from pressure-time histories across a range of thermodynamic conditions, as described in Chapter 3. The heat release analysis (HRA) could potentially create a better understanding of the links between LTHR, ITHR and auto-ignition behaviour of fuels and their blends, and offer additional targets for the development of detailed chemical kinetic models. Also, the knock propensity of a specific fuel can be changed by changing the LTHR/ITHR behaviour, as a result of fuel blending, or additives [336]. In this study, the impacts of *n*-butanol blending with TRF on the LTHR, ITHR and HTHR of the fuels and their blends are further explored.

6.2.1   Heat release analysis for experiments and simulations

Figure 6.5 shows the trends in normalised LTHR measurements as functions of the time-integrated, or accumulated heat release (aHR), with increasing temperatures for a) pure TRF, b) B10 and c) B85. An amount of LTHR is represented as the time-integrated heat release from the end of compression, through the peak heat release rate (HRR) at the first-stage ignition delay time, to the infection point in HRR just before the onset of the main ignition event. Figure 6.6 presents an example for a B10/TRF mixture at 727 K, illustrating this definition for both experimentally derived and computed normalised aHR. The gasoline TRF surrogate shows the anticipated LTHR at temperatures above 700 K. At the lowest compression temperature tested in this study, 679 K, the LTHR and HTHR merge together. However, within the NTC, an abrupt end to LTHR, that defines the first-stage ignition delays, is apparent as the temperature is raised from the transition point with a maximum peak HRR. This is reached at 783 K for the considered conditions. It is consisted with the minimum total ignition delay time detected within NTC region for this fuel, as shown in Chapter 5.
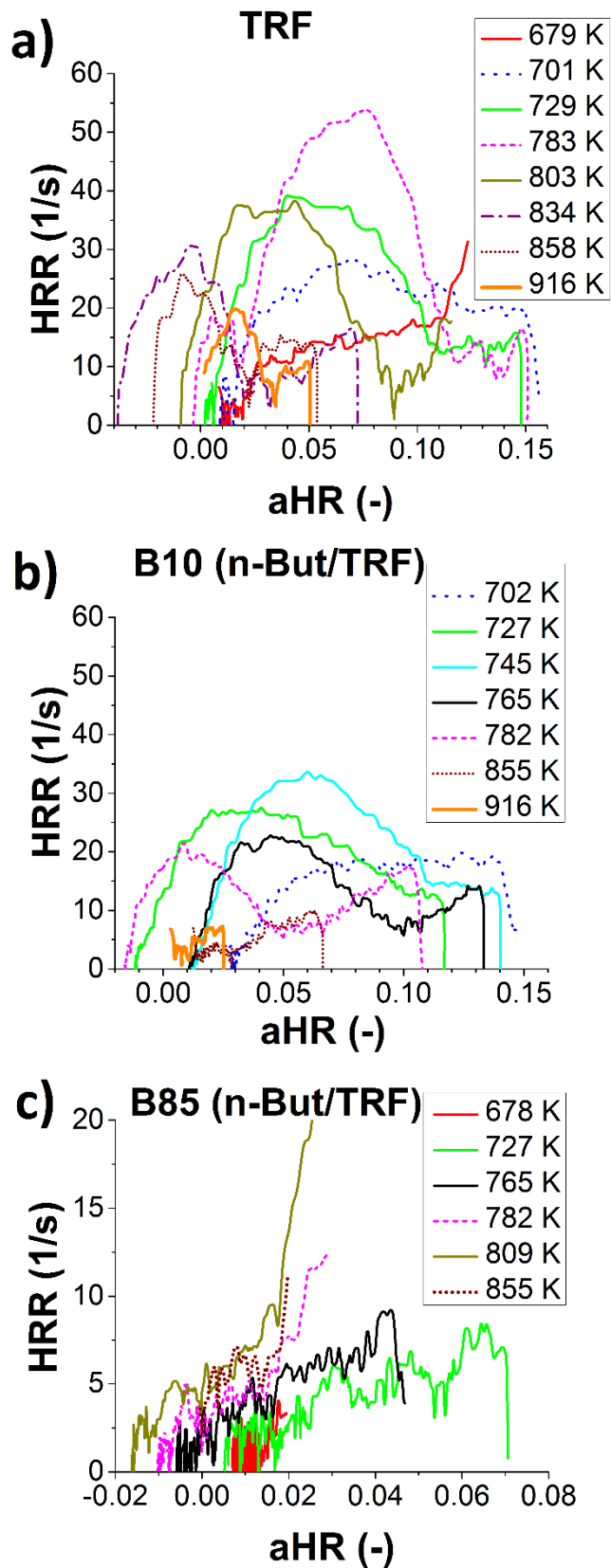
Figure 6.5: Comparisons of normalised experimental heat release rate (HRR) against accumulated heat release (aHR) at different temperatures for three fuel blends a) TRF, b) B10 and c) B85.
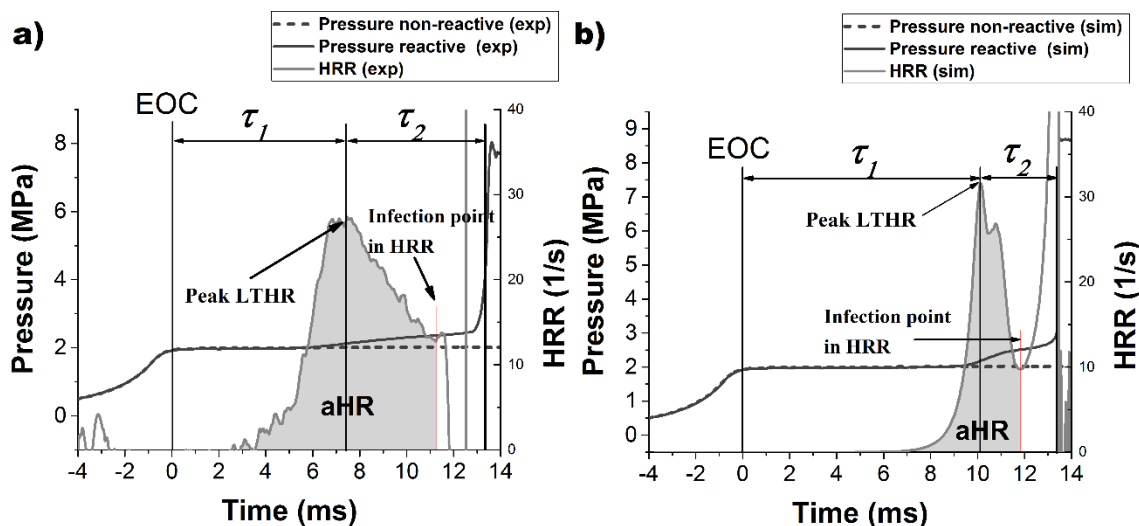
Figure 6.6: Representative a) experimental/experimentally derived, and b) modelled non-reactive and reactive pressure traces, and associated normalised heat release rates (HRRs). The accumulated heat release (aHR) is highlighted in gray. 10% vol *n*-butanol/TRF blend at 727 K stoichiometric conditions and a pressure of 2 MPa.

As temperature is further increased for the TRF mixture, the preliminary exothermicity is reduced. Similarly to the observations made in Chapter 5, where *n*-butanol addition acted as an octane enhancer in the low temperature region, an addition of *n*-butanol to the blends reduces LTHR as well as aHR (Figure 6.7). This manifests in longer total ignition delay times for B85 at these temperatures, compared to the lower *n*-butanol blends, illustrated in Figures 5.8 - 5.11. From Figure 6.7 it can be seen that the aHR is gradually decreasing with an increase in the *n*-butanol content within the TRF blends with few temperatures as exeptions for B10. For B10 a maximum peak HRR is reported at 745 K, with just over a half of that for TRF, observed at 783 K. A further increase in *n*-butanol content in blends further supresses the LTHR. At the highest blend ratio covered in this study, B85, LTHR becomes very weak and merges with HTHR, making it even more difficult to be identified, with HRR peaks becoming very similar in magnitude across the whole temperature range.
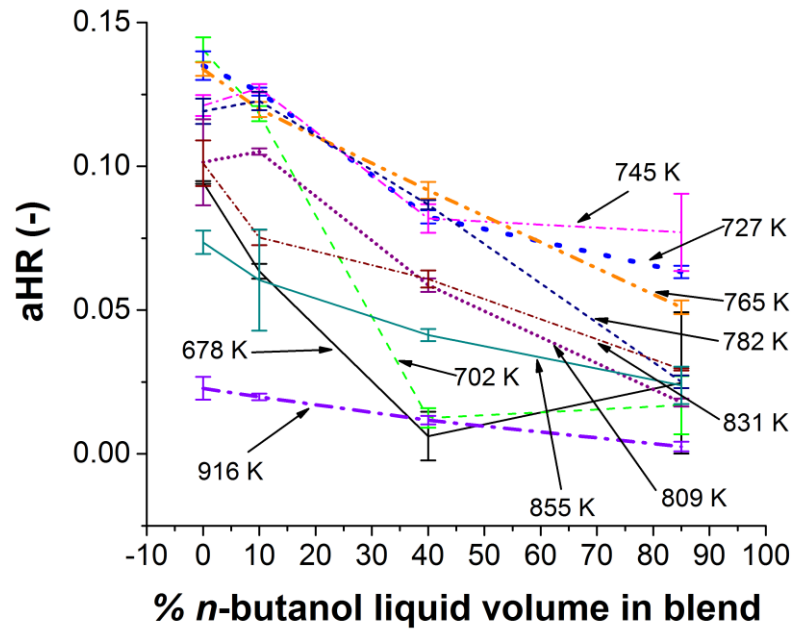
Figure 6.7: Effects of *n*-butanol addition to TRF at different blending ratios on accumulated heat release (aHR) derived from experimental data, reported as averages, at different temperatures, stoichiometric conditions, and a pressure of 2 MPa.

The experimental averages over 3-5 runs and simulated results of normalised heat release rates HRRs for TRF, B10, B40 and B85, at three temperatures are presented in Figure 6.8. The traces are aligned at the point of maximum pressure rise for the main ignition, in order to facilitate comparison between the different fuel blends on the same axes. The overall trends of LTHR, expressed by the detailed chemical kinetic mechanism, compares favourably with the experimental measurements, where an increase in *n*-butanol concentration is found to supress the reactivity of the system and decrease the magnitude of LTHR. However, the modelled preliminary heat release behaviour does not match experimental observations and there are some noticeable discrepancies in the magnitude of heat release behaviour between the simulation and experimentally derived results, especially at low and intermediate temperatures for pure TRF and low *n*-butanol/TRF blends. These are also the fuels and conditions at which the predicted first-stage and the second-stage ignition delay times are found to encounter the most differences compared to the experimental results. Not surprisingly, as their definitions are based on heat release profiles. The heat release profiles derived from experimental data are broader in time compared to simulated profiles, with the peak HRRs lower at low temperature of 701/702 K and higher at 761/765 K and 916 K compared to the experimental measurements. On the other hand, as can be seen from Figures 5.15 – 5.18, the model predictions of total

223

ignition delay times are in a relatively good agreement with experimental measurements at low temperatures for these fuels. This in turn suggests that the model has been designed and tuned to accurately represent the global targets, but not specifically the intricacy of thermochemistry. The underlying chemistry of heat release and reactions that control heat release are now investigated.
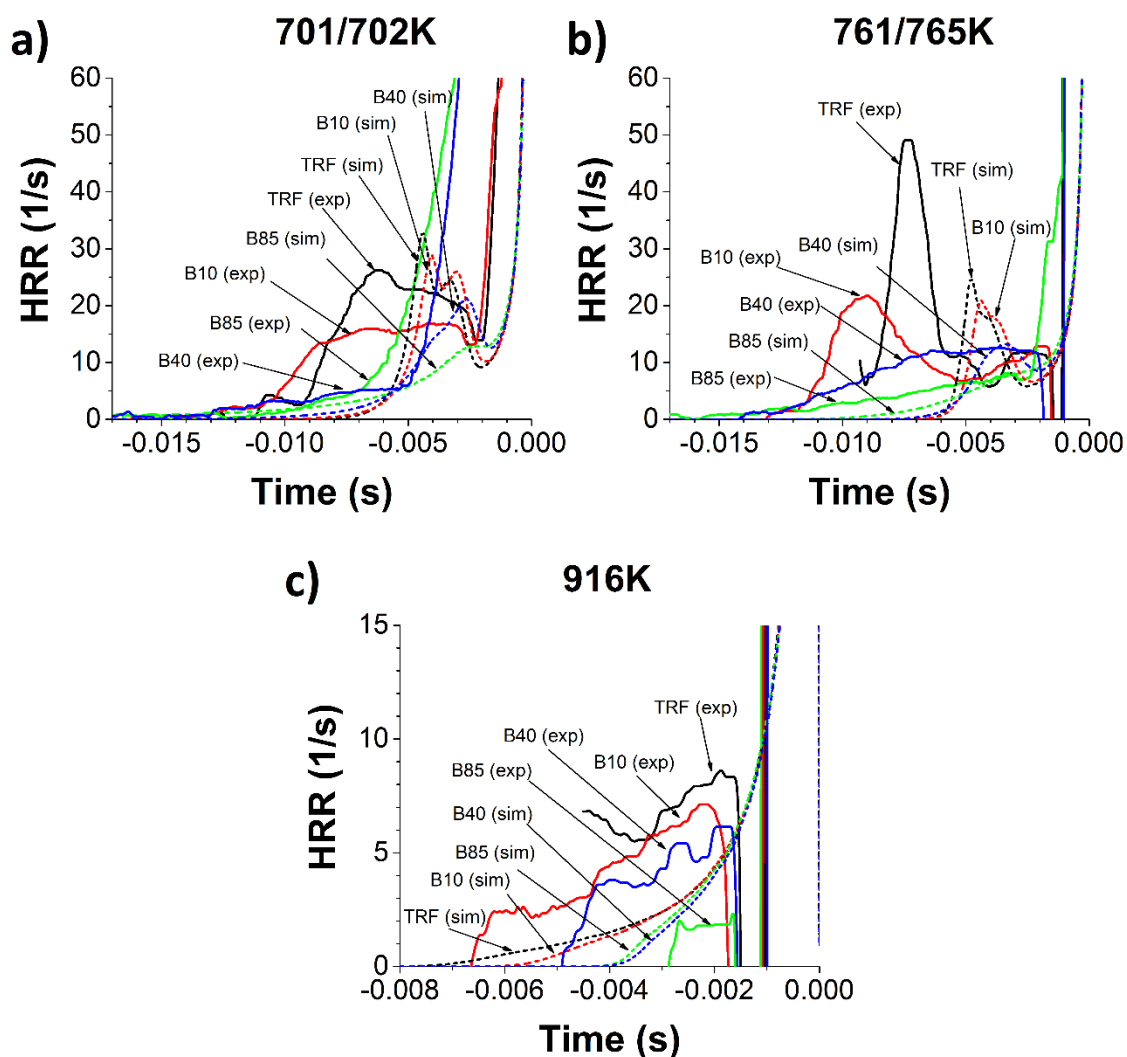
Figure 6.8: Comparisons of experimentally derived averages and modelled heat release rate (HRR) for TRF, B10, B40 and B85 at three temperatures a) 701 K (*n*-butanol/TRF blends) or 702 K (TRF), b) 761 K (TRF) or 765 K (*n*-butanol/TRF blends) and c) 916 K at stoichiometric conditions, and a pressure of 2 MPa.

Figure 6.9 presents comparisons between experimentally derived and simulated accumulated heat releases, aHRs, against *n*-butanol concentration within TRF at three different temperatures, stoichiometric conditions and a pressure of 2 MPa. The model is found to quite accurately predict aHR for blends at a high temperature of 916 K, which is consistent with its relatively good performance in predicting total ignition delay times at

this temperature as shown in Figures 5.15 -5.18. Here, LTHR get weaker and results in apparent HRR profiles becoming similar to single-stage ignition behaviour due to the mixture temperature entering the high temperature chemistry regime. However, the detailed chemical model seems to significantly under-estimate aHRs for all blends within the NTC at the intermediate temperature of 761/765 K, especially for pure TRF and B10 where a substantial LTHR is associated with these blends. At 701/702 K, modelled aHRs is lower than the derived from measurements for pure TRF and B10, but higher for all other blends.
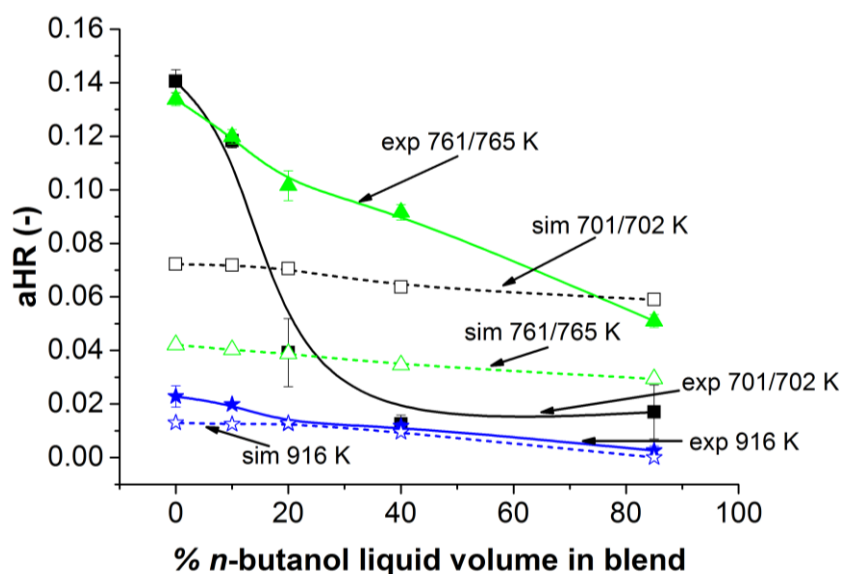
Figure 6.9: Comparisons between experimentally derived and modelled accumulated heat release (aHR) as functions of n-butanol concentration within the TRF blends at three temperatures of 701 K (n-butanol/TRF blends) or 702 K (TRF), 761 K (TRF) or 765 K (n-butanol/TRF blends) and 916 K at stoichiometric conditions, and a pressure of 2 MPa.

6.2.2 Chemical kinetic analysis of heat release rates

Brute-force sensitivity analyses for peak LTHR, peak ITHR, peak HTHR and low temperature aHRs were performed to better understand the kinetic effects of n-butanol addition on the LTHR and ITHR. Hence, the first stage ignition delays and peculiar NTC behaviour, as well as to identify reactions controlling the accumulated LTHR. Figure 6.10 shows the normalised sensitivity coefficients for the peak of LTHR for pure TRF, B10, B20, B40 and B85 n-butanol TRF mixtures at two temperatures of a) 678 K and b) 761 K (TRF) or 765 K (n-butanol/TRF blends) stoichiometric conditions and a pressure of 2 MPa. Figure 6.10, Figure 6.12 and Figure 6.13 sumarise the 10 most sensitive reactions at each of two/three temperatures and at each of the n-butanol/TRF blending ratios. Full

details of the methodology of the brute-force sensitivity analysis used here are in Section 3.3.7.

The brute-force sensitivity analysis computed the sensitivity of the output to each reaction in the mechanism by increasing each reaction rate A-factor by 10% from its nominal value, in turn, while all other parameters retained their base values. The local sensitivity coefficient was defined using Equation (3.9) as a difference in peak HRR values of LTHR, ITHR, HTHR or low temperature aHRs between the new and baseline case, normalised by the latter. Then each calculated sensitivity coefficient was normalised by the maximum sensitivity coefficient at each temperature. Hence the reaction with the largest effect on the predicted output target has a sensitivity index of 1. A positive sensitivity index correlates to lower peak HRR values or aHRs. It implies that increasing the A-factor by 10% of particular reaction rate decreases the reactivity of the system. At the same time, a negative sensitivity index results in higher peak HRR values or aHRs. Hence, it promotes the ignition process. Note, this differs from the interpretation of the sensitivity index for ignition delay times or excitation times, where a positive sensitivity index still indicates a decrease in the magnitude of the target output, but in this case it promotes the reactivity of the system, and vise versa.
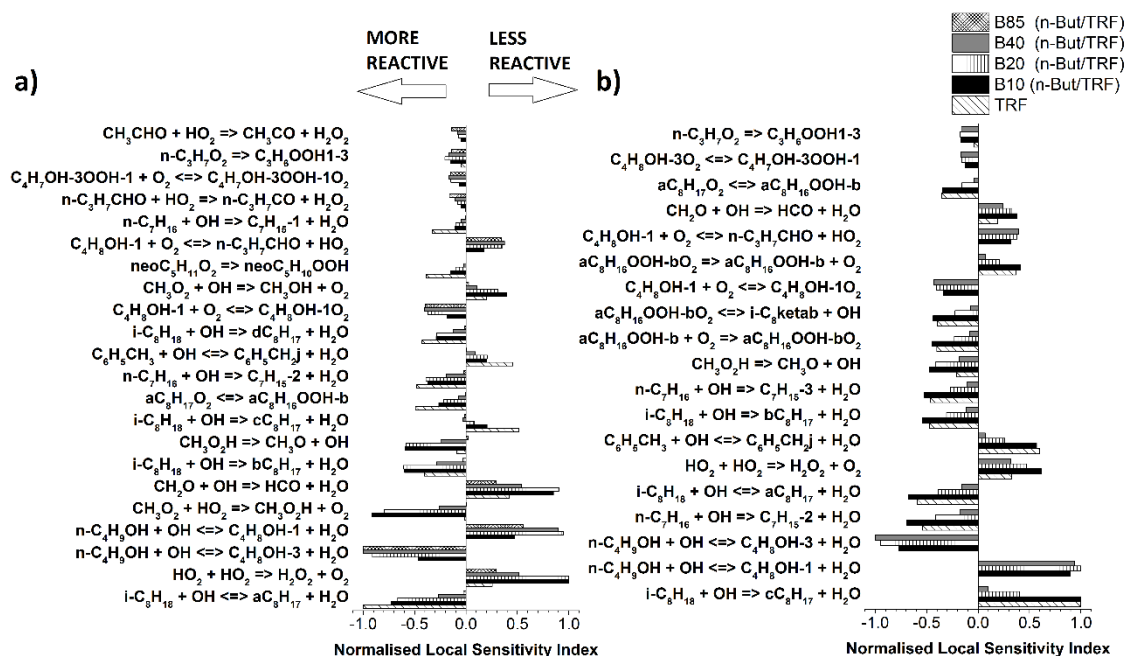
Figure 6.10: Normalised brute-force local sensitivity indices for LTHR peak at a) 678K and b) 765 K for pure TRF surrogate mixture, 10%, 20%, 40% and 85% vol *n*-butanol +TRF blend at stoichiometric conditions, and a pressure of 2 MPa.

226

As anticipated, H-atom abstraction reactions from parent fuel molecules by OH play a key role in defining the peak HRR value of LTHR, and subsequentely control the first-stage ignition delay. This is consistent with previous studies on first-stage ignition delays such as [87, 149, 252, 337]. For the pure TRF at 678 K H-atom abstraction by OH from *iso*-octane from the primary site, $iC_8H_{18}+OH\leftrightarrow aC_8H_{17}+H_2O$, has the largest negative sensitivity and increases the oxidation processes. As mentioned in the discussion of sensitivity analyses of total ignition delay times in Sections 5.6 and 5.7, the reactions of *iso*-octane with OH show the site specificity. The reactions causing formation of primary iso-octyl (aC_8H_{17}, dC_8H_{17}) and secondary *iso*-octyl ($bC8H17$) display negative sensitivity, resulting in an increased peak HRR value of LTHR, and hence promoting reactivity and decreasing first stage ignition delay times. On the other hand, the H-atom abstraction from iso-octane, leading to formation of tertiary *iso*-octyl (cC_8H_{17}) radicals, feature positive sensitivity, thus subsequently reducing the magnitude of the peak LTHR value and prolonging the first-stage ignition delay times. Furthermore, as discussed in Section 2.1.7 about low temperature hydrocarbon oxidation processes, all these *iso*-octyl radicals react with O_2 forming *iso*-octylperoxy, and subsequently $aC_8H_{17}O_2, bC_8H_{17}O_2$ and $dC_8H_{17}O_2$ undergo internal isomerisation. These hydroperoxy iso-octyl radicals hence promote chain branching, ultimately leading to the formation of keto-hydroperoxides which contribute to early heat release. In contrast, $cC_8H_{17}O_2$ is mainly consumed via conversion either to di-isobutylene and HO_2, or to a cyclic ether and an OH radical. Therefore, the entire reaction mechanism containing cC_8H_{17} is not chain branching, but acts as an OH radical scavenger inhibiting, or slowing down, the low temperature chemistry and delaying the final ignition [149]. Also, H abstraction from toluene ($C_6H_5CH_3+OH\leftrightarrow C_6H_5CH_2j+H_2O$) is featured in the sensitivity analysis, which inhibits a positive sensitivity reducing the reactivity of the system, and increasing the first-stage ignition delay time.

For the two highest *n*-butanol blends tested, B40 and B85, at this lowest temperature of 678 K, H abstraction via OH from the γ-carbon site ($nC_4H_9OH+OH\leftrightarrow C_4H_8OH\text{-}3+H_2O$) has the largest sensitivity, causing the peak HRR of LTHR to increase in magnitude. Here, it is competing with H abstraction via OH from the α-carbon site ($nC_4H_9OH+OH\leftrightarrow C_4H_8OH\text{-}1+H_2O$). The addition of *n*-butanol interferes with the low temperature oxidation processes, here leading to the reduction of the magnitude of LTHR, and ultimately retarding the time at which the end gas attains the auto-ignition temperatures at which H_2O_2 rapidly decomposes. The chain termination reaction

$HO_2+HO_2 \rightarrow H_2O_2+O_2$ has the largest positive sensitivity for B10 and B20 n-butanol/TRF blends, reducing the reactivity of the system and prolonging the first-stage as well as total ignition delay times. Other reactions that are featured in the sensitivity analysis at these two blending ratios are $CH_3O_2+HO_2 \rightarrow CH_3O_2H+O_2$ and $CH_2O+OH \rightarrow HCO+H_2O$.

At 765K, there was no apparent peak in LTHR for B85 n-butanol/TRF blend, which showed a more Arrhenius temperature dependence behaviour of total ignition delay times. At this temperature reactions inhibiting reactivity are found to play a key role, with H abstraction reactions from the tertiary site of iso-octane playing a key role for pure TRF and B10, and H abstraction via OH from the α-site of n-butanol for B20 and B40. This slows down, or inhibits, the low temperature chemistry and delays the final ignition. Similarly to total ignition delay time sensitivity, n-butanol chemistry plays an important role even for the low n-butanol/TRF blend (B10). It is also seen that as temperature increases to 765 K, the competition between the forward and reverse channels becomes increasingly important. This is consistent with observations of Liang and Law [338]. In particular, the reverse reaction of $aC_8H_{16}OOH\text{-}bO_2$, through $aC_8H_{16}OOH\text{-}bO_2 \rightarrow aC_8H_{16}OOH\text{-}b + O_2$, competing with $aC_8H_{16}OOH\text{-}bO_2 \leftrightarrow i\text{-}C_8ketab + OH$, an important chain branching reaction which can further decompose and form more OH radicals. This results in acceleration of the low temperature oxidation processes. Hence, the contributions and importance of $aC_8H_{16}OOH\text{-}bO_2$ increase with an increase in temperature, while its reverse channels consume this species, making it a rate-limiting species controlling first stage ignition.

Further analyses on the controlling chemistry for low temperature oxidation have been conducted by exploring dominant reactions influencing the low temperature accumulated heat release (aHR). Figure 6.11 summarises the top 8 most sensitive reactions for LTHR aHR for pure TRF, B10, B20, B40 and B85 n-butanol TRF mixtures at the two temperatures of a) 678 K and b) 761 K (TRF) or the 765 K (n-butanol/TRF blends) stoichiometric conditions, and a pressure of 2 MPa. Consistent with the sensitivity analysis for HRR peak of LTHR (Figure 6.10), H-atom abstraction reactions from parent fuel molecules by OH play a key role in driving LTHR, in particular $iC8H_{18}+OH \leftrightarrow aC_8H_{17}+H_2O$. This dominates sensitivities for pure TRF at 678 K. However, H abstraction via OH from the n-butanol α-carbon site is found to dominate sensitivity for B40 and B85 rather than H abstraction via OH from the γ-carbon site. Also $HO_2+HO_2 \rightarrow H_2O_2+O_2$, which controls the rate of formation of H_2O_2, is shown to be important in affecting first-stage ignition delay for B10 and B20 n-butanol/TRF blends, reducing the

reactivity of the system. Chapter 5 highlighted that temperature-dependent reaction rates for a site-specific H abstraction by both OH and HO_2 for each of the fuel blend components are required to enhance the performance of the detailed chemical kinetic model in predicting total ignition delay times. This is also required for improving model prediction of first-stage ignition processes and low temperature oxidation. Moreover, in the low temperature combustion region, thermochemistry has been shown to be as important as the reaction rates. A study by Hughes et al. [339] shows in particular the thermochemistry of peroxy alkylhydroperoxide radical (•OOQOOH) is especially important in propane oxidation. The authors highlighted that the heat of formation of n-$O_2C_3H_6OOH$ contributes up to 70% of the overall variance of the first-stage temperature, first-stage ignition and second-stage ignition outputs, with up to a 200 K decrease of the first-stage temperature when the heat of formation of peroxy alkylhydroperoxide radical, is increased by just +15 kJ mol^{-1}.

Figure 6.11: Normalised brute-force local sensitivity indices for accumulated LTHR at a) 678K and b) 765 K for pure TRF surrogate mixture, 10%, 20%, 40% and 85% vol *n*-butanol +TRF blend at stoichiometric conditions and a pressure of 2 MPa.

In the combined KAUST/LLNL scheme, the thermodynamic properties of all species for LLNL gasoline surrogate mechanism of Mehl et al. [143] and for the *n*-butanol scheme of Sarathy et al. [57] were evaluated using the THERM program, developed by Ritter and Bozzeli, implementing Benson's group additivity method. NASA polynomials are usually calculated by fitting to tables of thermochemical and thermodynamic properties, which are either experimental values or calculated using theoretical methods [117]. Such

evaluations may not always enclose the latest data. Also, for the larger species, the input parameters are often estimated, derived from a low number of measurements or from single theoretical studies [117]. This implies a higher degree of uncertainty and possible errors in the heats of formation for this species. Ghosh et al. [340] revealed that there is a significant variation between CBS-QB3, CBS-APNO, and G4MP2 methods (in the range of 0.5-6.2 kcal/mol) in the calculated heats of formation for the large oxygenated hydrocarbons. Currently, there is a lack of reliable standard reference heats of formation for (1) ketones and esters, (2) hydrocarbon species of liquid-fuel molecular weight, (3) oxygenated species typical of lignocellulosic biofuels and (4) oxygenated species typical of the alkylperoxy radical low temperature degenerated branching combustion mechanism[340]. Any imprecise, or inconsistently, derived heat of formation will have crucial effects on equilibrium constants [340]. It is speculated, that in the KAUST/LLNL scheme, the uncertainties of heats of formation of the larger species (such as alkylperoxy radical, alkylhydroperoxide radical, and peroxy alkylhydroperoxide radical) are relatively high. This is believed to result in observed discrepancies between the simulated and experimentally derived LTHR in Figure 6.8. More accurate experimental estimations and theoretical calculations of heats of formation, especially for the larger hydrocarbon species, can significantly improve the mechanism performances in predicting LTHR, first-, second-, and total-stage ignition delay times.

A distinctive auto-ignition phenomena with multiple-stage heat release behaviour, where more than two distinct stages exist, has been reported in [274, 333-335]. Generally, intermediate temperature heat release (ITHR) is merged with HTHR, rarely exhibiting a distinct stage of heat release. However, at low temperatures, heat release analysis for TRF and B10 has shown heat release to occur in three distinct stages (see Figure 6.8). Brute-force sensitivity analyses for the peak of ITHR for pure TRF, B10, B20, B40 and B85 n-butanol/TRF mixtures at temperatures of a) 678 K and b) 761 K (TRF) or 765 K (n-butanol/TRF blends) stoichiometric conditions at 2 MPa are presented in Figure 6.12. The reactions governing the maximum value of ITHR are similar across the two temperatures for the different n-butanol/TRF blends. However their ranking does vary. Conforming to the LTHR analysis, the B85 n-butanol/TRF mixture did not show a multi-stage heat release behaviour at 765 K but a more Arrhenius ignition behaviour. Contrary to expectations, at this intermediate temperature of 765K, the pure TRF simulations did not exhibit a distinct three-stage ignition behaviour, with a distinct peak in ITHR either.

Therefore, in this temperature sensitivity analysis, only for three low concentration *n*-butanol blends are presented, namely B10, B20 and B40 (Figure 6.12 (b)).

As pressure rises and inter-stage gas temperature increases with the LTHR during first-stage ignition, reactions involving HO_2 radicals become more reactive at the higher temperatures. These dominate reactivity, indicated by the sensitivity analysis in Figure 6.12. The major chain branching reaction $CH_3 + HO_2 \rightarrow CH_3O + OH$ is an important reaction for HO_2 consumtion and has displayed a highly negative sensitivity. This is especially so for pure TRF and low *n*-butanol/TRF blends, resulting in increased peak HRR value of ITHR, and hence promoting reactivity. In addition, the resulting methoxy radicals (CH_3O) are unstable and easily decompose to form H and CH_2O. Also, reaction $CH_2O + HO_2 \rightarrow HCO + H_2O_2$ is highlighted by the sensitivity analysis, and is an important contributor to the local maximum of ITHR. An alternative channel is the chain termination reaction $CH_3 + HO_2 \rightarrow CH_4 + O_2$, which inhibits reactivity leading to a decrease of the HRR peak value of ITHR.
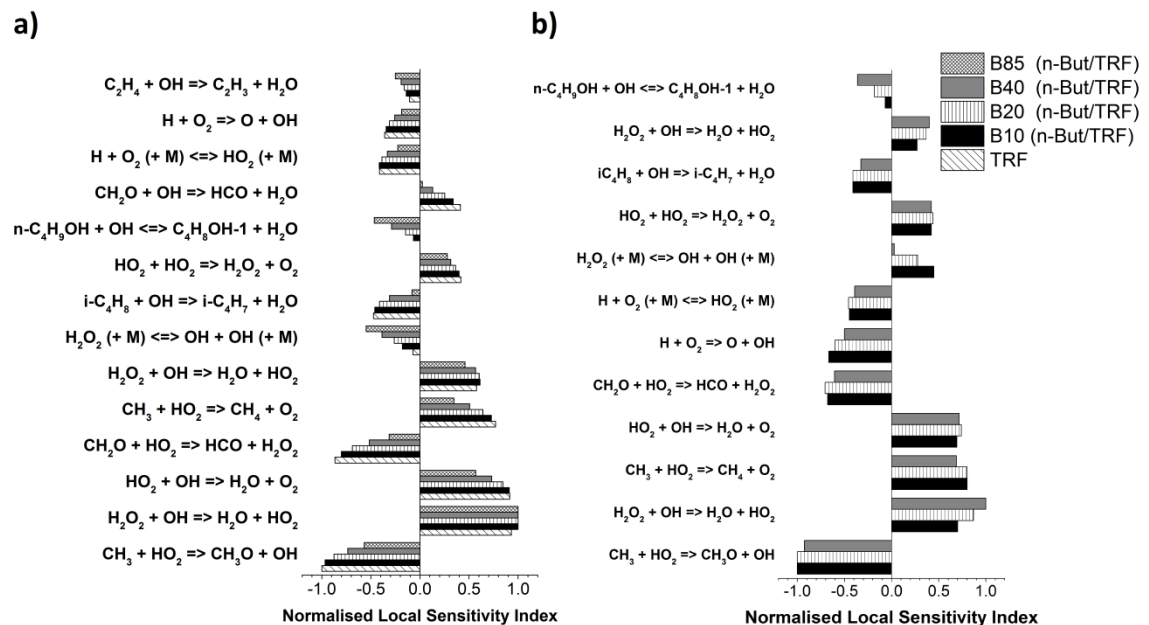
Figure 6.12: Normalised brute-force local sensitivity indices for ITHR peak at a) 678K and b) 765 K for pure TRF surrogate mixture, 10%, 20%, 40% and 85% vol *n*-butanol +TRF blend at stoichiometric conditions and 2 MPa.

Vuilleunier et al. [100] have shown formaldehyde (CH_2O) to be present in significant concentrations during the ITHR, and is quickly consumed, during HTHR, making CH_2O chemiluminescence a good marker for measurements in ITHR experiments. Griffiths et al. [335] were the first to highlight the importance of CH_2O as a molecular intermediate

to HO_2 formation and heat release rate in the second stage of hydrocarbon two-stage ignition. This can form through the methyl radical oxidation reaction pathway, $CH3 \rightarrow CH_3O_2 \rightarrow CH_3O_2H \rightarrow CH_3O \rightarrow CH_2O$. Onda et al. [341] showed in their study on CH_2O and OH laser-induced fluorescence and chemiluminescence measurements for methane weak flames in a micro flow reactor. Improving rate constants of reactions related to CH_2O chemistry, significantly improved their mechanism predictions for ignition delay times at the intermediate temperatures where RCM data are used.

Agbro et al. [42] showed that there is a sharp rise in production of CH_2O during the NTC stage. The substantial CH_2O concentration during the ITHR, can potentially explains the reasons behind the appearance of a distinct peak in ITHR. On the other hand, *n*-butanol addition to gasoline is found to promote CH_2O emissions, due to the partial oxidation of *n*-butanol by the hydroxyl in molecule [342]. An increased formaldehyde formation owing to *n*-butanol addition to TRF can therefore be a probable cause of why three-stage ignition behaviour is observed for a low concentration *n*-butanol/TRF blends at 765 K, and not for pure TRF. The detailed chemical model quite substantially under-predicted second-stage ignition delays for low *n*-butanol/TRF blends as can be seen from Figure 6.1. This could be a leading cause of the lower values in the predicted total ignition delay times, compared to the experimental measurements in the NTC region.

The major opposition to the reactivity increase of the system is the reaction $H_2O_2 + OH \leftrightarrow H_2O + HO_2$. It has duplicate entries and competes with $H_2O_2 (+M) \leftrightarrow OH + OH (+M)$ by consuming H_2O_2. H_2O_2 is accumulated through the reaction $HO_2 + HO_2 \rightarrow H_2O_2 + O_2$, as highlighted in sensitivity analyses in Figure 6.10 at low temperatures. This is a metastable molecule during the LTHR of first-stage ignition, until the temperature and pressure rises high enough to rapidly decompose to two OH radicals. This leads to degenerate branching and an explosive growth of OH radicals, ultimately resulting in the final-stage of heat release (HTHR), and hence auto-ignition. In addition, the termination reactions $HO_2 + HO_2 \rightarrow H_2O_2 + O_2$ and $HO_2 + OH \rightarrow H_2O + O_2$ counteract the explosive character, and reduce the peak HRR value of ITHR. On the other hand, $H + O_2 \rightarrow O + OH$ is also found to be important contributor to ITHR, which is also a dominant contributor to HTHR for all fuels at 916 K, as illustrated in Figure 6.13.

Figure 6.13 presents the normalised sensitivity coefficients for the peak of HTHR for pure TRF, pure *n*-butanol, B10, B20, B40 and B85 *n*-butanol TRF mixtures at three temperatures of a) 678 K b) 761 K (TRF) or 765 K (*n*-butanol/TRF blends), in addition

to c) 916 K stoichiometric conditions and 2 MPa. The HTHR stage is almost independent of fuel type and is primarily controlled by hydrogen related and CO-to-CO$_2$ chemistry. This is consistent with observations made in [274, 343]. Sjöberg et al. [343] suggested that when final CO oxidation takes place, the composition of the charge is very similar, regardless of the structure of the original fuel molecule. Hence, at the same temperature, the ranking of the reactions appears to be very similar. At 678 K and 765 K, $CO + OH \rightarrow CO_2 + H$ is a dominant reaction regardless of the fuel, and is a major heat generating reaction. Another significant heat producing reaction is the chain branching $H + O_2 \rightarrow O + OH$. This is known to be important at high temperatures. It dominates sensitivities at 916 K, resulting in the main stage ignition. Small opposition to the explosive character of this stage is provided by $CO_2 + H \rightarrow CO + OH$ at 678 K, while reaction $H + H_2O \rightarrow OH + H_2$ is featured at the higher temperatures.
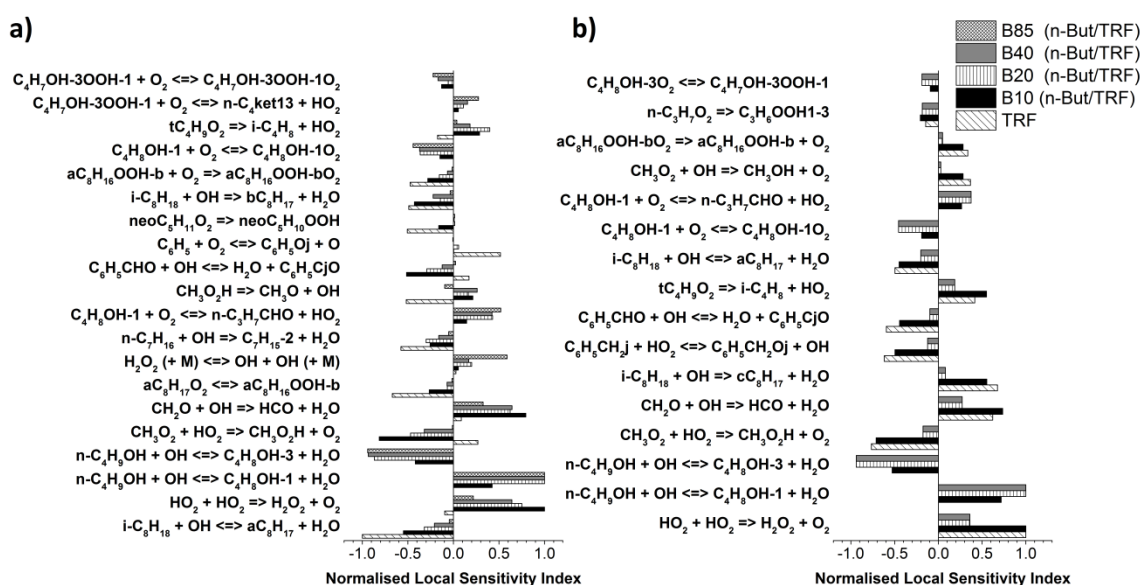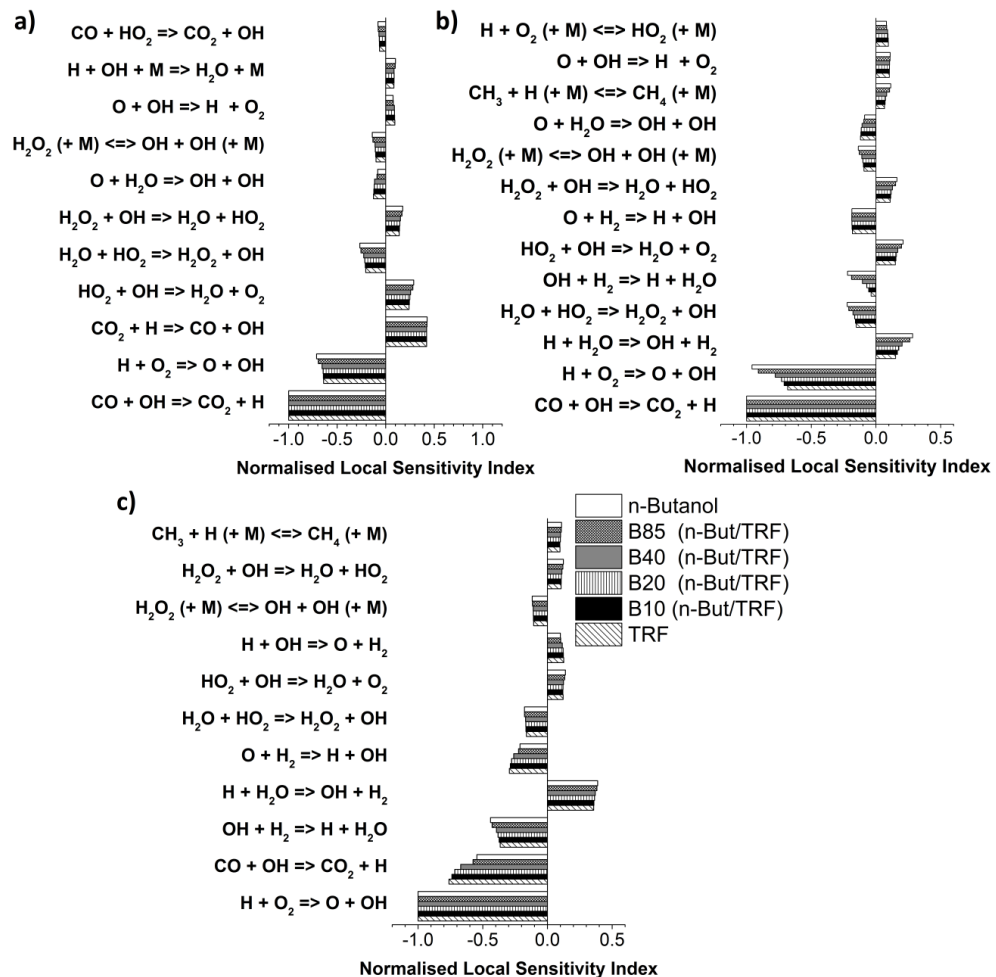

Figure 6.13: Normalised brute-force local sensitivity indices for HTHR at a) 678 K b) 765 K and c) 916 K or pure TRF surrogate mixture, 10%, 20%, 40% and 85% vol *n*-butanol +TRF blend and pure *n*-butanol at stoichiometric conditions at a pressure of 2 MPa.

6.3 Excitation times

6.3.1 Modelling excitation times for pure *n*-butanol, TRF and their blends

Severe engine knock is related to the strong and rapid heat release into the developing pressure wave arising from the rate of change of the heat release rate within the hot spot. The duration of heat release is determined by the excitation time, τ_e. The excitation time is defined as the time from the point where the heat release rate is 5% of the maximum heat release rate to the instant where that maximum value is attained. This combustion characteristic plays a key role in chemical-acoustic interaction and detonation development. Figure 6.14 presents a summary of excitation times, τ_e, modelled using variable volume simulations for TRF, *n*-butanol fuel and their blends under stoichiometric conditions at pressure of 2 MPa and 678-916 K. The results suggest that in the high to intermediate temperature range, the τ_e values fall onto a single one curve for the various fuels. There is practically no apparent effect of *n*-butanol addition to TRF blends nor obvious influence from NTC chemistry. The excitation times show an almost linear correlation with temperature. There is however an apparent increase in the τ_e value at the two lowest temperatures, with lower *n*-butanol/TRF of B10 and B20 blends behaving more like the pure TRF mixture at 678 and 702 K, and B40 at 702 K. The higher blend of B85 behaves more like pure *n*-butanol at 678 and 702 K. This potentially implies that the fuel composition only becomes important at low temperatures and τ_e is not fuel-specific at higher temperatures. Dealing with the order of microseconds, makes it very difficult to measure τ_e accurately in the current experimental configuration. Predictions of τ_e are entirely based on the performance of the detailed chemical kinetic scheme. To test whether the behaviour and trends in τ_e are consistent over the different detailed chemical mechanisms, additionally, variable volume simulations of τ_e have been performed using the POLIMI detailed chemical scheme.

Figure 6.15 compares predictions of τ_e using the KAUST/LLNL and the POLIMI detailed chemical mechanisms for the lowest and the highest *n*-butanol/TRF blend, B10 and B85, respectively. Similarly to the earlier observations, in the high to intermediate temperature region there is no apparent fuel specificity of τ_e predictions using the POLIMI scheme with all τ_e falling onto the same curve. Moreover, both mechanisms predicted similar τ_e at these temperatures. However, at the lower temperatures there are some differences in predictions of τ_e between two schemes with the jump in τ_e values at 745 K for the POLIMI mechanism. Interestingly, the crossover of τ_e trends between two blends using the

234

POLIMI scheme is observed at 678 K where τ_e is longer for B10 fuel compared to the B85 blend, whereas τ_e predictions using the KAUST/LLNL scheme are consistently longer for B85 at this temperature. To examine the role of fuel specificity and the key reactions that influence τ_e, local sensitivity analysis has been carried out.
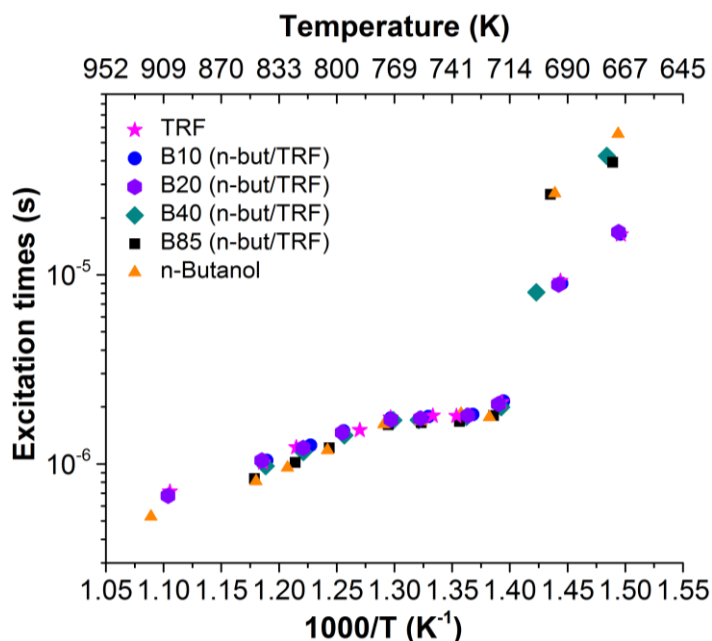
Figure 6.14: Comparisons of excitation times of various fuels and fuel blends under stoichiometric conditions and 2 MPa. Simulations performed using the KAUST/LLNL scheme.
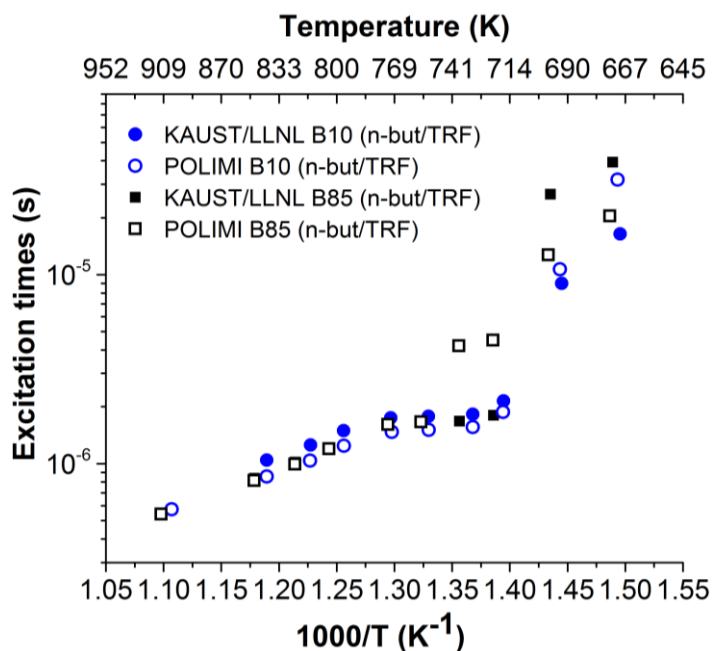
Figure 6.15: Comparisons of the KAUST/LLNL and the POLIMI detail chemical mechanism predictions of excitation times for B10 and B85 at stoichiometric conditions and 2 MPa.

6.3.2 Chemical kinetic analysis of excitation times

Because all fuels decompose to basically the same set of small C_1-C_3 hydrocarbons, high temperature auto-ignition processes are rather insensitive to fuel structure. These smaller hydrocarbons oxidise to yield CO and CO_2. Hence, the high temperature combustion chemistry is mostly dominated by small molecule, hydrogen related and CO-to-CO_2 chemistry, and follows similar high temperature chemistry pathways. As result, the lack of fuel specificity in the τ_e chemistry may be expected in this high temperature region. On the other hand, the inhibition of auto-ignition at low temperatures depends on the molecular structure of the fuel. This is derived from fuel's specific reaction pathways that supress low-temperature exothermic reactions [101]. It might therefore be expected that τ_e chemistry at low temperatures is fuel specific.

Despite apparent differences in excitation times between different fuels and their blends, as well as between mechanisms at low temperatures, as seen from Figure 6.14 and Figure 6.15, local brute-force sensitivity analyses for τ_e have not shown the anticipated fuel-specific reactions. Figure 6.16 shows the normalised sensitivity coefficients for excitation times for a) pure TRF surrogate mixture; b) 10% vol n-butanol +TRF blend; c) 20% vol n-butanol +TRF blend; d) 40% vol n-butanol +TRF blend; e) 85% vol n-butanol +TRF blend and f) pure n-butanol fuel, at three temperatures, under stoichiometric conditions at 2 MPa. Here, the 6 most influential reaction sensitivities at each of the three temperatures are reported. The smaller C_1-C_4 molecule chemistry dominates sensitivities and primarily controls τ_e. A positive sensitivity index correlates a decrease of τ_e magnitude, while a negative sensitivity index results in increased values of τ_e. Interestingly, two reactions featured in Figure 6.13 for peak values of HTHRs which contribute to high temperate heat release generation, in particular, $CO + OH \rightarrow CO_2 + H$ and $H + O_2 \rightarrow O + OH$, are found to dominate sensitivity analysis for τ_e, leading to a decrease in τ_e magnitude. These are also the same two reactions which dominate sensitivy analysis of τ_e for methane/air at high pressure of 10 MPa, as seen from Figure 4.15 (b). These reactions compete with $CO_2 + H \rightarrow CO + OH$ for pure TRF and low n-butanol/TRF blends, whereas a major opposition is shown by $HO_2 + OH \rightarrow H_2O + O_2$ and $H_2O_2 + OH \leftrightarrow H_2O + HO_2$ reactions for the highest B85 n-butanol/TRF blend and for pure n-butanol. These reactions slow down the reactivity of the system and result in longer τ_e. Also contributions of inhibiting reactions are seen to increase with an increase in n-butanol concentration, within n-butanol/TRF blends. This can potentially explain the apparent jump in τ_e values at lower temperatures, observed in Figure 6.14.
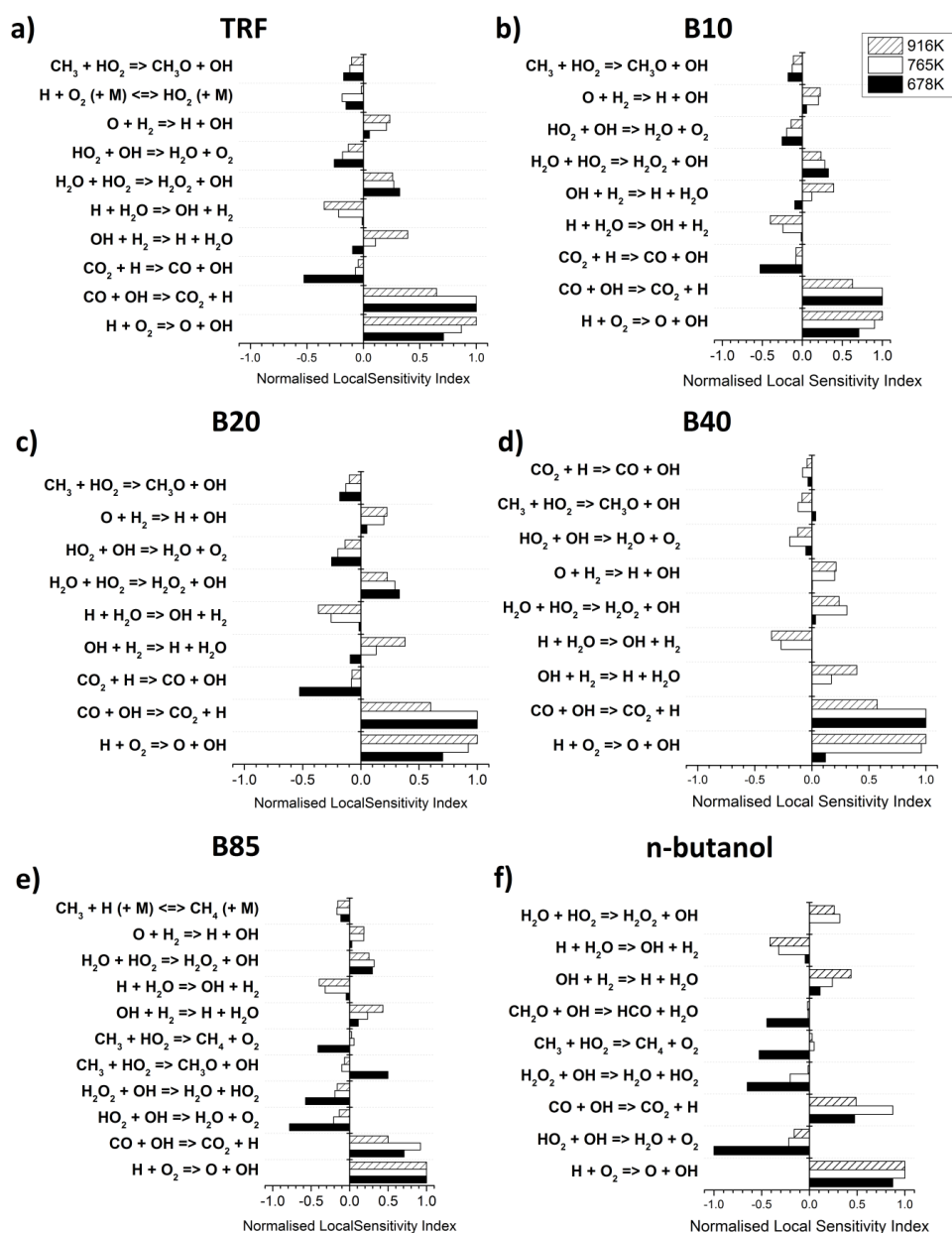
Figure 6.16: Normalised brute-force local sensitivity indices for excitation time for a) pure TRF surrogate mixture; b) 10% vol n-butanol +TRF blend; c) 20% vol n-butanol +TRF blend; d) 40% vol n-butanol +TRF blend; e) 85% vol n-butanol +TRF blends and f) pure n-butanol fuel at 3 temperatures, $\varphi=1$ and P=2 MPa.

In addition to the apparent dominance of these reactions in sensitivity analyses for excitation times of all the fuels studied here, specifically methane/air, TRF, *n*-butanol and *n*-butanol/TRF blends, the reaction $HO_2 + OH \rightarrow H_2O + O_2$ is also featured in all fuel sensitivity analyses that are presented in Figure 4.15 (b) and Figure 6.16. Also $H + O_2$ $(+M) \leftrightarrow HO_2 (+M)$ is highlighted in results for both sensitivity analyses for methane/air and pure TRF fuels. This reaction is known to enhance the rate of production of HO_2 radicals in high pressure systems. Despite apparent similarities in the dominant reactions

in sensitivity analyses between different fuels, generally the ranking importance of these reactions varies between fuels.
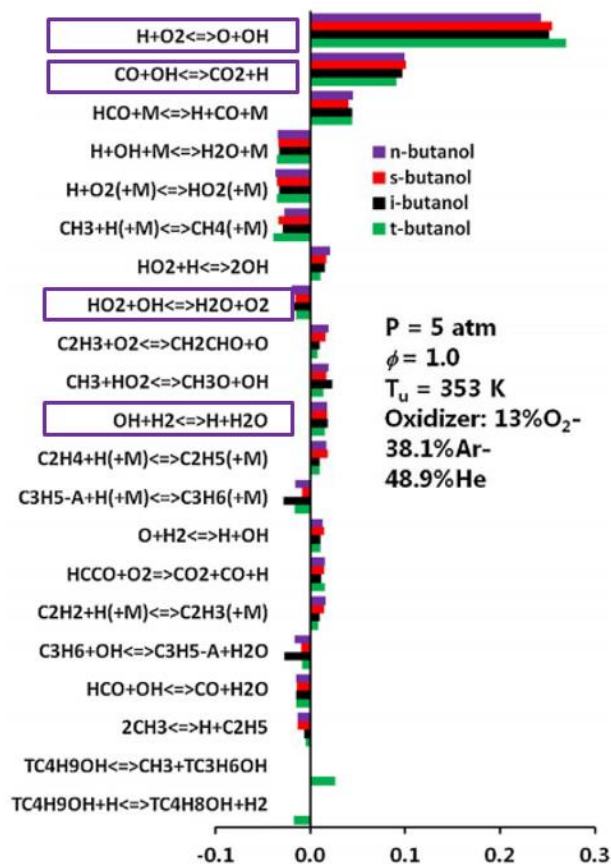
Figure 6.17: Normalised brute-force local sensitivity indices for flame speed of the stoichiometric 1-D planar flame for the butanol isomers at 0.5 MPa using Sarathy et al. [88] mechanism from an earlier study of laminar flame speeds for butanol isomers [344].

It is noteworthy, that the two dominant reactions for τ_e, namely $CO + OH \rightarrow CO_2 + H$ and $H + O_2 \rightarrow O + OH$, are found to dominate the sensitivity analysis for flame speeds [344]. An example of the normalised rate constant sensitivity indices for flame speeds of the stoichiometric 1-D planar flame for the butanol isomers at 0.5 MPa, using the Sarathy et al. [88] mechanism, are illustrated in Figure 6.17. This is adopted from the earlier study of laminar flame speeds for butanol isomers by Wu and Law [344]. The Sarathy et al. [88] mechanism is an earlier version of the n-butanol scheme of Sarathy et al. [57]. The study of Wu and Law [344] measured laminar flame speeds and Markstein lengths for four butanol isomers at pressures of 0.1 to 0.5 MPa. They also conducted computational and flame chemistry analysis. Similarly to τ_e, flame speeds are the most sensitive parameters to the kinetics of hydrogen, carbon monoxide, and the small C_1-C_3 hydrocarbons. Also consistent with τ_e, the results for the flame speed sensitivity analysis lack fuel specificity,

signifying that flame speed kinetics of butanol isomers are not significantly different from that of the other heavy hydrocarbons [344]. The other two reactions highlighted by both sensitivity analyses for τ_e in the present study, and for flame speeds that of Wu and Law [344] for pure n-butanol are $HO_2 + OH \rightarrow H_2O + O_2$ and $OH + H_2 \rightarrow H + H_2O$. This suggests that there is a certain level of crossover of sensitive reactions for τ_e with flame speed sensitivity reactions. Since it is extremely difficult to measure excitation times precisely in current experiments, it is difficult to constrain a mechanism against it. On the other hand, an accurate detailed model predictions of flame speeds as well as HTHR would create accurate predictions of τ_e, since the same chemistry is influencing these properties.

6.4   Characterisation of engine knock and detonation

As discussed earlier in this Chapter, there are different low, intermediate, and high temperature chemical kinetics involved in the auto-ignition processes for large hydrocarbon fuels. In Sections 2.1.12 and 2.1.13, different auto-ignition modes, including detonation, flame propagation and thermal explosion, can be generated by a hot spot. These auto-ignition modes can be located relative to a detonation peninsula, which indicates the bounds of the detonation region and is illustrated in Figure 6.18. Here the ratio of acoustic to auto-ignitive velocity, ξ, is plotted against the reactivity parameter, ε, which indicates the resistance time within the hot spot of the pressure pulse that is triggered by the rate of change of heat release, to the duration of the heat release, τ_e [90, 96, 97, 302]. The details on detonation theory and its governing equations were given in Sections 2.1.13 and 3.4.2.

For large hydrocarbons which exhibit NTC behaviour, auto- ignition can appear at lower temperatures compared to that at the higher temperatures within the NTC region. The NTC region itself, which is common under realistic engine conditions, presents difficulties in interpretation. In particular, the calculation of global activation energies, required in auto-ignition analyses and dependence on an Arrhenius correlation. In this study, activation energies for auto-ignition were derived by global fitting data to the relationship:

$$\frac{E}{R} = \frac{\ln(\tau_a) - \ln(\tau_b)}{\left(\frac{1}{T_a} - \frac{1}{T_b}\right)} \tag{6.1}$$

Here, E is an effective activation energy, with conditions a and b representing the values at the highest and the lowest temperatures tested, and T is the temperature at the end of compression. This calculation imposes uncertainties in deriving global activation energies due to its limitation of the simple Arrhenius-law. On the other hand, a local fit of the activation energies becomes possible. In fact, when the local fit of activation energies for pure TRF and low n-butanol/TRF blends was used, the magnitude of ξ decreased in the NTC region, sufficient to move few data points in Figure 6.18 inside the bounds of the detonation peninsula (see Appendix A).
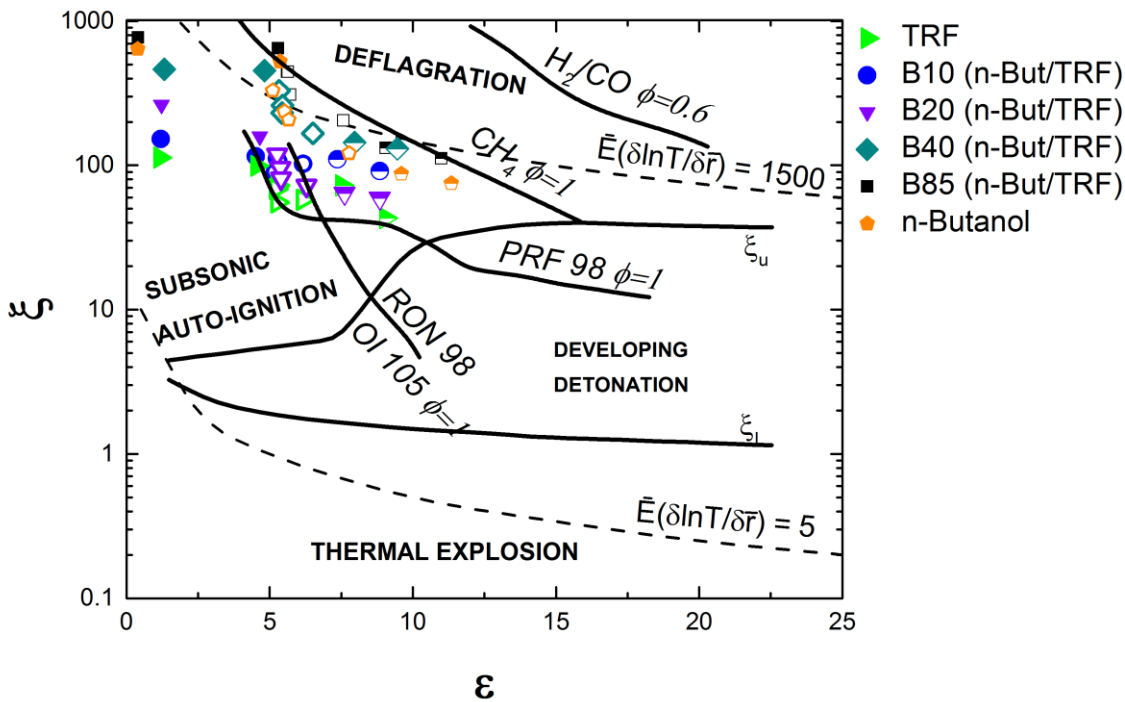
Figure 6.18: Detonation peninsula diagram of Bradley et al. [91] for 10%, 20%, 40% and 85% vol n-butanol blends with TRF, as well as neat TRF and n-butanol fuels, at stoichiometric conditions and a pressure of 2 MPa (from this work). For comparisons, isentropic compression curves for different fuels showing propensity for detonation adopted from an earlier study of auto-ignition in engines [94] are also presented. Filled symbols are in a temperature range 678-727 K. Opened symbols are in a temperature range 727-831 K. Half open symbols are in the temperature range 831-916 K.

The NTC region is a regime in which $\partial\tau/\partial T$ can become negative or zero, and as ignition delay temperature dependence becomes less Arrhenius, the magnitude of ξ correspondingly decreases and becomes negative. This subsequently implies positive critical temperature gradients, and consequently auto-ignition appears first at cold spots,

rather than hot spots, in the NTC regime, which thereafter can generate developing detonations. This has also been suggested by Bradley [45], Bradley and Kalghatgi [97] for low octane number fuels, Grogan et al. [345] for mild ignition using Damköhler number theory, Dai et al. [303] for n-heptane mixtures. In their work, Dai et al. [303] have shown that NTC behaviour does not significantly change the auto-ignition modes as long as ξ and ε are fixed. Consequently this implies that, similarly to hot spots, cold spots can also result in knock in engines with fuels that exhibit NTC behaviour and the temperature is within the NTC regime.

On the assumption that these generalised auto-ignition regimes are relevant to different fuels, the assessment of knocking propensity based on τ_i and τ_e of n-butanol/TRF blends in comparison with that of other fuels was performed and is expressed in terms of the detonation peninsula framework in Figure 6.18. At the temperature and pressure conditions tested in this study, all fuels and their blends lay outside the detonation development region avoiding the peninsula. Pure TRF and low n-butanol/TRF blends, in particular B10 and B20, are apparently close to the isentropic compression curves for the PRF 98, $\varphi=1$, and surrogate gasoline, with OI=105, $\varphi=1$, RON=98 from [94]. The PRF 98, $\varphi=1$, entered the detonation peninsula at a pressure of 6.5 MPa and 925 K, whereas the surrogate OI=105, $\varphi=1$, RON=98 was found to enter the detonation peninsula only at a pressure exceeding 7.5 MPa and a temperature of 950 K [94] which are considerably higher compared to the thermodynamic conditions in the current study with the pressure of 2 MPa and temperature range between 678 – 916 K. Therefore, it is possible that in case of severe operating conditions and high ε, compression curves for pure TRF and low n-butanol/TRF blends can enter the peninsula resulting in developing detonation, hence severe knock.

Interestingly, the pure n-butanol fuel and higher n-butanol/TRF blends, namely B40 and B85, are spread closer to the compression curve of methane and within the potential deflagration/subsonic auto-ignition transition region, which has been identified in Chapter 4 (Sections 4.7 and 4.8). It is marked by the region close to $\bar{E}(\delta lnT/\delta\bar{r}) = 1500$ represented by the dotted curves in Figure 6.18 and the hatched transition regime in Figure 6.19, in which auto-ignitive and deflagrative regimes can coexist. In Chapter 4, there were no clear boundaries between these two regimes partially due to uncertainties about the details of hot/cold spot structures. In Chapter 4 Section 4.8, low values of $\bar{E}(\delta lnT/\delta\bar{r})$ are commonly linked to stable detonations, whereas higher values can be related to an increased likelihood of deflagrative flame propagation. It can be seen that

deflagration is favoured by higher *n*-butanol concentrations within TRF blends in Figure 6.19. This complements the observations made in Section 5.2 about pressure-time history profiles, where longer ignition delay times with a gradual pressure increase were suggested as representative of conventional knock. On the other hand, pressure traces with steep pressure rise and high frequency oscillations near the maximum pressure, were indicative of strong ignition, detonations, and super-knock. The latter were found to occur at higher temperature conditions and for lower *n*-butanol/TRF blends in Chapter 5. Therefore, an addition of *n*-butanol to TRF, increases ξ values and potentially reduces the fuel propensity to detonation. Moreover, it can be seen that these high *n*-butanol/TRF concentrations mixtures seem to avoid crossing into the region of developing detonation in Figure 6.18. However, one must be careful in interpreting of $\bar{E}(\delta lnT/\delta \bar{r})$ values, since excessively high values of this parameter might impair experimental measurements of τ_i in an RCM.
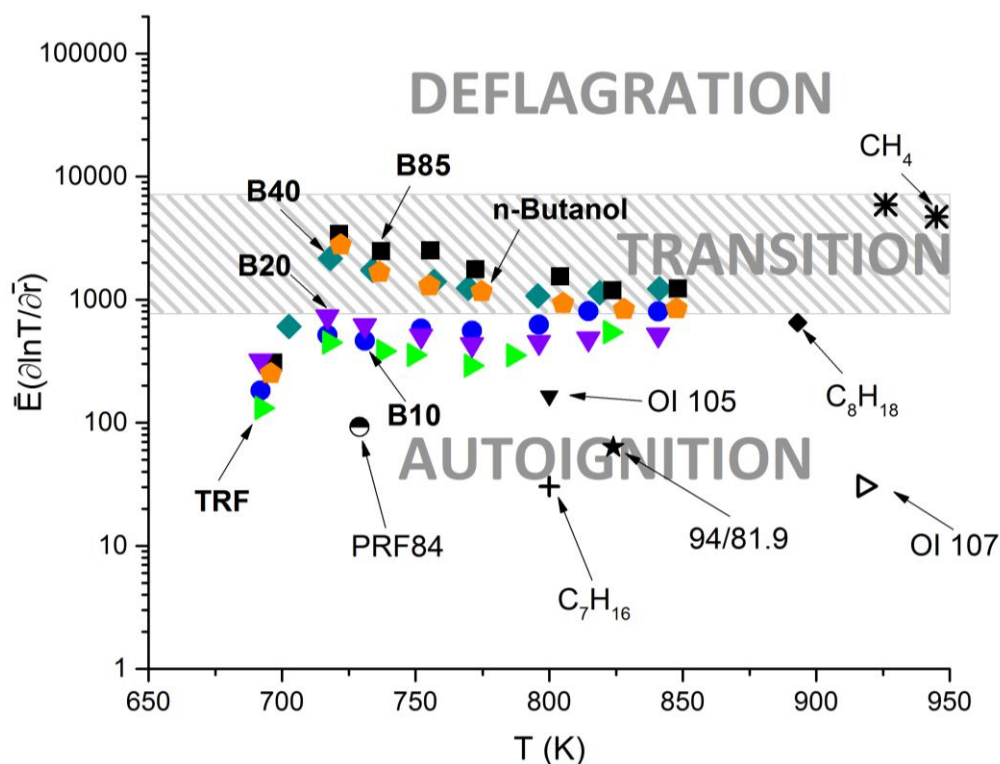
Figure 6.19: (a) $\bar{E}(\delta lnT/\delta \bar{r})$ as a function of *T* and *P* for stoichiometric TRF, *n*-butanol, B10, B20, B40 and B85 *n*-butanol/TRF blends compared to engine operational data of different fuels. Details in Table 4.3. (b) Three regimes of reaction propagation.

Overall, the results presented in Figure 6.18 and Figure 6.19 suggest that the RCM is operating in the regime associated with strong or uniform ignition, where uncontrolled auto-ignition is not likely occur. An occurrence of non-uniform auto-ignition is usually

more commonly observed in the NTC region [276]. In the present work, the fuels with apparent NTC auto-ignition behaviour, namely pure TRF and lower n-butanol/TRF blends, were found to lie below the suggested mixed deflagration/auto-ignition transition regime. The high n-butanol/TRF concentrations mixtures and pure n-butanol $\bar{E}(\delta lnT / \delta\bar{r})$ values stretch across the hatched transition regime in Figure 6.19, in which auto-ignitive and deflagrative regimes can coexist. Therefore, a particular caution was taken in conducting these experiments in order to eliminate possible causes of non-uniform auto-ignition. This included the precautions taken to ensure the initial charge temperature uniformity, regular cleaning and checks of the combustion chamber, thorough purging of the combustion chamber to remove inter-test contamination, as well as repetition of experiments to ensure reproducibility and consistency between experimental measurements. Therefore, the reported experimental ignition delay times can be used as a reliable validation targets for detailed chemical kinetic models when the experimental uncertainties and physics inside the combustion chamber are addressed.

Figure 6.18 demonstrates that the low temperature chemistry in the cases of cold spots and NTC region for pure TRF and low n-butanol/TRF blends has little effect on the detonation development in the detonation peninsula framework based on the ξ-ε diagram, only slightly decreasing ξ values in the present set up. This could potentially be attributed to the fact that the reaction front propagation is primarily driven by the heat release during the HTHR, while LTHR has a secondary effect on the chemical-acoustic interactions. On the contrary, the LTHR behaviour has a significant effect on the knocking intensity which is briefly discussed in the next section. Moreover, neither ξ nor ε could be known with great accuracy.

In order to determine ξ in Equation (2.22), the general value of temperature gradient $\partial T/\partial r$ is required, where temperature elevations at hot spot centres decline linearly with their radius, up to r_0 [45]. Values of this gradient are rarely known, however a selection of this datum value in the current estimations facilitates the comparison of auto-ignition properties of various fuels to be made. Following [90], a temperature gradient value of $(\partial T/\partial r)= -2$ K/mm was chosen based on engine and other measurements. On the other hand ξ is extremely sensitive to the temperature variation within the hot/cold spot interior which can considerably effect the calculation of the detonation peninsula and shift the detonation development regime [346].

Simultaneously, providing various physical-chemical properties of fuels, different hot spot magnitudes ($r_0 = 1 - 12$ mm) can be adopted in Equation (2.23), where small sizes of hot spots would struggle to sustain the auto-ignition, while the large ones would result in laminar flame propagation governed by molecular transport [94]. In the present study, a hot spot radius is assumed to be 5 mm, which corresponds to the turbulent flow length scales and heterogeneities in SI engines and is consistent with the assumptions made in Chapter 4 for methane calculations. In general, within the detonation peninsula framework, omitting a reactivity gradient and mass divergence prevents a developing detonation from propagating outside the hot spot interior. However, a developing detonation can occur outside the hot spot for some reactive mixtures or continue to propagate into the main mixture outside the hot spot with damaging consequences [45, 346]. On the other hand, even more damaging would be strongly developing detonations within numerous hot spots [45, 90]. This has been experimentally demonstrated by Pan and Sheppard [347]. The authors have shown that as auto-ignition fronts travelled towards each other from adjacent hot spots, pressure fronts ahead of them caused temperature and pressure rise of the reactants, which in turn resulted in further auto-ignition events, violent reaction and shock waves. The subsequent coupling of reaction fronts and pressure shock waves would lead to a self-sustaining detonation at low ξ and high ε [45].

Moreover, the detonation development regime is bounded by upper and lower limits, ξ_u and ξ_l, which calculations were based on $0.5\,H_2 - 0.5\,CO$ fuel mixed with air at various equivalence ratios [91]. This detonation development regime can be considerably quantitatively different for larger hydrocarbon fuels as has been suggested by Pan et al. [346], due to different physical-chemical properties of fuels that control auto-ignition delay times, diffusion and transport processes. Also, the detonation development is strongly controlled by pressure wave and heat release interplay. However, the accuracy of excitation times is presently entirely based on the performance of the detailed chemical kinetics in use due to the lack of experimental validations. Moreover, in Chapter 4 an alternative definition for the excitation time has been suggested which can result in even larger differences of the detonation peninsula, especially differences among the upper limits for detonation development. These uncertainties and limitations of the theory may cause substantial discrepancies of the detonation peninsula for various fuels and under various combustion chamber configurations. Further research is required to determine the important factors of key parameters for various fuels and their characteristics in realistic reactive flow configurations to achieve quantitative prediction of engine knock. This

would help to evaluate the scope of the detonation peninsula for various fuels and advance the understanding into knocking inhibition through fuel design and optimisation.

6.5   Combustion processes, strong and mild ignition

The maximum pressure and knocking severity are significantly affected by the combustion mode during the localised auto-ignition phenomenon, where it can strengthen the pressure wave similar to conventional knock in mild ignition, whereas developing detonation can result in extremely high amplitude of shock waves similar to super-knock in strong ignition. In SI engines, the end gas can be linked to isentropic compression processes until the knock onset by assuming that any heat losses are neglected. Wang and Liu [39] suggested that processes during the event of super-knock can successfully be linked to developing detonation processes in the RCM. The authors suggested that in the event of detonation in the RCM, auto-ignition temperatures and pressures, as well as amplitudes of pressure oscillations are consistently higher compared to that of supper knock in engines. They emphasised that super-knock in SI engines is due to detonations. This statement can be supported by the knock intensity parameter proposed by Rudloff et al. [283]. Therefore, compared to developing detonation within the peninsula in an RCM, knock and its accompanying consequences would be more violent during SI engine operation.

For the cases of higher temperature conditions and low n-butanol/TRF or n-butanol/gasoline concentrations, a steep pressure rise of more than 8 MPa was observed in Section 5.2 within a very short time. Then, strong pressure oscillations were observed with large amplitudes which are indicative of strong ignition phenomena and can be potentially related to detonations and super-knock events in gasoline engines. Nonetheless, despite displaying lower $\bar{E}(\delta lnT/\delta \bar{r})$ values for lower n-butanol/TRF blends and pure TRF, which are characteristic of more stable detonations with more devastating effect in case of engine knock as illustrated in Figure 6.19, none of the studied fuels were found to enter the bounds of detonation peninsula in Figure 6.18. To further assess and characterise auto-ignition events, another non-dimensional parameter, π, proposed by Rudloff et al. [283], is adopted in the present analysis. This knock intensity parameter exploits a reference pressure P_{AI} at the instance of auto-ignition, the apparent peak experimental pressure P_{max_exp}, as well as the peak pressure calculated from theoretical isochoric combustion based on the initial auto-ignition conditions P_{max_isoc}:

$$\pi = \frac{\Delta P_{exp}}{\Delta P_{isoc}} = \frac{P_{\max\_exp} - P_{AI}}{P_{\max\_isoc} - P_{AI}} = \frac{P_{\max\_exp} - P_{AI}}{\dfrac{(n-1)Q}{V_{cyl}}} \tag{6.2}$$

where n is the polytropic coefficient $(PV^n = const)$ and is equal to the specific heat ratio of the test mixture, γ, for an isentropic process, V_{cyl}, the actual cylinder volume, Q, the remaining energy in the end gases at the moment of auto-ignition. The remaining energy, Q, depends on the lower heating value of the fuel, *LHV*, and the mass of fuel at the moment of auto-ignition, and can be calculated by:

$$Q = LHV * m_0 * (1 - BMF) \tag{6.3}$$

where *LHV* is the lower heating value of the fuel, m_0 is the initial mass of the fuel, *BMF* is the burned mass fraction.

In this study, the knock intensity parameter, π, was calculated using the second expression in Equation (6.2). Here, the peak pressure, P_{max_exp}, was extracted from the experimental pressure trace. The pressure at the instance of auto-ignition, P_{AI}, was also deduced from experimental pressure trace at the time where the maximum rate of pressure rise was observed, and the peak pressure for the isochoric combustion, P_{max_isoc}, was calculated using the constant volume simulations in CANTERA.

Figure 6.20 examines the knock intensity of TRF and B10, B40, B85 *n*-butanol/TRF blends in attempt to further analyse and characterise the effects of *n*-butanol addition to TRF on auto-ignition phenomenon. Here, the knock intensity parameter π is plotted against a) non-dimensional reactivity parameter, ε, b) non-dimensional resonance parameter describing the incidence of coupling mechanism, ξ, c) inverse temperature and d) ignition delay times, in order to explore possible links and dependences between these parameters. Knock intensities are reported as averages of 2-4 consequent runs made at each test condition with errors of one standard deviation. To ensure reliability of the data, some of the runs were excluded from this analysis due to unrealistically high π values compared to other consequent runs at the same conditions. This can potentially be caused by the transducer characteristics, which would have a significant impact on the pressure oscillations and representative apparent peak experimental pressures. However this would not have affected the accuracy of ignition delay times.
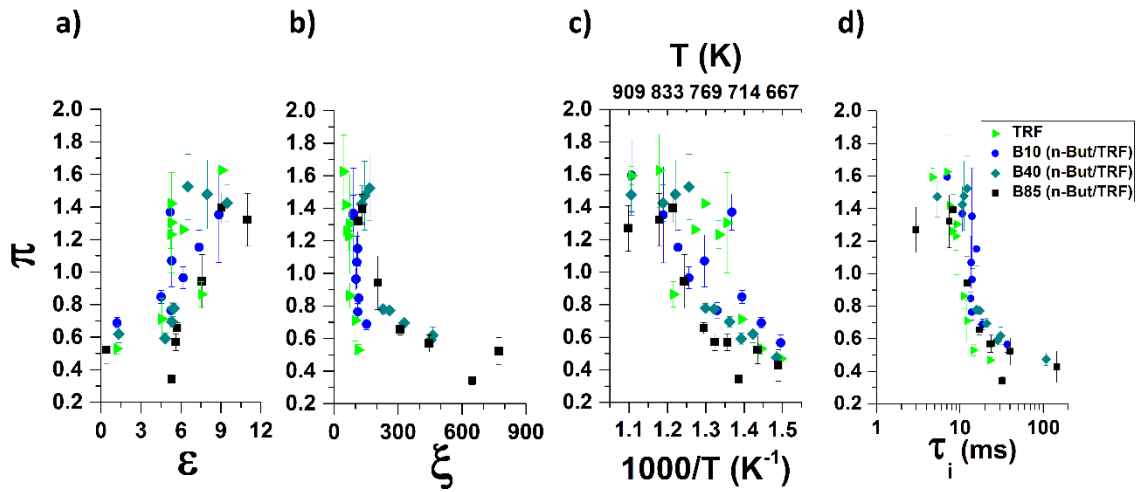
Figure 6.20: Knock intensity parameter, π, as function of a) non-dimensional reactivity parameter, ε, b) non-dimensional resonance parameter describing the incidence of coupling mechanism, ξ, c) inverse temperature and d) ignition delay times for pure TRF, B10, B40 and B85 for the temperature range 678 K - 916 K. P=2 MPa, φ=1.0.

Figure 6.20 shows that the number of events in which π exceeds 1 (which may be representative of strong knock occurrences) gradually decreases with an increase in n-butanol content within the fuel blends. Pure TRF, B10, B40 and B85 exhibit 6, 5, 4 and 3 of these instances, respectively. This may indicate that the addition of n-butanol to TRF improves the fuel resistance to engine knock and reduces its severity, which is consistent with the observations of Agbro et al. [348]. Figure 6.20 (d) displays an almost linear trend between knock intensity and ignition delay time, where the knock severity is reduced with an increase of ignition delay times. This supports the theory that fuels with longer ignition delay times are more likely to exhibit better knock resistance and show better performances under more violent engine operating conditions. This would be beneficial to modern boosted-downsizing SI engines.

In a study by Kalghatgi and Bradley [349], the authors successfully demonstrated in their experimental work that, as engine operation moves from normal combustion to knocking combustion and thermal explosion, ξ quickly decreases while ε increases in magnitude. In the present study, this observation is supported by representative higher knock intensities at higher ε, and lower ξ values. It is observed that knock intensity increases with an increase in ε magnitude in Figure 6.20 (a), and a decrease in ξ value in Figure 6.20 (b). As discussed earlier, there are several uncertainties involved in the calculation of ε and ξ values, which might also affect the estimation of knock intensity. These include the absence of accurate hot/cold spot properties and their localisation, as well as

compositional heterogeneities. However, the evidence that elevated π values are systematically observed for high ε and low ξ values, could imply that these neglected sources have a weaker effect on knock intensity. This conclusion is consistent with the observations of Rudloff et al. [283].

For the current work, it is observed that *n*-butanol addition to TRF fuel shifts mixtures into the deflagrative/auto-ignitive transition regime and away from the developing detonation in Figure 6.18 and Figure 6.19. Also it was demonstrated in Chapter 5 that addition of *n*-butanol to TRF supresses the NTC behaviour, while in Section 6.2 it was shown that LTHR heat release decreases and eventually disappears as *n*-butanol content continues to increase within the blends. Earlier in this chapter it was shown that NTC behaviour plays an important role in the reactivity of the species pool and auto-ignition phenomenon, including development of multi-stage ignition. Meanwhile, Figure 6.20 (c) shows that in the intermediate temperature region where NTC behaviour is apparent for pure TRF and B10 mixtures, knocking intensity is significantly increased for these fuels. At the compression temperature of 745 K TRF has a π value of 1.30 and B10 a π value of 1.37, whereas for higher blends with more Arrhenius ignition delay temperature dependence as demonstrated in Chapter 5 for B40 and B85, the magnitude of π is comparatively lower with π=0.70 B40 and π=0.60 for B85. At the highest compression temperature tested in this study, 916 K, π attains levels of 1.59, 1.59, 1.47 and 1.27 for TRF, B10, B40 and B85, respectively. Hence, the presence of the NTC region not only alters the LTHR and auto-ignition behaviour but also has a significant effect on the knocking intensity, as well as the timing of knocking occurrence, which is consistent with observations in [350].

In general, both TRF and B10 showed quite large variability in π magnitude in the NTC region. Also, the experimental uncertainties of TRF and B10 in the NTC region are higher compared to the higher *n*-butanol/TRF blends. These experimental uncertainties are indicated by the error bars of the one standard deviation of repeated experiments in Figure 6.20. In fact, both the variability in π magnitude and the standard deviation of repeated experiments in the NTC region reduce at the higher *n*-butanol/TRF blends. Agbro et al.[348] highlighted that blending of 20% vol *n*-butanol with TRF or gasoline reduced cyclic variability of the measured peak pressure compared to that of pure TRF or gasoline. Low cyclic variability is desired in SI operations, since high cyclic variability can limit the engine operating range and efficiency [275]. Therefore, this implies a possible link between the NTC behaviour and cyclic variability. It is possible that the

fuels which exhibit NTC behaviour would have a higher cyclic variability in a real engine compared to those with Arrhenius type temperature behaviour. Also, an addition of *n*-butanol to TRF or gasoline probably would directly reduce the magnitude of the cyclic variability. However, further research is required to confirm this theory.

At the beginning of this research, it was debatable whether *n*-butanol is a viable alternative fuel for the use within SI engines and advanced engine technologies. *N*-butanol has lower octane numbers compared to that of ethanol and similar to that of gasoline fuel. Hence, it was questionable whether an addition of *n*-butanol to gasoline would result in significant anti-knock performances of the blend. The present research, has shown that an addition of *n*-butanol to the TRF and a gasoline improves the auto-ignition resistance of the blend at low temperatures. Based on the results presented in Figure 6.18, *n*-butanol/TRF mixtures have demonstrated similar or improved performances compared to that of pure TRF, PRF 98, or RON 98 and OI 105, avoiding the region of developing detonation. At blend ratios of 40% or above of *n*-butanol, mixtures are found to lie close to the compression curve of CH_4, which is known to have good anti-knock properties. This suggests that even when the compression curves of high *n*-butanol/TRF mixtures are extrapolated to turbo-charged conditions, they will most likely avoid the detonation peninsula. B40/TRF blend has also shown a reduced NTC behaviour and a reduced LTHR. Since it is believed that LTHR and the NTC behaviour is strongly related to octane sensitivity [101], it is believed that *n*-butanol can reduce octane sensitivity of the blend. This would result in improved performances of *n*-butanol/TRF or *n*-butanol/gasoline in the practical engine technologies. Therefore, *n*-butanol is a viable anti-knock fuel additive in SI technologies. Although, a further research on cost, NO_x and PM emissions of *n*-butanol and its blends with gasoline is required to assess its overall viability.

6.6 Conclusions

In this study, experimental and modelling investigations of multiple-stage ignition behaviour and associated heat release were carried out for B10, B20, B40 and B85 *n*-butanol/TRF blends, as well as their pure components in the temperature range of 678-916 K and a pressure of 2MPa under stoichiometric conditions. The heat release analyses on the acquired experimental RCM pressure-time measurements were performed to further analyse the auto-ignition behaviour of the studied fuels and examine effects of *n*-butanol addition on LTHR, ITHR, HTHR and aHR for these fuels. These analyses inform

model development and facilitate further assessment of predictive capability of the chemical kinetic scheme, as well as investigations into abnormal combustion processes.

Two-stage ignition behaviour was found for pure TRF and low n-butanol/TRF blends in experimental measurements in the temperature region between approximately 678-831 K (depending on fuel) under stoichiometric conditions and a pressure of 2.0 MPa. Within the experimental study, addition of n-butanol to TRF increased first-stage ignition delay times in the low temperature region, while in the intermediate temperature regime first-stage ignition delays were found to initially increase in magnitude for B10 and then to decrease for B40. For detailed chemical simulations, the mechanism was found to capture the overall trends of the first-stage ignition delay times and overall low temperature heat release. However, modelled preliminary heat release behaviour did not match the experimentally derived data in terms of the magnitude of heat release, especially at low and intermediate temperatures for pure TRF and low n-butanol/TRF blends. On the other hand, in Chapter 5 it was shown that the model was capable of predicting overall ignition delay times relatively well. This potentially suggests that the detailed chemical mechanism has been designed and tuned to accurately represent global targets such as overall ignition delays, but that errors may exist within the thermochemistry. It is speculated that there are large uncertainties in the heats of formation of the larger species (such as alkylperoxy radicals, alkylhydroperoxide radicals, and peroxy alkylhydroperoxide radicals) the model. More accurate experimental estimations and theoretical calculations of heats of formations, in particular for larger hydrocarbons, could substantially enhance the predictive capability of the detailed chemical kinetic schemes.

Brute-force sensitivity analyses for peak values of LTHR, ITHR, HTHR and low temperature aHR were performed to better understand the kinetic effects of n-butanol addition to TRF. Consistent with previous studies, H abstraction reactions from parent fuel molecules by OH were found to be dominant in LTHR and aHR sensitivity analysis across the blends. Similarly to total ignition delay times, H abstraction via OH from the α-, and γ-carbon sites of n-butanol via OH, played a key role in defining LTHR for high n-butanol/TRF blends. On the other hand, for pure TRF, H-atom abstraction from *iso*-octane was important, and showed site specificity.

The presence of multiple-stage heat release behaviour, where more than two distinct stages are present was found for pure TRF and B10. Interestingly, TRF simulations did not show a distinct three-stage ignition behaviour with a distinct peak in ITHR at the

intermediate temperature of 761 K, while lower n-butanol blends exhibited this peculiar multi-stage behaviour at a temperature of 765 K. This potentially can be explained by the fact that n-butanol addition to TRF increases the formaldehyde formation, leading to its increased accumulation during LTHR, resulting in a distinct peak in ITHR. Sensitivity analyses on the peak value for ITHR showed that $CH_3+HO_2 \rightarrow CH_3O +OH$ plays a key role in promoting reactivity of the system, resulting in an increased magnitude for ITHR. On the other hand, $H_2O_2+OH \leftrightarrow H_2O+HO_2$ showed major opposition to the reactivity.

The modelling study of excitation times, τ_e, showed that at high to intermediate temperatures excitation times values fall on the same curve regardless of the detailed chemical model or the fuel composition studied here. The LTHR has some indirect influence on the τ_e magnitude resulting in observed scatter at low temperatures. On the other hand, brute-force sensitivity analyses for τ_e did not show fuel specific reactions with smaller C_1-C_4 molecule chemistry being dominant. The same two dominant reactions that control HTHR, namely $CO + OH \rightarrow CO_2 + H$ and $H + O_2 \rightarrow O + OH$, were found to dominate sensitivity analyses for τ_e for pure TRF and n-butanol fuels and their blends. Moreover, these are also the same two reactions that were featured in sensitivity analyses for τ_e for methane-air at high pressure in Chapter 4. A strong crossover of sensitive reactions for τ_e with flame speed sensitivity reactions and HTHR suggests that constraining mechanisms against flame speeds would also result in accurate predictions of τ_e, which are known to be difficult to be experimentally measured.

Finally, non-dimensional diagrams were introduced to analyse combustion mode and knock intensity. At the temperatures and pressures tested, all n-butanol/TRF blends and their pure components were found to lay outside the bounds of the developing detonation region. For large hydrocarbons which exhibit NTC behaviour, the auto-ignition was suggested to initially appear from cold spots rather than hot spots and thereafter generate detonations. The existence of NTC behaviour can potentially not only alter the LTHR and auto-ignition behaviour, but also lead to an increase in the knock intensity. Also, an addition of n-butanol to TRF was found to not only suppress LTHR but also to reduce knock intensity and shift fuels towards the deflagrative/auto-ignitive transition region in the detonation diagram. A possible link between the NTC behaviour and cyclic variability was also suggested.

7. Summary, Conclusions and Further Study

This thesis has provided an improved understanding of the importance and influence of the key combustion characteristics of methane, *n*-butanol, TRF, *n*-butanol/TRF and *n*-butanol/gasoline fuel blends. Namely, further insights were provided on excitation times, single-stage, multi-stage ignition delay times and associated heat release rates, as well as the interaction of these characteristics in combustion and auto-ignition processes. The detailed chemistry that governs these processes was also studied for different fuels to improve the current understanding of abnormal combustion events. This was achieved through measurements in a rapid compression machine and detailed chemical kinetic modelling investigations of the auto-ignition phenomena, with an accompanying theoretical analysis. Details on the methodology and descriptions of the approaches were provided in Chapter 3. The subsequent sections summarise the contributions, major findings and conclusions of this thesis, together with recommendations for future research.

7.1 Contributions

- The work has provided valuable RCM data for the ignition delay times of *n*-butanol/ TRF and *n*-butanol/ gasoline (RON 95 and MON 86.6) blends, for use in model assessment and improvement. This includes first-stage, second-stage and total ignition delay data. Also, non-reactive experimental volume profiles *n*-butanol/TRF blends are provided (in the Supplementary Materials of [267]). The theoretical work, detailed in Section 6.4, showed that the experimental ignition delay time data can be used as a reliable validation target for detailed chemical kinetic models, when the experimental uncertainties and physics inside the combustion chamber are taken into account.

- Severe engine knock is associated with the strong and rapid heat release deposition into a developing pressure wave within the hot spot. This is defined by the excitation time, which plays an important role in the chemical-acoustic interaction and detonation development. This work has provided novel data on excitation time for methane (over a temperature range of 700 - 1800 K, at 0.1, 4, 6 and 10 MPa), *n*-butanol, toluene reference fuel (TRF) and *n*-butanol/TRF blends (over a temperature range of 678 - 916 K, at 2 MPa).

- This investigation has shown that the heat release analysis methodology proposed by Goldsborough et al. [252] can be successfully applied to examine preliminary

exothermicity for a range of fuels. In the current work, the preliminary exothermicity of *n*-butanol/TRF blends were examined. The heat release rates derived from the RCM experimental measurements can be used as additional target data in the refinement and development of chemical kinetic mechanisms.

- This work has advanced understanding of the factors that controlling abnormal ignition events, such as such as knock, super-knock, deflagration and developing detonation for methane, *n*-butanol, TRF and *n*-butanol/TRF blends.

- Through a brute-force sensitivity analysis, this study has investigated the chemistry controlling heat releases, ignition delay times and excitation times. An improved understanding was obtained regarding the chemical kinetic properties of these processes, as well as the important reactions that drive these processes.

7.2 Summary of research findings

7.2.1 Computational study of methane/air auto-ignition behaviour

- The computational study of methane/air auto-ignition behaviour was performed over a temperature range between 700 and 1800 K at 0.1, 4, 6 and 10 MPa. Despite the adequate performance of the reduced global scheme in simulating ignition delay times, it was unable to predict accurately τ_e, which was under-estimated by an order of the magnitude. This suggests that while the model can be tuned to adequately represent global targets, it is unable to replicate other important parameters. Due to their intricacy, combustion processes and auto-ignition phenomena require detailed kinetic simulations to improve the understanding of these processes and their interactions.

- Ignition delay times, excitation times, and overall heat release rate were shown to be governed by quite different chemistry at atmospheric pressure compared to higher pressures. This resulted in apparent discrepancies in these characteristic behaviours, and associated ignition processes. Excitation times were shown to be governed by third body reactions, which are known to be more sensitive at higher pressures. Reactions $H + O_2 \leftrightarrow O + OH$ and $HO_2 + OH \leftrightarrow H_2O + O_2$ were found to be important for the excitation times for methane, as well as *n*-butanol and TRF blends, in Chapter 6. The dominance of hydrogen, carbon monoxide and small hydrocarbons in these sensitivities implies that there are little fundamental differences between the kinetics of methane excitation times and other fuels.

- Accurate evaluations of τ_i and τ_e allowed the examination of the tendency of CH_4 to detonate, and to compare it against other practical fuels relative to the detonation peninsula on the ξ/ε diagram. Also, these combustion characteristics were used to examine the CH_4 link to deflagrative and auto-ignitive regimes, and the possible transition regime between those in terms of the $\bar{E}(\delta lnT/\delta \bar{r})$ parameter. High $\bar{E}(\delta lnT/\delta \bar{r})$ values might suggest the deflagrative flame propagation and the uncertainty of experimental measurements of τ_i in an RCM. It has been featured that rapid compression machines should operate within the auto-ignitive regime.

- A stoichiometric CH_4/air showed very good anti-knock in comparison with those of other fuels.

7.2.2 Experimental and modelling study of the impacts of *n*-butanol blending on the auto-ignition behaviour of gasoline and its surrogate mixture at low temperatures

- The study presented in Chapter 5 demonstrated while that the TRF surrogate showed a reasonable performance in replicating the auto-ignition response of gasoline, it was unable to accurately replicate the intricacies of auto-ignition behaviour within the NTC region. For low *n*-butanol blends, the agreement between the TRF and gasoline blend was worse in the NTC regime than at lower temperatures, showing a higher degree of non-linear blending behaviour of mixtures. The improved agreement for the higher blends could be attributed to the large alcohol concentration within these blends. Matching compositional modelling of both RON and MON did not result in any major improvement of the surrogate performance in replicating the auto-ignition response of gasoline blends in the NTC. This implies that additional components within the surrogate may be required in order to effectively represent the chosen gasoline. However, this may also increase the level of uncertainty within the chemical mechanism representing the surrogate within simulations.

- This study explored effects of blending an alcohol fuel (*n*-butanol) with fuel that exhibits an NTC (gasoline, TRF) on auto-ignition behaviour of the blend. *N*-butanol showed octane boosting capabilities at low temperatures, where ignition delay times increased with an increase in *n*-butanol concentration within the *n*-butanol/TRF. At higher temperatures, the behaviour reversed as the chain

branching routes from H abstraction from the γ-site of *n*-butanol became more dominant. The NTC response was found to flatten with increasing *n*-butanol for both TRF and gasoline blends, almost disappearing at the highest blend tested of 85%. This blend exhibited a more Arrhenius-type temperature dependency.

- For the lower blends, the largest discrepancies between the simulations and experiments were seen in the NTC region where a large number of reactions contribute to the uncertainty in predicting τ_i.

- For the higher blends, the largest discrepancies were noted in the low temperature region, indicating that uncertainties within the low temperature *n*-butanol chemistry need to be addressed.

7.2.3 Characterisation of auto-ignition phenomenon and heat release analysis

- Similarly to total ignition delay trends, an increase in *n*-butanol concentration resulted in increased first-stage ignition delay times in the low temperature region. Here, the *n*-butanol addition to the blends reduces LTHR, manifesting in longer ignition delay times. A brute-force sensitivity analysis for LTHR peak HRR showed that H abstraction via OH from the γ-carbon site and the α-carbon site of *n*-butanol are the two dominant reactions for B40 and B85. These are the two reactions that were highlighted by the brute-force sensitivity analysis of the total ignition delay times. This indicates an increasing importance of the first-stage ignition delay and low temperature chemistry on the total ignition delay time at these temperatures. Moreover, these are the conditions where the largest discrepancies between experimental and simulated total ignition delay times were observed for the higher *n*-butanol/TRF blends. Accurate, temperature-dependent, reaction rates for site specific H abstraction by both OH and HO_2, for each of the fuel blend components are necessary, in order to improve the agreement between numerical simulations and experimental data.

- Results showed that accurate determination of the first-stage ignition delay does not ultimately lead to accurate prediction of total ignition delays. At the same time, there were cases when the model was unable to predict accurately LTHR but still resulted in satisfactory prediction of total ignition delays, when compared to experimental observations. This hints that the model potentially has been designed and tuned to represent accurately global targets, but not specifically the intricacy of thermochemistry. It is believed that there is a high degree of

255

uncertainty, and possible errors in the heat of formation for some species within the mechanism. More accurate experimental estimations and theoretical calculations of heats of formation can enhance the mechanism performances in predicting first-, second- and total-stage ignition delay times.

- The excitation time is an important combustion parameter for the characterisation of the transition to detonation, and also the stability of detonation waves. It was shown that, in the high to intermediate temperature range, the τ_e values fall onto one curve for different fuels. There was practically no apparent effect of n-butanol addition to TRF blends, nor any obvious influence from NTC chemistry. However, there was an evident rise in the τ_e value at the two lowest temperatures covered in this study. This is potentially attributed to preliminary exothermicity processes, related to cool flame chemistry. Brute-force sensitivity analyses showed that smaller C_1-C_4 molecule chemistry dominates sensitivities and primarily controls τ_e. Some degree of crossover of sensitive reactions for τ_e with flame speed sensitivity reactions was noticed. This suggests that constraining the mechanism against flame speeds can also result in accurate predictions of excitation times, since it is extremely difficult to measure excitation times directly in the current experimental facility.

- Finally, non-dimensional diagrams were introduced to analyse combustion mode and knock intensity. At the temperatures and pressures tested, all n-butanol/TRF blends and their pure components were found to lie outside the bounds of the developing detonation region. It was shown that the existence of NTC behaviour may not only alter the LTHR and auto-ignition behaviour, but also lead to an increase in the knock intensity. The number of events where π reaches values above 1 (which may be representative of strong knock occurrences) gradually decreases with an increase of n-butanol content within the fuel blends. The addition of n-butanol to TRF increases ξ values and reduces the fuel propensity to detonation. At high n-butanol/TRF concentrations, mixtures were found to avoid crossing into the region of developing detonation. They were found to lie close to the compression curve of CH_4, which was shown to have good anti-knock properties. Hence, n-butanol is a viable anti-knock fuel additive in SI technologies.

7.3 Recommendations for future research

- In this thesis it was shown that the proposed TRF surrogate fails to capture accurately auto-ignition behaviour in the NTC region. In the modelling work, it was shown that matching RON and MON in the development of the surrogate did not resolve the agreement between the surrogate and gasoline blends in the NTC region. After invaluable conversations with Dr. S. W. Wagnon and Prof. W. J. Pitz, it is suggested that addition of a fourth component, 1-hexane, can improve surrogate performances in representing gasoline auto-ignition behaviour. An introduction of an olefin representative in the mixture can result in higher octane sensitivity [351]. Also, 1-hexene is recommended due to its widely validated chemical kinetic model [352]. On the other hand, the studied gasoline (RON =95, MON=87) contains 4.7% vol of the oxygenated compound, ethanol. Matching the oxygenated content of the gasoline in the representative surrogate mixture will also result in an improved surrogate performance. However, increasing the number of components within the surrogate mixture also increases the complexity of the detailed chemical mechanism and associated uncertainties. Instead, it is suggested to test the surrogate performances in representing the auto-ignition behaviour of the research gasoline, which does not include an ethanol compound.

- There are some features of the experimental facility that can be improved or developed. For example, the introduction of optical access to the current experimental set-up would enable the study of hot spot auto-ignition and associated auto-ignition modes. By utilising RCM and high-speed imaging of CH_2O and OH chemiluminescence, the mechanism of hot-spot induced deflagration to detonation can be studied. As presented in Chapter 6, CH_2O chemiluminescence is a good marker for measurements of ITHR. Therefore, this can facilitate further studies in three-stage heat release processes. Optical access and high speed imaging could also enable the research of the auto-ignition transition to detonation and the mechanism of super-knock. However, due to the detrimental force of detonation to the optical parts, it might be problematic to repeatedly trigger super-knock in an optical facility to study the detailed mechanism of end gas auto-ignition. Also, further development of the rig can provide a means of measuring excitation times directly. Excitation times are of the order of microseconds, thus ultra-high speed photography is required for a sufficient temporal resolution.

- Finally, an experimental and modelling studies of the effects of *n*-butanol addition on the auto-ignition, heat release rates and knock properties of gasoline and its surrogate in a SI engine is recommended. Although the *n*-butanol octane enhancing properties at low temperatures have been reported in this work, it would be of interest to examine its auto-ignition and combustion behaviour in a real gasoline engine. This could facilitate a better understanding of the chemical processes affecting knock onsets within engines.

Appendix A
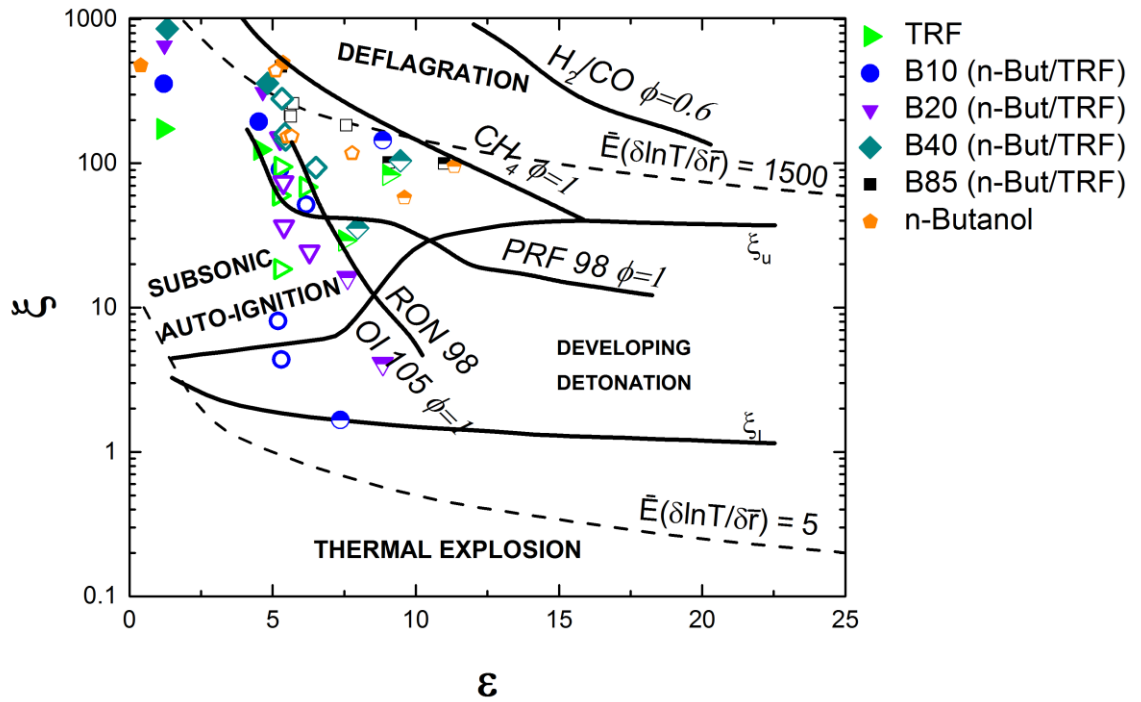
Figure A.1: Detonation peninsula diagram of Bradley et al. [91] for 10%, 20%, 40% and 85% vol *n*-butanol blends with TRF, as well as neat TRF and *n*-butanol fuels. Reported ξ values employed the local activation energies. For comparisons isentropic compression curves for different fuels showing propensity for detonation adopted from an earlier study of auto-ignition in engines [94] are also presented. Filled symbols are in the temperature range 678-727 K. Opened symbols are in the temperature range 727-831 K. Half open symbols are in the temperature range 831-916K. P=2 MPa, φ=1.0.

References

1. ExxonMobil. *Outlook for Energy: A View to 2040.* [Online]. 2016. [Accessed 17 September 2019]. Available from: https://cdn.exxonmobil.com/~/media/global/files/outlook-for-energy/2016/2016-outlook-for-energy.pdf

2. BP Global. *BP Energy Outlook: 2019 edition.* [Online]. 2019. [Accessed 15 June 2019]. Available from: https://www.bp.com/content/dam/bp/business-sites/en/global/corporate/pdfs/energy-economics/energy-outlook/bp-energy-outlook-2019.pdf

3. International Energy Agency. *World Energy Outlook 2017.* [Online]. 2017. [Accessed]. Available from: https://www.iea.org/weo2017/

4. Mathews, A.P. Renewable energy technologies: panacea for world energy security and climate change? *Procedia Computer Science.* 2014, **32**, pp.731-737.

5. Bessou, C., Ferchaud, F., Gabrielle, B. and Mary, B. Biofuels, greenhouse gases and climate change. In: *Sustainable Agriculture Volume 2.* Dordrecht: Springer, 2011, pp.365-468.

6. BP Global. *BP Statistical Review of World Energy.* [Online]. 2019. [Accessed 26 August 2019]. Available from: https://www.bp.com/content/dam/bp/business-sites/en/global/corporate/pdfs/energy-economics/statistical-review/bp-stats-review-2019-full-report.pdf

7. Sarathy, S.M., Farooq, A. and Kalghatgi, G.T. Recent progress in gasoline surrogate fuels. *Progress in Energy and Combustion Science.* 2017.

8. Kalghatgi, G. Is it really the end of internal combustion engines and petroleum in transport? *Applied Energy.* 2018, **225**, pp.965-974.

9. Canada's oil & natural gas producers. *2018 Economic Report Series: Canada's role in the world's future energy mix.* [Online]. 2018. [Accessed 15 February 2019]. Available from: https://www.capp.ca/publications-and-statistics/publications/317291

10. World Energy Council. *World energy outlook 2017.* [Online]. 2017. [Accessed 15 February 2019]. Available from: https://www.iea.org/weo2017/

11. ExxonMobil. *Energy demand: Three drivers.* [Online]. 2019. [Accessed 28 August 2019]. Available from: https://corporate.exxonmobil.com/Energy-and-environment/Energy-resources/Outlook-for-Energy/Energy-demand#threeDrivers

12. ExxonMobil. *Energy Supply.* [Online]. 2019. [Accessed 29 August 2019]. Available from: https://corporate.exxonmobil.com/Energy-and-environment/Energy-resources/Outlook-for-Energy/Energy-supply#liquids

13. International Energy Agency. *World Energy Outlook 2016: Part B: Special Focus on Renewable Energy.* [Online]. 2016. [Accessed 26 August 2019]. Available from: https://www.iea.org/media/publications/weo/WEO2016SpecialFocusonRenewableEnergy.pdf

14. Kalghatgi, G. and Johansson, B. Gasoline compression ignition approach to efficient, clean and affordable future engines. *Proceedings of the Institution of Mechanical Engineers, Part D: Journal of Automobile Engineering.* 2018, **232**(1), pp.118-138.

15. Yan, F., Winijkul, E., Streets, D., Lu, Z., Bond, T. and Zhang, Y. Global emission projections for the transportation sector using dynamic technology modeling. *Atmospheric Chemistry and Physics.* 2014, **14**(11), pp.5709-5733.

16. EDGAR European Commission. *Joint Research Centre (JRC)/Netherlands Environmental Assessment Agency (PBL), Emission Database for Global Atmospheric Research (EDGAR): Fossil CO2 & GHG emissions of all world countries.* [Online]. 2017. [Accessed 7 August 2019]. Available from:

https://edgar.jrc.ec.europa.eu/booklet2017/CO2_and_GHG_emissions_of_all_world_countries_booklet_online.pdf

17. European Commission. *Climate change consequences.* [Online]. 2019. [Accessed 26 August 2019]. Available from: https://ec.europa.eu/clima/change/consequences_en

18. Church, J.A., White, N.J., Domingues, C.M., Monselesan, D.P. and Miles, E.R. Sea-level and ocean heat-content change. In: *International Geophysics*. Elsevier, 2013, pp.697-725.

19. Meyssignac, B. and Cazenave, A. Sea level: a review of present-day and recent-past changes and variability. *Journal of Geodynamics.* 2012, **58**, pp.96-109.

20. Nerem, R., Plag, H. and Jules-Plag, S. *GLOBAL CHANGE | Sea Level Change.* Elsevier, 2015.

21. World Health Organisation. *Ambient air pollution - a major threat to health and climate.* [Online]. 2018. [Accessed 26.08.2018]. Available from: https://www.who.int/airpollution/ambient/policy-governance/en/

22. United Nations Climate Change. *The Paris Agreement.* [Online]. 2018. [Accessed 15 August 2019]. Available from: https://unfccc.int/process/the-paris-agreement/what-is-the-paris-agreement

23. United Nations Climate Change. *Nationally Determined Contributions (NDCs).* [Online]. 2019. [Accessed 17 September 2019]. Available from: https://unfccc.int/process-and-meetings/the-paris-agreement/nationally-determined-contributions-ndcs

24. European Commission. *Climate strategies and targets.* [Online]. 2019. [Accessed 26 August 2019]. Available from: https://ec.europa.eu/clima/policies/strategies_en

25. European Commission. *Renewable energy: Progress reports.* [Online]. 2019. [Accessed 27 August 2019]. Available from: https://ec.europa.eu/energy/en/topics/renewable-energy/progress-reports

26. European Commission. *Renewable Energy – Recast to 2030 (RED II).* [Online]. 2019. [Accessed 8 September 2019]. Available from: https://ec.europa.eu/jrc/en/jec/renewable-energy-recast-2030-red-ii

27. Department for Business Energy and Industry Strategy. *2018 UK Greenhouse Gas Emissions, Provisional Figures.* [Online]. 2019. [Accessed 26 August 2019]. Available from: https://assets.publishing.service.gov.uk/government/uploads/system/uploads/attachment_data/file/790626/2018-provisional-emissions-statistics-report.pdf

28. Committee on Climate Change. *Reducing carbon emissions.* [Online]. 2019. [Accessed 29 August 2019]. Available from: https://www.theccc.org.uk/tackling-climate-change/reducing-carbon-emissions/

29. International Energy Agency. *Hydrogen production and distribution.* [Online]. 2007. [Accessed 19 September 2019]. Available from: https://iea-etsap.org/E-TechDS/PDF/P12_H2_Feb2014_FINAL%203_CRES-2a-GS%20Mz%20GSOK.pdf

30. U.S. Energy Information Administration. *International Energy Outlook* [Online]. 2013. [Accessed 15 November 2018]. Available from: https://www.eia.gov/outlooks/ieo/

31. Royal Academy of Engineering. *Suistainability of liquid fuels.* [Online]. 2017. [Accessed 14 September 2019]. Available from: https://www.raeng.org.uk/publications/reports/biofuels

32. Remmert, S., Cracknell, R., Head, R., Schuetze, A., Akehurst, S., Turner, J. and Popplewell, A. Octane response in a downsized, highly boosted direct injection spark ignition engine. *SAE International Journal of Fuels and Lubricants.* 2014, **7**(1), pp.131-143.

33. Mansfield, A.B., Wooldridge, M.S., Di, H. and He, X. Low-temperature ignition behavior of iso-octane. *Fuel.* 2015, **139**, pp.79-86.

34. Richards, G., McMillian, M., Gemmen, R., Rogers, W.A. and Cully, S. Issues for low-emission, fuel-flexible power systems. *Progress in Energy and Combustion Science.* 2001, **27**(2), pp.141-169.

35.   Goyal, G., Warnatz, J. and Maas, U. Numerical studies of hot spot ignition in H2–O2 and CH4-air mixtures. In: *Symposium (International) on Combustion 23*: Elsevier, 1991, pp.1767-1773.

36.   Lutz, A.E., Kee, R.J., Miller, J.A., Dwyer, H.A. and Oppenheim, A.K. Dynamic effects of autoignition centers for hydrogen and C1, 2-hydrocarbon fuels. In: *Symposium (International) on Combustion 22*: Elsevier, 1989, pp.1683-1693.

37.   Kalghatgi, G. Knock onset, knock intensity, superknock and preignition in spark ignition engines. *International Journal of Engine Research.* 2018, **19**(1), pp.7-20.

38.   Kalghatgi, G., Algunaibet, I. and Morganti, K. On knock intensity and superknock in SI engine. *SAE 2017-01-0689.* 2017.

39.   Wang, Z., Liu, H. and Reitz, R.D. Knocking combustion in spark-ignition engines. *Progress in Energy and Combustion Science.* 2017, **61**, pp.78-112.

40.   Kumar, K., Zhang, Y., Sung, C.-J. and Pitz, W.J. Autoignition response of n-butanol and its blends with primary reference fuel constituents of gasoline. *Combustion and Flame.* 2015, **162**(6), pp.2466-2479.

41.   Agbro, E., Tomlin, A.S., Lawes, M., Park, S. and Sarathy, S.M. The influence of n-butanol blending on the ignition delay times of gasoline and its surrogate at high pressures. *Fuel.* 2017, **187**, pp.211-219.

42.   Agbro, E., Tomlin, A.S., Zhang, W., Burluka, A., Mauss, F., Pasternak, M., Alfazazi, A. and Sarathy, S.M. Chemical Kinetic Modeling Study on the Influence of n-Butanol Blending on the Combustion, Autoignition, and Knock Properties of Gasoline and Its Surrogate in a Spark-Ignition Engine. *Energy & Fuels.* 2018, **32**(10), pp.10065-10077.

43.   AlRamadan, A.S., Badra, J., Javed, T., Al-Abbad, M., Bokhumseen, N., Gaillard, P., Babiker, H., Farooq, A. and Sarathy, S.M. Mixed butanols addition to gasoline surrogates: Shock tube ignition delay time measurements and chemical kinetic modeling. *Combustion and Flame.* 2015, **162**(10), pp.3971-3979.

44.   Zhang, P., Ji, W., He, T., He, X., Wang, Z., Yang, B. and Law, C.K. First-stage ignition delay in the negative temperature coefficient behavior: Experiment and simulation. *Combustion and Flame.* 2016, **167**, pp.14-23.

45.   Bradley, D. Autoignitions and detonations in engines and ducts. *Philosophical Transactions of the Royal Society A: Mathematical, Physical and Engineering Sciences.* 2012, **370**(1960), pp.689-714.

46.   Sandia National Laboratories. *Combustion Research Facility: Chemistry of Autoignition.* [Online]. 2018. [Accessed 25 November 2018]. Available from: https://crf.sandia.gov/combustion-research-facility/combustion-chemistry/combustion-kinetics/chemistry-of-autoignition/

47.   Pulkrabek, W.W. *Engineering fundamentals of the internal combustion engine.* American Society of Mechanical Engineers Digital Collection. 2004.

48.   Montoya, J.P.G., Olsen, D.B. and Amell, A.A. Engine operation just above and below the knocking threshold, using a blend of biogas and natural gas. *Energy.* 2018, **153**, pp.719-725.

49.   Zhen, X., Wang, Y., Xu, S., Zhu, Y., Tao, C., Xu, T. and Song, M. The engine knock analysis–An overview. *Applied Energy.* 2012, **92**, pp.628-636.

50.   Shu, G., Pan, J. and Wei, H. Analysis of onset and severity of knock in SI engine based on in-cylinder pressure oscillations. *Applied Thermal Engineering.* 2013, **51**(1-2), pp.1297-1306.

51.   Active Standard ASTM D2700. *Standard test method for motor octane number of spark-ignition engine fuel.* . 2013.

52.   Bradley, D. and Head, R. Engine autoignition: The relationship between octane numbers and autoignition delay times. *Combustion and Flame.* 2006, **147**(3), pp.171-184.

53.   Badra, J.A., Bokhumseen, N., Mulla, N., Sarathy, S.M., Farooq, A., Kalghatgi, G. and Gaillard, P. A methodology to relate octane numbers of binary and ternary n-heptane,

iso-octane and toluene mixtures with simulated ignition delay times. *Fuel.* 2015, **160**, pp.458-469.

54. Kalghatgi, G.T. The outlook for fuels for internal combustion engines. *International Journal of Engine Research.* 2014, **15**(4), pp.383-398.

55. AlAbbad, M., Badra, J., Djebbi, K. and Farooq, A. Ignition delay measurements of a low-octane gasoline blend, designed for gasoline compression ignition (GCI) engines. *Proceedings of the Combustion Institute.* 2019, **37**(1), pp.171-178.

56. Yang, Y., Dec, J.E., Sjöberg, M. and Ji, C. Understanding fuel anti-knock performances in modern SI engines using fundamental HCCI experiments. *Combustion and Flame.* 2015, **162**(10), pp.4008-4015.

57. Sarathy, S.M., Oßwald, P., Hansen, N. and Kohse-Höinghaus, K. Alcohol combustion chemistry. *Progress in Energy and Combustion Science.* 2014, **44**, pp.40-102.

58. Mittal, V. and Heywood, J.B. The shift in relevance of fuel RON and MON to knock onset in modern SI engines over the last 70 years. *SAE International Journal of Engines.* 2010, **2**(2), pp.1-10.

59. Cisek, J. and Szlachta, Z. Correlation between autoignition delay and cetane number of rape fuels at varied diesel engine work conditions. In: *27st International Scientific Conference on Combustion Engines KONES*, 2001.

60. Patil, C., Varade, S. and Wadkar, S. A Review of Engine Downsizing and its Effects. *International Journal of Current Engineering and Technology, Special Issue-7 (March 2017), E-ISSN.* 2017, pp.2277-4106.

61. Petchers, N. *Combined heating, cooling & power handbook: technologies & applications: an integrated approach to energy resource optimization.* Fairmont Press, 2003.

62. Alriksson, M. and Denbratt, I. *Low temperature combustion in a heavy duty diesel engine using high levels of EGR.* SAE Technical Paper, 2006.

63. Yao, M., Zheng, Z. and Liu, H. Progress and recent trends in homogeneous charge compression ignition (HCCI) engines. *Progress in Energy and Combustion Science.* 2009, **35**(5), pp.398-437.

64. Distaso, E., Amirante, R., Calò, G., De Palma, P., Tamburrano, P. and Reitz, R. Investigation of Lubricant Oil influence on Ignition of Gasoline-like Fuels by a Detailed Reaction Mechanism. *Energy Procedia.* 2018, **148**, pp.663-670.

65. Wang, Z., Qi, Y., He, X., Wang, J., Shuai, S. and Law, C.K. Analysis of pre-ignition to super-knock: hotspot-induced deflagration to detonation. *Fuel.* 2015, **144**, pp.222-227.

66. Bendu, H. and Murugan, S. Homogeneous charge compression ignition (HCCI) combustion: Mixture preparation and control strategies in diesel engines. *Renewable Sustainable Energy Reviews.* 2014, **38**, pp.732-746.

67. Pachiannan, T., Zhong, W., Rajkumar, S., He, Z., Leng, X. and Wang, Q. A literature review of fuel effects on performance and emission characteristics of low-temperature combustion strategies. *Applied Energy.* 2019, **251**, p.113380.

68. Christensen, M., Hultqvist, A. and Johansson, B. *Demonstrating the multi fuel capability of a homogeneous charge compression ignition engine with variable compression ratio.* SAE Technical Paper, 1999.

69. Zhao, H. *HCCI and CAI engines for the automotive industry.* Elsevier, 2007.

70. Christensen, M. and Johansson, B. *Supercharged homogeneous charge compression ignition (HCCI) with exhaust gas recirculation and pilot fuel.* SAE Technical Paper, 2000.

71. Desantes, J.M., López, J.J., García-Oliver, J.M. and López-Pintor, D. A phenomenological explanation of the autoignition propagation under HCCI conditions. *Fuel.* 2017, **206**, pp.43-57.

72. Mohamed, C. *Autoignition of hydrocarbons in relation to engine knock.* Ph.D. thesis, University of Leeds, 1997.

73. Griffiths, J.F. and Barnard, J.A. *Flame and combustion.* CRC Press, 1995.

74. Koivisto, E. *Ignition and combustion of future oxygenated fuels in compression-ignition engines.* Ph.D. thesis, University College London, 2015.

75. Materego, M. *Auto-ignition characterisation of synthetic fuels via Rapid Compression Machine*. Ph.D. thesis, University of Leeds, 2016.

76. Pilling, M.J. *Low-temperature combustion and autoignition.* Elsevier, 1997.

77. Battin-Leclerc, F., Blurock, E., Bounaceur, R., Fournet, R., Glaude, P.-A., Herbinet, O., Sirjean, B. and Warth, V. Towards cleaner combustion engines through groundbreaking detailed chemical kinetic models. *Chemical Society Reviews.* 2011, **40**(9), pp.4762-4782.

78. Agbro, E. *Experimental and chemical kinetic modelling study on the combustion of alternative fuels in fundamental systems and practical engines*. Ph.D. thesis, University of Leeds, 2017.

79. Glassman, I., Yetter, R.A. and Glumac, N.G. *Combustion.* Academic press, 2014.

80. Simmie, J.M. Detailed chemical kinetic models for the combustion of hydrocarbon fuels. *Progress in Energy and Combustion Science.* 2003, **29**(6), pp.599-634.

81. Westbrook, C.K. and Dryer, F.L. Chemical kinetic modeling of hydrocarbon combustion. *Progress in Energy and Combustion Science.* 1984, **10**(1), pp.1-57.

82. Goldsborough, S.S., Hochgreb, S., Vanhove, G., Wooldridge, M.S., Curran, H.J. and Sung, C.-J. Advances in rapid compression machine studies of low-and intermediate-temperature autoignition phenomena. *Progress in Energy and Combustion Science.* 2017, **63**, pp.1-78.

83. Cavaliere, A. and de Joannon, M. Mild combustion. *Progress in Energy and Combustion Science.* 2004, **30**(4), pp.329-366.

84. Chen, B., Wang, Z., Wang, J.-Y., Wang, H., Togbé, C., Alonso, P.E.Á., Almalki, M., Mehl, M., Pitz, W.J. and Wagnon, S.W. Exploring gasoline oxidation chemistry in jet stirred reactors. *Fuel.* 2019, **236**, pp.1282-1292.

85. Curran, H.J. Developing detailed chemical kinetic mechanisms for fuel combustion. *Proceedings of the Combustion Institute.* 2018.

86. Griffiths, J. Reduced kinetic models and their application to practical combustion systems. *Progress in Energy and Combustion Science.* 1995, **21**(1), pp.25-107.

87. Yu, L., Mao, Y., Li, A., Wang, S., Qiu, Y., Qian, Y., Han, D., Zhu, L. and Lu, X. Experimental and modeling validation of a large diesel surrogate: Autoignition in heated rapid compression machine and oxidation in flow reactor. *Combustion and Flame.* 2019, **202**, pp.195-207.

88. Sarathy, S.M., Vranckx, S., Yasunaga, K., Mehl, M., Oßwald, P., Metcalfe, W.K., Westbrook, C.K., Pitz, W.J., Kohse-Höinghaus, K. and Fernandes, R.X. A comprehensive chemical kinetic combustion model for the four butanol isomers. *Combustion and Flame.* 2012, **159**(6), pp.2028-2055.

89. Pelucchi, M., Bissoli, M., Rizzo, C., Zhang, Y., Somers, K., Frassoldati, A., Curran, H. and Faravelli, T. A Kinetic Modelling Study of Alcohols Operating Regimes in a HCCI Engine. *SAE International Journal of Engines.* 2017, **10**(2017-24-0077), pp.2354-2370.

90. Bates, L., Bradley, D., Paczko, G. and Peters, N. Engine hot spots: Modes of auto-ignition and reaction propagation. *Combustion and Flame.* 2016, **166**, pp.80-85.

91. Bradley, D., Morley, C., Gu, X. and Emerson, D. Amplified pressure waves during autoignition: relevance to CAI engines, SAE paper 2002-01-2868. 2002.

92. Zeldovich, Y.B. Regime classification of an exothermic reaction with nonuniform initial conditions. *Combustion and Flame.* 1980, **39**(2), pp.211-214.

93. Ciccarelli, G. and Dorofeev, S. Flame acceleration and transition to detonation in ducts. *Progress in Energy and Combustion Science.* 2008, **34**(4), pp.499-550.

94. Bates, L. and Bradley, D. Deflagrative, auto-ignitive, and detonative propagation regimes in engines. *Combustion and Flame.* 2017, **175**, pp.118-122.

95. König, G., Maly, R., Bradley, D., Lau, A. and Sheppard, C. Role of exothermic centres on knock initiation and knock damage. *SAE transactions.* 1990, pp.840-861.

96. Gu, X., Emerson, D. and Bradley, D. Modes of reaction front propagation from hot spots. *Combustion and Flame.* 2003, **133**(1-2), pp.63-74.

97. Bradley, D. and Kalghatgi, G. Influence of autoignition delay time characteristics of different fuels on pressure waves and knock in reciprocating engines. *Combustion and Flame.* 2009, **156**(12), pp.2307-2318.

98. Leppard, W.R. The chemical origin of fuel octane sensitivity. *SAE transactions.* 1990, pp.862-876.

99. Dryer, F.L. Chemical kinetic and combustion characteristics of transportation fuels. *Proceedings of the Combustion Institute.* 2015, **35**(1), pp.117-144.

100. Vuilleumier, D., Selim, H., Dibble, R. and Sarathy, M. *Exploration of heat release in a homogeneous charge compression ignition engine with primary reference fuels.* SAE Technical Paper, 2013.

101. Westbrook, C.K., Mehl, M., Pitz, W.J. and Sjöberg, M. Chemical kinetics of octane sensitivity in a spark-ignition engine. *Combustion and Flame.* 2017, **175**, pp.2-15.

102. Saisirirat, P., Foucher, F., Chanchaona, S. and Mounaïm-Rousselle, C. Spectroscopic measurements of low-temperature heat release for homogeneous combustion compression ignition (HCCI) n-heptane/alcohol mixture combustion. *Energy & Fuels.* 2010, **24**(10), pp.5404-5409.

103. Saisirirat, P., Togbé, C., Chanchaona, S., Foucher, F., Mounaim-Rousselle, C. and Dagaut, P. Auto-ignition and combustion characteristics in HCCI and JSR using 1-butanol/n-heptane and ethanol/n-heptane blends. *Proceedings of the Combustion Institute.* 2011, **33**(2), pp.3007-3014.

104. Najafabadi, M.I. and Aziz, N.A. Homogeneous charge compression ignition combustion: challenges and proposed solutions. *Journal of combustion.* 2013, **2013**.

105. Westbrook, C., Pitz, W. and Curran, H. Auto-ignition and chemical kinetic mechanisms of HCCI combustion. *HCCI and CAI engines for the automotive industry.* 2007, pp.433-445.

106. Shibata, G., Oyama, K., Urushihara, T. and Nakano, T. *Correlation of low temperature heat release with fuel composition and HCCI engine combustion.* SAE Technical Paper, 2005.

107. Tanaka, S., Ayala, F. and Keck, J.C. A reduced chemical kinetic model for HCCI combustion of primary reference fuels in a rapid compression machine. *Combustion and Flame.* 2003, **133**(4), pp.467-481.

108. Kuwahara, K., Tada, T., Furutani, M., Sakai, Y. and Ando, H. Chemical kinetics study on two-stage main heat release in ignition process of highly diluted mixtures. *SAE International Journal of Engines.* 2013, **6**(1), pp.520-532.

109. Shibata, G., Oyama, K., Urushihara, T. and Nakano, T. *The effect of fuel properties on low and high temperature heat release and resulting performance of an HCCI engine.* SAE Technical Paper, 2004.

110. Pan, J., Wei, H., Shu, G., Chen, Z. and Zhao, P. The role of low temperature chemistry in combustion mode development under elevated pressures. *Combustion and Flame.* 2016, **174**, pp.179-193.

111. Kang, D., Lilik, G., Dillstrom, V., Agudelo, J., Lapuerta, M., Al-Qurashi, K. and Boehman, A.L. Impact of branched structures on cycloalkane ignition in a motored engine: Detailed product and conformational analyses. *Combustion and Flame.* 2015, **162**(4), pp.877-892.

112. Herbinet, O. and Dayma, G. Jet-stirred reactors. In: *Cleaner combustion.* Springer, 2013, pp.183-210.

113. Hanson, R.K. and Davidson, D.F. Recent advances in laser absorption and shock tube methods for studies of combustion chemistry. *Progress in Energy and Combustion Science.* 2014, **44**, pp.103-114.

114. Bradley, D., Lawes, M. and Materego, M. Interpretation of Auto-ignition Delay Times Measured in Different Rapid Compression Machines. In: *25th International Colloquium on the Dynamics of Explosions and Reactive systems, 2-7 August, Leeds.* 2015.

115. Atef, N., Kukkadapu, G., Mohamed, S.Y., Al Rashidi, M., Banyon, C., Mehl, M., Heufer, K.A., Nasir, E.F., Alfazazi, A. and Das, A.K. A comprehensive iso-octane combustion

model with improved thermochemistry and chemical kinetics. *Combustion and Flame.* 2017, **178**, pp.111-134.

116. Denisov, E., Sarkisov, O. and Likhtenshtein, G.I. *Chemical Kinetics: Fundamentals and Recent Developments.* Elsevier, 2003.

117. Turányi, T. and Tomlin, A.S. *Analysis of kinetic reaction mechanisms.* Springer, 2014.

118. Lindemann, F., Arrhenius, S., Langmuir, I., Dhar, N., Perrin, J. and Lewis, W.M. Discussion on "the radiation theory of chemical action". *Transactions of the Faraday Society.* 1922, **17**, pp.598-606.

119. Warnatz, J., Maas, U. and Dibble, R.W. *Combustion: physical and chemical fundamentals, modeling and simulation, experiments, pollutants formation,* . Berlin: Springer. 1999.

120. Robinson, P.J. and Holbrook, K.A. Unimolecular reactions. 1972.

121. Atkins, P.W. *Physical chemistry*. New York: W. H. Freeman,. 1990, p. 995 pp.

122. Golden, D.M. Gas phase homogeneous kinetics. In: *Low-temperature chemistry of the atmosphere*. Springer, 1994, pp.69-92.

123. Gilbert, R., Luther, K. and Troe, J. Theory of thermal unimolecular reactions in the fall‐off range. II. Weak collision rate constants. *Berichte der Bunsengesellschaft für physikalische Chemie.* 1983, **87**(2), pp.169-177.

124. Miller, J.A. and Klippenstein, S.J. Dissociation of propyl radicals and other reactions on a C3H7 potential. *The Journal of Physical Chemistry A.* 2013, **117**(13), pp.2718-2727.

125. Daly, S. *Chemometrics-based Approach for Predicting Low Temperature Combustion Engine Fuel Performance*. MSc thesis, Oregon State University, 2016.

126. Goodwin, D. *Cantera: Object-oriented software for reacting flows.* [Online]. 2005. [Accessed 17 October 2017]. Available from: http://www.cantera.org

127. Weber, B.W. and Sung, C.-J. UConnRCMPy: Python-based data analysis for rapid compression machines. *arXiv preprint arXiv:1706.01984.* 2017.

128. Design Reaction. CHEMKIN 10131. *Reaction Design.* 2013.

129. Cuoci, A., Frassoldati, A., Faravelli, T. and Ranzi, E. A computational tool for the detailed kinetic modeling of laminar flames: Application to C2H4/CH4 coflow flames. *Combustion and Flame.* 2013, **160**(5), pp.870-886.

130. LOGE. *LOGEresearch v 1.10 (LOGE AB).* [Online]. [Accessed 9 March 2019]. Available from: http://www.logesoft.com/loge-software

131. Pitsch, H. and Bollig, M. FlameMaster: A C++ computer program for 0D combustion and 1D laminar flame calculations. 2015.

132. Deutschmann, O., Tischer, S., Correa, C., Chatterjee, D., Kleditzsch, S., Janardhanan, V., Mladenov, N., Minh, H., Karadeniz, H. and Hettel, M. *DETCHEM Software Package, 2.Karlsruhe*. 2014.

133. Kintech Lab. *Chemical WorkBench.* [Online]. [Accessed 9 March 2019]. Available from: http://www.kintechlab.com/products/chemical-workbench/

134. Jones, A.C. and Hitchman, M.L. *Chemical vapour deposition: precursors, processes and applications.* Royal Society of Chemistry, 2009.

135. Shahangian, N., Keshavarz, M. and Jazayeri, S. Performance and combustion characteristics analysis of HCCI engine operation with diesel like fuels. *Oil & Gas Science and Technology-Revue de l'IFP.* 2009, **64**(4), pp.521-532.

136. Bourgeois, N. *Numerical study of multi-dimensional effects in Rapid Compression Machines*. Ph.D. thesis, Université Catholique de Louvain and Vrije Universiteit, 2017.

137. Coniglio, L., Bennadji, H., Glaude, P.A., Herbinet, O. and Billaud, F. Combustion chemical kinetics of biodiesel and related compounds (methyl and ethyl esters): experiments and modeling–advances and future refinements. *Progress in Energy and Combustion Science.* 2013, **39**(4), pp.340-382.

138. Frenklach, M., Wang, H. and Rabinowitz, M.J. Optimization and analysis of large chemical kinetic mechanisms using the solution mapping method—combustion of methane. *Progress in Energy and Combustion Science.* 1992, **18**(1), pp.47-73.

139. de Oliveira, L.P., Hudebine, D., Guillaume, D. and Verstraete, J.J. A review of kinetic modeling Methodologies for complex processes. *Oil & Gas Science and Technology–Revue d'IFP Energies nouvelles.* 2016, **71**(3), p.45.

140. Faravelli, T., Manenti, F. and Ranzi, E. *Mathematical Modelling of Gas-Phase Complex Reaction Systems: Pyrolysis and Combustion.* Elsevier Science, 2019.

141. Abianeh, O.S., Oehlschlaeger, M.A. and Sung, C.-J. A surrogate mixture and kinetic mechanism for emulating the evaporation and autoignition characteristics of gasoline fuel. *Combustion and Flame.* 2015, **162**(10), pp.3773-3784.

142. Ahmed, A., Goteng, G., Shankar, V.S., Al-Qurashi, K., Roberts, W.L. and Sarathy, S.M. A computational methodology for formulating gasoline surrogate fuels with accurate physical and chemical kinetic properties. *Fuel.* 2015, **143**, pp.290-300.

143. Mehl, M., Pitz, W.J., Westbrook, C.K. and Curran, H.J. Kinetic modeling of gasoline surrogate components and mixtures under engine conditions. *Proceedings of the Combustion Institute.* 2011, **33**(1), pp.193-200.

144. Chaos, M., Zhao, Z., Kazakov, A., Gokulakrishnan, P., Angioletti, M. and Dryer, F.L. A PRF+ toluene surrogate fuel model for simulating gasoline kinetics. In: *5th US combustion Meeting*, 2007, pp.25-28.

145. Gauthier, B., Davidson, D.F. and Hanson, R.K. Shock tube determination of ignition delay times in full-blend and surrogate fuel mixtures. *Combustion and Flame.* 2004, **139**(4), pp.300-311.

146. Vanhove, G., Petit, G. and Minetti, R. Experimental study of the kinetic interactions in the low-temperature autoignition of hydrocarbon binary mixtures and a surrogate fuel. *Combustion and Flame.* 2006, **145**(3), pp.521-532.

147. Kukkadapu, G., Kumar, K., Sung, C.-J., Mehl, M. and Pitz, W.J. Experimental and surrogate modeling study of gasoline ignition in a rapid compression machine. *Combustion and Flame.* 2012, **159**(10), pp.3066-3078.

148. Puduppakkam, K.V., Liang, L., Naik, C.V., Meeks, E. and Bunting, B.G. *Combustion and emissions modeling of a gasoline HCCI engine using model fuels.* SAE Technical Paper, 2009.

149. Kukkadapu, G., Kumar, K., Sung, C.-J., Mehl, M. and Pitz, W.J. Autoignition of gasoline surrogates at low temperature combustion conditions. *Combustion and Flame.* 2015, **162**(5), pp.2272-2285.

150. Javed, T., Lee, C., AlAbbad, M., Djebbi, K., Beshir, M., Badra, J., Curran, H. and Farooq, A. Ignition studies of n-heptane/iso-octane/toluene blends. *Combustion and Flame.* 2016, **171**, pp.223-233.

151. Dooley, S., Won, S.H., Chaos, M., Heyne, J., Ju, Y., Dryer, F.L., Kumar, K., Sung, C.-J., Wang, H. and Oehlschlaeger, M.A. A jet fuel surrogate formulated by real fuel properties. *Combustion and Flame.* 2010, **157**(12), pp.2333-2339.

152. Dooley, S., Won, S.H., Heyne, J., Farouk, T.I., Ju, Y., Dryer, F.L., Kumar, K., Hui, X., Sung, C.-J. and Wang, H. The experimental evaluation of a methodology for surrogate fuel formulation to emulate gas phase combustion kinetic phenomena. *Combustion and Flame.* 2012, **159**(4), pp.1444-1466.

153. Benson, S.W. *Thermochemical kinetics: Methods for the estimation of thermochemical data and rate parameters*. New York: John Wiley and Sons, Inc. 1976.

154. Yuan, H., Lu, Z., Chen, Z., Yang, Y., Brear, M.J., Anderson, J.E. and Leone, T. Oxidation of ethanol and hydrocarbon mixtures in a pressurised flow reactor. *Combustion and Flame.* 2019, **199**, pp.96-113.

155. Knop, V., Pera, C. and Duffour, F. Validation of a ternary gasoline surrogate in a CAI engine. *Combustion and Flame.* 2013, **160**(10), pp.2067-2082.

156. Pera, C. and Knop, V. Methodology to define gasoline surrogates dedicated to auto-ignition in engines. *Fuel.* 2012, **96**, pp.59-69.

157. Foong, T.M., Morganti, K.J., Brear, M.J., da Silva, G., Yang, Y. and Dryer, F.L. The octane numbers of ethanol blended with gasoline and its surrogates. *Fuel.* 2014, **115**, pp.727-739.

158. Badra, J., AlRamadan, A.S. and Sarathy, S.M. Optimization of the octane response of gasoline/ethanol blends. *Applied Energy.* 2017, **203**, pp.778-793.

159. Yuan, H., Yang, Y., Brear, M.J., Foong, T.M. and Anderson, J.E. Optimal octane number correlations for mixtures of toluene reference fuels (TRFs) and ethanol. *Fuel.* 2017, **188**, pp.408-417.

160. AlRamadan, A.S., Sarathy, S.M., Khurshid, M. and Badra, J. A blending rule for octane numbers of PRFs and TPRFs with ethanol. *Fuel.* 2016, **180**, pp.175-186.

161. Wang, H. and Sheen, D.A. Combustion kinetic model uncertainty quantification, propagation and minimization. *Progress in Energy and Combustion Science.* 2015, **47**, pp.1-31.

162. vom Lehn, F., Cai, L. and Pitsch, H. Sensitivity analysis, uncertainty quantification, and optimization for thermochemical properties in chemical kinetic combustion models. *Proceedings of the Combustion Institute.* 2018.

163. Tomlin, A.S. The role of sensitivity and uncertainty analysis in combustion modelling. *Proceedings of the Combustion Institute.* 2013, **34**(1), pp.159-176.

164. Turanyi, T. Applications of sensitivity analysis to combustion chemistry. *Reliability Engineering & System Safety.* 1997, **57**(1), pp.41-48.

165. Rabitz, H., Kramer, M. and Dacol, D. Sensitivity analysis in chemical kinetics. *Annual review of physical chemistry.* 1983, **34**(1), pp.419-461.

166. Dunker, A.M. The decoupled direct method for calculating sensitivity coefficients in chemical kinetics. *The Journal of chemical physics.* 1984, **81**(5), pp.2385-2393.

167. He, K., Androulakis, I.P. and Ierapetritou, M.G. On-the-fly reduction of kinetic mechanisms using element flux analysis. *Chemical Engineering Science.* 2010, **65**(3), pp.1173-1184.

168. Yabe, T. and Sekine, Y. Methane conversion using carbon dioxide as an oxidizing agent: A review. *Fuel Processing Technology.* 2018, **181**, pp.187-198.

169. Thiruvengadam, A., Besch, M., Padmanaban, V., Pradhan, S. and Demirgok, B. Natural gas vehicles in heavy-duty transportation-A review. *Energy Policy.* 2018, **122**, pp.253-259.

170. Bae, C. and Kim, J. Alternative fuels for internal combustion engines. *Proceedings of the Combustion Institute.* 2017, **36**(3), pp.3389-3413.

171. Yan, F., Xu, L. and Wang, Y. Application of hydrogen enriched natural gas in spark ignition IC engines: from fundamental fuel properties to engine performances and emissions. *Renewable and Sustainable Energy Reviews.* 2017.

172. Gogolev, I.M. and Wallace, J.S. Performance and emissions of a compression-ignition direct-injected natural gas engine with shielded glow plug ignition assist. *Energy Conversion and Management.* 2018, **164**, pp.70-82.

173. Cho, H.M. and He, B.-Q. Spark ignition natural gas engines—A review. *Energy Conversion and Management.* 2007, **48**(2), pp.608-618.

174. Mendoza Orbegoso, E.M., Silva, L.F., Junior, N. and André, R. On the predictability of chemical kinetics for the description of the combustion of simple fuels. *Journal of the Brazilian Society of Mechanical Sciences and Engineering.* 2011, **33**(4), pp.492-505.

175. Tingas, E.A., Manias, D.M., Sarathy, S.M. and Goussis, D.A. CH 4/air homogeneous autoignition: A comparison of two chemical kinetics mechanisms. *Fuel.* 2018, **223**, pp.74-85.

176. Enikolopyan, N. Kinetics and mechanism of methane oxidation. In: *Symposium (International) on Combustion 7*: Elsevier, 1958, pp.157-164.

177. Bowman, C.T. Non-equilibrium radical concentrations in shock-initiated methane oxidation. In: *Symposium (International) on Combustion*: Elsevier, 1975, pp.869-882.

178. Olson, D. and Gardiner Jr, W. Combustion of methane in fuel-rich mixtures. *Combustion and Flame.* 1978, **32**, pp.151-161.

179. Prince, J.C. and Williams, F.A. Short chemical-kinetic mechanisms for low-temperature ignition of propane and ethane. *Combustion and Flame.* 2012, **159**(7), pp.2336-2344.

180. Wang, H., You, X., Joshi, A.V., Davis, S.G., Laskin, A., Egolfopoulos, F., Law, C.K. and Version II, U.M. *High-temperature combustion reaction model of H2/CO/C1-C4 Compounds.* 2007.

181. Wang, H., Dames, E., Sirjean, B., Sheen, D., Tangko, R., Violi, A., Lai, J., Egolfopoulos, F., Davidson, D. and Hanson, R. A high-temperature chemical kinetic model of n-alkane (up to n-dodecane), cyclohexane, and methyl-, ethyl-, n-propyl and n-butyl-cyclohexane oxidation at high temperatures. *JetSurF version.* 2010, **2**(2), p.19.

182. Ranzi, E., Frassoldati, A., Grana, R., Cuoci, A., Faravelli, T., Kelley, A. and Law, C. Hierarchical and comparative kinetic modeling of laminar flame speeds of hydrocarbon and oxygenated fuels. *Progress in Energy and Combustion Science.* 2012, **38**(4), pp.468-501.

183. Metcalfe, W.K., Burke, S.M., Ahmed, S.S. and Curran, H.J. A hierarchical and comparative kinetic modeling study of C1– C2 hydrocarbon and oxygenated fuels. *International Journal of Chemical Kinetics.* 2013, **45**(10), pp.638-675.

184. Li, Y., Zhou, C.-W., Somers, K.P., Zhang, K. and Curran, H.J. The oxidation of 2-butene: A high pressure ignition delay, kinetic modeling study and reactivity comparison with isobutene and 1-butene. *Proceedings of the Combustion Institute.* 2017, **36**(1), pp.403-411.

185. Zhou, C.-W., Li, Y., O'Connor, E., Somers, K.P., Thion, S., Keesee, C., Mathieu, O., Petersen, E.L., DeVerter, T.A. and Oehlschlaeger, M.A. A comprehensive experimental and modeling study of isobutene oxidation. *Combustion and Flame.* 2016, **167**, pp.353-379.

186. Burke, U., Somers, K.P., O'Toole, P., Zinner, C.M., Marquet, N., Bourque, G., Petersen, E.L., Metcalfe, W.K., Serinyel, Z. and Curran, H.J. An ignition delay and kinetic modeling study of methane, dimethyl ether, and their mixtures at high pressures. *Combustion and Flame.* 2015, **162**(2), pp.315-330.

187. Lopez, J.G., Rasmussen, C.T., Hashemi, H., Alzueta, M., Gao, Y., Marshall, P., Goldsmith, C.F. and Glarborg, P. Experimental and Kinetic Modeling Study of C2H2 Oxidation at High Pressure. *International Journal of Chemical Kinetics.* 2016, **48**(11), pp.724-738.

188. Hughes, K., Turányi, T., Clague, A. and Pilling, M.J.I.J.o.C.K. Development and testing of a comprehensive chemical mechanism for the oxidation of methane. *International Journal of Chemical Kinetics.* 2001, **33**(9), pp.513-538.

189. Mohr, A. and Raman, S. Lessons from first generation biofuels and implications for the sustainability appraisal of second generation biofuels. *Energy Policy.* 2013, **63**, pp.114-122.

190. Nigam, P.S. and Singh, A. Production of liquid biofuels from renewable resources. *Progress in Energy and Combustion Science.* 2011, **37**(1), pp.52-68.

191. Saladini, F., Patrizi, N., Pulselli, F.M., Marchettini, N. and Bastianoni, S. Guidelines for emergy evaluation of first, second and third generation biofuels. *Renewable and Sustainable Energy Reviews.* 2016, **66**, pp.221-227.

192. Correa, D.F., Beyer, H.L., Possingham, H.P., Thomas-Hall, S.R. and Schenk, P.M. Biodiversity impacts of bioenergy production: microalgae vs. first generation biofuels. *Renewable and Sustainable Energy Reviews.* 2017, **74**, pp.1131-1146.

193. Leong, W.-H., Lim, J.-W., Lam, M.-K., Uemura, Y. and Ho, Y.-C. Third generation biofuels: A nutritional perspective in enhancing microbial lipid production. *Renewable and Sustainable Energy Reviews.* 2018, **91**, pp.950-961.

194. Jeswani, H.K., Falano, T. and Azapagic, A. Life cycle environmental sustainability of lignocellulosic ethanol produced in integrated thermo‐chemical biorefineries. *Biofuels, Bioproducts and Biorefining.* 2015, **9**(6), pp.661-676.

195. Department of Communications, C.A.a.E. *Biofuels Obligation Scheme Policy Statement April 2018.* [Online]. 2019. [Accessed 10 September 2019]. Available from: https://www.dccae.gov.ie/documents/Biofuels%20Obligation%20Scheme%20Policy%20Statement.pdf

196. Guo, M., Song, W. and Buhain, J. Bioenergy and biofuels: History, status, and perspective. *Renewable and Sustainable Energy Reviews.* 2015, **42**, pp.712-725.

197. Klass, D.L. *Biomass for renewable energy, fuels, and chemicals.* Elsevier, 1998.

198. Renewable Fuel Association. *2018 Ethanol Industry Outlook.* [Online]. 2018. [Accessed 25 April 2019]. Available from: https://ethanolrfa.org/wp-content/uploads/2018/02/NECfinalOutlook.pdf

199. Kaup, F. *The sugarcane complex in Brazil.* Cham: Springer, 2015.

200. Feng, H., Liu, D., Yang, X., An, M., Zhang, W. and Zhang, X. Availability analysis of using iso-octane/n-butanol blends in spark-ignition engines. *Renewable Energy.* 2016, **96**, pp.281-294.

201. Szwaja, S. and Naber, J.D. Combustion of n-butanol in a spark-ignition IC engine. *Fuel.* 2010, **89**(7), pp.1573-1582.

202. Choi, C.-Y. and Reitz, R.D. An experimental study on the effects of oxygenated fuel blends and multiple injection strategies on DI diesel engine emissions. *Fuel.* 1999, **78**(11), pp.1303-1317.

203. Siwale, L., Kristóf, L., Adam, T., Bereczky, A., Mbarawa, M., Penninger, A. and Kolesnikov, A. Combustion and emission characteristics of n-butanol/diesel fuel blend in a turbo-charged compression ignition engine. *Fuel.* 2013, **107**, pp.409-418.

204. Awad, O.I., Mamat, R., Ali, O.M., Sidik, N., Yusaf, T., Kadirgama, K. and Kettner, M. Alcohol and ether as alternative fuels in spark ignition engine: A review. *Renewable Sustainable Energy Reviews.* 2018, **82**, pp.2586-2605.

205. Ricardo, H.R. The high-speed internal-combustion engine. 1953.

206. Bock, B., Bell, A. and Floweday, G. *Investigation into the Influence of Charge Cooling and Autoignition Chemistry on the Greater Knock Resistance of Ethanol over Iso-octane.* SAE Technical Paper, 2013.

207. Milpied, J., Jeuland, N., Plassat, G., Guichaous, S., Dioc, N., Marchal, A. and Schmelzle, P. Impact of fuel properties on the performances and knock behaviour of a downsized turbocharged DI SI engine–Focus on Octane Numbers and latent heat of vaporization. *SAE International Journal of Fuels and Lubricants.* 2009, **2**(1), pp.118-126.

208. Lee, S., Speight, J.G. and Loyalka, S.K. *Handbook of alternative fuel technologies.* crc Press, 2014.

209. International Energy Agency. IEA Energy Technology Essentials: Biofuel Production. 2007.

210. Kumar, S., Singh, N. and Prasad, R. Anhydrous ethanol: A renewable source of energy. *Renewable and Sustainable Energy Reviews.* 2010, **14**(7), pp.1830-1844.

211. Niven, R.K. Ethanol in gasoline: environmental impacts and sustainability review article. *Renewable and Sustainable Energy Reviews.* 2005, **9**(6), pp.535-555.

212. Thangavelu, S.K., Ahmed, A.S. and Ani, F.N. Review on bioethanol as alternative fuel for spark ignition engines. *Renewable and Sustainable Energy Reviews.* 2016, **56**, pp.820-835.

213. Yusri, I., Mamat, R., Najafi, G., Razman, A., Awad, O.I., Azmi, W., Ishak, W. and Shaiful, A. Alcohol based automotive fuels from first four alcohol family in compression and spark ignition engine: a review on engine performance and exhaust emissions. *Renewable and Sustainable Energy Reviews.* 2017, **77**, pp.169-181.

214. Biofuel. *Major producers by region: North America.* [Online]. 2010. [Accessed 10 June 2016]. Available from: http://biofuel.org.uk/north-america.html/

215. Vancoillie, J. and Verhelst, S. Modeling the combustion of light alcohols in SI engines: a preliminary study. In: *FISITA 2010 World Automotive Congress*: International Federation of Automotive Engineering Societies, 2010.

216. da Silva Trindade, W.R. and dos Santos, R.G. Review on the characteristics of butanol, its production and use as fuel in internal combustion engines. *Renewable and Sustainable Energy Reviews.* 2017, **69**, pp.642-651.

217. Park, C., Choi, Y., Kim, C., Oh, S., Lim, G. and Moriyoshi, Y. Performance and exhaust emission characteristics of a spark ignition engine using ethanol and ethanol-reformed gas. *Fuel.* 2010, **89**(8), pp.2118-2125.

218. Yu, A.S.O., de Souza Nascimento, P.T., Nigro, F.E.B., Frederick, B.W.B., Varandas, A., Vieira, S.F.A. and Rocha, R.L. The evolution of flex-fuel technology in Brazil: the Bosch case. In: *Technology Management for Global Economic Growth (PICMET), 2010 Proceedings of PICMET'10:*: IEEE, 2010, pp.1-11.

219. Gu, X., Huang, Z., Li, Q. and Tang, C. Measurements of laminar burning velocities and Markstein lengths of n-butanol– air premixed mixtures at elevated temperatures and pressures. *Energy & Fuels.* 2009, **23**(10), pp.4900-4907.

220. Baral, N.R. and Shah, A. Techno-economic analysis of cellulosic butanol production from corn stover through acetone–butanol–ethanol fermentation. *Energy & Fuels.* 2016, **30**(7), pp.5779-5790.

221. Wigg, B.R. A study on the emissions of butanol using a spark ignition engine and their reduction using electrostatically assisted injection. 2011.

222. Brekke, K. Butanol an energy alternative. *Ethanol Today.* 2007, pp.36-39.

223. Wu, M., Wang, M., Liu, J. and Huo, H. *Life-cycle assessment of corn-based butanol as a potential transportation fuel.* Argonne National Laboratory, 2007.

224. Yusoff, M., Zulkifli, N., Masjuki, H.H., Harith, M., Syahir, A., Kalam, M., Mansor, M., Azham, A. and Khuong, L. Performance and emission characteristics of a spark ignition engine fuelled with butanol isomer-gasoline blends. *Transportation Research Part D: Transport and Environment.* 2017, **57**, pp.23-38.

225. Moss, J.T., Berkowitz, A.M., Oehlschlaeger, M.A., Biet, J., Warth, V., Glaude, P.-A. and Battin-Leclerc, F. An experimental and kinetic modeling study of the oxidation of the four isomers of butanol. *The Journal of Physical Chemistry A.* 2008, **112**(43), pp.10843-10855.

226. Weber, B.W. and Sung, C.-J. Comparative autoignition trends in butanol isomers at elevated pressure. *Energy & Fuels.* 2013, **27**(3), pp.1688-1698.

227. Stranic, I., Chase, D.P., Harmon, J.T., Yang, S., Davidson, D.F. and Hanson, R.K. Shock tube measurements of ignition delay times for the butanol isomers. *Combustion and Flame.* 2012, **159**(2), pp.516-527.

228. Gu, X., Huang, Z., Wu, S. and Li, Q. Laminar burning velocities and flame instabilities of butanol isomers–air mixtures. *Combustion and Flame.* 2010, **157**(12), pp.2318-2325.

229. Haas, F.M., Ramcharan, A. and Dryer, F.L. Relative reactivities of the isomeric butanols and ethanol in an ignition quality tester. *Energy & Fuels.* 2011, **25**(9), pp.3909-3916.

230. Yang, Z., Wang, Y., Yang, X., Qian, Y., Lu, X. and Huang, Z. Autoignition of butanol isomers/n-heptane blend fuels on a rapid compression machine in N2/O2/Ar mixtures. *Science China Technological Sciences.* 2014, **57**(3), pp.461-470.

231. Yasunaga, K., Mikajiri, T., Sarathy, S.M., Koike, T., Gillespie, F., Nagy, T., Simmie, J.M. and Curran, H.J. A shock tube and chemical kinetic modeling study of the pyrolysis and oxidation of butanols. *Combustion and Flame.* 2012, **159**(6), pp.2009-2027.

232. Zheng, Z., Li, C., Liu, H., Zhang, Y., Zhong, X. and Yao, M. Experimental study on diesel conventional and low temperature combustion by fueling four isomers of butanol. *Fuel.* 2015, **141**, pp.109-119.

233. Merola, S.S., Tornatore, C., Marchitto, L., Valentino, G. and Corcione, F.E. Experimental investigations of butanol-gasoline blends effects on the combustion process in a SI engine. *International Journal of Energy and Environmental Engineering.* 2012, **3**(1), p.6.

234. Wang, C., Prakash, A., Aradi, A., Cracknell, R. and Xu, H. Significance of RON and MON to a modern DISI engine. *Fuel.* 2017, **209**, pp.172-183.

235. Cracknell, R., Warnecke, W., Redmann, J.-H. and Goh, T.K. Oktanbedarf bei modernen aufgeladenen Ottomotoren. *MTZ-Motortechnische Zeitschrift.* 2015, **76**(7-8), pp.16-21.

236. Cracknell, R., Warnecke, W., Redmann, J.-H. and Goh, T.K. Octane requirements of modern downsized boosted gasoline engines. *MTZ worldwide.* 2015, **76**(7-8), pp.4-7.

237. Tsao, G.T. A novel 4A process ready for commercial production of ethanol, butanol and hydrogen from cellulosics. In: *Biofuels Symposium, Stewart Center, Purdue University, West Lafayette, Indiana*, 2008.

238. Busche, R.M. and Allen, B. Technoeconomics of butanol extractive fermentation in a multiphase fluidized bed bioreactor. *Applied Biochemistry and Biotechnology.* 1989, **20**(1), p.357.

239. Ezeji, T.C., Qureshi, N. and Blaschek, H.P. Butanol fermentation research: upstream and downstream manipulations. *The chemical record.* 2004, **4**(5), pp.305-314.

240. Ezeji, T.C., Qureshi, N. and Blaschek, H.P. Bioproduction of butanol from biomass: from genes to bioreactors. *Current opinion in biotechnology.* 2007, **18**(3), pp.220-227.

241. Noorani, K.E., Akih-Kumgeh, B. and Bergthorson, J.M. Comparative high temperature shock tube ignition of C1– C4 primary alcohols. *Energy & Fuels.* 2010, **24**(11), pp.5834-5843.

242. Stranic, I., Pyun, S.H., Davidson, D.F. and Hanson, R.K. Multi-species measurements in 1-butanol pyrolysis behind reflected shock waves. *Combustion and Flame.* 2012, **159**(11), pp.3242-3250.

243. Stranic, I., Pyun, S.H., Davidson, D.F. and Hanson, R.K. Multi-species measurements in 2-butanol and i-butanol pyrolysis behind reflected shock waves. *Combustion and Flame.* 2013, **160**(6), pp.1012-1019.

244. Vasu, S.S. and Sarathy, S.M. On the high-temperature combustion of n-butanol: shock tube data and an improved kinetic model. *Energy & Fuels.* 2013, **27**(11), pp.7072-7080.

245. Zhu, Y., Davidson, D.F. and Hanson, R.K. 1-Butanol ignition delay times at low temperatures: An application of the constrained-reaction-volume strategy. *Combustion and Flame.* 2014, **161**(3), pp.634-643.

246. Vranckx, S., Heufer, K., Lee, C., Olivier, H., Schill, L., Kopp, W., Leonhard, K., Taatjes, C. and Fernandes, R. Role of peroxy chemistry in the high-pressure ignition of n-butanol– Experiments and detailed kinetic modelling. *Combustion and Flame.* 2011, **158**(8), pp.1444-1455.

247. Heufer, K., Fernandes, R., Olivier, H., Beeckmann, J., Röhl, O. and Peters, N. Shock tube investigations of ignition delays of n-butanol at elevated pressures between 770 and 1250 K. *Proceedings of the Combustion Institute.* 2011, **33**(1), pp.359-366.

248. Black, G., Curran, H., Pichon, S., Simmie, J. and Zhukov, V. Bio-butanol: Combustion properties and detailed chemical kinetic model. *Combustion and Flame.* 2010, **157**(2), pp.363-373.

249. Karwat, D.M., Wagnon, S.W., Wooldridge, M.S. and Westbrook, C.K. On the combustion chemistry of n-heptane and n-butanol blends. *The Journal of Physical Chemistry A.* 2012, **116**(51), pp.12406-12421.

250. Weber, B.W., Kumar, K., Zhang, Y. and Sung, C.-J. Autoignition of n-butanol at elevated pressure and low-to-intermediate temperature. *Combustion and Flame.* 2011, **158**(5), pp.809-819.

251. Yang, Z., Qian, Y., Yang, X., Wang, Y., Wang, Y., Huang, Z. and Lu, X. Autoignition of n-butanol/n-heptane blend fuels in a rapid compression machine under low-to-medium temperature ranges. *Energy & Fuels.* 2013, **27**(12), pp.7800-7808.

252. Goldsborough, S.S., Santner, J., Kang, D., Fridlyand, A., Rockstroh, T. and Jespersen, M.C. Heat release analysis for rapid compression machines: Challenges and opportunities. *Proceedings of the Combustion Institute.* 2019, **37**(1), pp.603-611.

253. Mumby, R.D. *Experimental Characterisation of Fuel Blends*. Ph.D. thesis, University of Leeds, 2016.

254. Affleck, W. and Thomas, A. An opposed piston rapid compression machine for preflame reaction studies. *Proceedings of the Institution of Mechanical Engineers.* 1968, **183**(1), pp.365-387.

255. Mittal, G. *A rapid compression machine–design, characterization, and autoignition investigations*. Ph.D. thesis, Case Western Reserve University, 2006.

256. Desgroux, P., Gasnot, L. and Sochet, L. Instantaneous temperature measurement in a rapid-compression machine using laser Rayleigh scattering. *Applied Physics B.* 1995, **61**(1), pp.69-72.

257. Griffiths, J., Jiao, Q., Kordylewski, W., Schreiber, M., Meyer, J., Knoche, K.J.C. and flame. Experimental and numerical studies of ditertiary butyl peroxide combustion at high pressures in a rapid compression machine. 1993, **93**(3), pp.303-315.

258. Sung, C.-J. and Curran, H.J. Using rapid compression machines for chemical kinetics studies. *Progress in Energy Combustion Science Technology.* 2014, **44**, pp.1-18.

259. Wagnon, S.W. *Chemical Kinetics for Advanced Combustion Strategies*. Ph.D. thesis, 2014.

260. Yaws, C.L. and Gabbula, C. *Yaws" Handbook of Thermodynamic and Physical Properties of Chemical Compounds.* Knovel, 2003.

261. Wallner, T., Miers, S.A. and McConnell, S. A comparison of ethanol and butanol as oxygenates using a direct-injection, spark-ignition engine. *Journal of Engineering for Gas Turbines Power.* 2009, **131**(3), p.032802.

262. Zhang, Y., Somers, K.P., Mehl, M., Pitz, W.J., Cracknell, R.F. and Curran, H.J. Probing the antagonistic effect of toluene as a component in surrogate fuel models at low temperatures and high pressures. A case study of toluene/dimethyl ether mixtures. *Proceedings of the Combustion Institute.* 2017, **36**(1), pp.413-421.

263. Mittal, G. and SUNG*, C.-J. A rapid compression machine for chemical kinetics studies at elevated pressures and temperatures. *Combustion Science Technology.* 2007, **179**(3), pp.497-530.

264. Weber, B.W. *GitHub account.* [Online]. [Accessed 17 October 2016]. Available from: https://github.com/bryanwweber/CanSen

265. Smith, G.P., Golden, D.M., Frenklach, M., Moriarty, N.W., Eiteneer, B., Goldenberg, M., Bowman, C.T., Hanson, R.K., Song, S. and Gardiner Jr, W.C. *GRI-Mech 3.0.* [Online]. 1999. [Accessed 15 May 2016]. Available from: http://www.me.berkeley.edu/gri_mech

266. Huang, J., Hill, P.G., Bushe, W.K. and Munshi, S.R. Shock-tube study of methane ignition under engine-relevant conditions: experiments and modeling. *Combustion and Flame.* 2004, **136**(1), pp.25-42.

267. Gorbatenko, I., Tomlin, A.S., Lawes, M. and Cracknell, R.F.J.P.o.t.C.I. Experimental and modelling study of the impacts of n-butanol blending on the auto-ignition behaviour of gasoline and its surrogate at low temperatures. 2019, **37**(1), pp.501-509.

268. McGillen, M.R., Baasandorj, M. and Burkholder, J.B. Gas-phase rate coefficients for the OH+ n-, i-, s-, and t-butanol reactions measured between 220 and 380 K: Non-arrhenius behavior and site-specific reactivity. *The Journal of Physical Chemistry A.* 2013, **117**(22), pp.4636-4656.

269. Seta, T., Nakajima, M. and Miyoshi, A. High-temperature reactions of OH radicals with benzene and toluene. *The Journal of Physical Chemistry A.* 2006, **110**(15), pp.5081-5090.

270. Ranzi, E., Frassoldati, A., Stagni, A., Pelucchi, M., Cuoci, A. and Faravelli, T.J.I.J.o.C.K. Reduced kinetic schemes of complex reaction systems: fossil and biomass‐derived transportation fuels. 2014, **46**(9), pp.512-542.

271. Pelucchi, M., Bissoli, M., Cavallotti, C., Cuoci, A., Faravelli, T., Frassoldati, A., Ranzi, E. and Stagni, A. Improved kinetic model of the low-temperature oxidation of n-heptane. *Energy & Fuels.* 2014, **28**(11), pp.7178-7193.

272. Pelucchi, M. *Development of kinetic mechanisms for the combustion of renewable fuels*. Ph.D. thesis, 2017.

273. Ranzi, E., Dente, M., Goldaniga, A., Bozzano, G. and Faravelli, T. Lumping procedures in detailed kinetic modeling of gasification, pyrolysis, partial oxidation and combustion of

hydrocarbon mixtures. *Progress in Energy Combustion Science Technology.* 2001, **27**(1), pp.99-139.

274. Sarathy, S.M., Tingas, E.-A., Nasir, E.F., Detogni, A., Wang, Z., Farooq, A. and Im, H. Three-stage heat release in n-heptane auto-ignition. *Proceedings of the Combustion Institute.* 2019, **37**(1), pp.485-492.

275. Heywood, J.B. *Fundamentals of internal combustion engines.* New York: Tata McGraw Hills, 1988.

276. Fridlyand, A., Goldsborough, S.S., Al Rashidi, M., Sarathy, S.M., Mehl, M. and Pitz, W.J. Low temperature autoignition of 5-membered ring naphthenes: Effects of substitution. *Combustion and Flame.* 2019, **200**, pp.387-404.

277. Ritter, E.R. and Bozzelli, J.W.I.J.o.C.K. THERM: Thermodynamic property estimation for gas phase radicals and molecules. 1991, **23**(9), pp.767-778.

278. Burcat, A. and Ruscic, B. *Third millenium ideal gas and condensed phase thermochemical database for combustion (with update from active thermochemical tables).* Argonne National Laboratory, 2005.

279. Argonne National Laboratory. *Active Thermochemical Tables.* [Online]. 2016. [Accessed 16 August 2019]. Available from: https://atct.anl.gov/Thermochemical%20Data/version%201.122e/index.php#Uncertainties

280. Prosen, E. and Rossini, F. Heats of isomerization of the 18 octanes. *Journal of Research of the National Bureau of Standards.* 1945, **34**(2), pp.163-174.

281. Weber, B.W., Sung, C.-J. and Renfro, M.W. On the uncertainty of temperature estimation in a rapid compression machine. *Combustion and Flame.* 2015, **162**(6), pp.2518-2528.

282. Kalghatgi, G., Bradley, D., Andrae, J. and Harrison, A. The nature of 'superknock' and its origins in SI engines. In: *IMechE conference on internal combustion engines: performance fuel economy and emissions*, 2009, pp.8-9.

283. Rudloff, J., Zaccardi, J.-M., Richard, S. and Anderlohr, J.M. Analysis of pre-ignition in highly charged SI engines: Emphasis on the auto-ignition mode. *Proceedings of the Combustion Institute.* 2013, **34**(2), pp.2959-2967.

284. Hu, E., Li, X., Meng, X., Chen, Y., Cheng, Y., Xie, Y. and Huang, Z. Laminar flame speeds and ignition delay times of methane–air mixtures at elevated temperatures and pressures. *Fuel.* 2015, **158**, pp.1-10.

285. Herzler, J. and Naumann, C. Shock-tube study of the ignition of methane/ethane/hydrogen mixtures with hydrogen contents from 0% to 100% at different pressures. *Proc. Combust. Inst.* 2009, **32**(1), pp.213-220.

286. Trevino, C. and Mendez, F. Reduced kinetic mechanism for methane ignition. In: *Symposium (International) on Combustion 24*: Elsevier, 1992, pp.121-127.

287. Zeng, W., Ma, H., Liang, Y. and Hu, E. Experimental and modeling study on effects of N2 and CO2 on ignition characteristics of methane/air mixture. *Journal of Advanced Research.* 2015, **6**(2), pp.189-201.

288. Huang, J. and Bushe, W. Experimental and kinetic study of autoignition in methane/ethane/air and methane/propane/air mixtures under engine-relevant conditions. *Combustion and Flame.* 2006, **144**(1), pp.74-88.

289. Kim, S.-K., Yu, Y., Ahn, J. and Kim, Y.-M. Numerical investigation of the autoignition of turbulent gaseous jets in a high-pressure environment using the multiple-RIF model. *Fuel.* 2004, **83**(3), pp.375-386.

290. El Merhubi, H., Kéromnès, A., Catalano, G., Lefort, B. and Le Moyne, L. A high pressure experimental and numerical study of methane ignition. *Fuel.* 2016, **177**, pp.164-172.

291. Bates, L. *Characterisation of reaction propagation from auto-ignition.* Ph.D. thesis, University of Leeds, 2016.

292. Bates, L., Bradley, D., Gorbatenko, I. and Tomlin, A.S. Computation of methane/air ignition delay and excitation times, using comprehensive and reduced chemical

mechanisms and their relevance in engine autoignition. *Combustion and Flame.* 2017, **185**, pp.105-116.

293. Schreiber, M., Sakak, A.S., Lingens, A. and Griffiths, J. A reduced thermokinetic model for the autoignition of fuels with variable octane ratings. In: *Symposiom (International) on Combustion 25*: Elsevier, 1994, pp.933-940.

294. Aul, C.J., Metcalfe, W.K., Burke, S.M., Curran, H.J. and Petersen, E.L. Ignition and kinetic modeling of methane and ethane fuel blends with oxygen: A design of experiments approach. *Combustion and Flame.* 2013, **160**(7), pp.1153-1167.

295. Nagy, T., Valkó, É., Sedyó, I., Zsély, I.G., Pilling, M.J. and Turányi, T. Uncertainty of the rate parameters of several important elementary reactions of the H 2 and syngas combustion systems. *Combustion and Flame.* 2015, **162**(5), pp.2059-2076.

296. Varga, T., Olm, C., Nagy, T., Zsély, I.G., Valkó, É., Pálvölgyi, R., Curran, H. and Turányi, T. Development of a joint hydrogen and syngas combustion mechanism based on an optimization approach. *International Journal of Chemical Kinetics.* 2016.

297. Burke, M.P., Klippenstein, S.J. and Harding, L.B. A quantitative explanation for the apparent anomalous temperature dependence of OH+ HO 2= H 2 O+ O 2 through multi-scale modeling. *Proceedings of the Combustion Institute.* 2013, **34**(1), pp.547-555.

298. Zhang, Y., Huang, Z., Wei, L., Zhang, J. and Law, C.K. Experimental and modeling study on ignition delays of lean mixtures of methane, hydrogen, oxygen, and argon at elevated pressures. *Combustion and Flame.* 2012, **159**(3), pp.918-931.

299. Griffiths, J., MacNamara, J., Sheppard, C., Turton, D. and Whitaker, B. The relationship of knock during controlled autoignition to temperature inhomogeneities and fuel reactivity. *Fuel.* 2002, **81**(17), pp.2219-2225.

300. Griffiths, J.F. and Whitaker, B. Thermokinetic interactions leading to knock during homogeneous charge compression ignition. *Combustion and Flame.* 2002, **131**(4), pp.386-399.

301. Radulescu, M., Sharpe, G. and Bradley, D. A Universal Parameter Quantifying Explosion Hazards, Detonability and Hot Spot Formation: The χ Number. In: *Proceedings of the 7th International Seminar on Fire and Explosion Hazards. (D. Bradley, G. Makhviladze, V. Molkov, P. Sunderland, and F. Tamanini, Eds.)*, 2013, pp.617-626.

302. Bradley, D. and Shehata, M. Acceleration of laminar hydrogen/oxygen flames in a tube and the possible onset of detonation. *International Journal of Hydrogen Energy.* 2018, **43**(13), pp.6734-6744.

303. Dai, P., Chen, Z., Chen, S. and Ju, Y. Numerical experiments on reaction front propagation in n-heptane/air mixture with temperature gradient. *Proceedings of the Combustion Institute.* 2015, **35**(3), pp.3045-3052.

304. Robert, A., Richard, S., Colin, O. and Poinsot, T. LES study of deflagration to detonation mechanisms in a downsized spark ignition engine. *Combustion and Flame.* 2015, **162**(7), pp.2788-2807.

305. Sankaran, R., Im, H.G., Hawkes, E.R. and Chen, J.H. The effects of non-uniform temperature distribution on the ignition of a lean homogeneous hydrogen–air mixture. *Proceedings of the Combustion Institute.* 2005, **30**(1), pp.875-882.

306. Strozzi, C., Mura, A., Sotton, J. and Bellenoue, M. Experimental analysis of propagation regimes during the autoignition of a fully premixed methane–air mixture in the presence of temperature inhomogeneities. *Combustion and Flame.* 2012, **159**(11), pp.3323-3341.

307. Mansfield, A.B. and Wooldridge, M.S. High-pressure low-temperature ignition behavior of syngas mixtures. *Combustion and Flame.* 2014, **161**(9), pp.2242-2251.

308. Merchant, S.S., Goldsmith, C.F., Vandeputte, A.G., Burke, M.P., Klippenstein, S.J. and Green, W.H. Understanding low-temperature first-stage ignition delay: Propane. *Combustion and Flame.* 2015, **162**(10), pp.3658-3673.

309. Wang, Z., Liu, H., Song, T., Qi, Y., He, X., Shuai, S. and Wang, J. Relationship between super-knock and pre-ignition. *International Journal of Engine Research.* 2015, **16**(2), pp.166-180.

310. Qi, Y., Wang, Z., Wang, J. and He, X. Effects of thermodynamic conditions on the end gas combustion mode associated with engine knock. *Combustion and Flame.* 2015, **162**(11), pp.4119-4128.

311. Tanaka, S., Ayala, F., Keck, J.C. and Heywood, J.B. Two-stage ignition in HCCI combustion and HCCI control by fuels and additives. *Combustion and Flame.* 2003, **132**(1-2), pp.219-239.

312. Mehl, M., Chen, J.-Y., Pitz, W.J., Sarathy, S.M. and Westbrook, C.K. An approach for formulating surrogates for gasoline with application toward a reduced surrogate mechanism for CFD engine modeling. *Energy & Fuels.* 2011, **25**(11), pp.5215-5223.

313. Anderson, J., Kramer, U., Mueller, S. and Wallington, T. Octane numbers of ethanol– and methanol–gasoline blends estimated from molar concentrations. *Energy & Fuels.* 2010, **24**(12), pp.6576-6585.

314. Waqas, M.U., Mohammed, A., Masurier, J.-B. and Johansson, B. *Blending Octane Number of 1-Butanol and Iso-Octane with Low Octane Fuels in HCCI Combustion Mode.* SAE Technical Paper, 2018.

315. Kalghatgi, G., Babiker, H. and Badra, J. A simple method to predict knock using toluene, n-heptane and iso-octane blends (TPRF) as gasoline surrogates. *SAE International Journal of Engines.* 2015, **8**(2), pp.505-519.

316. Morgan, N., Smallbone, A., Bhave, A., Kraft, M., Cracknell, R. and Kalghatgi, G. Mapping surrogate gasoline compositions into RON/MON space. *Combustion and Flame.* 2010, **157**(6), pp.1122-1131.

317. Lee, C., Ahmed, A., Nasir, E.F., Badra, J., Kalghatgi, G., Sarathy, S.M., Curran, H. and Farooq, A. Autoignition characteristics of oxygenated gasolines. *Combustion and Flame.* 2017, **186**, pp.114-128.

318. Mehl, M., Faravelli, T., Giavazzi, F., Ranzi, E., Scorletti, P., Tardani, A. and Terna, D. Detailed chemistry promotes understanding of octane numbers and gasoline sensitivity. *Energy & Fuels.* 2006, **20**(6), pp.2391-2398.

319. Jameel, A.G.A., Naser, N., Issayev, G., Touitou, J., Ghosh, M.K., Emwas, A.-H., Farooq, A., Dooley, S. and Sarathy, S.M. A minimalist functional group (MFG) approach for surrogate fuel formulation. *Combustion and Flame.* 2018, **192**, pp.250-271.

320. Dooley, S., Won, S.H. and Dryer, F.L. Surrogate fuels and combustion characteristics of liquid transportation fuels. In: *Computer Aided Chemical Engineering*. Elsevier, 2019, pp.513-602.

321. Jameel, A.G.A., Naser, N., Emwas, A.-H., Dooley, S. and Sarathy, S.M. Predicting fuel ignition quality using 1H NMR spectroscopy and multiple linear regression. *Energy & Fuels.* 2016, **30**(11), pp.9819-9835.

322. Welz, O., Zádor, J., Savee, J.D., Sheps, L., Osborn, D.L. and Taatjes, C.A. Low-temperature combustion chemistry of n-butanol: principal oxidation pathways of hydroxybutyl radicals. *The Journal of Physical Chemistry A.* 2013, **117**(46), pp.11983-12001.

323. Agbro, E. and Tomlin, A.S. Low temperature oxidation of n-butanol: Key uncertainties and constraints in kinetics. *Fuel.* 2017, **207**, pp.776-789.

324. Haas, F.M., Chaos, M. and Dryer, F.L. Low and intermediate temperature oxidation of ethanol and ethanol–PRF blends: An experimental and modeling study. *Combustion and Flame.* 2009, **156**(12), pp.2346-2350.

325. Mittal, G., Burke, S.M., Davies, V.A., Parajuli, B., Metcalfe, W.K. and Curran, H.J. Autoignition of ethanol in a rapid compression machine. *Combustion and Flame.* 2014, **161**(5), pp.1164-1171.

326. Hébrard, E., Tomlin, A.S., Bounaceur, R. and Battin-Leclerc, F. Determining predictive uncertainties and global sensitivities for large parameter systems: A case study for n-butane oxidation. *Proceedings of the Combustion Institute.* 2015, **35**(1), pp.607-616.

327. Kim, D., Westbrook, C.K. and Violi, A. Two-stage ignition behavior and octane sensitivity of toluene reference fuels as gasoline surrogate. *Combustion and Flame.* 2019, **210**, pp.100-113.

328. Ribaucour, M., Minetti, R., Sochet, L., Curran, H., Pitz, W. and Westbrook, C. Ignition of isomers of pentane: an experimental and kinetic modeling study. *Proceedings of the Combustion Institute.* 2000, **28**(2), pp.1671-1678.

329. Westbrook, C.K. Chemical kinetics of hydrocarbon ignition in practical combustion systems. *Proceedings of the Combustion Institute.* 2000, **28**(2), pp.1563-1577.

330. Wilson, D. and Allen, C. A comparison of sensitivity metrics for two-stage ignition behavior in rapid compression machines. *Fuel.* 2017, **208**, pp.305-313.

331. Min, K., Valco, D.J., Oldani, A., Kim, K., Temme, J., Kweon, C.-B.M. and Lee, T. Autoignition of varied cetane number fuels at low temperatures. *Proceedings of the Combustion Institute.* 2019, **37**(4), pp.5003-5011.

332. Westbrook, C., Curran, H., Pitz, W., Griffiths, J., Mohamed, C. and Wo, S. The effects of pressure, temperature, and concentration on the reactivity of alkanes: Experiments and modeling in a rapid compression machine. In: *Symposium (international) on combustion*: Elsevier, 1998, pp.371-378.

333. Battin-Leclerc, F., Buda, F., Fairweather, M., Glaude, P., Griffiths, J., Hughes, K., Porter, R. and Tomlin, A. The Effect of Formal Mechanism Reduction on Simulated Propane Autoignition and a Quantitative Assessment of the Impact of Uncertainties in Parameter Values. *Proceedings of the European Combustion Meeting.* 2005.

334. Shi, Z., Zhang, H., Wu, H. and Xu, Y. Ignition properties of lean DME/H2 mixtures at low temperatures and elevated pressures. *Fuel.* 2018, **226**, pp.545-554.

335. Griffiths, J., Hughes, K. and Porter, R. The role and rate of hydrogen peroxide decomposition during hydrocarbon two-stage autoignition. *Proceedings of the Combustion Institute.* 2005, **30**(1), pp.1083-1091.

336. Westbrook, C.K. and Pitz, W.J. *Detailed kinetic modeling of autoignition chemistry.* SAE Technical Paper, 1987.

337. Yu, L., Wang, S., Wang, W., Qiu, Y., Qian, Y., Mao, Y. and Lu, X. Exploration of chemical composition effects on the autoignition of two commercial diesels: Rapid compression machine experiments and model simulation. *Combustion and Flame.* 2019, **204**, pp.204-219.

338. Liang, W. and Law, C.K. Theory of first-stage ignition delay in hydrocarbon NTC chemistry. *Combustion and Flame.* 2018, **188**, pp.162-169.

339. Hughes, K.J., Griffiths, J.F., Fairweather, M. and Tomlin, A.S. Evaluation of models for the low temperature combustion of alkanes through interpretation of pressure–temperature ignition diagrams. *Physical Chemistry Chemical Physics.* 2006, **8**(27), pp.3197-3210.

340. Ghosh, M.K., Howard, M.S. and Dooley, S. Accurate and standard thermochemistry for oxygenated hydrocarbons: A case study of ethyl levulinate. *Proceedings of the Combustion Institute.* 2019, **37**(1), pp.337-346.

341. Onda, T., Nakamura, H., Tezuka, T., Hasegawa, S. and Maruta, K. Initial-stage reaction of methane examined by optical measurements of weak flames in a micro flow reactor with a controlled temperature profile. *Combustion and Flame.* 2019, **206**, pp.292-307.

342. Yang, B., Yao, M., Cheng, W.K., Zheng, Z. and Yue, L. Regulated and unregulated emissions from a compression ignition engine under low temperature combustion fuelled with gasoline and n-butanol/gasoline blends. *Fuel.* 2014, **120**, pp.163-170.

343. Sjöberg, M. and Dec, J.E. An investigation into lowest acceptable combustion temperatures for hydrocarbon fuels in HCCI engines. *Proceedings of the Combustion Institute.* 2005, **30**(2), pp.2719-2726.

344. Wu, F. and Law, C.K. An experimental and mechanistic study on the laminar flame speed, Markstein length and flame chemistry of the butanol isomers. *Combustion and Flame.* 2013, **160**(12), pp.2744-2756.

345. Grogan, K.P., Goldsborough, S.S. and Ihme, M. Ignition regimes in rapid compression machines. *Combustion and Flame.* 2015, **162**(8), pp.3071-3080.

346. Pan, J., Dong, S., Wei, H., Li, T., Shu, G. and Zhou, L. Temperature gradient induced detonation development inside and outside a hotspot for different fuels. *Combustion and Flame.* 2019, **205**, pp.269-277.

347. Pan, J. and Sheppard, C.G.W. A theoretical and experimental study of the modes of end gas autoignition leading to knock in SI engines. *SAE transactions.* 1994, pp.1925-1947.

348. Agbro, E., Zhang, W., Tomlin, A.S. and Burluka, A. Experimental Study on the Influence of n-Butanol Blending on the Combustion, Autoignition, and Knock Properties of Gasoline and Its Surrogate in a Spark-Ignition Engine. *Energy & Fuels.* 2018, **32**(10), pp.10052-10064.

349. Kalghatgi, G.T. and Bradley, D. Pre-ignition and 'super-knock' in turbo-charged spark-ignition engines. *International Journal of Engine Research.* 2012, **13**(4), pp.399-414.

350. Terashima, H. and Koshi, M. Mechanisms of strong pressure wave generation in end-gas autoignition during knocking combustion. *Combustion and Flame.* 2015, **162**(5), pp.1944-1956.

351. Singh, E., Badra, J., Mehl, M. and Sarathy, S.M. Chemical kinetic insights into the octane number and octane sensitivity of gasoline surrogate mixtures. *Energy & Fuels.* 2017, **31**(2), pp.1945-1960.

352. Mehl, M., Vanhove, G., Pitz, W.J., Ranzi, E.J.C. and Flame. Oxidation and combustion of the n-hexene isomers: A wide range kinetic modeling study. 2008, **155**(4), pp.756-772.